ELECTROSPUN MUCOADHESIVE POLYMERIC MEMBRANES

MEDHA SURENDRANATH

PhD THESIS

2024

SREE CHITRA TIRUNAL INSTITUTE FOR MEDICAL SCIENCES AND TECHNOLOGY, TRIVANDRUM

An Institution of National Importance established by an Act of the Indian Parliament
(Act No.52 of 1980)
Dept. of Science and Technology, Govt. of India
www.sctimst.ac.in

ELECTROSPUN MUCOADHESIVE POLYMERIC MEMBRANES

A THESIS SUBMITTED BY

MEDHA SURENDRANATH

TO

SREE CHITRA TIRUNAL INSTITUTE FOR MEDICAL SCIENCES AND TECHNOLOGY, TRIVANDRUM.

IN PARTIAL FULFILMENT OF THE REQUIREMENTS

FOR THE AWARD OF

DOCTOR OF PHILOSOPHY

2024

DECLARATION

I, Medha Surendranath, hereby certify that I had personally carried out the work depicted in the thesis titled, "Electrospun Mucoadhesive Polymeric Membranes" under the direct supervision of Dr. P. Ramesh, Scientist, Division Polymeric Medical Devices, Biomedical Technology Wing, Sree Chitra Tirunal Institute for Medical Sciences and Technology, Thiruvananthapuram, Kerala, India. No part of this thesis has been submitted for the award of any other degree or diploma prior to this date.

Medha Surendranath

Date: 07.02.2024

CERTIFICATE BY THE RESEARCH GUIDE

SREE CHITRA TIRUNAL INSTITUTE FOR MEDICAL SCIENCES AND TECHNOLOGY
BIOMEDICAL TECHNOLOGY WING, POOJAPPURA
THRIUVANANTHAPURAM- 695011, INDIA
(An Institute of National Importance under Govt. of India)
Phone- (91)0471-2520221 Fax- (91)0471-2341814 www.sctimst.ac.in

Dr. P. Ramesh

Scientist G- Senior Grade

Division of Polymeric Medical Devices

This is to certify that Medha Surendranath, Division of Polymeric Medical Devices of this institute has fulfilled the requirements prescribed for the Ph.D. degree of the Sree Chitra Tirunal Institute for Medical Sciences and Technology, Trivandrum.

The thesis entitled; "Electrospun Mucoadhesive Polymeric Membranes" was carried out under my direct supervision. No part of the thesis was submitted for the award of any degree or diploma prior to this date.

Dr. P. Ramesh

Date: 07.02.2024

CERTIFICATE BY THE RESEARCH CO-GUIDE

SREE CHITRA TIRUNAL INSTITUTE FOR MEDICAL SCIENCES AND TECHNOLOGY
BIOMEDICAL TECHNOLOGY WING, POOJAPPURA
THRIUVANANTHAPURAM- 695011, INDIA
(An Institute of National Importance under Govt. of India)
Phone- (91)0471-2520221 Fax- (91)0471-2341814 www.sctimst.ac.in

Dr. Rekha M. R.

Scientist G

Division of Biosurface Technology

This is to certify that Medha Surendranath, Division of Polymeric Medical Devices of this institute has fulfilled the requirements prescribed for the Ph.D. degree of the Sree Chitra Tirunal Institute for Medical Sciences and Technology, Trivandrum.

The thesis entitled; "Electrospun Mucoadhesive Polymeric Membranes" was carried out under my direct supervision. No part of the thesis was submitted for the award of any degree or diploma prior to this date.

Dr. Rekha M. R.

Date: 07.02.2024

APPROVAL OF THE THESIS

The thesis entitled

Electrospun Mucoadhesive Polymeric Membranes

Submitted by

Medha Surendranath

for the degree of

Doctor of Philosophy

of

SREE CHITRA TIRUNAL INSTITUTE FOR MEDICAL SCIENCES AND TECHNOLOGY, TRIVANDRUM

is evaluated and approved by

Dr. P. Ramesh
(Guide) 30/1/2024

30/1/2024
.....(Name and signature of examiner)
Prof. Manickam Jayakannan.
(Examiner)

TABLE OF CONTENT

ACKNOWLEDGEMENT

It is genuine pleasure and gratitude to acknowledge the people who have whole heartedly supported me to write this thesis.

I would take this opportunity to thank CSIR, India for the financial assistance that helped me to complete this research work. I also would like to thank Head, BMT wing and Director SCTIMST for providing the facilities for carrying out the research experiments. I would like to thank Dean, Registrar, Deputy Registrar and all the staff of academic section for their help.

I would like to express my deep sense of thanks to my supervisor Dr. P. Ramesh, for extending his continuous support and guidance throughout my journey towards this thesis. I am extremely grateful to him for giving me all the freedom and confidence to carry out my research experiments and for always encouraging me to think out of the box ideas.

Dr. Rekha M. R, my co-guide had been constantly helping me in every stage of my research. I have no words to thank her for giving me insights and inspiration through the whole of my PhD program. I thank other members of my Doctoral Advisory Committee, Dr. P. V. Mohanan, Dr. Anil Kumar P. R, and Dr. Prakash Nair for their timely suggestions.

I would like to extend my gratitude to Dr. Renjith, Mr. Willi Paul, Ms. Nimi, Dr. Sasikala and Dr. Radhakumari of Central Analytical Facility for helping me to complete texture analysis, DSC, FTIR and TGA analysis. I take this opportunity to thank Dr. Manoj Komath and Dr. Nishad of Division of Bioceramics for the SEM analysis of my samples. I would like to acknowledge Dr. Anil Kumar P.R, Dr. Naresh Kasoju, Mr. Vinodkumar and students of Division of Tissue Culture for providing fluorescent imaging facilities.

I am thankful to Dr. Rekha M. R and students of Division of Biosurface Technology for UV spectrophotometer analysis of samples. I am grateful to Dr. P. V. Mohanan and Joseph Xavier of Division of Toxicology for helping me to get done the confocal imaging of samples. I am extremely thankful to Dr. Sachin J. Shenoy and members of Division of Laboratory Animal Science for the efforts taken to provide me carcass tissue samples of porcine buccal mucosa.

I also acknowledge Dr. Prabha D. Nair, Dr. Lynda V. Thomas and students of Division of Tissue Engineering and Regenerative Technology for the water contact angle analysis of my samples.

I delighted to express my gratitude to my own team of Division of Polymeric Medical Devices, Dr. Roy Joseph, Dr. Gijo Raj, Ms. Jasmin Joseph and Dr. Chandrasekhar for their sincere support during my tenure. I am indebted to my fellow lab mates, Dr. Resmi R, Ms. Prima S, Ms. Athira M, Ms. Athira K. R, Ms. Swetha P. V, Ms. Sarah, Ms. Theerdha, Ms. Prathyusha, Mr. Saravana Perumal, Mr. Ansar, Mr. Nikhil Prasad, Ms. Sruthi S, Mr. Rahul R. K, Ms. Sithara, Ms. Aleesha, Ms. Reshmi, Ms. Gopika V Gopan, Ms. Dhanya C. S, Ms. Gopika Ramesh, Dr. Anand, Mr. Adarsh and Ms. Arya for extending a positive atmosphere in the lab and for being with me in my good and bad times.

I would like extend my thanks to National Institute for Interdisciplinary Science and Technology and Central Laboratory for Instrumentation and Facilitation for XPS, TGA and XRD facilities

I am glad of thanking Mr. Jaison Jospeh and Ms. Mini K Philip for offering me moral and mental support all the time. I am grateful to Mr. Aravind Venugopal for the emotional support which kept me going through my thick and thin.

I am extremely grateful to Mr. C. K Lukose (late) and Dr. V. Venugopal for your objective understanding on my abilities and limitations and for the constant care and motivation. I am really appreciating you both for being my god fathers. I extend my deep sense of gratitude to Dr. D. Surendranath and Ms. Mary Surendranath (my parents) who were acting as my strong pillars of support in my life and never left me in doubt of their love for me.

Medha Surendranath

LIST OF FIGURES

LIST OF TABLES

ABBREVIATIONS

APBA	3-aminophenyl boronic acid
ATR	Attenuated Total Reflectance
BBB	Blood Brain Barrier
BRB	Blood Retinal Barrier
CD	Circular Dichroism
CMC	Carboxymethyl cellulose
CNS	Central Nervous System
CY	Cysteine
DMA	Dynamic Mechanical Analysis
DMEM	Dulbecco Modified Eagles Medium
DMF	Dimethylformamide
DMSO	Dimethyl sulfoxide
DSC	Differential Scanning Calorimetry
DTNB	5,5'-dithiobis-(2-nitro benzoic acid)
EDC	N-(3-dimethylaminopropyl)-N'-ethylcarbodiimide
EDTA	Ethylenediaminetetraacetic acid
FBS	Fetal Bovine Serum
FTIR	Fourier Transform Infrared
HPMC	Hydroxypropyl methylcellulose
MTT	3-[4,5-dimethylthiazol-2-yl]-2,5 diphenyl tetrazolium bromide
MUZ	Mucin crosslinked Zein
MUZPVP	Mucin crosslinked Zein/PVP blend
NSAID	Non-Steroidal Anti-Inflammatory Drug

PAA	Polyacrylic acid
PBS	Phosphate Buffered Saline
PBST	PBS containing 0.1 % triton-X-100
PCL	Polycaprolactone
PEG	Polyethylene glycol
PEO	Polyethylene oxide
PFA	Paraformaldehyde
PL	Propranolol Hydrochloride
PVA	Polyvinyl alcohol
PVP	Polyvinylpyrrolidone
RBM	Ring Breathing Mode
SEM	Scanning Electron Microscope
SSD	Sum of Square Deviation
TEER	Transepithelial electrical resistance
TGA	Thermogravimetric Analysis
TNB	2-nitro-5-thiobenzoate
TNBS	Trinitrobenzene sulfonic acid
UTM	Universal Testing Machine
XPS	X-ray Photon Spectroscopy
XRD	X-ray Diffraction

NOTATIONS

ωA	Specific thermodynamic work of adhesion
γb	Surface tension of bioadhesive polymer
γt	Surface tension of the substrate
γbt	Interfacial tension
σ	Fracture strength
E	Youngs modulus
L	Critical crack length
ε	Fracture energy
D	Bulk density
d	Apparent density
R^2	Correlation coefficient
R_t	Resistance at time t
R_0	Initial resistance
R_b	Resistance of trans well insert in the absence of cell monolayer
P_{app}	Permeation coefficient
M_v	Viscosity average molecular weight
n	Nonbonding molecular orbital
π^*	Anti-bonding π molecular orbital

SYNOPSIS

The phenomenon of adhesion of a material onto the surface of mucosal tissue is termed as mucoadhesion. Mucoadhesion happens in two stages – first, the material comes in contact with the mucosal surface and secondly it establishes contact via spreading over the mucosal surface. The first stage is called contact stage and the second stage is called consolidation stage. The polymers exhibiting mucoadhesive properties attributing to their charge, hydrophilicity and ability to establish non-covalent interactions have already been broadly investigated. Recently extensive research has been carried out to study the mucoadhesive properties of functionalised polymers. Functionalised polymers have been investigated in the perspective of causing enhanced and targeted adhesion onto the mucosal surface through covalent and electrostatic attractions. Thiol fucntionalisation, cationic functionalisation, acrylate functionalisation, boronic acid functionalisation, catechol functionalisation, maleimide functionalisation are some of the examples.

The application of the concept of mucoadhesion to the field of drug delivery was initiated during 1980s. Conventional drug delivery systems follow the oral administration of drugs to the patients. The poor oral bioavailability of drugs due to hepatic first-pass metabolism is the main concern of conventional drug delivery. In that scenario, alternative methods of drug delivery have been proposed. Mucoadhesive drug delivery is a non-conventional method of drug delivery where drug molecules are facilitated to permeate through the epithelial surface of different mucosal tissues and get absorbed into the systemic circulation. Poor absorption, low bioavailability and interaction of drug with the acidic gastric environment can be overcome in the mucosal delivery system. In mucosal drug delivery, the drug directly gets absorbed into the

systemic circulation and the hepatic first-pass metabolism is bypassed. Mucoadhesive drug delivery is a boon to geriatric and paediatric patients and patients suffering from swallowing difficulty due to dysphagia conditions.

Mucoadhesive polymers loaded with drug molecules of interest have been processed in the form of electrospun membranes in the present work. Electrospun membranes enable good drug entrapment due to the high surface-to-volume ratio and porosity. The porous architecture of electrospun membranes can be tuned to obtain desired rates of drug release.

Zein is a natural protein and is electrospinnable. Zein can be electrospun in various solvent systems like aqueous ethanol, aqueous propanol, acetic acid etc. The major limitation associated with electrospun zein is its brittleness and poor mechanical properties. A gentle soft touch could cause damage to the electrospun membrane of zein alone. Therefore, the purpose of this research work is to overcome the mechanical limitations of the electrospun zein membrane and to develop a better mucoadhesive drug delivery formulation out of it.

Based on the above-mentioned knowledge available, the hypothesis formulated for this research is,

'Would electrospun zein matrix be suitable as a biocompatible, and non-cytotoxic mucoadhesive system'

The main objectives of this study include,

1. To develop zein electrospun matrix strengthened by crosslinking and blending.

2. To study various drugs used for the treatment of cardiac-neuro diseases and select those which are having low bioavailability. And load the selected drug into the electrospun polymer matrix.
3. To study the drug release kinetics.
4. To study the mucoadhesive capacity of the polymer matrix.
5. To study the physico-chemical characteristics of the polymer matrix.
6. To study the cell- material interactions of the polymer matrix.

The design of the study has been done in such a way that two categories of blend systems of zein have been prepared. The first category is Zein/Polyethylene oxide (PEO) blend and the second is Zein/Polyvinyl pyrrolidone (PVP) blend. Different crosslinking mechanisms and functionalisation have been tried in both systems.

Zein/PEO blend category includes UV crosslinked Zein/PEO and Thiol modified Zein/PEO electrospun membrane systems. Zein/PVP blend system includes Thermally crosslinked Zein/PVP, Mucin crosslinked Zein/PVP and Zein/APBA (3-aminophenyl boronic acid) conjugated PVP electrospun membrane systems. The physico-chemical characterisations of all these membranes have been done in this piece of research. In all the above five systems, propranolol hydrochloride (PL) was incorporated as the drug of interest. Propranolol hydrochloride has been chosen because of its low oral bioavailability of around 15-23 %. The cytotoxicity evaluation, *in-vitro* drug permeation study and evaluation of epithelial cell transport have been carried out in RPMI 2650 cells, which are nasal epithelial cells. *Ex-vivo* drug permeation studies of PL have been done through porcine buccal mucosal tissue.

The entire study is presented in five chapters. Chapter 1 elaborately discusses the background and introduction of the work. It explains in detail the structure and function of mucosa and mucin, theories of mucoadhesion, mucoadhesive polymers and functionalised polymers called second-generation polymers, advantages of mucoadhesive drug delivery devices and its global importance, a brief discussion about the electrospun zein and its limitations and the current strategies adopted in this work for the fabrication of mucoadhesive electrospun drug delivery systems.

Chapter 2 of the thesis is an exhaustive literature review which includes the various research outputs in the field of mucoadhesive drug delivery in general. The chapter includes a detailed review of the structure and properties of mucosa and mucin, mucoadhesion and its theories, transepithelial transport mechanisms, a comparative analysis of mucoadhesive drug delivery and conventional drug delivery, literature references for different mucoadhesive drug delivery systems, first and second generation mucoadhesive polymers, fabrication techniques for mucoadhesive drug formulations, advantages of electrospun polymers for buccal and nasal adhesive drug delivery, electrospun zein and its various available crosslinking methods, Polyethylene oxide , Polyvinyl pyrrolidone and Propranolol hydrochloride.

In Chapter 3, experimental methods for the analysis of materials are elaborated. It also discusses the grade and specifications of materials used in this research. Experimental methods have been categorised into six. Section 2.2.1 discusses the synthesis of modified zein polymers which comprises thiol modification and mucin crosslinking of zein. Section 2.2.2 discusses the preparation of polymer solutions for all five systems in different solvent mixtures. Section 2.2.3 deals with the drug-loading mechanism in the polymer solutions. Section 2.2.4 tabulates the electrospinning parameters for all five electrospun membrane systems. Section 2.2.5 is about the various post-

electrospinning crosslinking techniques employed in the research which include, UV crosslinking and thermal crosslinking. Section 2.2.6 includes the physico-chemical characterisations, drug release studies and biological characterisations. Physico-chemical characterisation techniques include Scanning Electron Microscopy (SEM) for the surface morphological analysis, Fourier Transform InfraRed (FTIR), UV-Visible and Raman spectroscopy for the functional group analysis, Circular Dichroism (CD) spectroscopy for conformational analysis of protein, Density method of porosity analysis, Water contact angle analysis for wettability studies, Ellman's assay for thiol group estimation, TNBS assay for amino group estimation, Thermogravimetric (TGA) and Differential Scanning Calorimetric (DSC) analysis for thermal characterisations, X-ray Diffraction (XRD) analysis for the evaluation of crystallinity, X-ray Photon Spectroscopy (XPS) for elemental composition analysis, Universal Testing Machine (UTM) analysis for static mechanical property evaluation, Dynamic Mechanical Analysis (DMA) for dynamic mechanical property analysis, and Texture analysis for mucoadhesion studies. The calculation of drug entrapment percentage, drug loading percentage and the percentage cumulative release in PBS are included under drug release studies. Drug release studies also contain finding the best fitting mathematical model for the cumulative drug release profile. Biological characterisations include direct contact assay, MTT assay, Live/dead assay, F-actin staining, Immunostaining of beta-catenin proteins, Transepithelial Electrical Resistance (TEER) evaluation, *in-vitro* drug permeation studies and *ex-vivo* drug permeation studies.

In Chapter 4, the results of experiments and their elaborate discussions are included. Zein/PEO and Zein/PVP polymer blend electrospun membranes were fabricated after various crosslinking and functionalisation. UV crosslinked Zein/PEO membrane showed improved mechanical properties after crosslinking due to the conformational

changes of zein from alpha-helix to beta-sheet. UV crosslinking has also resulted in the breakage of disulfide bonds in the terminals of zein to free thiol groups which enhanced the mucoadhesion. Thiol modified Zein/PEO membranes also showed enhanced mucoadhesion due to the presence of increased thiol groups. Among different formulations of thiol modified Zein/PEO, the 30 % modified sample showed maximum force of adhesion. Evaluations of thermally crosslinked Zein/PVP showed radical-mediated crosslinking of PVP under high temperatures. High temperature treatment also resulted in the conformational change of zein from alpha-helix to beta-sheet. These changes contributed to the improved mechanical and mucoadhesive properties. Further, high temperature treatment caused breakage of disulfide bonds in the structure of zein which contributed towards enhanced mucoadhesion. Mucin crosslinked Zein/PVP was tested for amino group concentration using TNBS assay and found to have 38 % of crosslinking. The cohesive interpenetration of mucin in the polymer system and mucin in mucosa contributed towards the highest value of mucoadhesion. APBA conjugated PVP/Zein has resulted in about 97 % of conjugation as per UV spectroscopy quantification. Evaluation of drug entrapment had shown poor PL entrapment in Mucin crosslinked Zein/PVP due to compatibility issues of PL and mucin in the solvent system. Boronate ester-mediated adhesion to the cis-diol groups of oligosaccharide side chains in mucin resulted in an increased value of mucoadhesion. Unlike all the other systems, APBA conjugated PVP/Zein electrospun membrane was hydrophobic. All the systems were non-cytotoxic to RPMI 2650 cells. The treatment of materials hasn’t caused any disturbances to the epithelial cell junctions, which was confirmed by F-actin staining, immunostaining and TEER value evaluation. *In-vitro* drug permeation studies and *ex-vivo* drug permeation studies

confirmed the transcellular mechanism of transport of PL from all the five materials under study.

The results obtained from this study have been summarised in Chapter 5. Electrospun zein-based polymer blends with PEO and PVP were suitable materials for mucoadhesive drug delivery. A comparative analysis of physically crosslinked simple blends and functionally modified polymer blends was done. Functionally modified polymer blend systems were found to be performing well in terms of tensile strength, mucoadhesion, drug release in buffer (PBS) conditions, drug permeation *in-vitro* and drug permeation *ex-vivo*. Thiol modified Zein/PEO electrospun membrane can be described as the best system under Zein/PEO category. Mucin crosslinked Zein/PVP electrospun membranes were concluded as the best mucoadhesive system. APBA conjugated PVP/Zein electrospun membrane was also concluded as a good material for drug delivery applications.

The extended future work plan of the study is proposed. Citations are listed in the bibliographic section.

1 INTRODUCTION

The phenomenon of adhesion of material onto the surface of mucosal tissue is termed mucoadhesion. In general, the mucosa is composed of an epithelium and a basement membrane. The areolar connective tissue region found beneath the basement membrane is called lamina propria. Lamina propria is composed of blood vessels, nerves, glands etc (Groeger and Meyle, 2019). Different types of mucosal tissues are seen in the human body at various locations and those differ in their fine structure. Oral mucosa is composed of stratified squamous epithelium whereas ocular mucosa in the eye is composed of columnar epithelial cells in the basal layer with flattened polygonal cells in the outer layer. Epithelial cells in nasal mucosa are again columnar epithelial cells but it additionally contains cilia on their surface. Vaginal and rectal mucosa are composed of stratified squamous and cylindrical epithelial cells respectively.

Mucin is a glycoprotein and is a critical element of mucosal tissue. It is a large, and heavily glycosylated protein. The central protein core of mucin is composed of large tandem repeats of amino acids like serine, threonine and proline. The hydroxyl functionalities in these amino acids bind with oligosaccharide units via O-glycosylation. At the same time, the terminal regions of mucin are the least glycosylated (Bansil et al., 1995) and those areas are known as ‘naked protein regions’ (Yu et al., 2014). Certain portions of naked protein regions contain cysteine amino acids in higher concentration and those areas are termed cysteine-rich domains (Hanisch and Müller, 2000).

The mechanism of adhesion of materials on the surface of the mucosa can be explained in terms of different theories in different perspectives – wetting theory, adsorption theory, diffusion theory, electrostatic theory and fracture theory. In wetting theory, the extent of mucoadhesion increases with an increase in the wettability of materials (Peppas and

Bur2i, 1985; Shaikh, Raj Singh, Garland, A David Woolfson, et al., 2011). In adsorption theory, mucoadhesion is the result of secondary bonding interactions like van der Waals interactions, hydrogen bonding etc. with the mucosal surface (Mathiowitz et al., 1999). Diffusion theory explains mucoadhesion as the result of interpenetration of mucin chains of mucosa and polymer chains in the material of interest (Carvalho et al., 2010; Mathiowitz et al., 1999). Mucoadhesion has been explained by electrostatic theory in terms of electrostatic interaction between positively charged polymer material and negatively charged mucin (Mathiowitz et al., 1999). Fracture theory interprets mucoadhesion as the force required to separate material from the surface of the mucosa.

Recently, widespread research has been happening to explore the possibility of augmenting the mucoadhesive properties of polymers by polymer chain functionalisation. Mucoadhesive polymers like polyvinyl pyrrolidone (Vecchi et al., 2021), carboxymethyl cellulose, hydroxypropyl methylcellulose (Mortazavi and Moghimi, 2010), polyethylene glycol, chitosan (Khutoryanskiy, 2011), and polyacrylic acid (Lam et al., 2021). have been well studied (Mortazavi and Moghimi, 2010; Woodley, 2001). These polymers cause mucoadhesion due to physical interactions with the mucosal surface. Chemical interactions are the key feature of second-generation mucoadhesive polymers which are also known as functionalised polymers. Different functional groups can be conjugated on the polymer chain to establish chemical bond-mediated mucoadhesion. Thiol functionalisation (Puri et al., 2020; Zaman, Saeed, et al., 2021), boronic acid functionalisation (S Liu et al., 2015), catechol functionalisation (Waite and Tanzer, 1981), acrylate functionalisation (Eshel-Green and Bianco-Peled, 2016). and maleimide functionalisation (Matsumoto et al., 2016). are some of the methods which have been widely investigated. Functionalised polymers could adhere to the surface of mucosa for a much long time due to chemical interactions (Surendranath, R, et al., 2022).

Mucoadhesive polymers have been widely studied for drug delivery applications (Carvalho et al., 2010). Mucoadhesive drug delivery has been proposed as an alternative to conventional drug delivery. Conventional drug delivery reduces the oral bioavailability of drugs due to hepatic first-pass metabolism in the liver (Pamlényi et al., 2021). In that scenario, even though a high drug dosage is administered, only low concentration reaches the systemic circulation. Mucoadhesive drug delivery facilitates the direct absorption of the drug through mucosal epithelial cells to systemic circulation. Mucoadhesive drug delivery causes rapid absorption of the drug and protects the drug from harsh acidic gastric environments as well. Mucoadhesive drug delivery can be considered an advantageous method to deliver the drug in patients suffering from hard-to-swallow drugs such as those in the coma stage or suffering from dysphagia condition of Parkinson's disease.

Electrospinning is a versatile technique used for fabricating fibroporous membranes from polymer solutions. The miscible blending of drug and polymer in the suitable solvent or solvent mixture will lead to the formation of drug-incorporated nanofibres (Sun et al., 2019). The release of drugs from the nanosized fibres of electrospun membranes can either follow a diffusion or degradation-controlled mechanism. The versatility of electrospinning has further expanded to co-axial electrospinning, tri-axial electrospinning and multi-fluid electrospinning where complex architecture of fibrous membranes can be generated for controlled drug delivery applications (Ji et al., 2022).

Propranolol hydrochloride (PL) is a well-known synthetic beta-adrenergic receptor blocker drug given to patients suffering from cardiovascular irregularities. PL is advisable for hypertensive patients, or those suffering from angina pectoris (Patel et al., 2007). Though PL is commonly prescribed to give through an oral delivery route, it has a low oral bioavailability of 15-23 %. PL is highly susceptible to hepatic first-pass

metabolism. That being the case, PL is a good candidate to deliver through the mucosal route so that the bioavailability of the drug can be improved as the drug directly reaches systemic circulation. And also, only a low dosage of the drug is required to administer which could efficiently cause the required pharmacological action and frequent administration of the drug could be avoided.

Zein has been chosen as the basic polymer of interest in this study (Yao et al., 2007). Zein is a natural protein extracted from corn. It possesses disulfide linkages and due to which zein is capable of establishing mucoadhesion. The feasibility of electrospinning of zein is much higher using different solvent systems like aqueous alcohol, acetic acid, DMF (Dimethyl formamide) etc. But the main limitation associated with electrospun zein is its brittleness. Blending with synthetic polymers like polyethylene oxide (Surendranath, Rajalekshmi, et al., 2022) and polyvinyl pyrrolidone (Surendranath, Ramesan, et al., 2023) has been carried out to overcome the mechanical limitations of electrospun zein. Simply blending alone will not solve all the issues of poor mechanical character of electrospun zein. In that case, physical crosslinking methods like UV crosslinking and thermal crosslinking have been employed in this work. These crosslinking strategies would impart enhanced mechanical strength to the electrospun membrane of zein blends. Further ahead to crosslinking modification of polymer blends, polymer functionalisation has also been tried in this research. Thiol functionalisation using cysteine amino acid and boronate functionalisation using 3-aminophenyl boronic acid (APBA) have been also evaluated for the polymer blends of electrospun zein. As a novel approach of a mucoadhesive polymer system, a mucin-crosslinked zein electrospun membrane has also been developed. It’s a new approach proposal for cohesive interaction between mucin in the polymer system with mucin in the mucosal tissue.

Zein contains disulfide linkages and cysteine residues in its structure and is already known for its mucoadhesive properties. Crosslinking and functionalisation strategies improve the mucoadhesive properties along with mechanical properties. Physical crosslinking mechanisms like UV crosslinking and thermal crosslinking result in disulfide bond breakage in the zein structure. And also, these crosslinking techniques cause conformational changes in zein from alpha-helix to beta-sheet. The impact of these changes on the improvement in mechanical and mucoadhesive properties has been studied. Thermal crosslinking has been employed not only to crosslink zein chains but also to crosslink PVP chains. A radical-mediated mechanism of PVP crosslinking has already been reported in the literature during high temperature treatment. Thiol functionalisation has been done on the polymer chain of zein where a peptide bond-mediated conjugation happens in the presence of EDC crosslinker. Thiol functionalisation increases the presence of more free thiol groups on the polymer chain. Thiol groups establish mucoadhesion by forming disulfide bonds with the cysteine moieties of mucin glycoprotein. Boronate functionalisation has been done between the keto group of the pyrrolidone ring structure of PVP and the amino group of APBA through a Schiff base formation. Boronate functionalisation causes mucoadhesion by chemical interaction with the cis-diol groups of oligosaccharide side chains of mucin. The interaction results in the formation of a five-membered boronate ester complex formation. Mucin crosslinking to the zein polymer chain was done in the presence of an EDC crosslinker. The presence of mucin in the polymer system is an exciting shift in the role of mucin from facilitating mucoadhesion to a component in the drug delivery system.

The thesis evaluates five systems in detail- UV crosslinked Zein/PEO, Thiol-modified Zein/PEO, Thermally crosslinked Zein/PVP, Mucin crosslinked Zein/PVP and Zein/APBA conjugated PVP electrospun systems. The material synthesis,

electrospinning, crosslinking techniques and physico-chemical characterizations have been discussed in detail. The physico-chemical characterization includes Scanning Electron Microscopy (SEM), Fourier Transform Infrared (FTIR) Spectroscopy, UV-Visible Spectroscopy, Raman Spectroscopy, Circular Dichroism (CD) Spectroscopy, Density method of porosity calculation, Water contact angle analysis, Ellman's assay, TNBS assay, Thermogravimetric Analysis (TGA), Differential Scanning Calorimetry (DSC) Analysis, X-ray Diffraction (XRD) analysis, X-ray Photon Spectroscopy (XPS), Universal Testing Machine (UTM) analysis, Dynamic Mechanical Analysis (DMA) and Texture analysis. The PL-loaded electrospun membranes of all systems have been evaluated for drug entrapment and loading capacity efficiency. Drug release studies were conducted in Phosphate Buffered Saline (PBS). The cytocompatibility evaluation of the materials was done in nasal epithelial RPMI 2650 cells. Direct contact assay, MTT assay, and Live/dead assay were done for cytotoxicity analysis. F-actin staining and beta-catenin immunostaining were done to qualitatively evaluate the junctional integrity of epithelial cells after material treatment. The same has been confirmed quantitatively by TEER value evaluation. *In-vitro* drug permeation through epithelial cells has also been conducted. The drug permeation under *ex-vivo* conditions was also evaluated in the porcine buccal mucosa.

2 REVIEW OF LITERATURE

2.1 MUCOSA AND MUCIN – STRUCTURE AND PROPERTIES

The mucosal membrane is the inner layer of various body cavities and the outer covering of certain internal organs. It is composed of one or more layers of stratified squamous epithelial cells with connective tissues beneath (Groeger and Meyle, 2019). It is the layer of epithelial cells that face the inner cavity. The upper epithelial layer of the mucosa is semipermeable and avascular. The epithelium is composed of four layers- stratum basale, stratum spinosum, stratum granulosum and stratum corneum. The replenishment of

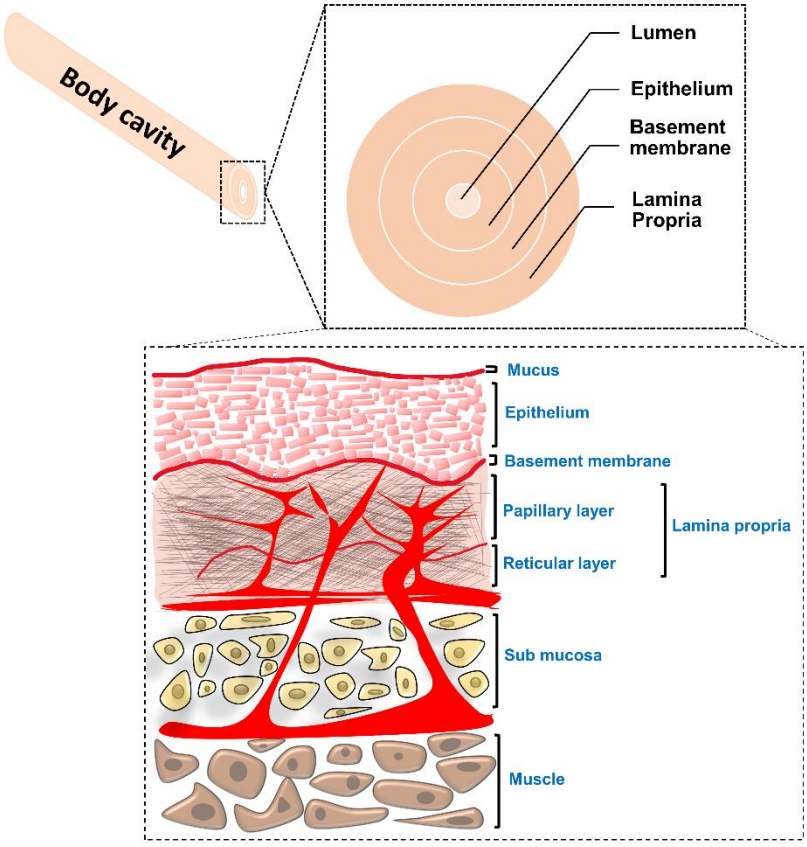

Figure 1 Structure of mucosa

epithelial cells occurs at the stratum corneum every 14 or 21 days (Kydd and Daly, 1982). The degree of keratinization of the epithelial layer varies according to the function of

mucosal tissue. Soft mucosal inner regions like the soft palate, alveoli, vestibular fornix, mouth floor, cheeks and lips are not keratinized, whereas gingival regions and hard palate inside the mouth are keratinized. The fibrous connective tissue beneath the epithelial layer is lamina propria which is mainly composed of fibroblast cells. There is a non-cellular basement membrane in between the epithelial layer and lamina propria which strongly connects both (Brizuela and Winters, 2022). The primary function of lamina propria is to provide mechanical support to the overlying epithelium. There are numerous blood capillaries found in lamina propria along with lymphatics and neural elements. Lamina propria is connected with the underneath submucosa which is associated with muscles, fat and salivary glands (Winning and Townsend, 2000). Figure 1 is a representation of the structure of mucosa.

The mucosal tissue is covered by mucus secreted by goblet cells. Mucus plays a critical role in facilitating protection, lubrication and adhesion. Mucus consists of water, mucin glycoprotein, electrolytes, fatty acids, phospholipids, cholesterol and proteins (Yu et al., 2014). Mucin is a macro-sized glycoprotein with molecular weight in the range of 0.5 to 20 MDa. It has a central protein backbone composed of a large number of tandem repeats of serine, proline and threonine. The hydroxyl groups of serine and threonine are linked to large carbohydrate groups via O-glycosidic covalent linkage. The carbohydrate side chains of mucin are composed of N-acetylgalactosamine, N-acetylglucosamine, fucose, galactose, sialic acid etc (Bansil and Turner, 2006). The central protein backbone has greater than 10 % cysteine domains also (Bell et al., 2003: 2). The terminal regions of mucin are not linked to carbohydrates and are hence termed as “naked protein regions”. The presence of negatively charged sialic acid and sulphate groups contributes to the negative charge of mucin at physiological pH. Due to the negative charge of mucin, it could easily attach to the surface of the mucosal epithelium. Mucin undergoes gelation

in aqueous media owing to electrostatic interactions, inter and intramolecular hydrogen bonding and disulphide bond formation. The viscoelastic property of mucin is controlled by the proportion of disulphide interaction present in the mucin (Hanisch and Müller, 2000).

2.2 MUCOADHESION

According to Leung and Robinson, mucoadhesion is the interaction of mucin with a polymer substrate (Sau-Hung Spence Leung and Robinson, 1987). Mucoadhesion would take place through three stages- adhering stage, the swelling and expanding stage and the interaction stage. The mucoadhesive material will come and contact with the mucosal surface in the first stage followed by swelling and expansion by absorbing moisture from the mucosa and finally, the material establishes certain chemical interactions with the surface to cause interpenetration of polymer chains with the chains of mucin glycoprotein (Mythri et al., 2011). The chains of mucoadhesive material diffuse within the chains of mucin by spreading over the surface of mucosa to initiate close surface contact. Both attraction and repulsion are possible between the material and mucosa but for a successful adhesion, the attraction forces must dominate (Carvalho et al., 2010). The kind of interaction taking place between the material and mucosa is highly dependent on the nature of drug formulation. So, the extent of interaction of drug loaded material and mucus is highly varying.

Two steps involved in the mechanism of mucoadhesion are the contact stage and the consolidation stage. The mucoadhesive material comes in contact with the mucous membrane during the contact stage. During the consolidation stage, material spreads over the mucous membrane and establishes contact with the mucosa after swelling (Hägerström, 2003).

In ocular formulations or vaginal formulations, the mucoadhesive system is attached mechanically over the mucosal surface. The aerodynamics of the organ plays a major role in the promotion of deposition, especially in the case of nasal route administration. Therefore, it is difficult to attach adhesive formulations directly over the mucous membrane in the gastrointestinal tract. Peristaltic motions may interfere with the contact of formulation to the gastro intestinal tract mucosal lining. Additionally, an undesirable adhesion in the oesophagus is also possible. Therefore, peristalsis and movement of organic fluids in the internal cavity are the controlling factors in mucoadhesion. When a material approaches the mucosal surface, it can either come in contact with repulsive forces like osmotic pressure, electrostatic repulsion, etc. or with attractive forces like van der Waals forces and electrostatic attraction. Therefore, to get attached to the mucosal lining, the particle must overcome this repulsive barrier (Carvalho et al., 2010; Mathiowitz et al., 1999).

Activation of mucoadhesive material in the consolidation stage is done by moisture. The moisture acts as a plasticizer in the system. Theories used to explain consolidated mucoadhesion are diffusion theory and dehydration theory. According to diffusion theory, mutual interpenetration of chains, supramolecular interactions and chemical interactions of mucoadhesive material and glycoproteins of the mucus are responsible for the mucoadhesion during the mutual interaction of both (Smart, 2005). Molecules possessing hydrogen bond-building functional groups- OH, -COOH, anionic surface charge; or flexible chains of polymers can interact and interpenetrate the mucus layer (Carvalho et al., 2010; Mathiowitz et al., 1999).

According to dehydration theory, unlike the interpenetration of the macromolecular polymer chains, the movement of water cause adhesion. Due to the difference in osmotic pressure, water enters the formulation until reaching the osmotic balance and the material

gelifies readily. So, there can be an increased time of contact between the formulation and mucus.

The mechanism of mucoadhesion is explained in terms of various theories- Wetting theory, Electrostatic theory, Diffusion theory, Adsorption theory and Fracture theory. No single theory could comprehensively explain mucoadhesion rather a combination of two or more can be relied upon (Kulkarni et al., 2023a).

2.2.1 Diffusion Theory

Diffusion theory can explain mucoadhesion in terms of the sufficient interpenetration of polymer chains and mucin chains that allow the formation of a semi-permanent bond (Jiménez-castellanos et al., 1993). Figure 2A is a schematic representation of the mechanism of adhesion according to diffusion theory. As the extent of interpenetration of polymer chains with mucin increases, the force of adhesion increases (Mathiowitz et al., 1999). The diffusion coefficient, flexibility and mobility of the mucoadhesive chains, and contact time increase the rate of interpenetration (Hägerström, 2003; Smart, 2005). Mutual solubility of the materials involved in adhesion is a pertinent factor in diffusion. For that, the materials should be similar in their chemical structure (Mathiowitz et al., 1999).

2.2.2 Adsorption Theory

There is a possibility for the formation of primary and secondary bonding between the adhesive surface and the mucosa. But primary bonding interactions like covalent bonding, ionic bonding etc. have an issue with it because they may result in permanent interactions with the mucosal tissue. Therefore, the most desirable is secondary interactions like van der Waals forces, hydrogen bonding, electrostatic interactions,

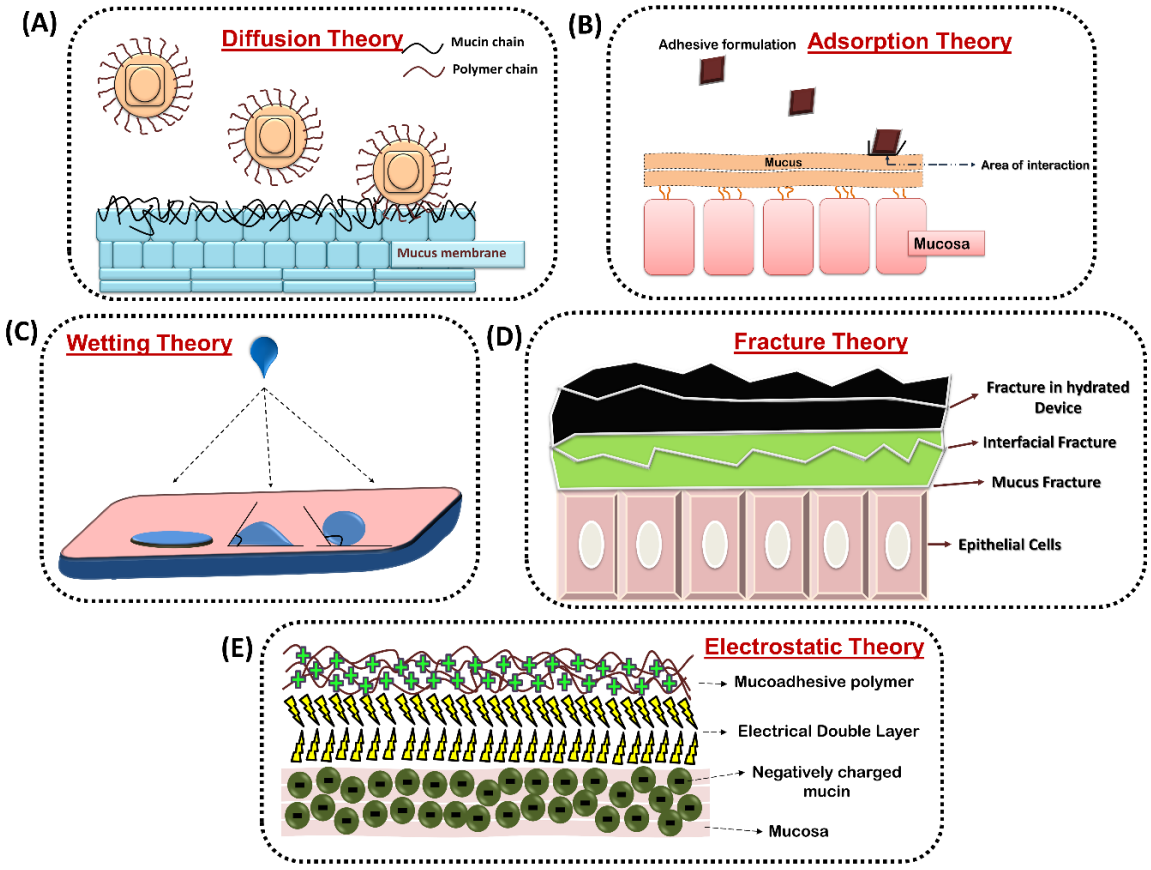

Figure 2 Schematic representations of theories of mucoadhesion – A) Diffusion theory, B) Adsorption theory, C) Wetting theory, D) Fracture theory and E) Electrostatic theory

hydrophobic interactions etc through the interaction area of mucus with material. This theory explains the mechanism of mucoadhesion in terms of secondary chemical interactions (figure 2B). Though these forces are individually weak, they are considered important because, a large number of interactions are possible in an intense adhesion (Mathiowitz et al., 1999).

2.2.3 Wetting Theory

This theory is applied to explain the mucoadhesion of liquid or low-viscosity bioadhesives (Peppas and Buri, 1985; Shaikh, Raj Singh, Garland, A David Woolfson, et al., 2011). According to wetting theory, adhesion is a piercing process. There occurs penetration of surface irregularities of mucosal membrane and chains of adhesive agents.

This kind of interpenetration produces anchors for adhesion (McBain and Hopkins, 1925). The wetting theory considers contact angle and work of adhesion into account. Generally, the lower the contact angle, the higher the affinity of the material towards the mucosal surface (figure 2C).

Dupre's equation shown as equation 1 explains the thermodynamic work done based on the surface tension of materials involved in adhesion:

$$\boldsymbol{\omega A = \gamma b + \gamma t - \gamma bt} \qquad \textbf{(1)}$$

where ωA is the specific thermodynamic work of adhesion and γb, γt, and γbt represent, the surface tensions of the bioadhesive polymer, the substrate, and the interfacial tension respectively.

2.2.4 Fracture Theory

Fracture theory is the most widely used theory to explain mucoadhesion. This theory describes mucoadhesion as the force required for separating two surfaces which were already adhered to. This theory studies bio adhesion by tensile apparatus by equation 2

$$\boldsymbol{\sigma = \frac{(E \times \in / L)}{2}} \qquad \textbf{(2)}$$

where σ is the fracture strength, ε fracture energy, E Youngs modulus of elasticity, and L is the critical crack length (Gu et al., 1988).

Fracture theory explains mucoadhesion through the force of separation of adhesive formulation and mucus membrane, unlike diffusion theory. Therefore, it can be used in calculating the force of adhesion of rigid or semi-rigid bioadhesive materials, because in such cases, there is no chance for the penetration of polymer chains into the mucus layer (Mathiowitz et al., 1999). Figure 2D is a schematic diagram explaining the fracture theory of mucoadhesion.

2.2.5 Electrostatic Theory

The electrostatic theory of adhesion is based on the assumption that the adhesive material and the mucosal membrane have opposite surface charges. When the formulation having a positive charge and negatively charged mucosal membrane comes in contact with each other, an electronic double layer will be formed in the interface due to the transfer of electrons between the two (figure 2E). The attractive forces within the electronic double layer will determine the mucoadhesion (Mathiowitz et al., 1999; Yu et al., 2014).

2.3 TRANSEPITHELIAL DRUG TRANSPORT MECHANISMS

Transepithelial drug transport happens through three pathways. Transport of drug molecules from the apical side to the basolateral side can happen through the transcellular pathway, paracellular transport or vesicular mechanism of transport (figure 3).

2.3.1 Transcellular transport

In the transcellular transport mechanism, molecules get transported across epithelial cells through the cell membrane. It is also known as intracellular transport. Transcellular transport of small nonpolar molecules happens according to the concentration gradient across the epithelia. They undergo transcellular diffusion from a lower concentration gradient to a higher concentration gradient (Yang and Hinner, 2015). Transcellular transport is not favourable for highly polar molecules and charged molecules. Nevertheless, highly polar water molecules pass across the cell membrane through water-transporting molecules known as aquaporins (Reuss, 2012). It is possible to have energy-utilised transport for moderately polar large-sized molecules across epithelial cells. Molecules such as sugars, peptides and amino acids make use of energy to get across the epithelial cell layer. Lipophilic prodrugs have been designed to cross the epithelial barrier via a transcellular pathway (Laksitorini et al., 2014).

2.3.2 Vesicular transport

Receptor-mediated transport across epithelia is also possible where receptors bind with the drug molecules like peptides, proteins, liposomes etc. and carry them across the

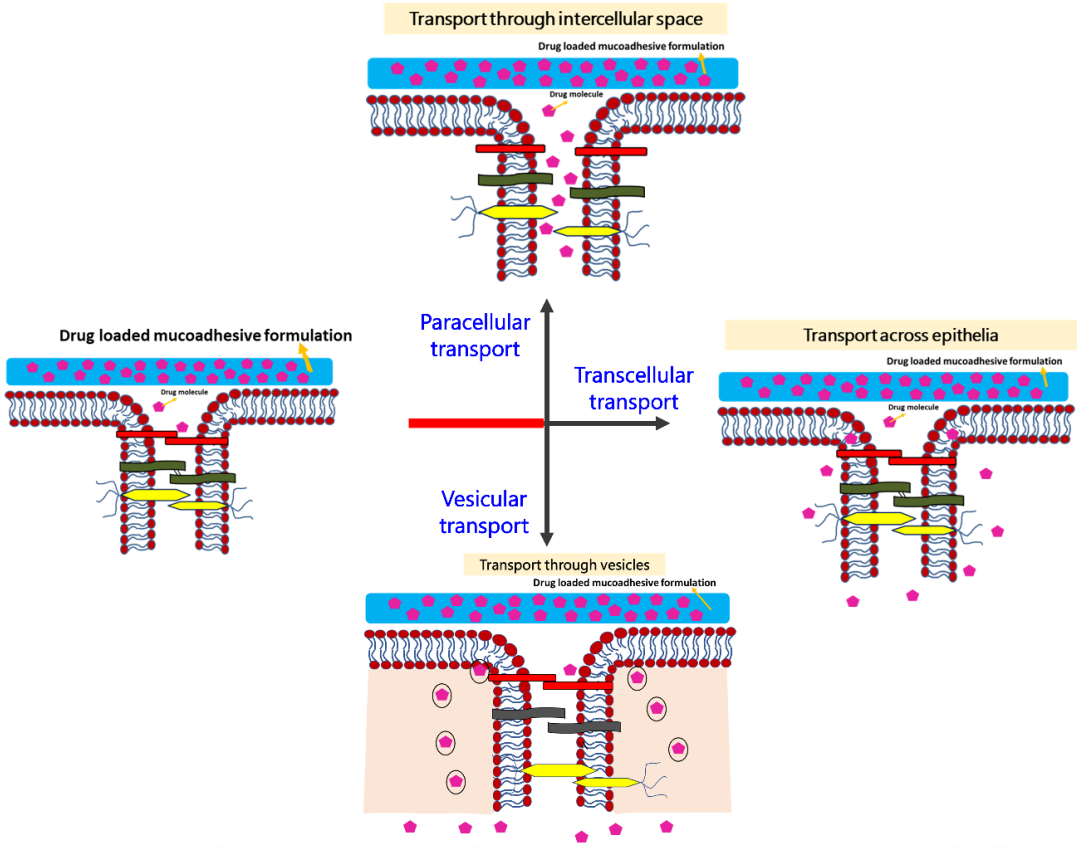

Figure 3: Schematic representation of transepithelial transport mechanisms- Paracellular transport, Transcellular transport and Vesicular transport

membrane (Liu et al., 2009). This mode of transport can happen either by making use of energy or without utilising energy (Yang and Hinner, 2015). In response to the changes in transmembrane potential, stress or light (Jin et al., 2020) ion channels like valinomycin, gramicidin A etc. facilitate ion transport across cell membranes (Becucci et al., 2008). These ion channels which are capable of complexing with charged ions are known as ionophores (Novilla, 2018).

2.3.3 Paracellular transport

In the paracellular transport mechanism, molecules get transported across cells via intercellular junctions. Epithelial cells are sealed among themselves employing cell adhesion molecules. The apical surface of the cell is sealed with tight junction. A tight junction is composed of proteins like claudin, occludin and junction adhesion molecules. Transport through tight junction can either follow pore pathway or leak pathway. Claudin-2 protein regulates the pore pathway and it has a molecular size cut off 3.5 A°. The leak pathway is regulated by the occludin protein of tight junction and it is a low-capacity pathway having a molecular size cut restriction of 7.5 A° (Weber, 2012). Dephosphorylation of occludin protein cause loss of tight junction integrity and increase molecule permeability. Adherens junction is seen to the basolateral side of the tight junction. It is composed of cadherin proteins which are calcium-dependent in action. Desmosomes seen below to adherens junction are composed of desmocollin and desmogelin proteins and facilitate cell-cell adhesion (Laksitorini et al., 2014).

Permeation enhancers are the specific molecules which facilitate the easy permeation of particles through cell junctions. Some examples of permeation enhancers are EDTA, surfactants, zona occludens toxins and fatty acids (Maher et al., 2019). They are capable of displacing zona occludens proteins in the epithelial cell junctions. Loss of junctional integrity can be quantitatively measured using TEER evaluation. Cationic polymers and thiolated polymers are also been explored for causing tight junction openings (Chen et al., 2018; Han et al., 2019; Yeh et al., 2011).

2.4 MUCOADHESIVE DRUG DELIVERY VS CONVENTIONAL DRUG DELIVERY

Mucoadhesive drug delivery is now being extensively studied to overcome the limitations of conventional oral delivery of pharmaceuticals. The conventional drug delivery technique is oral administration. Though oral administration of drug is commonly used, the bioavailability of the drug would be reduced depending on the extent of absorption of the drug across intestinal epithelium as well as first-pass metabolism. After intestinal absorption, the absorbed active drug would be entering the hepatic portal system and the portal vein would carry the same to the liver. First-pass metabolism occurs in the liver where the absorbed drug undergoes metabolism. The drug enters systemic circulation after first-pass metabolism and the bioavailability of active pharmaceutical would be greatly reduced (Kim and De Jesus, 2022). The drastic loss of drug concentration after first pass metabolism will cause dismal performance as well as administration of higher dosage formulations in the patient (Milligan and Saha, 2022).

Mucosal administration of the drug is highly preferred because of bypassing of first-pass metabolism. Mucosal administration of the drug facilitates direct absorption of the drug into the systemic circulation and thus enhances bioavailability (Kulkarni et al., 2023b). The preferred additional benefits of mucosal drug delivery are increased patient compliance, excellent accessibility and improved barrier permeability compared to transdermal drug delivery (Shaikh, Raj Singh, Garland, A David Woolfson, et al., 2011). The extent of keratinisation of the mucosa is not much extensive as skin and thus increases permeability (Hearnden et al., 2012).

The efficiency of mucosal transport of drugs varies according to the anatomy of mucus membranes at various body locations. Thickness, surface area permeability, and structural features of the mucosal membrane vary in different regions of the body and

thus, the method of drug delivery and the type of drug formulation also vary. It is to be noted that all drugs cannot be delivered through all types of mucosa. The selection of drugs for delivery through different mucosa is made by considering the physiological and anatomical features of the mucosal tissue. Similarly, all formulations of a drug cannot be applied to all mucosal surfaces. Selection of drugs is done based on the surface area and the location of the mucosal tissue in our body.

2.4.1 Oral mucosal delivery

Excellent blood supply, rapid repair, better permeability profile, higher surface area for absorption, lack of acidic environment like stomach and lack of enzymatic environment of small intestine makes oral mucosa advisable for local and systemic drug delivery (Hearnden et al., 2012). It was William Murrell who proposed the administration of nitroglycerin drops through oral mucosa to treat angina pectoris and reported that its therapeutic action was so quick compared to ordinary swallowing (Marsh and Marsh, 2000). By now, the list of drugs which are delivered through oral mucosa has been expanded and includes drugs like isosorbide dinitrate, nicotine, asenapine, prochlorperazine, selegiline, zolpidem etc.

2.4.1.1 Buccal adhesive drug delivery

Buccal adhesive drug delivery is the most commonly relied method of drug administration because of its convenience. The buccal mucosa is composed of epithelium, basement membrane, and connective tissues. Among different regions of the oral mucosa, buccal mucosa and sublingual are composed of soft palate nonkeratinized tissue while gingival mucosa is composed of hard palate keratinized tissue. The buccal epithelium has a thickness of approximately 500–800 μm and it is 40–50 cells thick. Turnover time for buccal epithelium is 5–6 days. The mucus secreted by salivary glands forms a thick layer

with 0.1–0.7 mm thickness. Intercellular materials derived from membrane-coating granules cause permeability barrier property to the oral mucosa (Woolfson et al., 1998). The blood flow to this region is approximately 2.4 mL min^{-1} cm^{-2} (Sattar et al., 2014). Local buccal drug therapy is mainly done using a variety of formulations like adhesive gels, tablets, films, ointments, patches and mouthwashes, for the treatment of periodontal disease, gingivitis etc. (Shaikh, Raj Singh, Garland, A David Woolfson, et al., 2011). Within the last five years, a significant number of studies have been reported regarding the development and evaluation of electrospun mucoadhesive drug delivery systems. Colley *et al* have done the pre-clinical evaluation of a mucoadhesive bi-layer patch consisting of PVP, PEO and Eudragit-made adhesive layer containing Clobetasol-17-propionate and PCL-made hydrophobic backing layer. The *in-vivo* studies in minipig models showed drug release at therapeutic doses and demonstrated prolonged adhesion (Colley et al., 2018). Clitherow *et al* have probed into the efficiency of mucoadhesive patches for the delivery of local anaesthetic like lidocaine, instead of injecting. They have demonstrated the development of lidocaine-loaded electrospun membranes and evaluated its release and permeation through the porcine buccal mucosa. Their suggestion was to use the mucoadhesive patch for rapid and sustained delivery of lidocaine (Clitherow et al., 2019). Voronova *et al* have investigated the potential of reduced graphene oxide-modified polyacrylic acid with cyclodextrin incorporated as a crosslinker for the delivery of insulin via buccal mucosa as well as eye cornea. The feasibility of the membrane for photothermal activation caused the release of insulin. The good heating capacity of the patch triggered efficient insulin release (Voronova et al., 2022). Drug loaded mucoadhesive formulations in the form of gels, tablet, films, patches or nanoparticles can be used for the local delivery of cancer drugs at oral cancer sites. This method of drug administration saves patients from the discomforts of surgical interventions and side

effect of radiation treatment (Das et al., 2023).

2.4.1.2 Sublingual drug delivery

The highly permeable area of oral mucosa is sublingual mucosa (Hearnden et al., 2012). The sublingual delivery of drug molecules is considered to be a promising alternative to conventional drug delivery. The thickness of the sublingual region of oral mucosa is about 100-200 μm with a surface area of 26.5 ± 4.2 cm^2 and it is 8-12 cells thick (Czerkinsky and Holmgren, 2012). Similar to buccal mucosa, sublingual mucosa is also non-keratinized. But, unlike buccal mucosa, blood flow to this region is of the order 1.0 mL min^{-1} cm^{-2} (Sattar et al., 2014). The absorption of active pharmaceuticals through sublingual mucosa also happens directly to the systemic circulation and thus bypasses hepatic first-pass metabolism (Hua, 2019). Sublingual delivery of drugs is usually formulated as tablets, wafers, sprays, films etc.

Baltzley *et al* have administrated ketorolac, a medication for migraine via chitosan-based nanoparticle spray. *In-vivo* model studies of the formulation were done in the rabbit model and evaluation of plasma concentration of ketorolac was carried out and compared with intravenous administration of drug. Nanoparticle sublingual spray formulation of ketorolac resulted in increased bioavailability of the drug compared to sublingual solution and intravenous administration (Baltzley et al., 2018). Li *et al* prepared PVP /PEG fast-dissolving electrospun patch for the sublingual delivery of carvedilol (Li et al., 2020). Lately, Paris *et al* have tried to deliver protein drugs through sublingual mucosa. The pH and the presence of gastric enzymes always restricted protein delivery through conventional methods. Since such hurdles could be easily avoided in sublingual delivery, protein administration to the systemic circulation is favoured. They have developed a

mucoadhesive patch of chitosan and hyaluronic acid by layer-by-layer methodology and evaluated protein release (Paris et al., 2021).

2.4.2 Nasal mucosal drug delivery

The normal human nasal mucosa is a highly vascularised network with an area of approximately 150 cm^2 and it is a relatively permeable membrane. The nasal cavity is lined with columnar cells, goblet cells, and basal cell lines. The nasal lining has pseudostratified ciliated columnar epithelium. Cilia help in preventing the entry of foreign particles, dust, microorganisms etc. Cilia are responsible for mucociliary clearance also (Ugwoke et al., 2005). Both keratinized and nonkeratinized epithelial cells are present in the nasal mucosa in various locations inside the cavity (Chaturvedi et al., 2011). Turn-over time for mucus is usually 15-20 min (Anand et al., 2012).

2.4.2.1 Nasal cavity-structure and Anatomy

The nasal cavity consists of a floor, a roof, a medial wall and a lateral wall. Each cavity is classified into three regions- nasal vestibule, respiratory region and olfactory region as shown in Figure 4. The nasal vestibule is the region known as the nostrils. Half of the region of the nasal vestibule is composed of keratinized squamous epithelium with vibrissae. The second half of the vestibule is composed of ciliated pseudostratified columnar epithelium. The main function of the respiratory region is to control humidity, and warmth and to protect the nasal cavity by eliminating debris particles entering (Sobiesk and Munakomi, 2022). The olfactory region of the nasal cavity is responsible for sensing smell. The olfactory receptors found in this region do this function. The olfactory mucosal cells contain bipolar neurons, the axons of which combine to form olfactory nerve or cranial nerve I. The cranial nerve I enters the brain through the cribriform plate.

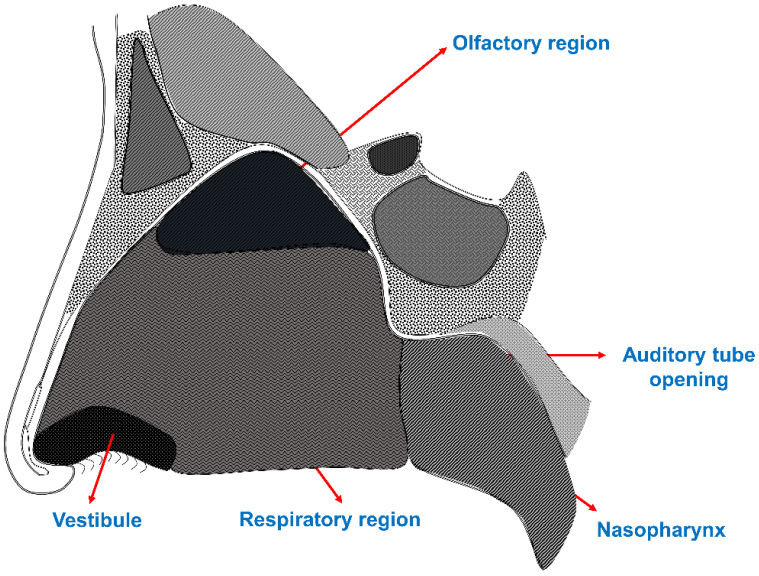

Figure 4 Sagittal section of nasal cavity with marking of different regions

2.4.2.2 Nasal pathways

The pathways through which drug is absorbed from the nasal cavity are classified as – systemic pathway, olfactory pathway and trigeminal pathway (figure 5). The drug is absorbed directly into the systemic circulation via a systemic pathway and to reach CNS (Central Nervous System) it has to cross BBB (Blood Brain Barrier). In the olfactory pathway drug is absorbed through olfactory epithelia. It will be further passed through the olfactory bulb to CNS. The drug is transported through the trigeminal nerve system in the trigeminal pathway (Khan et al., 2010). The olfactory pathway is further divided into two- intraneuronal and extraneuronal. The intraneuronal pathway is about the uptaking of drug molecules from the olfactory epithelium via endocytosis which then gets transported to the olfactory bulb via axonal transport. The extraneuronal pathway is about tight junction crossing of drug molecules through the olfactory epithelium and subsequently reaching the olfactory bulb. In this case, the drug will be reaching CNS within minutes whereas the intraneuronal pathway required hours or days to transport the drug to CNS (Ying, 2008).

The nasal cavity permits direct access to the CNS to circumvent the BBB (Illum, 2003). Commercially marketed nasal formulations of drugs such as sumatriptan, calcitonin and estradiol have been shown to have faster onset of action (Illum, 2002). The absorption of the drug through the olfactory region of the nasal cavity facilitates direct transport to the brain targeting CNS. Therefore, drugs for conditions like Parkinson's disease, Alzheimer's disease, migraine, depression and schizophrenia can be effectively transported to CNS via the nasal cavity rather than conventional methods where there is poor bioavailability due to hepatic first pass metabolism and BBB (Mittal et al., 2014). Direct administration of drugs like protein, peptides and nucleic acids is not advised to be done alone without a carrier. Because these kinds of molecules won't tolerate the harsh

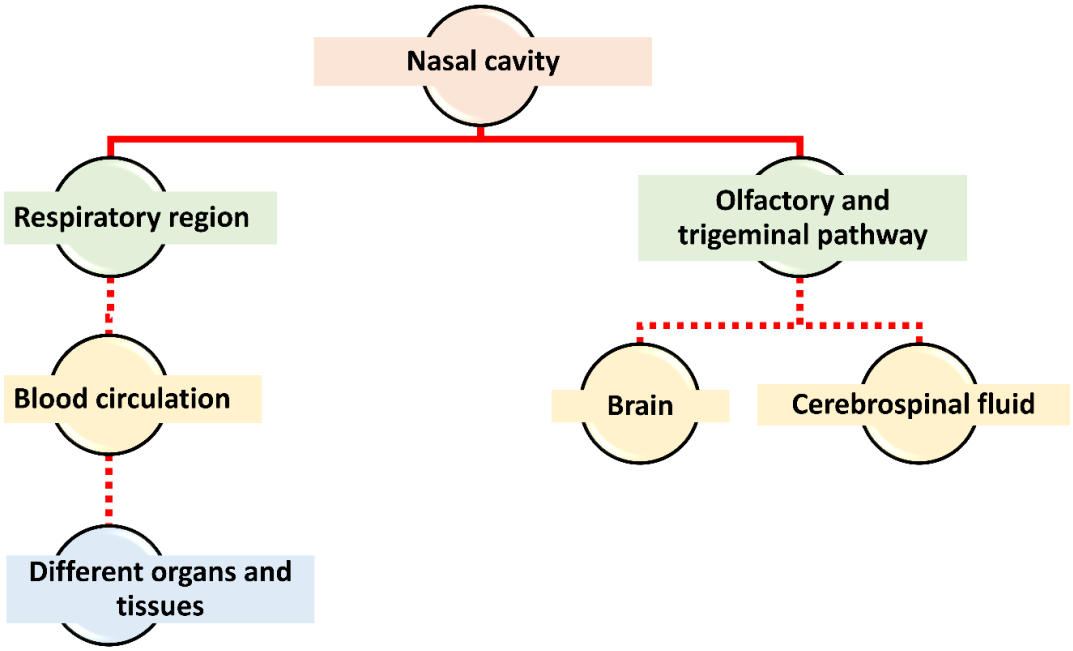

Figure 5 Flow chart describing nasal pathways

nasal environment. Polymeric carriers are preferred compared to peptide-based or lipid-based carriers because of their ability to deliver drugs at targeted locations (Rabiee et al., 2021).

The dry nasal syndrome is treated by applying nasal formulation in the nasal cavity. But, mucociliary clearance limits its use. A nasal adhesive film consisting of gellan gum and

carboxymethyl cellulose was fabricated by Laffleur *et al*. Improved bioadhesive result of this film convinced their proficiency in nasal drug delivery due to prolonged residence time (Laffleur, 2018). Porfiryeva *et al* have synthesized an acrylate polymer of Eudragit EPO for enhanced mucoadhesive properties for nasal delivery. Freeze-dried polymer samples were evaluated for their ability to cause mucosal adhesion (Porfiryeva et al., 2019). Gel-type formulations are much preferred for nasal administration because solution-type formulations could flow down from the nasal cavity. An *in-situ* gelling polymer system of gellan gum after reductive amination was developed for nasal administration. The newly added amino groups enabled enforced adhesion to mucus (Jelkmann et al., 2020).

2.4.3 Ocular mucosal drug delivery

Bowman's layer, Descemet's membrane, epithelium and endothelium together constitute cornea. The basal layer of epithelium contains columnar cells and the outermost layer contains flattened polygonal cells (Gaudana et al., 2010). Around 1.5 million goblet cells present in conjunctiva synthesize secretory mucins and peptides. Molecules of size up to 20,000 Da are permeable through conjunctival tissue and molecules of size up to 5000 Da are permeable through cornea. Turnover of the mucus layer occurs in approximately 15–20 h. Introducing mucoadhesive polymers in ocular drug delivery is a new trend. Due to the interaction of the mucoadhesive polymer with the mucus tissue in the eye precorneal residence time is increased. In liquid dosage forms, where the polymer solutions are fully hydrated, mucoadhesive performance is limited. Whereas small solid dosage forms show interesting performances over an extended period. So, sustained release can be modulated by composition and fabrication techniques (Ludwig, 2005). Nasolacrimal drainage, blinking, anatomical barriers and efflux pumps always challenge

researchers in developing ocular drug formulations. The Blood-Retinal Barrier (BRB) prevents drug entering from systemic circulation to the retina (Gorantla et al., 2020).

A different approach to developing supramolecular self-assembly of dexamethasone prodrug by succination was done by Cheng *et al.* The viscoelastic property of the above-mentioned supramolecular hydrogel extended prolonged corneal residence and also enabled enhanced corneal permeation owing to the nanofibrous structure of the hydrogel. The extended corneal residence helped to increase the bioavailability of dexamethasone also (Cheng et al., 2019). An *in-situ* gelling system based on hexanoyl glycol chitosan was proposed by Shi *et al* for ocular delivery of levofloxacin with enhanced bioavailability. The hexanoyl glycol chitosan hydrogel is a thermo-responsible hydrogel with typical sol-gel transition at 32 °C. The gelling property at 32 °C caused increased corneal retention time and bioavailability of levofloxacin compared to the simple aqueous solution of the same (Shi et al., 2019). Xu *et al* put forward valylvaline-mediated targeted delivery of dexamethasone by chitosan oligosaccharide-stearic acid nano micelles to the posterior segment of the ocular cavity. This transporter-mediated ocular delivery improved the bioavailability of dexamethasone in the posterior segments (Xu et al., 2020).

2.4.4 Rectal mucosal drug delivery

The surface area of rectal mucosa is approximately 300 cm^2. The rectum mainly functions to remove water. The epithelium in the rectal region is composed of cylindrical cells and goblet cells which secrete mucus. No villi-like structures are present on the rectal surface but rectal valves are seen as three major folds (Shaikh, Raj Singh, Garland, A David Woolfson, et al., 2011). Rectal delivery of drugs has been used for local delivery of laxatives, antipyretics and treatment of haemorrhoids. Localized rectal administration is

directly delivering a drug into the systemic circulation by portosystemic shunting (Purohit et al., 2018).

The use of rectal suppositories for sustained drug delivery has been widely studied with several drugs like morphine, diclofenac, zidovudine etc. Leithy *et al* have formulated diclofenac sodium -chitosan microspheres (E. S. El-Leithy et al., 2010). The same research group had again come up with developing a hydrogel system with Carbopol 934 and hydroxypropyl methylcellulose (HPMC) to deliver diclofenac-sodium chitosan microspheres for rectal application (Eman S. El-Leithy et al., 2010). This hydrogel system facilitated the subsequent controlled release of microspheres with no burst release. Liu *et al* proposed developing an *in-situ* gel system which is thermo-responsive for the rectal delivery of ibuprofen. A thermoresponsive gel system was prepared using poloxamer 407, HPMC and sodium alginate. The *in-vivo* studies in the rabbit model showed improved bioavailability of ibuprofen and the team has proposed the *in-situ* gel as an effective rectal formulation for non-steroidal anti-inflammatory drugs (NSAID) (Liu et al., 2018).

2.4.5 Vaginal mucosal drug delivery

The epithelial layer of vaginal mucosa consists of the lamina propria and stratified squamous epithelium. Though vaginal mucosa lacks a gland to secrete it is covered with vaginal fluid. Cervical mucus is one of the main components of vaginal fluid. During the menstrual cycle, the volume, viscosity, and pH of the cervical mucus vary. Age is also a determining factor for the physical properties of cervical mucus. In 7 days a turnover of around 10-15 layers of vaginal cells is observed (Valenta, 2005). The vaginal route is conventionally used for local delivery of antiviral, antifungal, antibacterial, antiprotozoal, anti-inflammatory and steroid drugs. It is a potential route for uterine targeting of active

agents like progesterone (Cicinelli et al., 2000). The concentration of vaginally administered progesterone is higher in the uterine artery than the radial artery indicating preferential distribution to the uterus. This direct local transport from the vagina to the uterus is termed the 'first uterine pass effect' (De Ziegler et al., 1997). Drug formulations like solutions, gels, suspensions, suppositories, creams, and tablets are used for vaginal drug delivery for a short time (Robinson and Bologna, 1994).

Krogstad *et al* designed a nanoparticle-releasing nanofibre composite for nanoparticle retention in the vaginal tract. PVP and PVA were chosen to fabricate nanofibre for the release of PEGylated PLGA nanoparticles loaded with antiretroviral drugs like etravirine. This nanofibre-mediated delivery of nanoparticles caused the retention of nanoparticles as well as drugs in the tract for a prolonged period (Krogstad et al., 2017). Effective release of contraceptive drugs like levonorgestrel and ethinylestradiol through an electrospun gelatin matrix was proposed by Painuly *et al.* The dual drug-loaded system offered sustained drug release for a prolonged period (Painuly et al., 2019). Metronidazole-mediated treatment of bacterial vaginosis is widely practised. Local application of metronidazole is preferred for pregnancy patients due to certain systemic side effects. Nanofibres were proposed by Tugcu-Demiroz *et al* as an effective formulation for local vaginal drug delivery. They have produced metronidazole-loaded PVP electrospun mucoadhesive fibre to treat bacterial vaginosis (Tuğcu-Demiröz et al., 2020).

2.5 MUCOADHESIVE POLYMERS

2.5.1 Cationic polymers

The reported cationic polymer used in mucoadhesive applications is chitosan (Khutoryanskiy, 2011). Chitosan consists of β-(1-4)-linked 2-amino-2-deoxy-D-

glucosamine and N-acetyl-D-glucosamine residues which are produced by deacetylation of chitin (crustacean exoskeleton). Chitosan is not water-soluble but dissolves in acid medium and a water-soluble salt of chitosan can be derived from it (Jabbal-Gill et al., 2012). It is widely used for biomedical applications like wound dressing, tissue engineering, antimicrobial applications, drug delivery etc due to excellent biocompatibility, non-toxicity and biodegradability (Cheung et al., 2015). These polymers exhibit cationic behaviour due to the protonation of amino functional groups under acidic pH. These positively charged species establish electrostatic interaction with sialic acids in mucin glycoprotein which is negatively charged (Casettari et al., 2012). Hence, chitosan is preferred for pH-sensitive drug delivery applications targeting the stomach as a tablet excipient. High molecular weight chitosan is more viscous causing slow release of pharmaceuticals from the polymer systems and prolonging therapeutic activity (Kofuji et al., 2005). Chitosan has been extensively studied for immunogenic properties via mucosal regions also (Jabbal-Gill et al., 2012).

Chemical modifications of chitosan are typically done in amino groups although, functionalisation of hydroxyl groups is also possible. Functional modifications of chitosan improve the water solubility of base chitosan polymer. Quaternisation of amino groups (Sajomsang et al., 2009), thiolation (Cesari et al., 2020), acrylation (Davidovich-Pinhas and Bianco-Peled, 2010), hydroxypropyl modification (Jabbal-Gill et al., 2012) and carboxy methyl modification (Fonseca-Santos and Chorilli, 2017) of chitosan have been investigated by various research groups.

Quaternary modification of the amino group of chitosan by methylation imparts persistent cationic nature to the polymer and thus improves mucoadhesion (Kulkarni et al., 2017). Though the force of adhesion is expected to increase with an increased degree of quaternization (Sajomsang et al., 2009), according to Nazar *et al* chitosan gels prepared

with a medium degree of quaternization and molecular weight have higher work of adhesion (Nazar et al., 2011). Carboxymethyl functionalization of chitosan provides amphoteric properties to chitosan which helps for drug delivery in acidic and basic pH (Upadhyaya et al., 2014) through protonation of amino groups at low pH and deprotonation of carboxylic groups at higher pH. Thiolation of chitosan has been reported to be carried by reagents like cysteine, thioglycolic acid, glutathione etc. In addition to electrostatic interactions, the additional interaction of thiol groups with the cysteine residues of mucin augments the mucoadhesive property (Cesari et al., 2020). Acrylate modification of chitosan is reported to follow the Michael-type reaction mechanism (Davidovich-Pinhas and Bianco-Peled, 2010). A schematic representation of acrylate group-mediated mucoadhesion is exhibited in figure 6.

2.5.2 Anionic polymers

Widely studied anionic polymers in mucoadhesive applications are polyacrylic acid and its derivatives. Alginate and carboxymethyl cellulose are also studied in the same category. Polyacrylic acid is a water-soluble polyelectrolyte with pendent carboxyl side chains. Polyalkanyl ester crosslinked polyacrylic acid is known as Carbopol and divinyl glycol crosslinked polyacrylic acid is Carbophil. Polyacrylic acid and it's all derivatives are known to be non-toxic and non-irritant. Crosslinked derivatives of polyacrylic acid readily absorb water, and swell and are therefore highly suitable for drug delivery applications (Ritthidej, 2011). The mechanism of interaction of anionic polymers in mucoadhesion is the establishment of hydrogen bond between anionic functional groups of polymer and oligosaccharide chains of mucin. This interaction causes an increase in viscosity and the formation of hydrogels with mucin (Soni et al., 2019). The linear polysaccharide derivative of alginic acid is known as sodium alginate. It is composed of 1,4-β-D-mannuronic acid and α-L-guluronic acid. The conversion of alginic acid to

sodium alginate improves water solubility also. When a monovalent ion like sodium is exchanged with a divalent ion like calcium in an aqueous alginate solution change to a gel structure. Alginate has been studied for various applications like tissue engineering, wound dressing, and drug delivery application due to its biocompatibility and non-toxicity (Fonseca-Santos and Chorilli, 2017). Most recently, alginate/gelatin spray dried microparticles have been developed for the treatment of vulvovaginal candidiasis by with the incorporation of Luliconazole into it. The mucoadhesive property of polyelectrolyte complex of alginate/gelatin facilitated better mucoadhesion on porcine vaginal mucosa (Szekalska et al., 2023). Carboxymethyl cellulose (CMC) is a cellulose-derived anionic polysaccharide with β-1-4 linked glucose subunits in which some of the hydroxyl groups are replaced with carboxymethyl groups to render water solubility (Cook et al., 2018; Grządka, 2012). The sodium salt of carboxymethyl cellulose is often used as an excipient in different drug dosage forms (da Silva et al., 2021).

Catechol modification of polyacrylic acid was reported by A. Li and Z. Xu *et* al. They have done dopamine hydrochloride modification of polyacrylic acid with cellulose fibres as reinforcement. This has been reported to cause improved adhesion compared to available glues (Li et al., 2019). Grafting of cellulose nanocrystals over polyacrylic acid was investigated by Vakili *et al* to improve mucoadhesion. They have evaluated the delivery of cancer drug cisplatin from the polymer system to treat colorectal cancer (Vakili et al., 2021). A similar modification of alginate with dopamine hydrochloride to introduce a catechol functional group was also done and found that the irreversible interaction of catechol groups with thiol groups of mucin caused improved mucoadhesion (Sahatsapan et al., 2020). Figure 6 gives an idea of the interaction of the catechol-modified polymer with the mucosa surface for mucoadhesion. A controlled release study of ibuprofen from interpenetrating microgels fabricated using polyacrylic acid and

sodium alginate ensured increased bioavailability. The system has caused gastric retainment of microgels for more than 12 h owing to its low density (Ramesh Babu et al., 2006). Tang *et al* fabricated polydopamine/carboxymethyl cellulose/polyacrylic acid (PAA) adhesive hydrogel as UV filtration membrane and skin care products. Dopamine was self-polymerized in a CMC solution followed by acrylic acid polymerisation to PAA and established crosslinking (Tang et al., 2021). Shihui *et al* synthesized CMC-poloxamer containing chemically crosslinked hydrogel which is dual pH and temperature sensitive for the release of nepafenac to increase ocular bioavailability. They found that the cumulative release of nepafenac is higher at 35 $^{\circ}$C and pH 7.4 (Yu et al., 2017).

2.5.3 Non-ionic polymers

Hydrophilic non-ionic polymers like hydroxypropyl methylcellulose, poloxamer, polyvinyl pyrrolidone and polyvinyl alcohol (PVA) are also well-investigated for their mucoadhesive properties even though, ionic polymers are desirable due to ionic interactions (Zhang et al., 2021) (Diaz-Salmeron et al., 2021) (Rohani Shirvan et al., 2021) (Vecchi et al., 2021). The highly viscous aqueous solutions of these polymers cause interpenetrating interactions with mucin glycoprotein chains. Hence, a diffusion model mechanism is expected for mucoadhesion. These polymers also possess wetting properties which enable wetting theory to interpret the mechanism (Shaikh, Raj Singh, Garland, A. David Woolfson, et al., 2011).

A pulsatile formulation of felodipine was formulated by Karavas *et* al by a miscible polymer blend of polyvinyl pyrrolidone and hydroxypropyl methylcellulose. A weak interaction between the hydroxyl group of HPMC and the carbonyl group of PVP was observed to enable the miscibility of the blend. The tablet formulation consisted of two layers- an internal layer containing felodipine and PVP alone and an external adhesive

layer containing PVP and HPMC (Karavas et al., 2006). A biphasic release profile of ofloxacin was observed from a nanofibrous matrix of gellan/polyvinyl alcohol with desired mucoadhesion in the gastric mucosa of the rat model. The nanofibres exhibited an initial burst release kinetics followed by a sustained release for 24 h (Vashisth et al., 2017). Edmans *et al* developed a dual-layer electrospun consisting of polyvinyl pyrrolidone/Eudragit containing adhesive layer containing lysozyme as an antimicrobial protein. Polycaprolactone (PCL) was introduced over the adhesive layer as a backing layer to enable the unidirectional release of lysozyme. It is observed that *Streptococcus ratti* growth was inhibited during the oral release of lysozyme (Edmans et al., 2020).

2.5.4 Thiol-modified polymers

The widely practised chemical modification to improve the mucoadhesion of a polymer is thiolation. An around 140-fold increase in mucoadhesion is observed after thiolation (Puri et al., 2020) due to the formation of a disulfide bond between the thiol group of polymer and thiol groups present in mucin glycoprotein (Duggan et al., 2017) as shown in figure 6. Thiolation is expected to be highly advantageous for oral delivery of protein and peptide drugs because of the ability of thiol groups to bind with divalent cations like zinc and magnesium. These divalent cations are co-factors for many of the proteases like aminopeptidases and carboxypeptidases. The binding of thiomers with these cations causes the inhibition of proteases (Bravo-Osuna et al., 2007). Polymers carrying various functional groups like amino, hydroxy and carboxylic groups have been reported to be thiolated using different techniques. Thiolation of amino groups has been done with thioglycolic acid (Kast and Bernkop-Schnürch, 2001), cysteine, thiobutylamidine, thioethylamidine, 4-mercaptobenzoic acid (Sarti and Bernkop-Schnürch, 2011) and 2-iminothiolane or traut's reagent (Bernkop-Schnürch et al., 2004). Molecules like cysteine, thioglycolic acid and N-acetyl cysteine form amide bond with the amino group

of the polymer chain whereas thiobutylamidine and thioethylamidine form amidine bonds with chitosan (Sarti and Bernkop-Schnürch, 2011). Thiolation of polymers with hydroxyl backbone was reported to be done with thiourea or 3-mercaptopropionic acid (Suchaoin et al., 2016). Gupta *et al* have reported the thiolation of polyvinyl alcohol with thioglycolic acid via an esterification reaction. The esterification reaction was carried out in the presence of sulphuric acid as a catalyst and the thiolated compound was precipitated in methanol (Gupta et al., 2013). Anionic polymers containing carboxylic functional groups were reported for thiolation with cysteine amino acid. The expected mechanism of thiolation is the formation of an amide bond (Bernkop-Schnürch and Steininger, 2000).

Kafedjiiski *et al* developed cysteine-conjugated hyaluronic acid for mucoadhesive drug delivery applications. They have studied the release profile of fluorescein isothiocyanate-dextrans as a model study and observed sustained release kinetics for 12 h (Kafedjiiski et al., 2007). A biphasic drug release profile of sodium diclofenac from thiolated poly(aspartic acid) was reported by Horvat *et al* as a promising system for ocular drug delivery. The prolonged residence time of the modified polymer on the mucosa caused an initial burst release in the first hour followed by a sustained release in the next 24 h (Horvát et al., 2015). Thioglycolic acid-mediated modification of gum ghatti has been reported by Puri *et al* as a novel excipient of the mucoadhesive tablet. The increased adhesion of the thiomer caused a retardant release of domperidone rather than a burst release (Puri et al., 2021). Zaman *et al* synthesized thiolated hemicellulose for sustained drug release and better therapeutic activity (Zaman, Bajwa, et al., 2021). Recently Leonard *et al* have investigated the potential of thiolated pectin-chitosan composite as a mucoadhesive drug delivery system of 5-flurouracil to treat colorectal cancer conditions (Leonard et al., 2023).

2.5.5 Boronic acid-modified polymers

Polymers functionalized with phenylboronic acid have gained tremendous attention for mucoadhesive drug delivery applications in the last decade. Boronic acid-modified

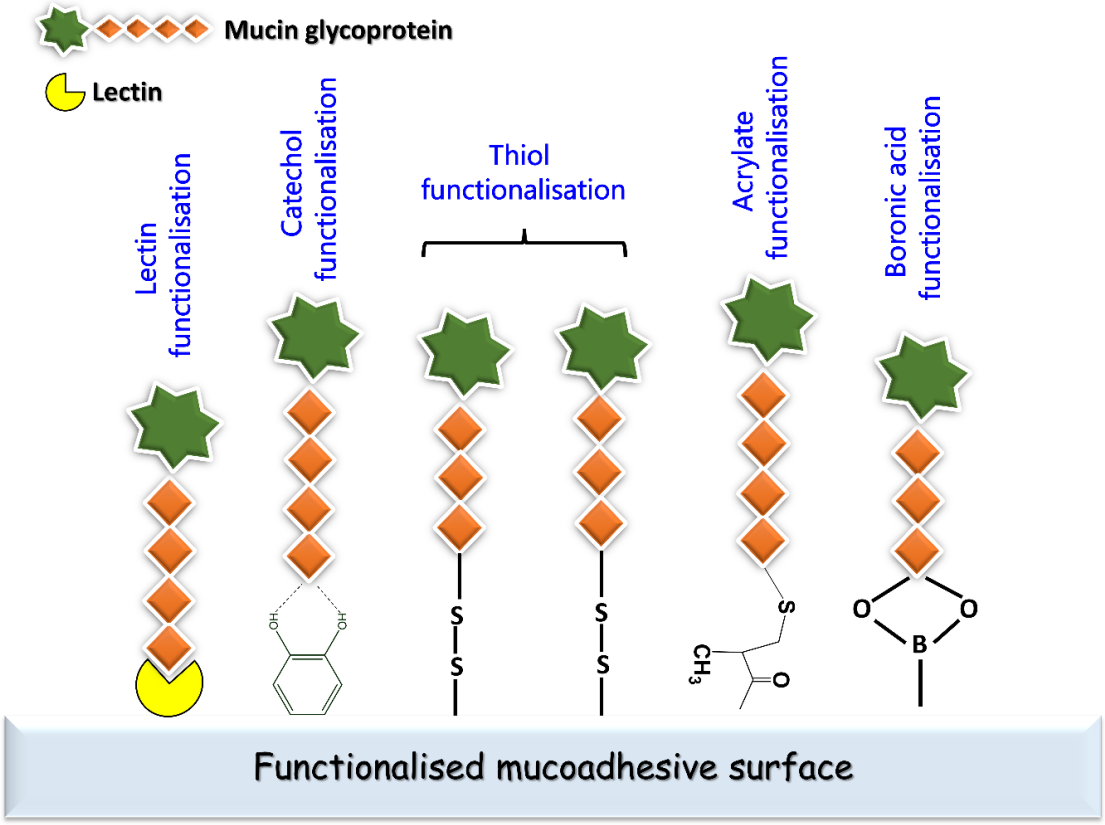

Figure 6: Schematic diagram representing mechanism of mucoadhesion of various functionalised polymers with mucin glycoprotein- Lectin functionalisation, Catechol functionalisation, Thiol functionalisation, Acrylate functionalisation and Boronate functionalisation are demonstrated.

polymers were known to target polysaccharides, glycoproteins, polyols, sugars etc. The complex formed between the boronic acid functionalized polymer and the target molecules is phenyl boronate ester (Singh et al., 2017) as shown in figure 6. The phenyl boronate ester formation is highly pH dependent in such a way that it forms an adduct with the hydroxyl group of targets when the pH of the medium is equal to greater than the pKa of the boronic acid. At pH above pKa, boronic acid forms a negatively charged tetragonal structure (boronate anion) which further binds with hydroxyl groups to form boronate cyclic esters. When the pH becomes lower than pKa, the cyclic ester complex

dissociates to form the trigonal boronic acid structure. Hence, boronate-modified polymers are not expected to bind with the hydroxy groups at neutral or acidic pH. The pH of most of the biological samples like urine, blood and saliva is between 6 to 8. Hence, modified boronic acids with a pKa value in the range of 8 are used for complex formation, eg., 3-aminophenyl boronic acid or 4-vinyl phenylboronic acid (Brooks and Sumerlin, 2016). As far as the structure of mucin is concerned, saccharide groups as well as sialic acid groups are prone to bind with boronic acid. The saccharide groups form boronate cyclic esters at higher pH conditions. On the contrary, sialic groups in mucin are reported to bind easily with boronic acid at neutral pH conditions (Brannigan and Khutoryanskiy, 2019).

The nanoparticles formed by the self-assembly of poly(D, L-lactide) and dextran were reported for enhanced mucoadhesion after surface functionalization with phenyl boronic acid. These particles were evaluated for release of cyclosporine A to treat anterior eye diseases. Due to augmented mucoadhesion, the particles got retained in the mucosa for a long time in the mice model. Compared to commercially available dosage forms, the nanoparticles facilitated prolonged drug release and reduced the drug administration frequency (S Liu et al., 2015). The precorneal turnover and relatively low permeability of corneal tissues make topical treatment of dry eye disease tricky. To tackle this limitation, Graeme Prosperi-Porta *et al* proposed phenylboronic acid-based polymeric micelles for anterior ocular drug delivery. They have synthesized and characterized poly(L-lactide)-b-poly(methacrylic acid-co-3-acrylamidophenylboronic acid) block copolymer micelles for Cyclosporine A release. The *in-vivo* evaluation done in Sprague-Dawley rats showed the potential of the material to improve the bioavailability of topically applied Cyclosporine A (Prosperi-Porta et al., 2016). Similarly, another group of researchers have reported 3-aminophenyl boronic acid tethered chondroitin sulphate-

based nano lipid carriers which showed a high affinity with the sialic groups of ocular mucins. This strong affinity has resulted in the prolonged delivery of dexamethasone from the lipid carriers to alleviate dry eye syndrome (Tan et al., 2019). Kolawole *et al* have prepared boronate-conjugated chitosan via EDC-NHS coupling by using 4-carboxyphenyl boronic acid. The same was evaluated for adhesion in urothelial mucosa with fluorescein sodium for release study. The mucoadhesion was found to increase with an increased degree of boronation. The prolonged residence time of the system in urothelial mucosa ensured the prolonged release of the drug too (Kolawole et al., 2019). The research group of Kolawole have recently proposed boronated chitosan/alginate mucoadhesive nanoparticles for cervical cancer drug delivery of paclitaxel also. The preparation of nanoparticles was done by ionic gelation method (Kolawole et al., 2023).

2.5.6 Lectin and antibodies

Lectins and antibodies belong to second-generation mucoadhesive polymers with specific binding potential. Lectins are also a class of glycoproteins which specifically bind to sugar molecules which is reversible as shown in figure 6. According to the specificity of binding with carbohydrates, lectins are classified as glucose-binding lectins, mannose-binding lectin, D-galactose binding lectin, L-fucose binding lectin, sialic acid binding lectin and 2-acetamido-2-deoxy-galactose binding lectin (Chettri et al., 2021). Lectins are reported for the transport of macromolecules across cell membranes via receptor-mediated adhesion. In this case, lectins get internalised by endocytosis and enable the transport of macromolecules through vesicular transport. Therefore, lectins are considered to be fascinating molecules with dual functionality- target specific adhesion and controlled release of macromolecular pharmaceuticals (Lehr, 2000).

Wheat germ agglutinin is a non-immunogenic lectin derivative isolated from *Triticum vulgaris.* It can specifically bind to sialic acid residues in the intestinal mucosa. Makhlof *et al* reported wheat germ agglutinin conjugated Carbopol for surface modification of cationic multilamellar vesicle liposomes. The positively charged liposome and negatively charged liposomes establish an electrostatic interaction. *In-vivo* studies confirmed the ability of the surface-modified liposomes to penetrate the intestinal barrier and enhance the systemic delivery of entrapped peptides in liposomes (Makhlof et al., 2011). Odorranalectin (OL) isolated from *Odorrana graham* can specifically bind to L-fucose which has greater expression on olfactory mucosa. S14G-HN is a promising anti-AD drug and finds it difficult to cross BBB. H. Wu *et al* reported surface engineering of PEG-ylated cubosomes with OL to deliver S14G-HN intranasally (Wu et al., 2012). Gao *et al* prepared an ethylcellulose/chitosan microsphere with PVA as a surfactant. The microspheres were surface activated with lectin via EDC mediation. The potential of the lectin-conjugated microspheres was evaluated for rivastigmine delivery to treat Alzheimer's disease and observed significantly improved performance in *in-vivo* experiments (Gao et al., 2021). Recently Putri *et al* proposed specific site adhesion of lectin conjugate alginate matrix system for better mucoadhesion and drug bioavailability (Putri et al., 2021). Antibodies provide site-selective binding over the mucosal surface. This property facilitate highly targeted drug delivery, especially to tumour tissues (Chowdary and Rao, 2004). The role of antibodies in the field of mucosal-targeted drug delivery is yet to explore by the science community.

2.6 FABRICATION TECHNIQUES FOR MUCOADHESIVE DRUG FORMULATIONS

2.6.1 Freeze drying

Freeze drying or cryodesiccation or lyophilization is the best drying method adopted to remove water from samples. This technique was started to practice on a laboratory scale in the 1880s and remained a laboratory technique till the 1930s (Adams et al., 2015). Unlike other dehydration techniques, freeze drying causes no change in the original structure and colour of samples (Jiang et al., 2013). The main components of a freeze-drying machine are a refrigerator system, vacuum system, control system, product chamber and condenser. The refrigerator system cools the condenser located inside. The purpose of the condenser is to collect the vapours being sublimed off and condense them back to solid (ice) which is removed after the entire procedure is over. Low pressure is required for water to sublime. Hence samples are kept in the product chamber under a deep vacuum condition which is well below the triple point of water. Sublimation is a phase transition where heat energy is added causing the product in the solid state to sublime.

Freeze drying is highly recommended for samples containing heat-sensitive molecules like proteins, microbes and pharmaceuticals. The basic principle of freeze drying is sublimation in which the transformation of ice to vapour takes place (Garcia-Amezquita et al., 2016). Freeze-dried polymer samples have been extensively studied for developing fast-dissolving oral drug delivery systems like tablets, wafers etc. (Siow et al., 2016). The highly porous structure of freeze-dried samples (figure 7) shows higher drug loading efficiency and water absorption capacity. AlHusban *et al* formulated a freeze-dried rapid disintegrating tablet and evaluated the feasibility of using amino acids as matrix-forming

agents (AlHusban et al., 2010). Elsharawy *et al* formulated and evaluated various lyophilized tablets containing duloxetine hydrochloride which is used for the treatment of depression. They have formulated a polymer combination of HPMC, Carbopol, chitosan and PVA in various concentrations and compared the performance *in vivo* (El Sharawy et al., 2017). Recently, Lal *et al* proposed the use of freeze-dried tablets for oral vaccine delivery. The entry of most the pathogens into human body is via mucosal linings at the nasal, buccal, rectal and vaginal regions. It is truly rational to immunize via the mucosal route to control the spread of infection to distal regions rather than relying on intramuscular and intravenous injections. The development of fast-dissolving freeze-dried tablets enables consumption of the tablet without added liquid and enables the patients themselves to use it. These advantages are expected to cause increased vaccination rates for large-scale immunization drives or in epidemic situations such as covid pandemic scenario (Lal, 2020).

2.6.2 Solvent casting

Solvent casting is a century-old, versatile and easiest method to prepare polymer films. It can be also defined as an air-dry method to remove solvent from a polymer sample. Polymer is dissolved in a suitable volatile solvent and spread on a substrate or mould. The solvent is dried without applying thermal or mechanical stress. The solvent casting of homogeneous solution on a uniform surface allows the fabrication of films with uniform thickness as shown in figure 7. This method is highly dependent on the volatility of the solvent – less volatile solvent takes more time to evaporate and high volatile solvent easily evaporates (Siemann, 2005).

Timur *et al* have carried out a comparative study of drug release from mono and bilayered mucoadhesive films and wafers. Cefuroxime axetil was taken as a model drug and HPMC

and chitosan were taken as polymers for the preparation of mucoadhesive films and wafers. Disintegration of HPMC was fast compared to chitosan and higher drug release was observed for wafer samples. Hence chitosan-based monolayer wafer facilitated the prolonged release of the drug. In the case of the bilayered wafer, a chitosan-based system with a drug-loaded on HPMC provided excellent adhesion and prolonged drug release (Timur et al., 2019). Mucoadhesive films based on gellan gum and pectin were designed by Prezotti *et al* for oral delivery. Curcumin was loaded into the film as a model and its release rates were evaluated (Prezotti et al., 2020). The solvent casting technique has been broadly used for fabricating mucoadhesive films for drug delivery applications. Extensive first-pass metabolism reduced the oral bioavailability of rizatriptan for migraine treatment. An investigation has reported the development of solvent-cast buccal films comprising Proloc, HPMS and Eudragit RS 100 for rizatriptan delivery. The mucosal delivery in rabbits showed a higher plasma level concentration of the drug following biphasic drug release kinetics (Nair et al., 2021).

2.6.3 Nanoparticles

In addition to established drug delivery formulations like tablets, ointments, gels and sprays, mucoadhesive nanoparticles have gleaned attention as a promising system for the controlled delivery of drug molecules (Hanafy et al., 2019). Ocular drug delivery studies highly rely on developing nanoparticulate systems because of increased viscosity and reduced drug drainage rate (Silva et al., 2017). As a carrier for drug molecules, nanoparticles can be of two types based on the structural organization of the polymer. Nanospheres are the kind of nanoparticles with a matrix model distribution of polymer and nanocapsules are the class of particles with a reservoir model distribution of polymer on the outer side (Barratt et al., 2001). Figure 7 diagrammatically describes the mechanism of nanoparticle production.

The successful techniques adopted to prepare nanoparticles are the emulsion solvent diffusion method, emulsification- reverse salting out and *in-situ* polymerisation (Takeuchi et al., 2001). In the emulsion solvent diffusion method, the polymer is dissolved in a solvent which is a partially-miscible solvent with water. Later, the solution is poured into a water container. Due to the immediate reduction of interfacial tension, the solvent diffuses out of the internal phase (containing polymer) to the aqueous phase. A large quantity of water is used in this method to accelerate solvent diffusion to the aqueous phase. This causes the polymer to enter a non-solvent phase where its aggregation is prevented by adding a stabilizer (María Pineda-Reyes et al., 2021). Pluronic F68, PVA and sodium taurodeoxycholate were reported to be used as aqueous phase stabilizers and soy lecithin as an organic phase stabilizer. The size of the nanoparticle is controlled by altering the stirring speed and stabilizer concentration (Vauthier and Bouchemal, 2009).

Emulsification-reverse salting out is another technique which has slight difference from the above method of preparation. The emulsion is prepared in a solvent which is completely miscible with water. Some electrolytes like magnesium chloride, calcium chloride and magnesium acetate in high concentration are used to emulsify the polymer solution in the aqueous phase. These compounds use water for their solubilisation. The precipitation of polymer is induced by pouring an excess amount of water which leads to a sudden drop of salt concentration and thus causes polymer solvent to migrate out (Vauthier and Bouchemal, 2009).

Well-characterized nanospheres are prepared by *in-situ* polymerisation of monomers in emulsions. *In-situ* emulsion polymerisation of poly cyano acrylates has been reported in which anionic polymerisation is taking place initiated by water itself. The drug molecules are loaded in the nanoparticle by dissolving in the polymerisation medium either before

adding monomer or after completing polymerisation (Couvreur et al., 1979). The percentage of drug adsorption on the nanoparticle is controlled by the hydrophobicity of the polymer and the specific surface area of the particle (Couvreur and Vauthier, 1991). Nanocapsules are obtained from interfacial polymerisation or polycondensation reactions of monomers in emulsions. The polymerisation of the monomer is expected to take place at the oil-water interface to produce nanocapsules. The monomers are solubilized in the water-miscible aqueous phase and then dispersed in water-containing surfactants. Polymerisation will be initiated at the interface which is initiated by ions in the aqueous phase (Barratt et al., 2001).

Aggregation of amphiphilic copolymers in aqueous media leads to the formation of spheroid polymeric micelles with a hydrophilic shell and hydrophobic core. These particles can be tuned to respond to external stimuli like pH, light, temperature, magnetic field, electric field etc. The influence of external factors regulates the release of drug molecules out of the micelle. Dendrimers are another class of tree-like polymers. Dendrimers possess a loosely packed core and tightly packed periphery structure and thus the core holds drug molecules. Poly(amidoamine) or PAMAM is extensively used for the synthesis of dendrimers (Masserini, 2013).

2.6.4 Electrospinning

Electrospinning is a widely used method to fabricate nano and micro-sized fibres from polymer solutions using electrostatic force (figure 7). Electrospun nanofibres have been widely investigated for biomedical applications, filtration, sensor applications and electrical applications because of several advantages like high surface-to-volume ratio, controllable porosity, and controllable properties by adjusting spinning parameters.

Natural, semi-synthetic and synthetic polymers have been exploited for fabricating electrospun fibres (Bhardwaj and Kundu, 2010).

Electrospinning setups can be classified into two – horizontal and vertical. With the expansion of the technology, various research groups have come forward with other sophisticated methods to fabricate complex nanofibrous structures (Stankus et al., 2006).

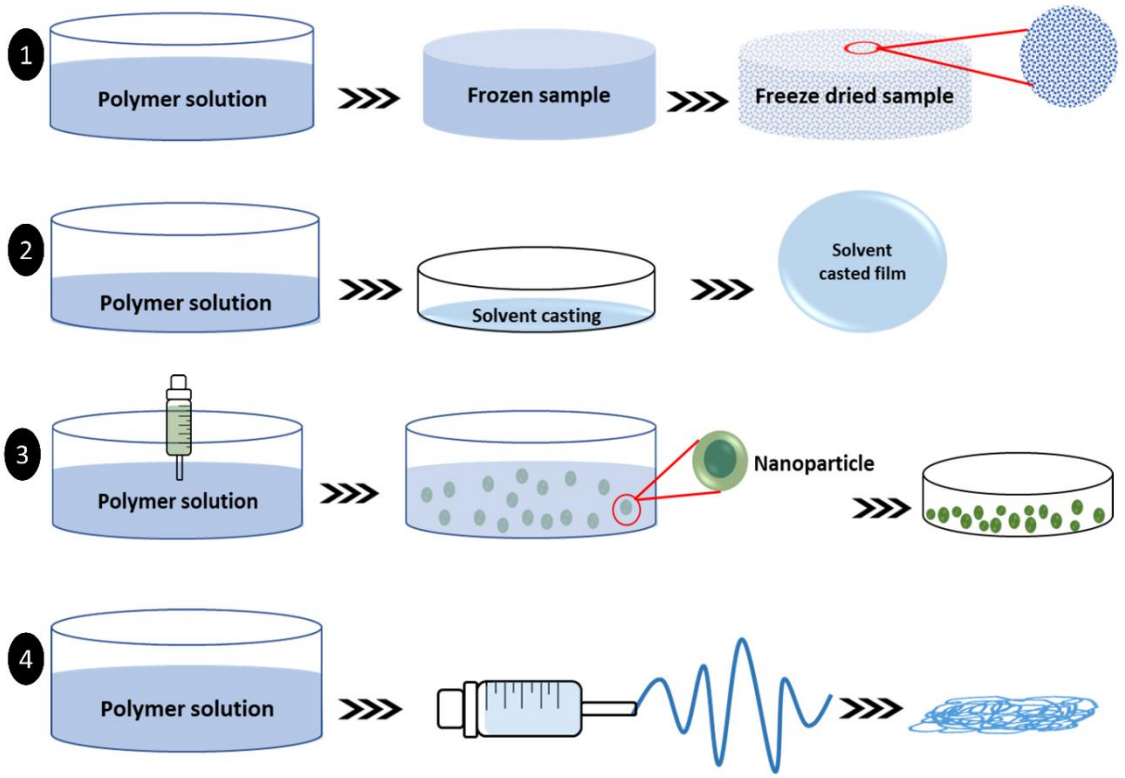

Figure 7 Diagrammatic representation of methods of preparation of drug delivery systems: - 1) Freeze-drying 2) Solvent casting 3) Nanoparticle preparation 4) Electrospinning

Typically, an electrospinning setup consists of a spinneret, a high-voltage power supply and a grounded collector (rotating mandrel, plate etc) (Liang et al., 2007). The polymer droplet at the end of the capillary tube will be held spherical by its surface tension. When the applied potential difference reaches a critical point and overcomes the surface tension of the droplet, a charged get will be ejected from the Taylor cone and further cause whipping of unstable jet between the spinneret and collector. During this whipping

motion, the highly volatile solvent will get evaporated leaving the polymer fibre alone over the collector (Taylor, 1969).

Electrospun materials are advised for drug delivery applications because of high loading and entrapment efficiency, ability to regulate release, process simplicity and cost-effectiveness (Chou et al., 2015). Simple blend electrospinning, co-electrospinning, side-by-side electrospinning, co-axial electrospinning and emulsion electrospinning are the various types of electrospinning setups used for fabricating drug-loaded fibres. Traditional electrospinning in which drug molecules are mixed with the polymer solution leads to the formation of drug-loaded nano fibres. Co-electrospinning includes two separate spinneret systems loaded with different polymer solutions and spun at the same time to a single collector. Unlike the co-electrospinning system, the side-by-side approach forms bicomponent fibres that had properties of both polymeric components. In this case, two polymer solutions meet up only at the terminal of the spinneret. Co-axial electrospinning is the technique to produce core-shell-like fibres from a concentric spinneret. Different polymers are filled in the inner and outer chambers where the electrostatic field is applied in both and facilitate electrostatic perturbations in both solutions. Drug-encapsulated nanofibres have been reported to be fabricated by co-axial electrospinning in which drug-loaded polymer is filled in the inner core and the protective polymer is filled in the outer core (Hu et al., 2014). Emulsion electrospinning also results in the formation of core-shell-like fibres where agglomeration of emulsion droplets occurs in the core and the polymer forms the outer shell (Yarin, 2011).

2.7 ELECTROSPUN POLYMERS FOR BUCCAL AND NASAL ADHESIVE DRUG DELIVERY

The development of electrospun polymeric matrices particularly for buccal and nasal adhesive drug delivery is the area of interest of this research work. The advantage of mucoadhesive nanofibres in drug delivery is that they facilitate a controlled rate of drug delivery either through polymer degradation or diffusion from the polymeric matrix. The mucoadhesive electrospun patches are also flexible enough and hence could be positioned in any part of mucosa (Pérez-González et al., 2019). Various mucoadhesive dosage forms are under investigation for buccal adhesive drug delivery among which, buccal patches developed through electrospinning offer great flexibility and comfort (Rohani Shirvan et al., 2019). The buccal route of drug administration is preferred because of its high administrability and milder environment for drug absorption (Mann et al., 2022). Even though the nasal mucosa site provides fast permeation of drugs across mucosa to the CNS and systemic circulation, only a few studies have reported electrospun matrices for nasal adhesive drug delivery. This is due to the lesser area of absorption and the lack of comfortability of the patient. However, reported literature results support the potential of an electrospun nasal adhesive drug delivery system and prove the improved bioavailability after nasal administration (Lee et al., 2017; Pérez-González et al., 2019).

2.8 ZEIN

Zein is a biocompatible polymer extracted from a major seed storage protein in corn. It is one of the known hydrophobic proteins due to the presence of nonpolar amino acids like leucine, proline etc. It is light cream coloured with a dielectric constant in the range of 4.9 to 5.0. The glass transition temperature of zein is 165 $^{\circ}$C and molecular weight varies from 9.6 to 44 kDa. (Paliwal and Palakurthi, 2014). Apart from biocompatibility,

zein has been extensively studied for its properties like elasticity and film-forming properties which make it suitable for controlled drug delivery, coating, and fabrication of fibrous membranes, films and plastics (Deng et al., 2018). Zein as a drug delivery system has been investigated for the release of proteins, peptides, vaccine delivery and DNA transfection. Zein is insoluble in water but soluble in an aqueous alcohol solution, therefore, can be easily precipitated by an anti-solvent approach to prepare nanoparticles (Paliwal and Palakurthi, 2014). Zein possesses a helical protein conformation in which nine homologous anti-parallel repeating units are stabilized by hydrogen bonds (SB Yang et al., 2016).

Table 1 Electrospinning parameters of zein in different solvent systems and the corresponding shape of fibres obtained

Solvent	Concentration (wt %)	Voltage (kV)	Fibre shape
60:40 EtOH/H_2O	27	20	Ribbon
70:30 EtOH/H_2O	27	20	Ribbon
80:20 EtOH/H_2O	27	20	Ribbon
90:10 EtOH/H_2O	27	20	Ribbon
60:40 IPA/H_2O	27	20	Ribbon
80:20 IPA/H_2O	27	20	Ribbon
80:20 MeOH/H_2O	30	20	Ribbon
Acetic acid	25	20	Round
Acetic acid	30	20	Ribbon

2.8.1 Electrospinning zein

Electrospinning of zein has been widely studied using various solvent systems like acetic acid, ethanol/water mixture, isopropyl alcohol/water mixture, methanol/water, and hexafluoro isopropyl alcohol (Miyoshi et al., 2005; Selling, Biswas, et al., 2007). The

electrospinning conditions and properties of zein solutions which have been explored yet are listed in the table above. The fibres prepared in ethanol/water mixture and isopropanol/water mixture were reported to be ribbon-like whereas those prepared in acetic acid are round in morphology at lower concentrations and ribbon-shaped at higher concentrations. This is expected to be due to the different evaporation speeds of the solvent. The evaporation of the solvent leads to a pressure difference between the inner and outer space of the fibre and causes tubular structure collapse. An increase in the concentration of the solution causes increased pressure difference and that's why a higher concentration of zein in acetic acid produce flat ribbon-shaped fibres (Li et al., 2013). Comprehensive information regarding the shape of the electrospun fibre of zein using different solvent systems is given in table 1.

2.8.2 Crosslinking of zein

Electrospun membranes of zein possess mechanical limitations like brittleness and low water stability. The nanofibres spun in aqueous ethanol don't permit the unfolding of zein protein conformation in such a way that bulky side groups of protein structure prevent ordered alignment. Due to plasticizing effect of water on zein, the nanofibres immediately swell, collapse and become film-like in aqueous conditions (Surendranath, Rajalekshmi, et al., 2022). Crosslinking can improve the water stability of zein matrices. Different crosslinking agents are available to crosslink zein.

Conventional crosslinking agents like formaldehyde and glutaraldehyde are practised by different groups. But the toxicity of the vapour used for crosslinking diminishes its excellency. As zein is a protein and possesses free amino groups, non-cytotoxic agents like polycarboxylic acids eg: citric acid, maleic acid (Yang et al., 1996), or free aldehyde-containing compounds eg: glucose, oxidized sucrose (P Liu et al., 2015; Xu et al., 2015) glyoxal (Selling et al., 2012), etc are recommended. But the main disadvantages of these

methods are time consumption and the use of high temperatures. These cross-linking techniques involve two stages, pre-crosslinking and post-crosslinking. Post-crosslinking is always a heating treatment for annealing modification of new chemical crosslinks formed. Polycarboxylic acid crosslinking demands heating around 120 °C and aldehyde group crosslinking favours heating at 150-170 °C (Koombhongse et al., 2001; Selling et al., 2012). Another crosslinking mechanism proposed by Reddy *et al* is alkali-catalyzed wet crosslinking (Reddy et al., 2009). In this mechanism, the crosslinking solution won't be added to the spinning dope and crosslinking will be done after electrospinning. But the matrix obtained after such a mechanism would be film-like and fails to satisfy the tasks of a porous electrospun matrix.

2.9 POLYETHYLENE OXIDE (PEO)

Polyethene oxide (PEO) is a crystalline, thermoplastic polymer with a chemical formula $H\text{-}(OCH_2CH_2)_n\text{-}OH$. It is a water-soluble polymer commercially available in a wide range of molecular weights from 200 to several million. Low molecular weight members of this group are generally known as polyethene glycol (PEG) and higher molecular weight members are known as polyethene oxide or polyoxyethylene (Lee et al., 1995). PEO is usually synthesized from the ring-opening polymerization of ethylene oxide (Stephan and Thomas, 2009). PEO has been well explored in various biomedical studies because of its non-toxic and non-immunogenic properties (Ottenbrite and Javan, 2005). The suitable solvents for electrospinning PEO are chloroform, ethanol, dimethyl formamide and water. Nanofibrous membranes of PEO were obtained from 3, 4, 7, and 7 wt% solutions in chloroform, ethanol, DMF and water respectively (Son et al., 2004).

Deitzel *et al* have reported electrospinning of PEO alone (Deitzel et al., 2001) and Son *et al* also probed into the effect of solution properties and polyelectrolyte on PEO

electrospinning. Yang *et al* have reported their study on the influence of environmental parameters on the electrospinning of PEO (Yang et al., 2006). Along with electrospinning of individual solutions of PEO, various blend solutions have also been evaluated to improve properties. Kianfar *et al* have developed photocrosslinked nanofibre mats containing a chitosan/PEO blend. The polycationic nature of chitosan always delimited its electrospinning ability which can be overcome by blending with PEO. Photo-crosslinking has caused improvement in water stability and thermal properties (Kianfar et al., 2019). Another blend of PEO with silk fibroin was prepared by Lan *et al* for antibacterial activity. Silk fibroin is a known polymer with good biocompatibility and biodegradability. The brittleness of silk fibroin has improved by blending with PEO. Moreover, silk fibroin/PEO blending has caused an excellent sustained release profile of gentamicin from the membrane (Lan et al., 2022).

2.10 POLYVINYL PYRROLIDONE (PVP)

Polyvinyl pyrrolidone is a linear polymer synthesized from 1-vinyl-2-pyrrolidone monomer units (Nair, 1998). Almost 80 years ago, PVP was first reported in a patent (Kurakula and Rao, 2020) by a German Scientist Walter J. Reppe. It is a water-soluble, stable and hygroscopic polymer. It is an amorphous fragile synthetic material used in a variety of applications (Ingole and Kumbharkhane, 2021). PVP possess excellent physiological compatibility, adhesion, complexation properties and low chemical toxicity (Yang et al., 2004). PVP possess amphiphilic properties owing to the presence of a polar lactam group and non-polar methylene moiety (Koczkur et al., 2015). Bognitzki *et al* first reported electrospinning of PVP polymer solution in 2001. They have prepared polylactide/PVP blend fibres using electrospinning (Bognitzki et al., 2001). Ethanol has been recommended as a single solvent system to electrospun PVP alone. Ethanol/DMF

50:50 mixture is also recommended for producing electrospun nanofibres of PVP. Electrospinning of PVP has been reported to happen within a concentration range of 4-10 % (w/v) which will slightly vary depending on the solvent system used (Yang et al., 2004).

Electrospun fibres of PVP have been extensively investigated for loading and delivering drug molecules. Ibuprofen-loaded fibres have been developed in 2009 by Yu *et al* as an oral fast-dissolving drug delivery system. The major advantage of PVP lies in the fact that it is a good carrier for the delivery of poorly water-soluble drugs as the drug-loaded membrane will dissolve in water immediately (Yu et al., 2009). 3-aminopropyltriethoxysilane functionalized PVP fibres have been studied for the pH-dependent release of curcumin and observed a moderate initial burst release followed by a sustained release (Kurniawan et al., 2017).

2.11 PROPRANOLOL HYDROCHLORIDE (PL)

Propranolol hydrochloride is a non-selective beta-adrenergic blocking drug which competitively inhibits the effects of catecholamines at the beta-adrenergic receptor. Propranolol is a white-coloured crystalline solid with a molecular weight of 295.80 amu and is readily soluble in water and ethanol. It is widely used to treat antihypertensive disorders (Javadzadeh et al., 2008). The antihypertensive action of propranolol includes decreasing cardiac output, inhibiting renin release and restricting synthetic nerve outflow from vasomotor centres in the brain. Propranolol is a lipophilic molecule and undergoes first-pass metabolism in the liver. The oral bioavailability of propranolol has been reported as 25 %. The peak plasma concentration of propranolol occurs about 1 to 4 hours after oral administration. The metabolism of propranolol mainly follows three routes-aromatic hydroxylation, N-dealkylation and side-chain oxidation. The major metabolites

of propranolol are propranolol glucuronide, naphthyloxylactic acid, glucuronic acid and sulfate conjugates of 4-hydroxy propranolol.

Sahoo *et al* have made a comparative study of propranolol hydrochloride release from a hydrophilic matric tablet developed from hydroxypropyl methylcellulose (HPMC) or Kollidone® SR. The release of propranolol from HPMC followed a first-order kinetics and the same from Kollidone® SR followed a zero-order kinetics (Sahoo et al., 2008). A comparative evaluation of the release profile of propranolol from uniaxially and co-axially electrospun matrices was evaluated by Oliveira *et al*. Poly(cyclodextrin) and poly (methacrylic acid) were electrospun to develop a delivery system for propranolol. The annealing process between poly(cyclodextrin) and poly (methacrylic acid) facilitated the formation of hydrophobic nanofibres to release propranolol. Uni-axially spun fibres exhibited burst release which was overcome by co-axially spun fibres (Oliveira et al., 2015). Another group of researchers reported an adhesive mat based on polyvinyl alcohol developed through an electrospinning technique for oral mucosal delivery of propranolol in paediatric patients (Pérez-González et al., 2022).

2.12 SCOPE AND OBJECTIVE OF THE PRESENT WORK

Several attempts have already been made to develop and evaluate electrospun membranes for mucoadhesive drug delivery applications using various available polymers. Zein protein is Generally Recognized As Safe and FDA approved for human applications (Kariduraganavar et al., 2019). The weak mechanical properties of electrospun zein membranes constrained the exploration of its potential applications. Hence, the potential of zein protein for mucoadhesive drug delivery has been less investigated. If it is possible to develop a mechanically sound, fibroporous electrospun membrane of zein for mucoadhesive applications, it would be a new information to add to the existing

knowledge. Additionally, mucoadhesive drug delivery formulations would be benefitting patients with improved bioavailability of drug and advantages of a non-invasive technique.

In that scenario, the objectives of the present scenario have been formulated as listed below.

1. To develop zein electrospun matrix strengthened by crosslinking and blending.
2. To study various drugs used for the treatment of cardiac-neuro diseases and select those which are having low bioavailability. And load the selected drug into the electrospun polymer matrix.
3. To study the drug release kinetics.
4. To study the mucoadhesive capacity of the polymer matrix.
5. To study the physico-chemical characteristics of the polymer matrix.
6. To study the cell- material interactions of the polymer matrix.

The primary objective of the foregoing research is to overcome the mechanical shortcomings of electrospun zein membranes by various methods like blending, crosslinking etc. The study also evaluates the possible functional modifications of zein to improve its mucoadhesive properties. This study involves blending zein with PEO or PVP for improving the mechanical as well as mucoadhesive properties of electrospun membranes. Physical crosslinking mechanisms like UV crosslinking and thermal crosslinking have been employed in this work as post-crosslinking techniques. Apart from simple polymer blending and physical crosslinking, functional modification has also been investigated. Thiol modification, boronic acid modification and mucin incorporation have been evaluated for electrospun membranes of zein blends.

Propranolol hydrochloride has been chosen for the current study to incorporate in electrospun membrane of zein blend or modified zein blend. The rationale for choosing propranolol hydrochloride is its low oral bioavailability, which is around 25 %. It is expected that the mucosal delivery of propranolol hydrochloride increases its bioavailability and consequently dosage frequency can be reduced. Propranolol hydrochloride being an antihypertensive drug, its mucoadhesive delivery will be a boon to the patients suffering from dysphagia conditions related to Parkinsons disease.

Drug release studies will be carried out in PBS medium of pH 7.4, *in-vitro* conditions through RPMI 2650 cells and *ex-vivo* conditions through porcine buccal mucosa. The mucoadhesive properties of the optimized electrospun membranes will be evaluated in porcine buccal mucosa using Texture analysis. Chemical characterizations like FTIR, UV, XPS, CD, Raman spectroscopies will be done. Thermal characterizations like TGA, DSC and DMA will also be done along with mechanical characterisation using UTM. Surface morphology will be evaluated using SEM and surface wettability will be also analysed.

The electrospun membranes with and without drug loading will be subjected to cytocompatibility evaluation using RPMI 2650 cells. Direct contact assay, MTT assay and Live/dead assay will be done. The influence of material on the epithelial integrity of RPMI 2650 cells will be investigated using F-actin staining, immunostaining of β-catenin protein of adherens junction and TEER (%) evaluation.

3 MATERIALS AND METHODS

3.1 MATERIALS

The materials used in this research work is listed below in table 2 with specifications and source.

Table 2 Name, specifications and source of materials used in the research work

Sl.No	Material	Grade/Specifications	Source
1.	3-aminophenyl boronic acid monohydrate	Purified powder	Sigma Aldrich, USA
2.	5,5-Dithiobis(2-nitrobenzoic acid)	Ellman's reagent, Minimum assay: 97.0 %	Himedia, India
3.	Antibiotic-antimycotic solution (100X)	Contains 10,000 units of Penicillin, 10,000 µg of Streptomycin and 25 µg of Amphotericin B in a 0.85 % saline solution. Effective against bacteria, fungi and yeast.	Genetix, Cell Clone, India
4.	Borax	ACS Reagent ≥ 99.5 %	Sigma Aldrich, USA
5.	Boric acid	≥ 99 %	Merck, India
6.	Calcium chloride	Fused, for elementary analysis	Sd fine Chemicals Ltd, India
7.	Cysteine hydrochloride monohydrate	European Pharmacopeia Reference Standard	Sigma Aldrich, USA
8.	Dipotassium hydrogen phosphate	Pro analysis	Merck, India
9.	Disodium hydrogen phosphate	Anhydrous for analysis EMSURE®, ACS Reag.Ph Eur	Merck, India

10.	DMSO	For DNA and peptide synthesis	Merck, India
11.	Dulbecco modified Eagle's Medium (DMEM-HG)	With high glucose, L-glutamine and sodium pyruvate	Sigma Aldrich, USA
12.	Ethanol	95 % purity	Himedia, India
13.	Fetal Bovine Serum (FBS)	South American Origin	Genetix, Cell Clone, India
14.	Goat anti-mouse polyclonal antibody	Goat pAb to Ms Ig G-Alexa Fluor® 488	Abcam
15.	Hoechst 33258	10 μg/mL solution	Origin Lab, India
16.	Hydrochloric acid	ACS reagent, 37 %	Merck, India
17.	Live dead kit	Double stain apoptosis detection kit,(Acridine orange/Ethidium bromide)	Origin Lab, India
18.	Magnesium chloride hexahydrate	For analysis EMSURE® ISO	Merck, India
19.	Magnesium sulfate heptahydrate	Pure, for analysis	Merck, India
20.	Monoclonal anti-beta catenin antibody	Puregene	Genetix, India
21.	MTT reagent A	Study of cell and mitochondrial health	Himedia, India
22.	Mucin from porcine stomach	Type III, bound sialic acid 0.5-1.5 %, partially purified powder	Sigma Aldrich, USA
23.	N-(3-dimethylaminopropyl)-N'-ethylcarbodiimide hydrochloride (EDAC or EDC)	Commercial grade, powder	Sigma Aldrich, USA

24.	Paraformaldehyde (PFA)	Reagent grade, crystalline	Sigma Aldrich, USA
25.	PEO	Average M_v = 6,00,000 Inhibited with 200-500 ppm, BHT	Sigma Aldrich, USA
26.	Phenol	For molecular biology	Merck, India
27.	Picrylsulfonic acid solution (TNBS)	5 %(w/v) in H_2O, Bioreagent suitable for the determination of primary amines	Sigma Aldrich, USA
28.	Potassium chloride	For analysis EMSURE® ISO	Merck, India
29.	Potassium dihydrogren phosphate	For analysis EMSURE® ISO	Merck, India
30.	Propranolol hydrochloride	Industrial grade	Microlabs Limited, India
31.	PVP	Average mol wt 3,60,000	Sigma Aldrich, USA
32.	Rhodamine/phallloidin	Invitrogen	Thermo Fisher scientific
33.	RPMI 2650	Nasal septum epithelial cells of a 52-year-old male patient with squamous cell carcinoma	NCCS, Pune, India
34.	Sodium chloride	EMSURE®	Merck, India
35.	Sodium hydrogen carbonate	For analysis	Merck, India
36.	Sodium hydroxide	Pellets for analysis	Merck, India
37.	Trans well inserts	Polycarbonate membrane, pore size 0.4 µm, Growth area 0.33 cm^2	Himedia, India
38.	Trypsin-EDTA 0.25 %	Contains 0.05 % Trypsin and 1 mM EDTA in	Himedia, India

		Hank's Balanced Salt Solution without calcium and magnesium sterile filtered Porcine parvovirus and mycoplasma tested.	
39.	Zein	Biological source maize, powder	Sigma Aldrich, USA
40.	α-D-glucose	Anhydrous 96 %	Sigma Aldrich, USA

3.2 METHODS

3.2.1 Synthesis of modified zein polymer

3.2.1.1 Thiol modification of zein

Thiol modification of zein was carried out using cysteine amino acid. The basic mechanism behind the modification is the conjugation reaction between amino group of zein and carboxyl group of cysteine via EDC crosslinking to set more thiol groups free on the polymer chain of zein. A 30 % (w/v) of zein solution was prepared in 8:2 EtOH/H_2O solvent at room temperature by magnetic stirring. The carboxylic acid groups of zein were activated for conjugation by adding 1-ethyl (dimethyl aminopropyl) carbodiimide (EDC) of 2 mM concentration. EDC of volume 20 µL was added by dissolving in KH_2PO_4 buffer of pH 8 (Majzoob et al., 2006). The activation reaction was continued for 45 min and later L-cysteine hydrochloride was added with concentration 5, 10, 15, 30 and 50 % (w/w). The solution was then stirred at room temperature again till complete dissolution. The solution was then solvent casted at 40 °C in air oven. The EDC crosslinking involves the formation of isourea by product at the end of the reaction which has to be removed off. Since zein is a water insoluble polymer system the isourea removal

was done so easy by washing the casted film in water. The washing was continued until the UV absorption peak of isourea vanishes in the washed off water samples. The washed film was then dried at 40 °C in air oven, crushed into small pieces and stored at room temperature.

3.2.1.2 Mucin crosslinking of zein

Mucin is a glycoprotein present in the mucosa of mucosal tissue surface. Mucin from porcine stomach was purchased and crosslinked with zein via EDC crosslinking. A 15 % (w/v) of zein solution was prepared in 7 mL EtOH. Another solution of mucin of concentration 0.5 % and 1 % (w/v) (0.5 g, and 1 g respectively) was prepared in 3 mL phosphate buffered saline (PBS) of pH 7.4 at room temperature. EDC was prepared of concentration of 2 mM and added to mucin solution. The EDC activation reaction was continued for 45 min by magnetic stirring. After activation, mucin and zein solutions were mixed by keeping the magnetic stirring on for one solution and stirred well till thorough mixing. The solution was then casted at 40 °C overnight. In this modification also, isourea by product of EDC activation has to be removed off, for which casted film was washed with distilled water isourea peak in UV spectra disappears. The washed film was again dried, crushed into small pieces and stored at room temperature. Mucin crosslinked zein films were represented as MUZ.

3.2.2 Preparation of polymer solution

3.2.2.1 Zein/PEO blend solution

The blend solution of zein with PEO was prepared in 8:2 EtOH/H_2O solvent mixture. Initially, zein solution of 30 % (w/v) concentration was prepared in 10 mL 8:2 EtOH/H_2O solvent at room temperature by magnetic stirring. To the above solution 5 % (w/w) of polyethylene oxide (PEO) was added and dissolved well.

3.2.2.2 Thiol-modified Zein/PEO solution

For all five compositions of thiol-modified zein, 33 % (w/v) was taken and dissolved in 10 mL of 8:2 EtOH/H_2O. Polyethylene oxide (PEO) was then added to the above solution in 3 % (w/w) concentration corresponding to the weight of zein in each composition. The whole mixture was dissolved well under magnetic stirring.

3.2.2.3 Zein/PVP solution

Zein solution of concentration 15 % (w/v) was prepared in 10 mL EtOH. Polyvinylpyrrolidone (PVP) of 5 % concentration (w/v) was added to the zein solution and mixed under magnetic stirring at room temperature.

3.2.2.4 Mucin crosslinked Zein/PVP solution

Mucin crosslinked zein film pieces were taken of weight 1.55 g and 1.6 g for three compositions crosslinked with 0.5 g mucin and 1 g mucin respectively. The film pieces were dissolved well in 10 mL 7:3 EtOH/PBS solvent mixture at room temperature. After completely dissolving the film, 5 % (w/v) of Polyvinylpyrrolidone (PVP) was added to the above and stirred well. The solution was designated as MUZPVP.

3.2.2.5 Zein/APBA conjugated PVP solution

3-aminophenyl boronic acid (APBA) was weighed out and dissolved in 10 mL EtOH at room temperature to prepare 10 mM, 20mM and 50 mM concentration solutions. 5 % (w/v) of PVP was added to the above solution and stirred under room temperature. Subsequently, 15 % (w/v) of zein was added to the solution and dissolved well.

3.2.3 Drug loading in the polymer solution

From reference literature it is concluded that propranolol hydrochloride (PL) have the non-cytotoxic concentrations of PL which falls in the range of 0.01 mM to 0.05 mM

(Hajighasemi and Mirshafiey, 2009). PL was loaded in five concentrations (0.01 mM, 0.02 mM, 0.03 mM, 0.04 mM and 0.05 mM) to all the above four polymer solutions prior electrospinning.

3.2.4 Electrospinning of polymer solution

The electrospinning of five of the polymer solutions mentioned above were carried out using 10 mL syringe fixed in KD Scientific Pump. High voltage was applied on the syringe needle for the formation of nanofibres using high-voltage power supply from Zeonics Systech, Bangalore (Surendranath, Rajalekshmi, et al., 2022). The various electrospinning parameters are listed in the table 3 below.

Table 3 Electrospinning parameters for various electrospun membrane systems

Polymer solution	Flow rate	Applied voltage	Mandrel rotation speed	Syringe needle used	Distance
Zein/PEO	5 mL/h	16 kV	1500 rpm	18 gauge	10 cm
Thiol-modified Zein/PEO	5 mL/h	15 kV	1500 rpm	18 gauge	10 cm
Zein/PVP	5 mL/h	15 kV	1500 rpm	18 gauge	10 cm
Mucin crosslinked Zein/PVP	5 mL/h	15 kV	1500 rpm	18 gauge	10 cm
Zein/APBA conjugated PVP	5 mL/h	15 kV	1500 rpm	18 gauge	10 cm

3.2.5 Post-electrospinning crosslinking technique

3.2.5.1 UV crosslinking of electrospun Zein/PEO membrane

The crosslinking of Zein/PEO electrospun membrane was done after electrospinning via UV irradiation. The electrospun membrane was placed in an UV chamber fixed with UV light of intensity 180 $\mu W/cm^2$ (Toshiba FL15sbl, 350 nm, 15W). The UV treatment was

done for 24 h and the material was stored at room temperature in self-lock cover after treatment.

3.2.5.2 Thermal crosslinking of electrospun Zein/PVP membrane

The physical crosslinking technique adopted for polyvinylpyrrolidone is thermal treatment. After electrospinning the membrane was placed in OV-11 vacuum oven for 10 h at 120 °C. After thermal crosslinking the material was taken off and stored in a self-lock cover at room temperature.

3.2.5.3 Thermal crosslinking of electrospun mucin crosslinked Zein/PVP membrane

The mucin crosslinked Zein/PVP electrospun membrane also requires a post-electrospinning physical crosslinking for which thermal treatment is preferred. The electrospun membrane was placed in OV-11 vacuum oven at 100 °C for 10 h. The crosslinked sample was kept in a self-lock cover and stored at room temperature.

3.2.6 Characterization methods

3.2.6.1 Physico-chemical characterizations

3.2.6.1.1 Scanning Electron Microscopy (SEM)

The surface morphology of the electrospun samples were analysed using scanning electron microscopy. The polymer samples were gold coated prior to make them conductive using Hitachi, E-1010 Ion sputter. Scanning electron microscope (FEI Quanta 200, Netherlands) was used to image surface morphology of the membrane by placing the samples on an aluminium stub under vacuum. SEM images were subjected to imageJ analysis to find out fibre diameter, directionality and fibre orientation.

3.2.6.1.2 Fourier Transform Infrared (FTIR) Spectroscopy

The degree of modification, extent of crosslinking and chemical composition of samples were evaluated based on Fourier Transform Infrared (FTIR) spectroscopy. Attenuated Total Reflectance (ATR) method was adopted for the analysis. Samples were evaluated in the form of electrospun polymer sheet, powder etc. The spectra were recorded in the range of 4000 – 400 cm^{-1} using PerkinElmer Series Spectrum two (USA).

3.2.6.1.3 Raman Spectroscopy

Raman spectroscopy was done to evaluate chemical composition of the polymer samples used. The Raman spectra was analysed using method adopted from Witec Manual. The instrument was calibrated using silicon calibration standard before experiment. The samples were immersed in water in a glass petri dish which is placed on the microscope table and observed using 60x water immersion objective and focused. Confocal Raman Microscope, alpha 300A, Witec Inc. Germany was used for imaging. The sample was then excited using 532 nm Laser and the spectra was recorded. The integration time was 2 s. The grating used was 600 lines/mm.

3.2.6.1.4 Circular Dichroism (CD) Spectroscopy

The circular dichroism spectroscopy was performed using Jasco 810 spectrometer equipped with Peltier thermostatic cell holders. The CD spectra was recorded as θ in millidegrees. Electrospun samples of interest were dissolved in appropriate solvents to perform the spectroscopy analysis. The measurements were taken by scanning within the range of 200 – 400 nm (Surendranath, Rajalekshmi, et al., 2022).

3.2.6.1.5 Porosity Analysis

The percentage of porosity was analysed by density method of calculation. Replicates of samples (n=6) were cut in the shape of disc having 2 cm diameter and weighed. The porosity was calculated by the equation 3 (Remya et al., 2018; Zhang et al., 2014),

$$\boldsymbol{Porosity}\ (\%) = \left(\mathbf{1} - \frac{\boldsymbol{d}}{\boldsymbol{D}}\right) \times \mathbf{100} \qquad \textbf{(3)}$$

Where d is the apparent density in g/cm^3 which is devoid of the density of the pores. D is the bulk density and the ratio of difference of apparent and bulk density gives to the bulk density gives the percentage porosity. The d and D are calculated by the below equation,

$$\boldsymbol{D} = \frac{\sum \boldsymbol{Mass\ of\ indivudual\ compounds}}{\sum\left(\boldsymbol{mass\ of\ indivudual\ compound} / \boldsymbol{density\ of\ indivudual\ compound}\right)} \qquad \textbf{(4)}$$

$$\boldsymbol{d} = \frac{\boldsymbol{Weight\ of\ electrospun\ sample}}{\boldsymbol{Area}\ (\boldsymbol{\pi r^2}) \times \boldsymbol{Thickness}(\boldsymbol{h})} \qquad \textbf{(5)}$$

3.2.6.1.6 Water Contact Angle Analysis

The wettability of polymer samples was analysed using casted films of the same. The polymer film was cut in 6 cm x 2 cm dimension and pasted on a glass slide. The contact angle was determined by adopting sessile drop method. OCA 15 Plus optical contact angle instrument was used for the analysis and images were obtained using SCA 20 software. Five replicates of imaging and measurements were taken for each sample and the mean value was taken.

3.2.6.1.7 Viscosity Measurement

Viscosity of the polymer solutions were measured using Anton Paar, Rolling-ball micro viscometer (Lovis 2000 M/ME). The measurement was done using 2.5 mm capillary at 37 °C with a rolling steel ball. The instrument measured the rolling time of the ball through the polymer solution based on Hoeppler's falling ball principle. Dynamic

viscosity, kinematic viscosity and shear rate were recorded from the instrument and kinematic viscosity is reported.

3.2.6.1.8 Ellman's Assay

The Ellman's assay was done to quantitatively evaluate the concentration of thiol groups in a sample. Ellman's reagent is chemically 5,5'-dithiobis-(2-nitrobenzoic acid) or DTNB in abbreviated form. The disulfide bond reacts with DTNB and get cleaved to 2-nitro-5-thiobenzoate (TNB^-) which further ionize to TNB^{2-} at neutral and alkaline pH which gives a yellow colour. Cysteine amino acid containing thiol functional group was used as reference material for preparing standard calibration curve within concentration range 500 µM to 15.6 µM. Ellman's reagent was prepared in KH_2PO_4 buffer of pH 8 in 4 mg/mL concentration. The absorbance was measured at 412 nm with KH_2PO_4 buffer as blank.

Thiol group estimation of desired samples was done by adding 100 µL of Ellman's reagent to the 0.01 g sample taken. It was then diluted to 2000 µL using KH_2PO_4 buffer. The absorbance was then taken immediately without keeping it for incubation. The corresponding concentration of thiol groups was calculated from the trendline equation of calibration curve.

3.2.6.1.9 TNBS Assay

Trinitrobenzene sulfonic acid (TNBSA) was used to quantitatively estimate the amount of primary amino groups in the sample. The basic mechanism of the estimation technique is that the TNBSA reacts with primary amino group of samples under test to rapidly form a chromogenic derivative which is yellow-orange in colour. The absorbance of chromogenic derivative was measured at 420 nm. The simple amino acid glycine is used as the standard for the calibration curve within concentration range 2.5 µg/mL to 0.015 µg/mL.

The estimation was done in borax-boric acid buffer of pH 9. The buffer was prepared by dissolving 0.47 g of boric acid and 0.25 g of borax in 100 mL distilled water and pH was adjusted to 9. The concentration of stock solution of TNBSA purchased was 5 % and it is diluted to 0.1 % using borax-boric acid buffer. The samples were weighed to 0.05 g and added with 500 µL of 0.1 % of TNBSA solution along with 1000 µL buffer and incubated at room temperature for 30 min. The coloured solution was then taken for UV spectroscopy to measure the absorbance. The solution was diluted to 10 times (300 µL sample solution and 2700 µL buffer) before measuring absorbance. The trendline equation of calibration curve was used to calculate the concentration of primary amino groups.

3.2.6.1.10 UV spectroscopy for the quantification of degree of APBA conjugation

Quantification of 3-aminophenyl boronic acid (APBA) was done using UV spectroscopy. The standard calibration curve of APBA in distilled water at 305 nm water prepared within 0 to 1 mM concentration. Pre-weighed samples were immersed in distilled water and UV absorbance was measured at pre-determined time periods at 305 nm. The corresponding concentration calculated from the calibration curve is the amount of APBA leached out from the samples. Triplicates of samples were evaluated. Degree of conjugation (%) was then calculated by the below equation 6.

$$\%\ \boldsymbol{Degree\ of\ conjugation} = \left(\frac{\boldsymbol{Initial\ APBA\ concentration - Leached\ out\ APBA\ concentration}}{\boldsymbol{Initial\ APBA\ concentration}}\right) \times \mathbf{100} \qquad \textbf{(6)}$$

3.2.6.1.11 Thermogravimetric (TGA) Analysis

The thermal stability and thermal decomposition of samples of interest were analysed using thermogravimetric analysis. Samples were taken in a sample container made of platinum cup and calcined alumina was taken as the reference material in another platinum cup container. Nitrogen atmosphere was maintained in the chamber and is heated from room temperature to 800 °C with a heating rate of 10 °C/min. The experiment

was done in SDT Q600 instrument. The output obtained was in terms of weight loss corresponding to temperature. Graph of percentage weight loss against temperature was plotted. The temperature corresponding to onset of weight loss and 50 % weight loss were noted. The pattern of thermal decomposition was also analysed.

3.2.6.1.12 Differential Scanning Calorimetry (DSC) Analysis

Differential Scanning Calorimetry is a technique to analyse the thermal properties of samples. ASTM standard D 3418-21 was used for the analysis in the instrument DSC Q20, USA. The entire analysis was carried out under nitrogen atmosphere and N_2 gas was purged at a flow rate of 50 mL/min. The samples were weighed in a Tzero pan and sealed. The sample pan and reference pan were placed carefully on the front and rear platforms respectively in the Tzero cell. The temperature scan was done in the range of -50 °C to 200 °C at a rate 10 °C/min. The DSC result gave information about glass transition temperature (T_g), melting temperature (T_m) and crystallization temperature (T_c).

3.2.6.1.13 X-ray diffraction (XRD) Analysis

X-ray diffraction (XRD) analysis was done in polymer samples to evaluate the crystallinity. Wide-angle X-ray Scattering measurement was carried out in XEUSS 2DSAXS/WAXS system using a Genixmicro source from Xenocs operated at 50 kV and 0.6 mA. The Cu Kα radiation (λ = 1.54 A^0) was collimated with a FOX2D mirror and two pairs of scattering fewer slits from Xenocs. The 2D- patterns were recorded on a Mar 345 image plate and processed using the Fit2D software. Silver behenate was used as standard material for calibration.

3.2.6.1.14 X-ray Photoelectron Spectroscopy

X-ray Photoelectron Spectroscopy (XPS) was used for the evaluation of elemental composition. Both survey spectra and high-resolution spectra were recorded using XPS,

PHI 5000 VersaProbe, II, ULVAC_PHI Inc.USA equipped with micro-focused monochromatic Al-Kα X-ray source. Survey spectra was recorded using 50 W power and 187.85 eV pass energy. High resolution spectra were recorded at 46.95 eV pass energy. The data was processed using PHI's Multipak software.

3.2.6.1.15 Universal Testing Machine (UTM) Analysis

The static mechanical properties of electrospun samples were analysed to evaluate the tensile strength, Youngs modulus and elongation at break (%). The analysis was carried out in Universal Testing Machine (UTM;Instron 3345, single column, UK). Dumbbell specimens were cut using pneumatic die cutter, ATS faar, Italy as per ISO 527-2 Type 5B. The experiment was done using 100 N load cell under a crosshead speed of 18 mm/min. A minimum of six specimens were analysed for each sample and stress-strain curve was obtained. All the required mechanical property informations were determined from the stress-strain result obtained.

3.2.6.1.16 Dynamic Mechanical Analysis (DMA)

Viscoelastic properties of polymer films are analysed using Dynamic Mechanical Analysis in Triton Thermoanalyzer DMA Tritec 2000. Tension mode of DMA analysis was used for sample testing. Samples of dimension 10 mm x 4 mm x 0.2 mm (L x W x H) were subjected to temperature sweep analysis from room temperature to 50 ºC at 1 Hz frequency. Storage modulus and tan delta versus temperature thermogram was plotted and analysed.

3.2.6.1.17 Mucoadhesion study using Texture analysis

Mucoadhesion was analysed using Texture analyser (TAXT Plus, Stable Micro Systems, UK). Samples were cut in 12 mm diameter disc shapes and attached to a probe using double sided adhesive tape. Carcass tissue of porcine buccal mucosa was collected

(IAEC/LAS/TR-005/Y20) and cut into 2 cm x 2 cm pieces before experiment. Mucosal tissue was mounted in a rig (Mucoadhesion Rig A/MUC) to which probe was lowered by applying a downward force of 50 g. The probe was allowed to stay on the surface of mucosa for 60 sec and then detached from the surface. The force required for the detachment was recorded. Force-distance curve was obtained from the Exponent software. The area under the curve denotes the work of adhesion.

3.2.6.2 Drug release study

3.2.6.2.1 Percentage of drug entrapment

The drug entrapment was calculated by drug dissolution study. Samples of size 1 cm x 1 cm were cut from the drug loaded electrospun membrane and dissolved in corresponding solvent system. The volume of solvent chosen is the same as the volume of polymer solution electrospun to prepare the membrane. Similarly, electrospun membranes without drug loaded was also dissolved in corresponding solvent system of volume equal to the electrospun polymer solution volume. Absorbance of propranolol hydrochloride loaded samples was measured at 290 nm with samples without drug dissolved in solvent as blank. Triplicates of measurements were taken for every formulation. The experimental concentration of entrapped drug was calculated from the absorbance based on trendline equation of calibration curve of propranolol hydrochloride. Electrospinning involves loss of certain amount of polymer due to fibre wastage hence the theoretical amount of drug loaded in the membrane won't be the same as dissolved in the solution. Therefore, theoretical amount of drug loaded or expected amount of drug was calculated corresponding to the final weight of electrospun membrane as given in the equation 7 below. The drug entrapment percentage is then calculated from the theoretical and

analysed amount of drug in the membrane. Drug entrapment was calculated for all the five formulations of each system by equation 8.

$$\textbf{\textit{Theoretical or expected amount of drug loaded in the membrane}} = \frac{\textbf{\textit{Final weight of membrane}} \times \textbf{\textit{dissolved amount of drug}}}{\textbf{\textit{Total weight of polymer taken for electrospinning}}} \quad \textbf{(7)}$$

$$\textbf{\textit{Drug entrapment}}\ (\%) = \frac{\textbf{\textit{Analysed amount of drug in the membrane}}}{\textbf{\textit{Theoretical amount of drug in the membrane}}} \times \mathbf{100} \quad \textbf{(8)}$$

3.2.6.2.2 Percentage of drug loading capacity

The loading capacity of a drug dosage formulation is the percentage weight of entrapped drug with respect to the total weight of membrane. The equation followed to calculate loading capacity (%) is given below. Loading capacity was calculated for all the five formulations of each system.

$$\textbf{\textit{Loading capacity}}\ (\%) = \frac{\textbf{\textit{Analysed amount of drug in the membrane}}}{\textbf{\textit{Total weight of the membrane}}} \times \mathbf{100} \quad \textbf{(9)}$$

3.2.6.2.3 Drug release kinetics

The membrane with highest loading capacity was selected for drug release kinetic analysis. Cumulative drug release concentration and cumulative drug release percentage were calculated after measuring the concentration of drug released to PBS. Another calibration curve of propranolol hydrochloride was prepared in PBS medium for this analysis. Membrane samples were cut in 1 cm x 1 cm dimension and immersed in 5 mL PBS of pH 7.4. At each pre-determined time periods, 3 mL of PBS were taken out for UV -visible spectroscopy analysis and replenished with fresh 3 mL PBS. The absorbance was measured at 290 nm. Cumulated drug concentration and drug release (%) were plotted against time.

3.2.6.2.4 Mathematical model fitting of drug release

The cumulative drug release percentage obtained was plotted against time and tried to fit with mathematical model of drug release. Up to 60 % of drug release data was chosen and fitted with mathematical equations of each mathematical model in Microsoft excel. Arbitrary values of constants were given for all models. The square deviation and sum of square deviation (SSD) of fitted value with real value obtained was calculated. Later, the sum of square deviation (SSD) was subjected to 'solver' operation in Excel by giving command to minimize the same by adjusting the value of constants of the equation. Once the SSD is solved, correlation coefficient (R^2) of new fit value with real value of cumulative drug release (%) was calculated. The mathematical model showing maximum value of R^2 was selected as the best fit model.

3.2.6.3 Biological characterizations

Biological evaluation of the membrane samples fabricated with and without drug loading was done in RPMI 2650 cells. RPMI 2650 cells were procured from National Centre for Cell Science (NCCS), Pune, India. RPMI 2650 cells belong to the class of epithelial (Kreft et al., 2015) cells collected from the nasal septum of a male patient with squamous cell carcinoma. RPMI 2650 cells were grown in High Glucose-Dulbecco modified Eagles Medium (DMEM) supplied from Sigma Aldrich supplemented with 10 % Fetal Bovine Serum (FBS) and 1 % antibiotic-antimycotic solution procured from Cellclone, India (Kürti et al., 2012).

3.2.6.3.1 Direct contact assay

Direct contact assay is the qualitative method of analysis of *in-vitro* cytotoxicity. Qualitative assessment of cytotoxicity of the materials was done in RPMI 2650 cells. Cells at a density of 1 x 10^5 cells/well were seeded in a 48 well plate and incubated at conditions - 37 °C, 5 % CO_2 and 95 % humidity until confluency. Electrospun samples

cut in 4 mm diameter were sterilized under UV irradiation and placed over the cell monolayer. The material-cell system was then again incubated at conditions- 37 °C, 5 % CO_2 and 95 % humidity for 24 h. Discs of tin coated PVC (Polyvinyl pyrrolidone) and UHMWPE (Ultra High Molecular Weight Polyethylene) treated cells were considered as the positive and negative control respectively. Six replicates of samples were analysed for each membrane system. After 24 h, phase contrast images of the material over cell monolayer were taken using Leica DMI 3000-B microscope to determine the cytotoxic influence of the material on the cell monolayer (Rajalekshmi et al., 2021).

3.2.6.3.2 MTT Assay

MTT assay is a quantitative cytotoxicity estimation technique. It is a colorimetric assay to measure the metabolic activity of cells and thus estimate the cell viability. MTT is chemically 3-(4,5-dimethylthiazol-2-yl)2,5-diphenyl tetrazolium bromide. RPMI 2650 cells were seeded in a 96 well plate at a density of 5 x 10^4 cells/well and incubated at conditions - 37 °C, 5 % CO_2 and 95 % humidity until confluency. Materials were cut in such a way that the total surface area is 6 cm^2. Such samples were sterilized under UV irradiation and immersed in sterile 1 mL PBS or DMEM complete media for 24 h at conditions like 37 °C, 5 % CO_2 and 95 % humidity. After 24 h, the extracts were collected. Once the cells achieve confluency, material extracts in PBS were added to the cell monolayer in the dilution ration of 1:10, where the dilution was done using 2X complete media. A minimum of six replicates were tested for each sample. After adding extracts, the cell-extract system was again incubated at 37 °C, 5 % CO_2 and 95 % humidity for 24 h. MTT reagent was prepared in PBS at a concentration of 5 mg/mL. After 24 h of incubation 20 µL of MTT reagent was added to each well and incubated for 4 h. Later, the reagent containing media was removed and the purple-coloured crystals in the wells are solubilized in 100 µL DMSO. The yellow coloured MTT dye will be

reduced to purple coloured formazan by the oxidoreductase enzymes in viable cells. Therefore, the amount of formazan complex formed will be representing the number of viable cells present. The quantity of formazan formed is determined by measuring the absorbance at 570 nm (Kumar et al., 2018). The negative control of the experiment was the cells without material treatment and positive control was the cells added with phenol. The percentage of cell viability was calculated from the equation 10 below.

$$\textbf{\textit{Cell viability}}\ (\%) = \frac{\textbf{\textit{Absorbance of the material added cells}}}{\textbf{\textit{Absorbance of the negative control cells}}} \times \mathbf{100} \qquad \textbf{(10)}$$

3.2.6.3.3 Live/dead assay

Live/dead assay is another technique for the qualitative evaluation of cytotoxicity via fluorescent imaging. Ethidium bromide/Acridine Orange (EtBr/AO) live/dead assay kit procured from Origin lab was used. Ethidium bromide stains the dead cells and visualize as red. Ethidium bromide is actually staining the nucleus of the dead cells because the dead cells lose the cytoplasmic membrane integrity. Acridine Orange selectively binds with the nucleic acid via intercalating with DNA and RNA through electrostatic interactions. RPMI 2650 cells were seeded in a 4 well plate at 1 x 10^5 cells/well density and incubated at 37 °C, 5 % CO_2 and 95 % humidity till confluency. The material extracts were added over the cell monolayer and the extraction was done in PBS for 24 h with electrospun samples of total surface are 6 cm^2. 10X dilution of the material extracts in 2X complete culture media was added over the cells and incubated at 37 °C, 5 % CO_2 and 95 % humidity for another 24 h. After 24 h, the media was removed and the cells were stained using Ethidium bromide/Acridine Orange staining kit. The concentration of stock solution of both Ethidium bromide and Acridine Orange is 1 mg/mL. Both of the stains were diluted to 20 µg/mL and mixed in 1:1 ratio. The dilution of Ethidium bromide was done in water and that of Acridine Orange in AO dilution buffer. The mixture of

stains of volume 50 µL was added to each well and added with additional 200 µL PBS. Fluorescent images were taken immediately within 10 min in Leica DMI 3000-B. Excitation and emission wavelength of Ethidium bromide are 301 nm and 603 nm respectively. The same for Acridine Orange are 500 nm and 526 nm respectively.

3.2.6.3.4 Actin staining

Table 4 Excitation and Emission wavelength of Rhodamine/phalloidin and Hoechst

Stain	Excitation wavelength (nm)	Emission wavelength (nm)
Rhodamine/phalloidin	540	565
Hoechst	361	497

Fluorescent staining of F-actin filaments gives an idea about the morphology and integrity of cell monolayer. Actin filaments were stained using rhodamine labelled phalloidin purchased from Sigma Aldrich and nucleus was counter stained using Hoechst procured from Origin Lab. Cells at a density of 2 x 10^5 cells were seeded in a coverslip in 12 well plate and incubated at 37 °C, 5 % CO_2 and 95 % humidity till confluency. The material extracts were added over the confluent cell monolayer in 10 X dilution. Material extraction and dilution were done following the already mentioned protocol. The extract added cells were again incubated at 37 °C, 5 % CO_2 and 95 % humidity for 24 h. Later, the cells were fixed in 4 % paraformaldehyde for 15 min followed by three times PBS wash. The fixed cells were kept at 4 °C in PBS overnight. 0.1 % Triton-X-100 was added to the fixed cells for 2-3 min to permeabilize. The methanol stock solution of Rhodamine phalloidin (6.6 µM) was diluted to 0.33 µM in PBS and 50 µL was added to the fixed cells in the coverslip in such a way that the stain spreads throughout the cell monolayer. The stained cells were kept at room temperature at dark condition for 15 – 30 min. Rhodamine stain washed using PBS three times. Hoechst was then added to counter stain nucleus. The stock concentration was 10 µg/mL which then diluted to 0.5 µg/mL in PBS.

The diluted Hoechst solution of volume 50 µL was added at dark condition to the coverslips and washed off after 2 min using PBS for three times. Fluorescent images of the stained cells were taken using Leica DMI 3000-B microscope. Excitation and emission wavelength of Rhodamine/phalloidin and Hoechst are listed in table 4.

3.2.6.3.5 TEER measurement

Transepithelial Electrical Resistance (TEER) evaluates the integrity and permeability of cell monolayer by measuring the electrical resistance across cell monolayer (Srinivasan et al., 2015). Trans membrane polycarbonate membrane inserts of 24 well plate of pore size 0.4 µm and area 0.33 cm^2 were used for the TEER measurement. RPMI 2650 cells at a density of 2 x 10^5 cells/well were cultured in the trans well inserts till the cell monolayer achieve constant transepithelial electrical resistance. The apical chamber containing cells was added with 200 µL media and basolateral chamber with 600 µL media. TEER measurement was done using Milli ERS voltmeter-chopstick electrode system. Once the TEER becomes constant, the cell seeded membrane system was equilibrated with HBSS solution for 1 h at 37 °C, 5 % CO_2 and 95 % humidity conditions. After equilibration, materials were placed in the apical chamber of the insert. TEER of the system was monitored for pre-determined time periods at 37 °C and analysed the influence of mucoadhesive material on the integrity of cell monolayer. TEER (%) values were calculated using the equation 11 below which indicates the change in the transepithelial electrical resistance.

$$\boldsymbol{TEER}\ (\%) = \frac{\boldsymbol{R_t - R_b}}{\boldsymbol{R_0 - R_b}} \times \mathbf{100} \qquad \textbf{(11)}$$

R_t is the resistance at time 't', R_0 is the initial resistance and R_b is the resistance of trans well insert in the absence of cell monolayer.

3.2.6.3.6 In-vitro drug permeation study

RPMI 2650 cells were cultured in a trans membrane insert in 24 well as in the above protocol. After achieving constant value of TEER measurement, media in the apical and basolateral compartments were removed and equilibrated with HBSS for 1 h at conditions - 37 °C, 5 % CO_2 and 95 % humidity. The drug loaded electrospun samples were placed over the cell monolayer after equilibration. Aliquots of permeated drug samples were removed from the basolateral chamber at pre-determined time periods and replenished with fresh HBSS. The samples were analysed using UV spectrometer at 290 nm and *in-vitro* drug permeation was studied. The apparent permeability coefficient (P_{app}) was calculated by the equation 12 below,

$$\boldsymbol{P_{app}} = \frac{\left(\boldsymbol{dQ}/\boldsymbol{dt}\right)}{\boldsymbol{A.C_0}} \qquad \textbf{(12)}$$

Where dQ/dt denotes the slope of the cumulative concentration vs time graph, A is the area of the insert and C_0 is the initial concentration.

3.2.6.3.7 Immunostaining of beta catenin junctional protein

The ability of electrospun membranes to open adherens junction of RPMI 2650 epithelial cell was evaluated via immunostaining junctional proteins. Cells were cultured in a coverslip at a density of 9 x 10^4 cells/coverslip. Membrane samples were placed over the cell monolayer after attaining confluency and incubated at 37 °C, 5 % CO_2 and 95 % humidity for 24 h. After 24 h, material was removed and cells were fixed using 4 % paraformaldehyde as per the protocol mentioned before. The fixed cells were permeabilized using PBS containing 0.1 % triton-X-100 (PBST) followed by PBS washing. The non-specific binding of antibody with the cellular receptors were blocked by incubating with 1 % BSA containing 22.52.mg/mL glycine in PBST for 10 min. Again, the cells incubated with 1:100 dilution of anti-beta catenin antibody procured from

Puregene for 1 h at room temperature under dark conditions. PBS washing was done for three times. Again, the cells were incubated with 1:100 dilution of Goat Anti-mouse IgG H&L (Alexa Fluor® 488) secondary antibody procured from abcam, USA, at room temperature (24 ± 3 °C) under dark. PBS washing was done again for three times. Counterstaining of nucleus was also done using Hoechst following the above-mentioned protocol. Later fluorescent imaging was done in Leica DMI 3000-B.

3.2.6.3.8 Ex-vivo drug permeation through porcine buccal mucosa

Porcine buccal mucosa was collected from sacrificed pigs from animal science laboratory (IAEC/LAS/TR-005/Y20). Tissue samples were transported to laboratory in Phosphate Buffered Saline (PBS) of pH 7.4. Non-keratinized epithelium of porcine buccal mucosa was separated from the connective tissues using scalpel blades and scissors within 6 h of tissue collection. During the separation process, the thickness of the epithelial tissue has to be assured to fall within 500 to 800 μm. In addition, heat separation-based splitting technique was employed to separate epithelial layer from connective tissue beneath. Heat separation was done by immersing porcine buccal mucosa in 0.9 % of NaCl solution (saline) at 60 ºC for just 1 min (Pinto et al., 2020). Franz diffusion cell apparatus was used for the *ex-vivo* drug permeation study. Tissue sample was mounted between a donor and receptor chamber in such a way that epithelial layer faces donor chamber (Kulkarni et al., 2009). The donor chamber was filled with 1 mL PBS and receptor chamber with 20 mL PBS. Later, PL loaded electrospun sample was placed on the top of the mucosa. The entire experimental setup was kept at 37 °C. At each predetermined time periods, 1 mL PBS was collected from the receptor chamber and replenished with fresh PBS. The amount of drug permeated across mucosa was quantified using UV spectroscopy at 290 nm. Permeation coefficient of *ex-vivo* drug permeation was calculated from the cumulative drug permeation curve using equation 12. Permeation coefficient was

compared with control system, where PL alone was added to the epithelial surface of mucosa.

4 RESULTS AND DISCUSSION

4.1 UV CROSSLINKED ZEIN/PEO ELECTROSPUN MEMBRANE AND ITS CHARACTERIZATION

4.1.1 Preparation, drug loading, electrospinning and crosslinking of Zein/PEO matrix

Electrospinning is the technique to generate nanosized fibres from a polymer solution in the presence of an external electric field. The electrospinning process is controlled by various factors like concentration of the polymer solution, applied electric potential, and polymer solution flow rate (Xue et al., 2019). Solutions of lower concentrations are less viscous and result in electrospraying or generate fibres with beads. Increasing the concentration of polymer solution increases viscosity and generates bead-free fibres (Dias Antunes et al., 2017; Koombhongse et al., 2001; Miri et al., 2016). It was observed that the optimised concentration of zein to obtain bead-free fibres is 33 % (w/v).

Five formulations of PL-loaded UV crosslinked Zein/PEO were prepared by incorporating 0.01 mM, 0.02 mM, 0.03 mM, 0.04 mM and 0.05 mM Propranolol hydrochloride (PL) into the polymer blend of zein and PEO.

The inherent limitation of electrospun zein fibres is their brittle nature (Shi et al., 2011). Synthetic polymers of high molecular weight are recommended to blend with zein solution to reduce brittleness and improve mechanical properties. Therefore, high molecular weight polyethylene oxide (PEO) of molecular weight (Mv = 600000) was blended with zein solution. Only 5 % (w/w) of PEO was blended with zein in 8:2 EtOH/H_2O mixture because a higher weight percentage of PEO resulted in increased

viscosity which is not suitable for electrospinning. Finally, 30 % (w/v) of zein and 5 % (w/w) PEO were blended in the solvent mixture.

The blending of zein with PEO alone can't resolve all the mechanical shortcomings of zein. The water stability and related issues remain to be solved. Crosslinking of polymer chains is a wise idea to resolve the problem and thus impart water stability to the system. In this study, crosslinking was carried out under UV irradiation. Optimization of the time of crosslinking was done by analysing the shrinkage and strength of the electrospun matrix under aqueous conditions. Details of the observations in the water stability study have shown in table 5. The electrospun matrix maintained its strength and shape under wet conditions after 24 h UV crosslinking.

Table 5 Observations of water stability studies

Time of crosslinking	Observation in water
0 h	Matrix immediately shrinks in water and loses strength and shape.
1 h	Matrix immediately shrinks in water and loses strength and shape.
4 h	Matrix shrinks in water and loses strength and shape.
9 h	Matrix shrinks in water and loses strength and shape.
16 h	Matrix slowly shrinks in water and loses strength and shape.
20 h	Matrix slowly shrinks in water and loses strength but maintains shape.
24 h	Matrix slowly shrinks in water but maintains strength and shape.

4.1.2 Water stability studies and percentage of water uptake

In the water stability study, the change in dimension and mechanical properties before and after UV crosslinking were analyzed. The dimensional changes for dry and wet samples of uncrosslinked and UV crosslinked Zein/PEO were almost similar. Since the

matrix shrinks in contact with water, the percentage of shrinkage is approximately 30 % in both cases. Though the percentage of shrinkage is the same in uncrosslinked and UV

Table 6 Table comprising tensile strength and Youngs modulus of dry and wet samples before and after crosslinking

	Tensile Strength (MPa)	Youngs Modulus (MPa)
Before crosslinking (Dry sample)	1.79 ± 0.29	186 ± 25
Before crosslinking (Wet sample)	0.10 ± 0.02	0.16 ± 0.07
After crosslinking (Dry sample)	3.52 ± 0.38	293 ± 37
After crosslinking (Wet sample)	0.11 ± 0.007	0.16 ± 0.06

crosslinked matrices, the stability of the matrix in water has improved after crosslinking. Therefore, the shrinkage might be due to the leaching of water-soluble PEO out of the matrix. Hence, it can be inferred that only zein is getting crosslinked under UV irradiation.

Both uncrosslinked and UV crosslinked Zein/PEO shrink in wet conditions. Tensile strength and Youngs modulus decrease for the wet samples (table 6). But the elongation at break of wet samples is more than two hundred times that of dry samples. Elongation at the break of the dry sample of UV crosslinked Zein/PEO is 9.5 ± 1.2 % which has increased to 487 ± 4 % for wet sample (figure 8A). This could be attributed to the plasticizing effect of water molecules. The high surface-to-volume ratio of the electrospun scaffold of Zein/PEO blend facilitates the entry of water molecules into the matrix. So, the flexibility of polymer molecules to slip over each other increases and because of that the elongation at break at wet conditions also increases to more than a

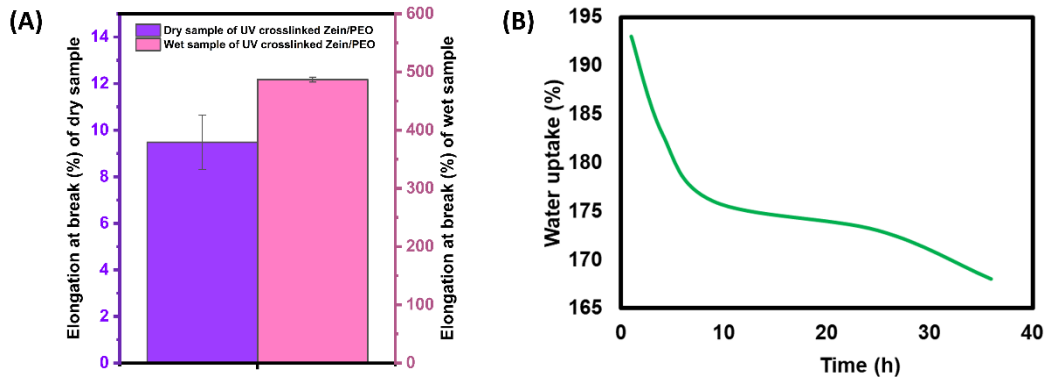

Figure 8 A) Bar diagram representation of elongation at break (%) of dry and wet samples of UV crosslinked Zein/PEO B) Graphical plot of percentage of water uptake

hundred-fold. It was observed that wet samples don't break within short extension but their tensile strength is very less. It elongates to a larger extent before breaking.

Water uptake studies of UV crosslinked Zein/PEO shows a decrease in the values of the percentage of water uptake (figure 8B). This indicates the leaching of certain components out of the electrospun matrix when immersed in water. This might have been the reason behind the reduction in the dimension of the matrix in water. As polyethylene oxide is a water-soluble polymer, we expect that PEO leaches out of the electrospun matrix. Therefore, a constant decrease is observed in the water uptake percentage of UV crosslinked Zein/PEO.

4.1.3 Fourier Transform Infra-red (FTIR) Spectroscopy

The FTIR spectrum of native zein is shown in figure 9A. It shows six characteristic peaks of protein structure (Corradini et al., 2014). The amide A peak which corresponds to N-H stretching vibration in the protein backbone was observed at 3280 cm^{-1}. The C=O stretching vibration also known as amide I vibration was observed at 1648 cm^{-1}. The peak at 1533 cm^{-1} corresponding to N-H bending vibration was also observed. This particular vibration is called amide II vibration. Another peak at 1242 cm^{-1} is due to C-N stretching

vibration. C-H stretching vibration was observed at 2947 cm^{-1} and C-H bending vibration was observed at 1447 $cm^{-1.}$

FTIR spectrum of polyethylene oxide (PEO) is shown in figure 9B. The backbone of PEO is composed of CH_2-CH_2 bonding. C-H stretching frequency was observed at 2871 cm^{-1} and C-H bending was observed at 1464 cm^{-1}. The terminal O-H bending was observed at 1342 cm^{-1}. The stretching vibration of the C-O bond in the principal chain of PEO was observed at 1096 cm^{-1}.

Uncrosslinked and UV crosslinked Zein/PEO showed FTIR peaks of amide A, amide I, amide II, C-H stretching, C-H bending, C-N stretching and C-O stretching (figure 9C and 9D respectively). A characteristic observation was in the shift of vibrational frequency of

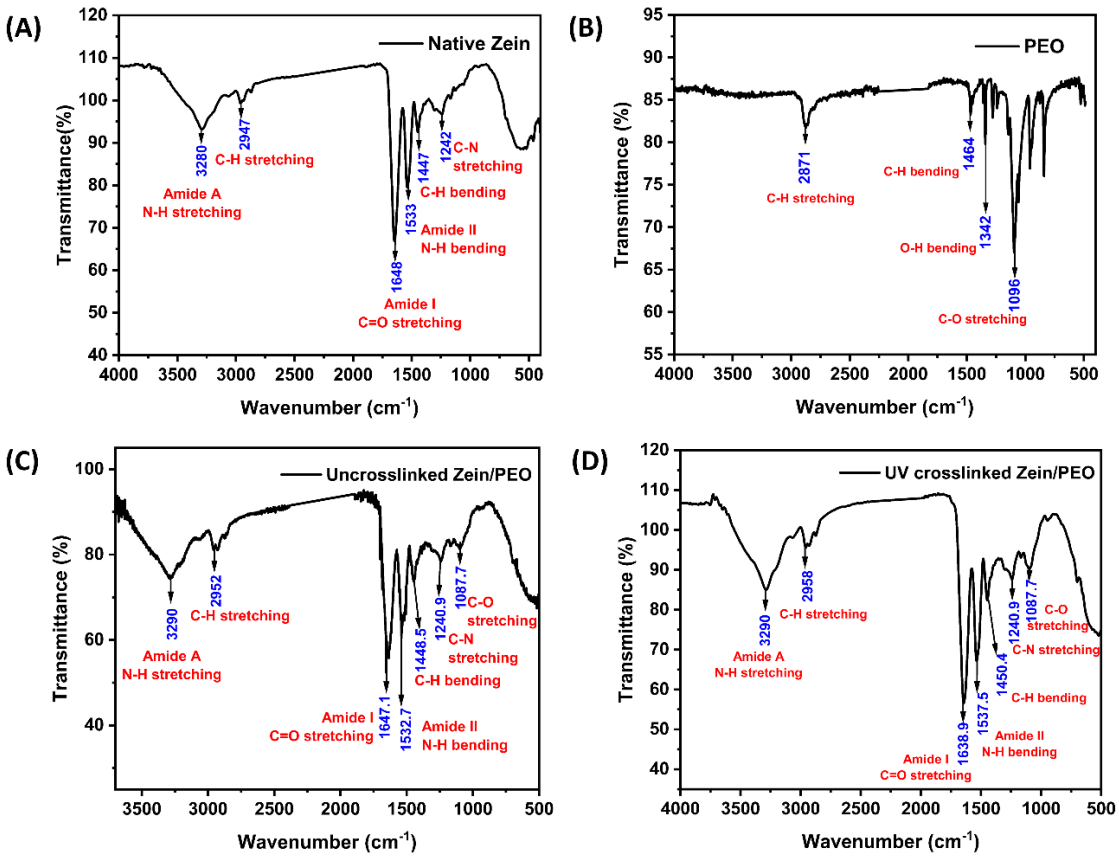

Figure 9:FTIR Spectrum of A) Native zein B) PEO C) Uncrosslinked Zein/PEO D) UV crosslinked Zein/PEO

amide I. FTIR peaks of amide linkage in the range of 1600-1700 cm^{-1} have certain indications towards the conformations of zein protein (Turasan and Kokini, 2017). Vibrational frequencies in the range of 1640-1650 cm^{-1} indicate random coil conformation, beta-sheet conformation has a vibrational frequency in the range of 1610-1640 cm^{-1} and beta-turn conformation shows a peak between 1660 cm^{-1} and 1700 cm^{-1}.

As already discussed, UV exposure to the electrospun matrix of Zein/PEO causes certain conformational changes in the secondary structure of the protein. Those changes were confirmed by FTIR spectra. Because the amide I vibration of the uncrosslinked sample appeared in the range of random coil conformation which changed to beta-sheet conformation after UV crosslinking.

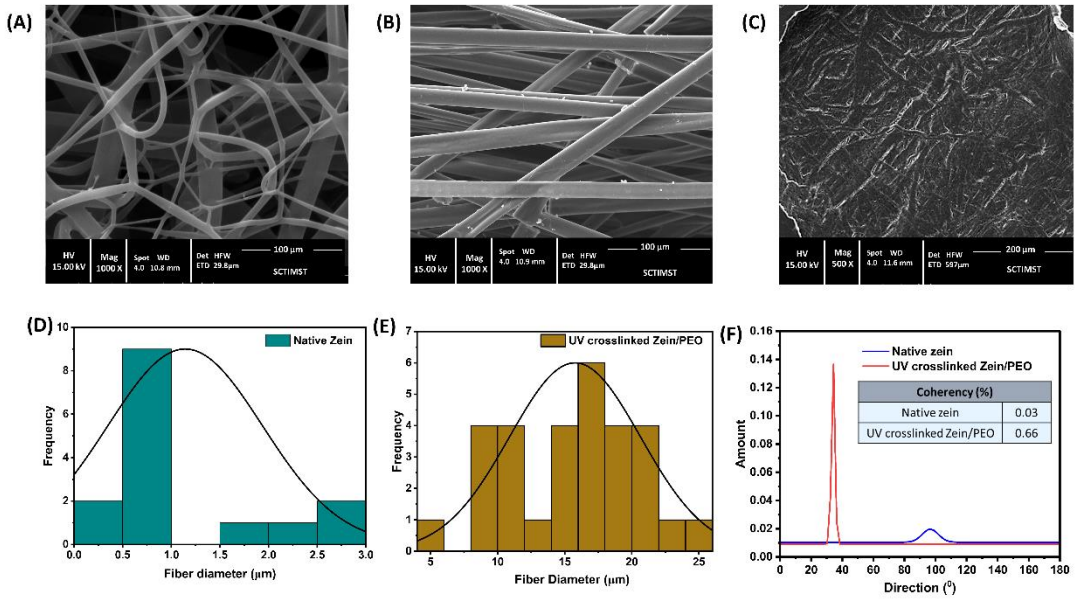

Figure 10 SEM images of A) Native zein B) UV crosslinked Zein/PEO C) UV crosslinked Zein/PEO after wetting (1000X magnification), Fibre diameter distribution of D) Native zein E) UV crosslinked Zein/PEO F) Directionality diagram shown with coherency (%) in the inset

4.1.4 Surface morphology analysis using SEM

Figures 10A and 10B show the morphology of fibres obtained during electrospinning of native zein alone and UV crosslinked Zein/PEO blend. Electrospinning of zein and its blends in EtOH/H_2O mixture as solvent results in the formation of ribbon-shaped fibres

(Yao et al., 2007). It is interesting to note that native zein shows randomly oriented fibres whereas with the addition of high molecular weight PEO, both uncrosslinked and UV crosslinked Zein/PEO show fibres with aligned geometry. This alteration in the alignment of fibre might be due to the increase in the viscosity of the polymer blend solution.

Table 7 Tabulated viscosity values of native zein and Zein/PEO blend solutions in 8:2 EtOH/H_2O solvent mixture

Sample	Viscosity (Centistokes)
Native Zein	67.45
Zein/PEO	247.65

The crosslinked electrospun matrix was cut into the dimension of 2 cm x 2 cm and kept in 1X PBS for 24 h and then dried. The dried matrix was brittle and hard. The SEM images of the matrices were taken and analyzed. Fused fibres were seen with the dissolution of fibres with complete closure of inter-fibre voids (Sadeghi-avalshahr et al., 2020) (figure 10C).

The electrospun fibres of Zein/PEO have an even distribution of fibre diameter. The range of fibre diameter of native zein is widely distributed (figure 10D). As evident from figure 10E, the fibre diameter of UV crosslinked Zein/PEO is much more uniform and distributed. The mean fibre diameter of native zein is 1 ± 0.8 µm and that of UV crosslinked Zein/PEO is 16 ± 5 µm. This increase is due to the increase in the viscosity of the blend solution. The viscosity of different polymer solutions was measured in Lovis 2000 M/ME rolling-ball viscometer. The change viscosity after PEO blending is tabulated in table 7.

Directionality analysis has shown a narrow directional distribution of electrospun fibres for UV crosslinked Zein/PEO compared to native zein (figure 10F). A flat gaussian curve of histogram indicate isotropic arrangement of fibres wherein a sharp peak corresponds to an aligned arrangement. To confirm that further, orientation plugin analysis was done

which calculates the value of coherency (%). Coherency is the degree to which the fibres are oriented. Its value close to 1 is highly aligned and 0 is isotropic. The abovementioned analysis has given the coherency (%) value of 0.03 for native zein, whereas that of UV crosslinked Zein/PEO is 0.66. These parameters actually substantiate the aligned geometry of electrospun UV crosslinked Zein/PEO fibres.

4.1.5 Thiol estimation using Ellman's assay and conformational analysis by Circular Dichroism Spectroscopy

Thiol estimation with and without adding $NaBH_4$ gave quantitative knowledge about the thiol concentrations in the free state and the total thiol concentrations. Zein, being the prolamin fraction of corn protein consists of a series of disulfide-linked oligomers of varying molecular weight and intramolecular disulfide-bonded polypeptides (Geraghty et al., 1981). The addition of the reducing agent reduces the disulfide bond to thiol functional groups.

DTNB (5,5′-dithiobis(2-nitrobenzoic acid) reacts with a free sulfhydryl group to yield a mixed disulfide and 2-nitro-5-thiobenzoic acid (TNB). The target of DTNB in this reaction is the conjugate base (R—S-) of a free sulfhydryl group. TNB is the yellow-coloured species produced in this reaction and it is analyzed using UV light of wavelength 412 nm.

The concentration of thiol groups of UV crosslinked and uncrosslinked Zein/PEO are shown in figure 11A. The concentration of thiol functional groups in crosslinked Zein/PEO was found to be higher than that of the uncrosslinked blend. There is a significant increase in thiol concentration from 187.8 ± 0.02 μM to 208.6 ± 3 μM (p-value 0.05). This is because more thiol groups become free after the breakage of disulfide

linkages under UV irradiation. The proposed mechanism for the change in disulfide bond breakage is shown in figure 11B.

Nonpolar aromatic amino acids like tyrosine, phenylalanine and tryptophan (Trp) absorb UV light to different degrees. Tryptophan is responsible for the absorbance of UV light by zein (Rhim et al., 1999). Upon absorption, they can transfer an electron to the nearby disulfide bonds formed between cysteine (Cys) amino acids, causing them to break. The Cys residues form a radical which goes to react with the Trp amino acid next to it.

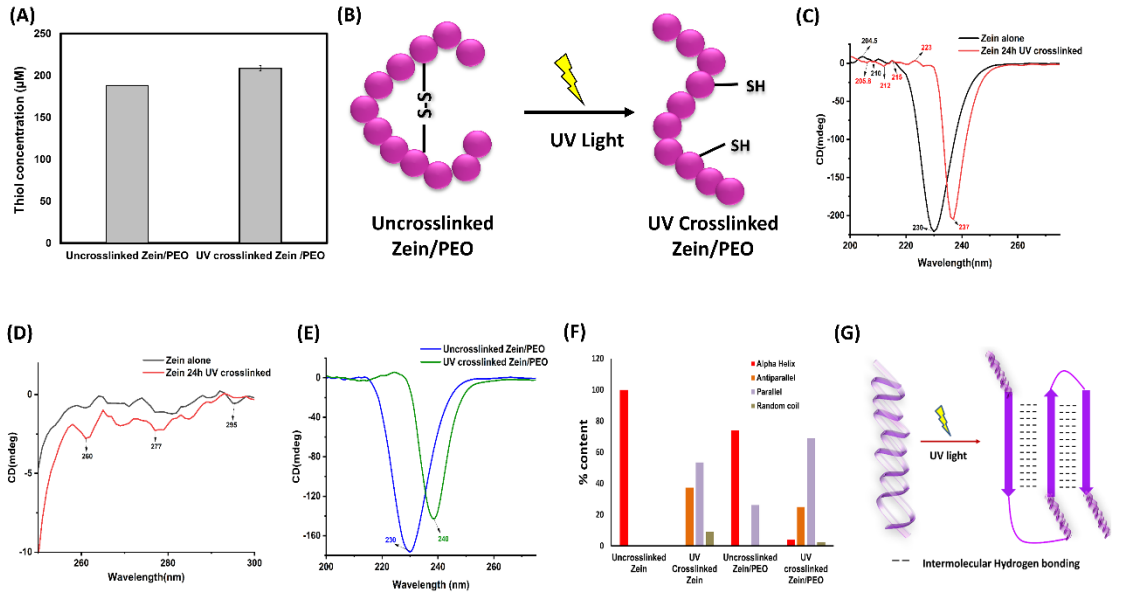

Figure 11 A) Thiol content of uncrosslinked and UV crosslinked Zein/PEO B) Schematic representation of terminal disulfide breakage upon UV irradiation C) Far UV CD spectra of zein and UV crosslinked zein D) Near UV CD spectra of zein and UV crosslinked Zein E) Far UV CD spectra of uncrosslinked and UV crosslinked Zein/PEO F) Graphical representation of % content of proteins conformations after Bestsel analysis G) Schematic diagram of conformation change of zein after UV irradiation

Circular dichroism (CD) studies were performed on Zein/PEO blends before and after crosslinking. According to the mechanism discussed above, UV crosslinking causes a reduction in disulfide linkage which will further lead to a decrease in extended coil content and an increase in β sheet structure (Selling, Hamaker, et al., 2007). CD spectra analysis of zein in 8:2 EtOH/H_2O solution before and after UV crosslinking was done. α

helix secondary structure of zein protein is confirmed by the presence of negative maxima at 208 nm and 222 nm (Paraman and Lamsal, 2011) corresponding to n→π* and π→π* transitions. Peaks observed in the far UV CD spectrum (figure 11C) show a slight red shift in absorption maxima to 210 nm and 230 nm in the uncrosslinked zein electrospun matrix. After UV crosslinking for 24 h, a further red shift is observed in the peaks to 212 nm and 237 nm. The intensity of peak at 230 nm has also decreased after UV crosslinking which implies the decreased alpha-helical conformation in the protein (Erickson et al., 2020). It is also observed that an additional positive peak is observed at 223 nm in UV crosslinked zein which is expected to be a contribution of aromatic side chains which become free after disulfide bond breakage on UV exposure (Woody, 1994) following electron transfer mechanism. The near UV CD spectrum (figure 11D) gives information about aromatic amino acids in the protein structure like tryptophan (295 nm) and tyrosine (277 nm) (Kelly et al., 2005). A similar trend is observed in the CD spectra of Zein/PEO electrospun matrices before and after UV crosslinking (figure 11E).

BeStSel (Beta Structure Selection) analysis helped with secondary structure determination and fold recognition from protein circular dichroism spectra. It has revealed conformational transformations occurring during UV crosslinking. Native zein electrospun membrane is showing 100 % alpha-helical conformation which changes to 37.3 % antiparallel beta-sheet and 53.5 % parallel beta-sheet conformations. Similarly, Zein/PEO blend electrospun membrane also showed conformational transformation during UV crosslinking. 73.9 % alpha-helical conformation in uncrosslinked Zein/PEO has changed to 3.9 % after UV crosslinking (figure 11F).

Therefore, the mechanism of conformational change during UV crosslinking is explained using the diagram (figure 11G). The proposed mechanism involves a transition from α helix to β sheet, which is a universal mechanism in α helix rich protein-rich materials

(Qin and Buehler, 2010). In the α helix, every backbone N-H group forms a hydrogen bonding to the backbone C=O group. Here, the hydrogen bonds appear within a polypeptide chain to create a helical structure. Beta sheets consist of beta strands connected laterally by hydrogen bonds. That means intra-molecular hydrogen bonds in α helix have changed to inter-molecular hydrogen bonds in β sheet. This change has increased the mechanical properties of the crosslinked Zein/PEO.

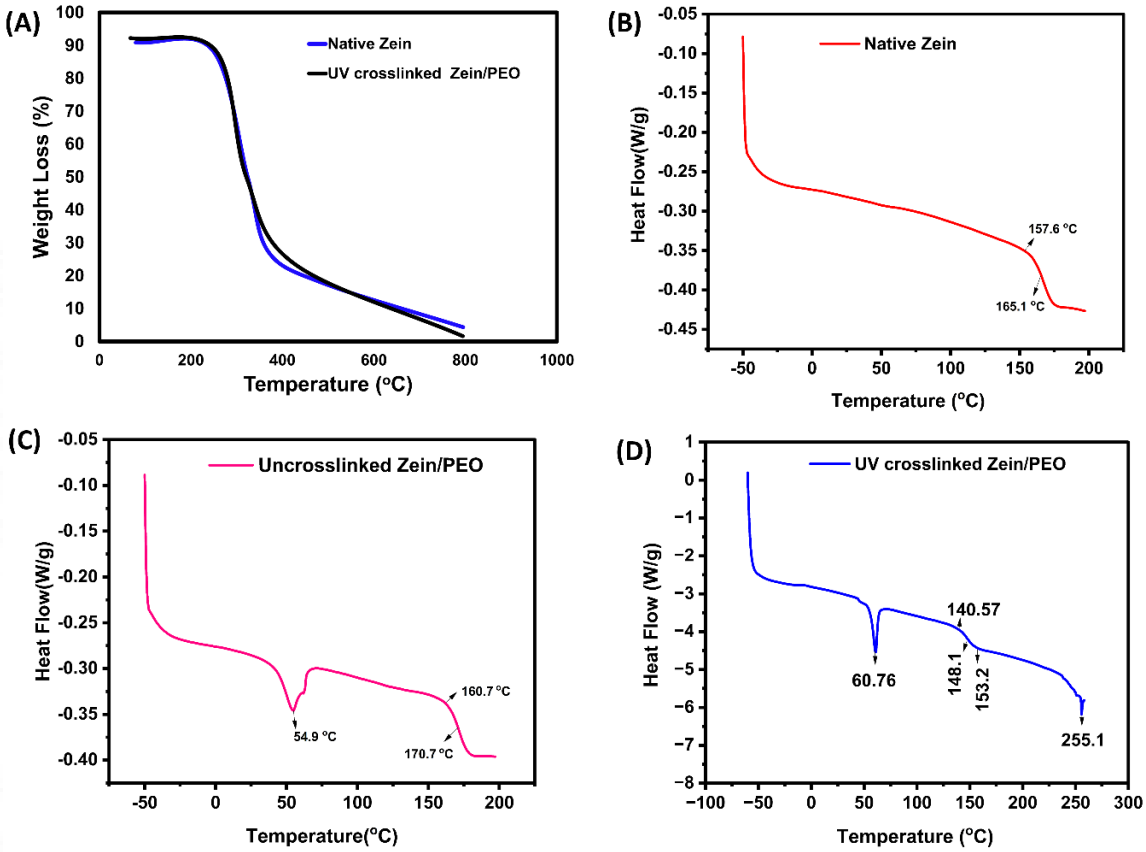

Figure 12 A) TGA thermogram of native zein and UV crosslinked Zein/PEO, DSC thermogram of B) Native zein C) Uncrosslinked Zein/PEO D) UV crosslinked Zein/PEO

4.1.6 Thermogravimetric analysis and Differential Scanning Calorimetry

The thermal decomposition pattern of UV crosslinked Zein /PEO followed the same trend as that of native zein. The onset of thermal degradation was observed at 250 °C for both samples as demonstrated in figure 12A and it got completed at 795 °C. Therefore, it can

be concluded that prolonged UV exposure for 24 h and blending with PEO haven't caused changes to the thermal decomposition pattern of the Zein/PEO electrospun matrix. Figure 12B-D exhibits the DSC curves of native zein, uncrosslinked Zein/PEO and UV crosslinked Zein/PEO respectively. Glass transition temperature is noted as the point of shift from the linear profile of the curve. In the case of native zein, this shift was observed between 157.6 °C and 165.1 °C. For uncrosslinked Zein/PEO glass transition was observed between 160.7 °C and 170.7 °C. But for UV crosslinked this shift happened between 140.6 °C and 153.2 °C. The glass transition temperature of native zein was observed at 162.6 °C whereas the same for uncrosslinked Zein/PEO was observed at 166.6 °C. A shift in glass transition temperature to 148.1 °C has been observed after 24 h UV crosslinking. In all Zein/PEO blend matrices, the melting point of PEO was observed as an endothermic dip at 60.7 °C. Literature has reported a protein unfolding peak at 314 °C for native zein (Muller et al., 2011). This has shifted to 255.1 °C after 24 h UV crosslinking. Though UV exposure is causing protein unfolding, the entire protein structure is not expected to undergo unfolding. Our research team has also reported complete unfolding of protein structure of zein after 40 h UV irradiation (Medha et al., 2023). That means prolong UV exposure cause complete unfolding of the protein structure of zein which is not happening in the case of 24 h long irradiation.

4.1.7 X-ray Diffraction analysis

Native zein fibres were reported to exhibit wide peaks at 9 ° and 20 ° which indicate the amorphous character of the polymer. XRD peaks of zein powder have been reported to match with nano fibres of zein (Ullah et al., 2019). Literature reports suggest a semi-crystalline property for PEO as sharp peaks were observed at 2θ values of 19.15 ° and 23.35 ° (Ahmed and Abdullah, 2019). Figure 13A represents the XRD curves of native zein, uncrosslinked Zein/PEO and UV crosslinked Zein/PEO. XRD spectra of native zein

demonstrated agreement with the reports as broad peaks are observed at 9 ° and 20 °. On account of PEO blending, two small peaks were observed in the XRD spectra of uncrosslinked Zein/PEO at 19.1 ° and 23.35 °. Those two peaks were not very sharp because the percentage composition of PEO in the entire polymer blend is only 5 % where zein is present in large amounts. The possible overlap of XRD peaks of zein and PEO at a 2θ value of 20 ° might have increased the broadness of peaks. Interesting observation

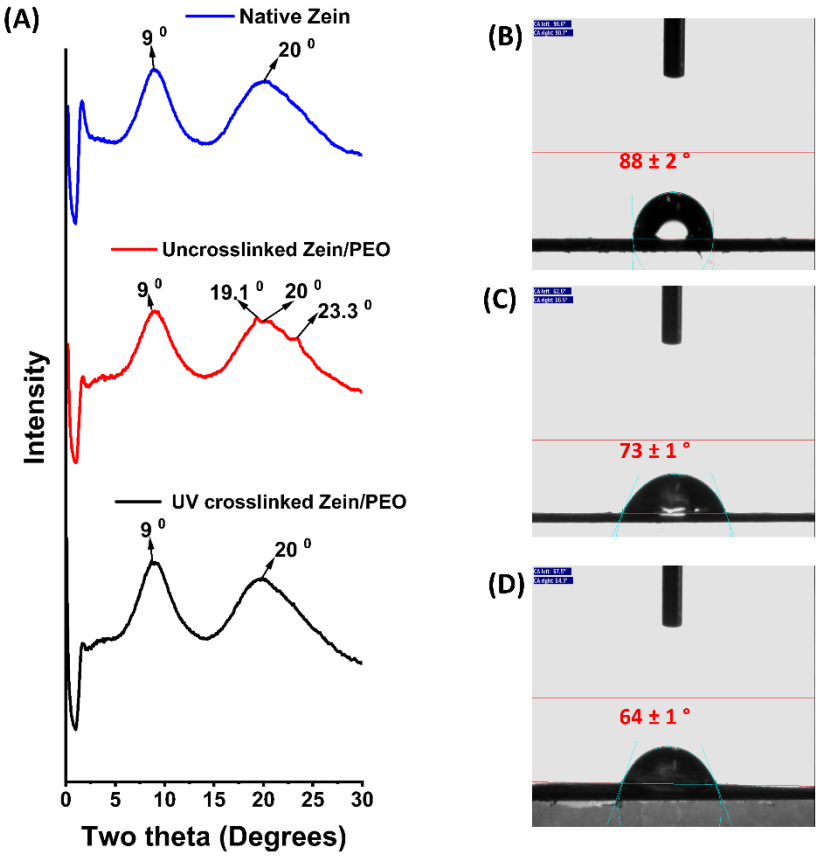

Figure 13 A) Stacked XRD spectra of native zein, uncrosslinked Zein/PEO and UV crosslinked Zein/PEO and water contact images of B) Native Zein C) Uncrosslinked Zein/PEO D) UV crosslinked Zein/PEO

after UV crosslinking is the disappearance of small peaks of PEO. UV crosslinked Zein/PEO showed a smooth broad peak at 20 ° and 9 ° (Ochoa Machiste et al., 2005). UV exposure to the polymer chains of PEO has been reported for causing decomposition.

Hence, the semi-crystalline structure of PEO might have got disrupted and smooth broad peaks of zein dominantly expressed in the XRD spectra.

4.1.8 Surface wettability analysis and Porosity evaluation

Due to the presence of hydrophobic aminoacids like proline, zein is hydrophobic (Luís et al., 2019). Figure 13B demonstrates the contact angle measurement image of native zein showing 88 ± 2 ° angle confirms the fact. Blending with PEO has impacted the hydrophilicity of the system. The contact angle observed in figure 13C considerably decrease to 73 ± 1 ° (p-value = 0.009). UV treatment for a prolonged period has been reported to facilitate an increase in hydrophilicity (Bhurke et al., 2007) and therefore, the

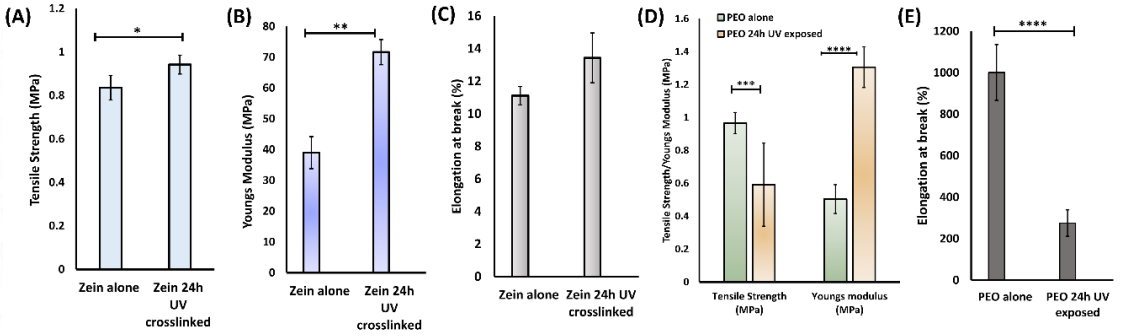

Figure 14 Graphical representation of A) Tensile strength of zein before and after UV crosslinking B) Youngs modulus of zein before and after UV crosslinking C) Elongation at break (%) of zein before and after UV crosslinking D) Tensile strength and Youngs modulus of PEO before and after UV irradiation E) Elongation at break (%) of PEO before and after UV irradiation

contact angle was further observed to reduce to 64 ± 1 ° (figure 13D). The contact angle of UV crosslinked Zein/PEO showed a significant decrease in value compared to native zein (p-value = 0.007) and uncrosslinked Zein/PEO (p-value = 0.01).

The fibrous membrane of UV crosslinked Zein/PEO was evaluated for porosity by the theoretical density method of calculation. The analysis revealed 68 ± 7 % porosity in the matrix.

4.1.9 Static mechanical property evaluation

Zein, PEO and Zein/PEO blend electrospun membranes were exposed to UV irradiation independently. The mechanical properties were evaluated. UV crosslinking of zein has resulted in a significant increase in tensile strength (p-value = 0.05) and Youngs modulus (p-value = 0.001) (figure 14A-B). Elongation at break (%) of zein before and after UV irradiation is graphically represented in figure 14C where there is no significant difference is observed. But interestingly, PEO after getting exposed to UV irradiation shows a significant reduction in tensile strength (p-value = 0.0001) and elongation at break (%) (p-value = 6.9×10^{-6}) (figure 14D and 14E). This might be due to the UV-initiated decomposition of PEO polymer chains under UV irradiation (Ochoa Machiste et al., 2005). A threefold decrease in elongation at break (%) is noticed for PEO after UV exposure.

The incorporation of PEO with zein has caused a significant increase in tensile strength from 0.69 ± 0.35 MPa to 1.79 ± 0.29 MPa (p-value 0.0009). The mechanical property evaluation of the electrospun matrix before and after crosslinking under UV irradiation also shows that the tensile strength of the matrix increases significantly after UV crosslinking as shown in figure 15A (p-value 0.0009). This increase of tensile strength from 1.79 ± 0.29 MPa of uncrosslinked Zein/PEO to 3.52 ± 0.38 MPa of UV crosslinked Zein/PEO (figure 15A) might be because of the strong inter-molecular H bonding in the crosslinked matrix with beta sheet conformation. Similarly, a significant difference (p-value <0.00005) is observed between the tensile strength of samples cut in longitudinal (3.52 ± 0.38 MPa) and transverse direction (0.22 ± 0.03 MPa). Longitudinal and transverse samples are represented as L and T respectively. This anisotropy is attributed to the aligned fibrous structure (Orkwis et al., 2020) of UV crosslinked Zein/PEO.

The blending of zein with PEO has augmented Youngs modulus from 47.4 ± 18.1 MPa to 186.5 ± 25.1 MPa (p-value 3.42 x10^{-5}) and UV crosslinking has improved the modulus further to 293 ± 37 MPa (p-value 0.007) as depicted in figure 15B. Anisotropy as in the case of tensile strength is observed for Youngs modulus also. Youngs modulus in the

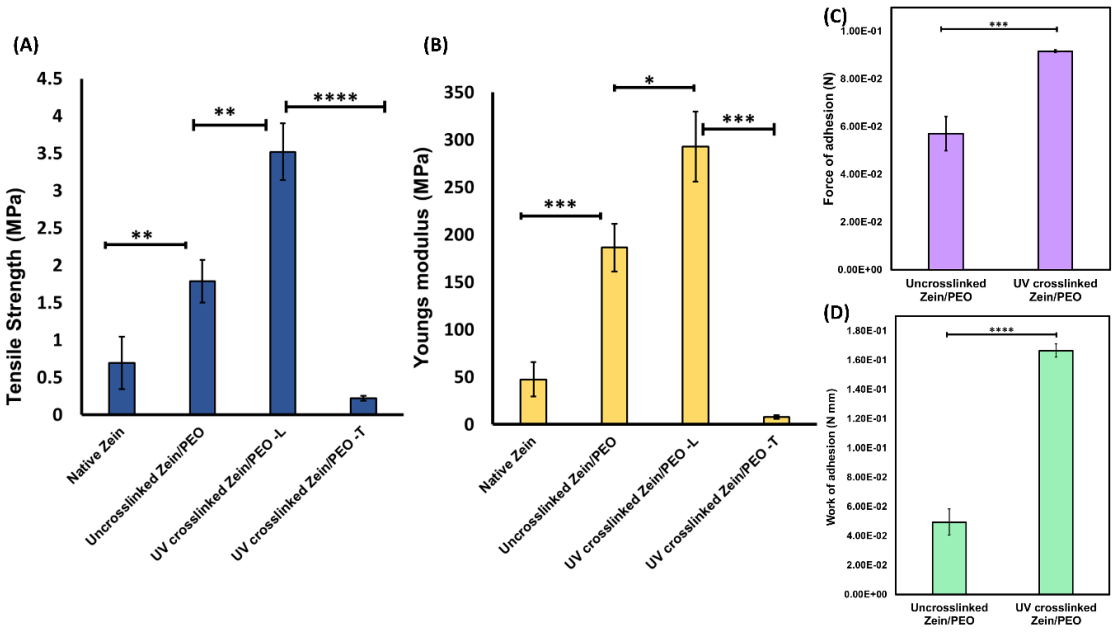

Figure 15 Graphical representation of A) Tensile strength of zein, uncrosslinked Zein/PEO, UV crosslinked Zein/PEO in longitudinal and transverse directions B) Youngs modulus of zein, uncrosslinked Zein/PEO, UV crosslinked Zein/PEO in longitudinal and transverse directions C-D) Force of adhesion and work of adhesion respectively of uncrosslinked and UV crosslinked Zein/PEO represented as bar graphs

longitudinal and transverse direction is 293 ± 37 MPa and 7.7 ± 1.2 MPa respectively. The negative influence of UV irradiation on the mechanical properties of PEO hasn't influenced the mechanical properties of the Zein/PEO blend electrospun membrane. Only less quantity of PEO is incorporated with zein to improve brittleness. Conformational changes of zein from alpha helix to beta sheet under UV irradiation would be the reason for this increased tensile property as zein contributes almost 95 % of the weight of the membrane. The exciting balancing between the positive and negative contributions of PEO and favourable contributions of zein after UV crosslinking has increased the mechanical property of the final UV crosslinked Zein/PEO matrix in total.

A quantitative microstructure model developed by Pai *et al.* explains the mechanical properties of fibrous membranes in terms of fibre diameter, junction lengths and radii of curvature of individual nanofibres (Pai et al., 2011). The blending of PEO has caused an increase in fibre diameter and thus resulted in higher junction length and radius of curvature (Xu et al., 2014). An increase in fibre diameter, junction length and radius of curvature increases the modulus of the individual fibres and eventually the modulus of the membrane as a whole. Therefore, it can be deduced from these data that both blending with PEO and UV crosslinking have contributed well to improving the mechanical properties of the electrospun UV crosslinked Zein/PEO matrix.

4.1.10 Evaluation of mucoadhesion by Texture analysis

Mucoadhesion is defined as the adhesive interaction between a material surface and a mucosal surface. Cationic and anionic functional groups, thiol groups, methacrylate groups etc. exhibit great potential for establishing adhesion with mucosal surfaces via different chemical interactions. Zein and PEO are capable of interacting with mucosa to a certain extent to get adhered to it. If so, a polymer blend of zein and PEO also cause mucoadhesion. The additional advantage of UV crosslinking of the Zein/PEO blend is not only to impart sufficient mechanical properties but also to augment mucoadhesive properties in terms of force of adhesion and work of adhesion. The force required to separate the uncrosslinked Zein/PEO electrospun membrane from the porcine buccal mucosal tissue is $5.7 \times 10^{-2} \pm 7.15 \times 10^{-3}$ N. And also, minimalistic work of $4.94 \times 10^{-2} \pm 8.88 \times 10^{-3}$ N mm is needed to be done to separate two surfaces from contact. UV crosslinking causes disulfide bond breakage and sets more thiol groups free in the protein chain of zein. The disulfide interaction of free thiol groups and cysteine moieties of mucin cause enhanced adhesion. In addition to that, conformational changes occurring to the alpha-helical conformation of zein to beta-sheet conformation could facilitate easy

penetration of the polymer chain with the mucin polymer chains. In that sense, diffusion theory and adsorption theory of mucoadhesion together influence the mucoadhesive property of UV crosslinked Zein/PEO. As a result of all these factors, the force of adhesion and work of adhesion of UV crosslinked Zein/PEO were statistically found to be significantly more than uncrosslinked Zein/PEO (p-values 0.0002 and 1.19×10^{-5} respectively). The force of adhesion of UV crosslinked Zein/PEO was observed to be $9.16 \times 10^{-2} \pm 5.30 \times 10^{-4}$ N and work of adhesion was noted as $1.66 \times 10^{-1} \pm 4.51 \times 10^{-3}$ N mm (figure 15C and 15D).

4.1.11 Evaluation of percentage entrapment

Evaluation of the percentage of drug entrapment of all five formulations was done by drug dissolution study. The percentage of drug entrapment was calculated based on values of actual drug-loaded, theoretical amount of drug entrapped and the experimental concentration of drug entrapped. Table 8 describes the values of all five formulations. For instance, F1 formulation was prepared by dissolving 130 μg of PL in the 5 mL zein/PEO polymer blend solution carrying a total of 1.575 g polymers (1.5 g zein and 0.075 g PEO). It is expected that the electrospun membrane collected will be having a weight of 1.575 g. But, during the electrospinning process, certain fibre wastage may happen. So, the collected membrane was having a total weight of only 1.237 g. The corresponding concentration of the drug expected to be entrapped on the fibrous membrane is then 102.14 μg, which is termed the theoretical concentration of the drug entrapped. Some pre-weighed pieces of the membrane were then dissolved in 8:2 EtOH/H_2O and analysed in a UV spectrometer at 290 nm to quantify the experimental concentration of the drug entrapped, which was 72.74 μg. F2 to F5 formulations were prepared by dissolving 260, 390, 520 and 650 μg of PL into the polymer solution. With respect to the weight of obtained electrospun membrane, the theoretical amount of PL

entrapped was calculated. Measurement of UV absorbance at 290 nm quantified the experimental amount of PL in the formulations. The blue colour bar demonstrated in figure 16A represents the percentage of drug entrapment. The highest drug entrapment percentage of 71.1 ± 1.7 % was observed for the F1 formulation. F2, F3, F4 and F5 demonstrated drug entrapment percentage of 47.6 ± 1.5 %, 23.4 ± 0.6 %, 24.8 ± 2 % and 23.5 ± 2.6 % respectively. The amount of drug entrapped is more for higher formulations, but the drug entrapment percentage is less because it is relatively less compared to the amount loaded. Inference of this particular observation is that, though a higher amount of drug is loaded into the electrospun membrane of UV crosslinked Zein/PEO, expected drug entrapment is not observed which might be due to the aggregation of drug molecules happening at higher concentrations and the subsequent non-uniform distribution of PL in the electrospun membrane.

Table 8 Tabulated calculations of the amount of drug-loaded, theoretical amount entrapped and experimental amount entrapped in F1-F5 formulations

Formulations	Amount of drug loaded (µg)	Theoretical amount of drug entrapped (µg)	Experimental amount of drug entrapped (µg)	Drug entrapment (%)
F1	130	102.14	72.74	71.1
F2	260	241.42	115.01	47.6
F3	390	273	63.85	23.4
F4	520	325.86	80.91	24.8
F5	650	515.04	121.03	23.5

4.1.12 Evaluation of percentage of drug loading

The drug loading capacity of a drug-entrapped membrane was stated based on the final weight of the electrospun membrane and the total amount of drug entrapped in the

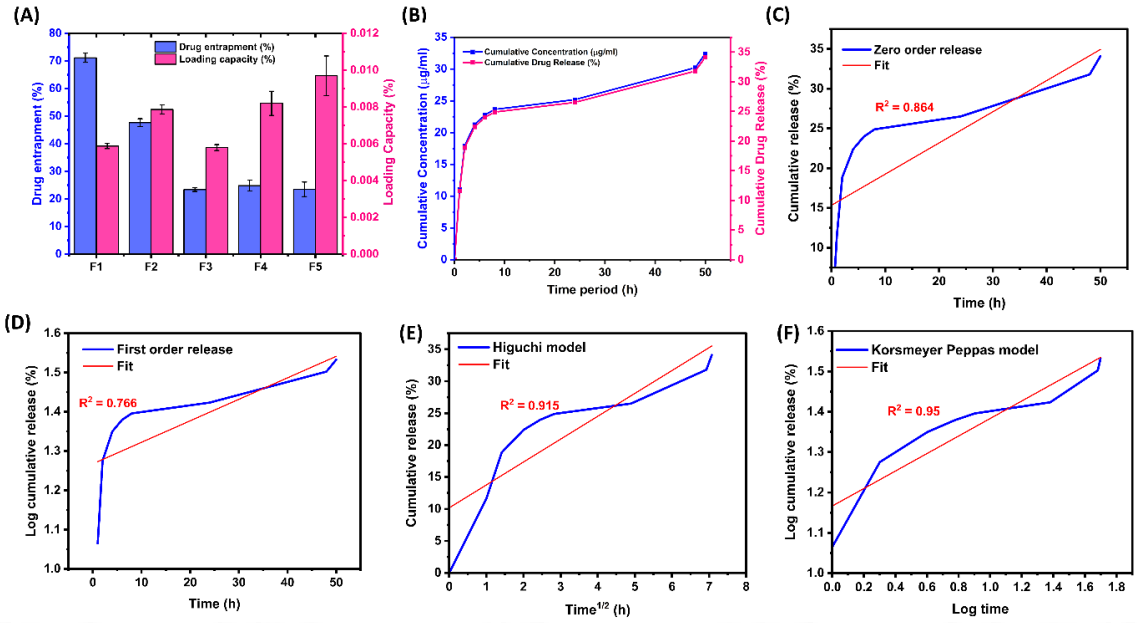

Figure 16 A) Drug entrapment (%) and loading capacity (%) represented as bar graph B) Drug release profile in PBS and mathematical models of drug release – C) Zero order kinetics D) First order kinetics E) Higuchi model of release F) Korsmeyer Peppas model of release

membrane. The experimental amount of drug entrapped was calculated for pre-weighed 1 cm x 1 cm pieces of membrane by UV spectroscopy. The total weight of the membrane and correspondingly the total amount of drug-loaded were calculated by multiplying the observations with the area of the membrane. Since the microgram level of PL is getting entrapped on the membrane having weight in the range of grams, the percentage of loading capacity is a small number. The loading capacity of the F1 formulation was calculated as 0.0059 ± 0.0001 %. F2, F3, F4 and F5 formulations have loading capacity percentage of 0.0079 ± 0.0002 %, 0.0058 ± 0.0002 %, 0.0081 ± 0.006 % and 0.0097 ± 0.001 % respectively. The highest loading capacity was observed for the F5 formulation. The percentage of drug loading is graphically represented in figure 16A.

4.1.13 Drug release kinetics studies and fitting with mathematical models

The release of PL from UV crosslinked Zein/PEO was analysed in Phosphate Buffered Saline (PBS) of pH 7.4. Release studies were carried out for 48 h in PBS media. UV absorbance of PL released into PBS was measured at 290 nm. Figure 16B represents the PL release profile from UV crosslinked Zein/PEO in PBS. PL release trend has an initial burst release followed by a sustained release profile. At the first hour of the release itself, 11.6 ± 2 % of PL got released into PBS media. After 24 h, PL release from the membrane reached 26.5 ± 2.5 %. The release sustained to 31.8 ± 2.3 % at 48 h. The release kinetics has to be analysed for fitting with existing mathematical models. Zero order, first order, Higuchi model and Korsmeyer Peppas models were evaluated. Figure 16C-9F Korsmeyer Peppas release model showed the best fit ($R^2 = 0.95$) with the release profile of PL from UV crosslinked Zein/PEO.

4.1.14 Direct contact assay for cytotoxicity evaluation

Direct contact assay evaluates the cytotoxicity of the materials by analysing the images of the cell monolayer after coming in contact with the material for 24 h. The untreated cell monolayer was considered as the control wherein the morphology of the cells would be seen intact. After treating the cell monolayer with UV-crosslinked Zein/PEO and PL-incorporated UV-crosslinked Zein/PEO, the changes that happened to the RPMI 2650 cells were analysed. Figure 17A-C shows the positive control, negative control and cell alone control images respectively wherein the original morphology of cells was seen. Figure 17D-E represents the images of RPMI 2650 cells treated with UV crosslinked Zein/PEO and PL-incorporated UV crosslinked Zein/PEO respectively. The dark colour region in the images indicates the materials placed over the cells. It can be inferred from

those images that cells are viable with original morphology after material treatment. Zein and PEO are already been reported for their non-cytotoxic properties (Surendranath, Rajalekshmi, et al., 2022). Incorporation of PL is also not causing cytotoxicity to the cells.

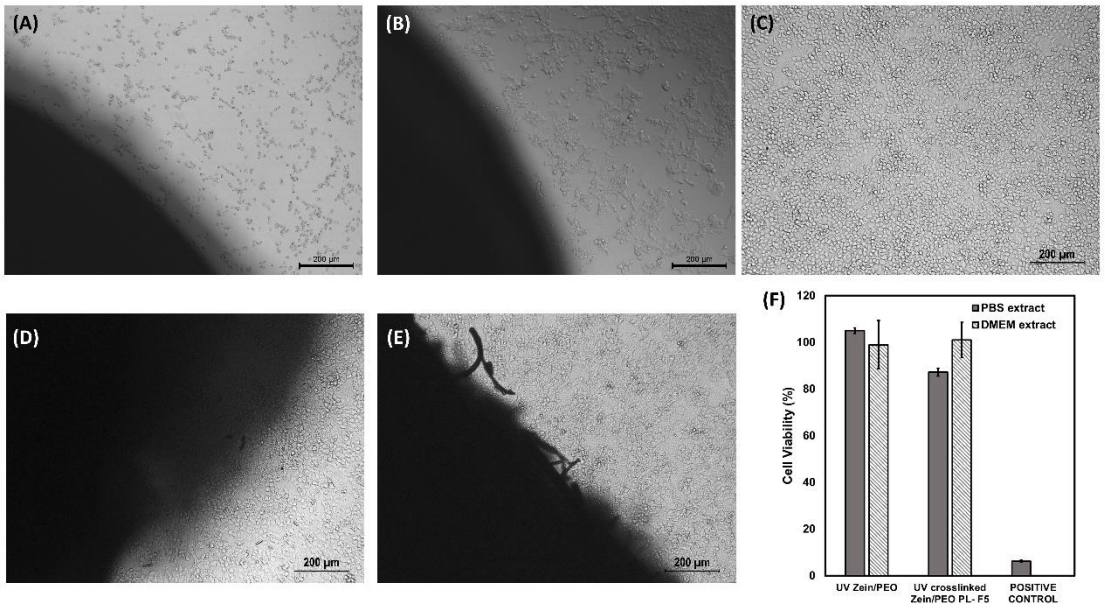

Figure 17 Phase contrast direct contact images (10X magnification) A) Positive control B) Negative control C) Cell alone control D) Cells treated with UV crosslinked Zein/PEO E) Cells treated with PL-incorporated UV crosslinked Zein/PEO and F) Graphical representation of cell viability (%) after MTT assay

4.1.15 MTT assay for cell viability evaluation

MTT assay determines the mitochondrial activity of viable cells and quantifies the percentage of viable cells. Viable cells are capable of converting MTT into formazan crystals which can be solubilized and quantified by measuring the absorbance at 570 nm. Material extracts were added to the cells and incubated for 24 h before adding MTT reagent. If the material extract supports cell growth MTT would be converted to formazan crystals. The quantity of formazan crystals is a direct indication of material toxicity. Figure 17F has represented cell viability (%) as a bar graph diagram. Material extraction was done in PBS and DMEM media. PBS extracts of UV crosslinked Zein/PEO resulted

in 105.1 ± 1.2 %. Cell viability of RPMI 2650 cells after treatment with the extracts of PL-incorporated UV crosslinked Zein/PEO was 87.2 ± 1.7 %. Similarly, DMEM extracts also showed more than 95 % of cell viability as shown in Figure 17D. Cytotoxic phenol-treated cells were considered as the positive control which showed 6.2 ± 0.3 % cell viability. These results confirmed the cytocompatibility of the materials under study.

4.1.16 Live/dead assay

Live/dead assay affirms the cytocompatibility of materials by fluorescent staining. Acridine orange was used to stain live cells which appeared green in colour. Ethidium bromide was used to stain dead cells and they appeared red in the images. Figure 18A-B represents images of untreated control cells which are fluorescent stained using acridine orange, and ethidium bromide. Figure 18C is the overlay of both. Similarly, figure 18D

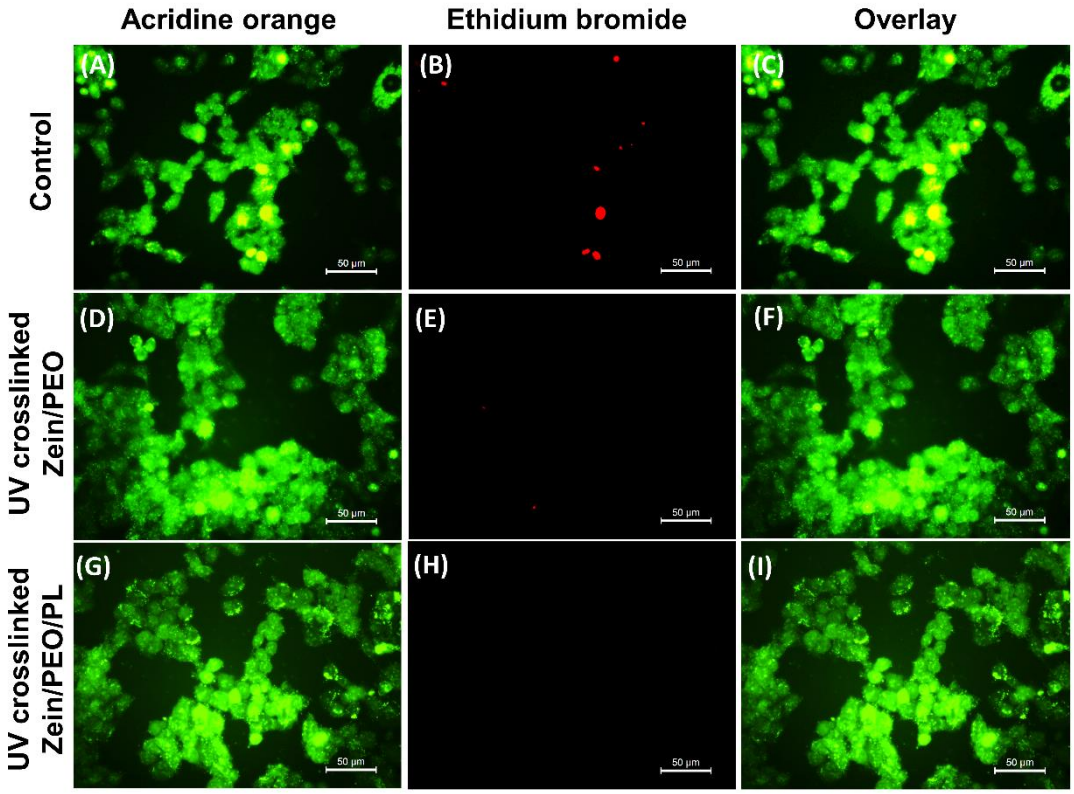

Figure 18 Live/dead staining images after acridine orange staining, ethidium bromide staining, and their overlay respectively of A-C) Untreated control cells D-F) UV crosslinked Zein/PEO treated cells G-I) PL-incorporated UV crosslinked Zein/PEO treated cells (40X magnification)

and 18E represents fluorescent images of cells treated with UV crosslinked Zein/PEO after acridine orange and ethidium bromide staining respectively. Figure 18F is the overlay of the previous two. Live/dead assay for PL-incorporated UV crosslinked Zein/PEO has been evaluated and represented in figure 18G-I. Live cell staining, dead cell staining and their overlay are demonstrated in figure 18G-I in respective order. In all the cases, the number of live cells in green colour are in abundance compared to dead cells in red colour. A higher population of live cells is evident for the cytocompatibility of the materials.

4.1.17 F-actin staining

The influence of materials on the integrity of F-actin cytoskeleton filaments plays a crucial role in deciding the mechanism of drug transport across epithelia. Paracellular transport of drug molecules happens through tight junctions. F-actin filaments critically regulate and support the architecture and maintenance of tight junctions (Van Itallie and Anderson, 2014). Hence, investigation of the solidity and integrity of F-actin filaments

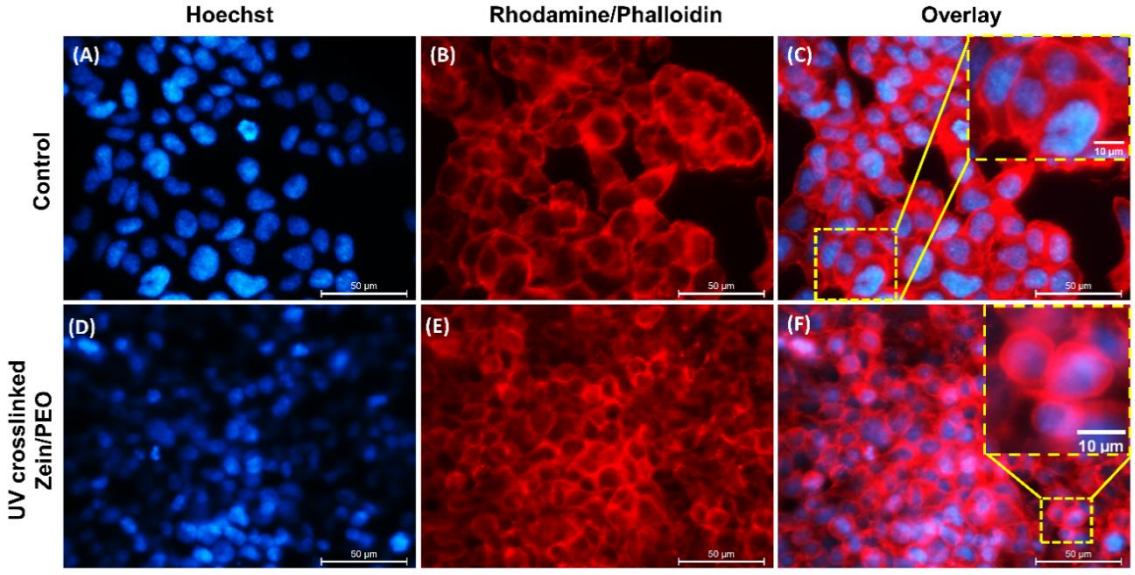

Figure 19 Fluorescent images of A) Nucleus staining of control cells B) F-actin staining of control cells C) Overlay of A and B, magnified overlay shown in inset D) Nucleus staining of UV crosslinked Zein/PEO treated cells E) F-actin staining of UV crosslinked Zein/PEO treated cells F) Overlay of D and E, magnified overlay shown in inset

would insight into the opening of the tight junction of epithelial cells. F-actin staining was done using rhodamine-labelled phalloidin. Figure 19 shows the F-actin-stained images of RPMI 2650 cells with the nucleus stained using Hoechst. Figure 19A-C represents the images of control cells which are non-treated with the material of interest. Figure 19A indicates nucleus staining which appears in blue, figure 19B represents the F-actin staining which appears in red and figure 19C represents the overlay of the previous two. The enlarged overlay image of a single RPMI 2650 epithelial cell is shown in the inset. Figure 19C can be taken as the reference for the integrity of cytoskeleton filaments. After treatment of RPMI 2650 cells with UV crosslinked Zein/PEO for 24 h, morphological evaluation of F-actin was done and demonstrated in figure 19D-F. The extensive filaments of F-actin were seen undisturbed after treatment with UV crosslinked Zein/PEO. Figure 19F has an image of the F-actin structure of a single cell shown in the inset which was maintaining the integrity as such. Therefore, zein and PEO are not causing an impact on the structure and morphology of actin filaments and thus the tight junction.

4.1.18 Immunostaining of beta-catenin proteins in adherens junction

Beta-catenin proteins are the constituents of adherens junctions seen in epithelial cells. A strong networking connection exists between beta-catenin proteins and F-actin filaments via alpha-catenins (Drees et al., 2005). And also, zonal occludens proteins mediate physical linkage between tight junctions and adherens junctions (Campbell et al., 2017). Fluorescent antibody staining of beta-catenin proteins of RPMI 2650 was done and evaluated for material-treated and non-treated cells. Figure 20A-C represents control cell images (Hoechst staining, beta-catenin staining and overlay respectively) which are

untreated. The integrity and coalition of beta-catenin proteins were observed to be intact in the images. The inset shown in the overlay image of control cells in figure 20C helps to figure out the morphology and structural continuity of beta-catenin proteins. Similarly, after treatment with UV crosslinked Zein/PEO structure and morphology of beta-catenin proteins were maintained as such. Figure 20D-F represents the nucleus staining, beta-

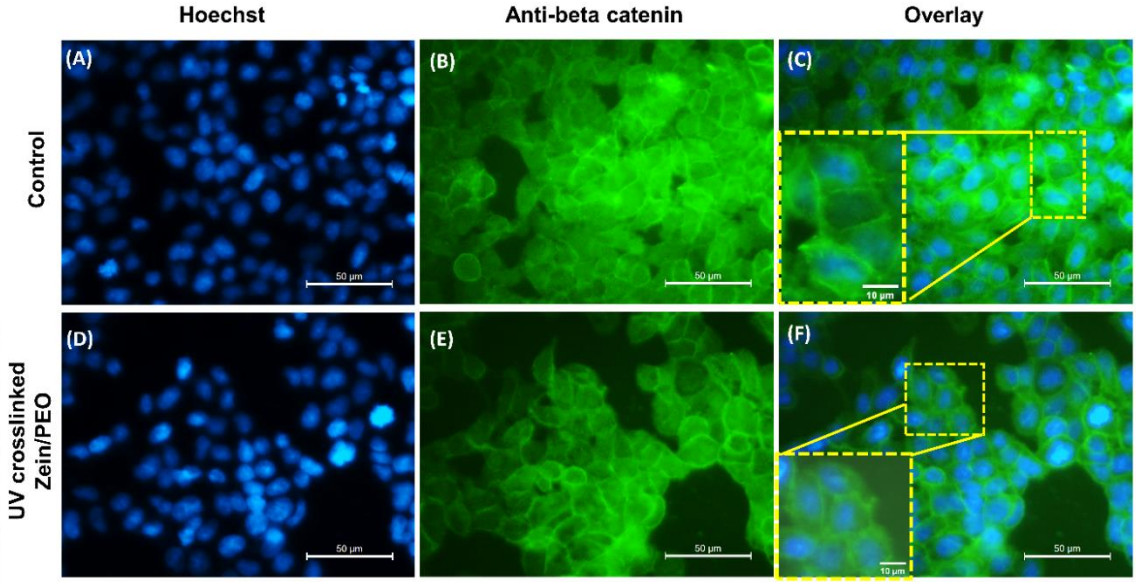

Figure 20 Fluorescent images of A) Nucleus staining of control cells B) Beta-catenin staining of control cells C) Overlay of B and C, magnified overlay shown in inset D) Nucleus staining of UV crosslinked Zein/PEO treated cells E) Beta-catenin staining of UV crosslinked Zein/PEO treated cells F) Overlay of D and E, magnified overlay shown in inset.

catenin staining and their overlay respectively. The inset of the overlay image in figure 20F is that of a single cell in which the structure of beta-catenin was observed to be undisturbed and continuous. These observations confirmed the F-actin staining results wherein no junctional opening can be observed.

4.1.19 TEER evaluation and *in-vitro* drug permeation

Transepithelial electrical resistance (TEER) is the quantitative evaluation of the barrier coalition of epithelial cells. Reduction in the epithelial electrical resistance would indicate a junctional opening. RPMI 2650 cell monolayer was assessed for its electrical resistance

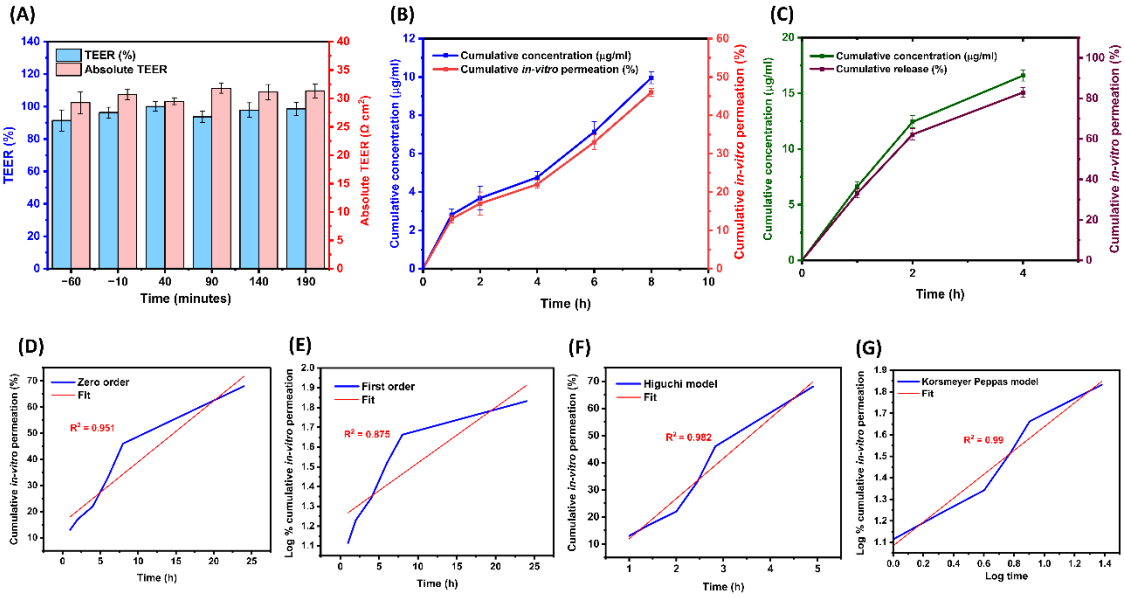

Figure 21 A) Double Y bar diagram representing TEER (%) and absolute TEER, Double Y diagram representing cumulative percentage of drug permeation and cumulative concentration of drug permeation of B) PL loaded UV crosslinked Zein/PEO C) 20 µg/mL PL control and mathematical models of drug permeation- D) Zero order E) First order F) Higuchi model G) Korsmeyer Peppas model

before and after material treatment. Figure 21A gives a bar diagram representation of change in TEER value and absolute TEER value before and after UV crosslinked Zein/PEO treatment. TEER measurement also goes on par with the results of fluorescent staining of F-actin and beta-catenin proteins. Because TEER values were observed to be constant before and after treatment with UV crosslinked Zein/PEO. The liquid-liquid interface culturing of RPMI 2650 cells was reported to have an absolute TEER value of approximately 30 Ωcm^2 (Kreft et al., 2015; Sibinovska et al., 2019). A similar result has been observed in the experiment also. Therefore, zein and PEO are not expected to cause perturbation to the epithelial electrical resistance of RPMI 2650 cells.

Drug permeation in the absence of a junctional opening has to be evaluated. If PL permeation happens only in the presence of a junctional opening, UV crosslinked Zein/PEO wouldn't be the right choice as an adhesive delivery vehicle for the drug. Hence, drug permeation through cell monolayer has been extensively investigated. PL-

loaded UV crosslinked Zein/PEO matrix took 8 h to release 46.4 ± 1.4 % and permeate across the epithelial monolayer as shown in figure 21B. PL solution of concentration 20 µg/mL in HBSS was the control in the experiment. PL solution was administered directly to the surface of the epithelial layer. It was noticed that 83 ± 2 % of PL permeated across the epithelial layer within 4 h (figure 21C). The fastest permeation in the control sample compared to the test samples was reflected in the values of the permeation coefficient. Permeation coefficient of UV crosslinked Zein/PEO and 20 µg/mL PL are 0.093 ± 0.002 cm/h and 0.565 ± 0.025 cm/h respectively. Though fast permeation is happening in the direct administration of drug molecules to the surface of the mucosa, it is not preferred because of local irritations and loss of drug due to saliva secretion. Mucoadhesive membrane carriers for PL drugs would facilitate targeted delivery for a prolonged period

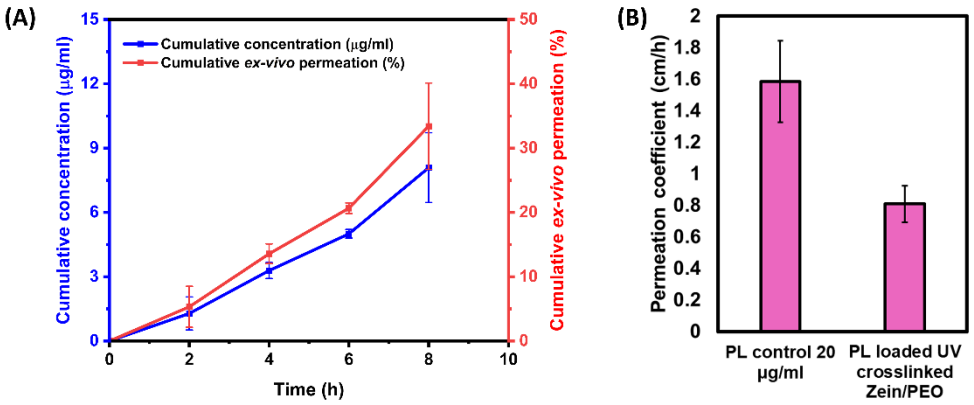

Figure 22 A) Cumulative *ex-vivo* drug permeation diagram B) Permeation coefficients of PL 20 µg/mL control and PL loaded UV crosslinked Zein/PEO represented as bar diagram

and prevent fast and uncontrolled release. Since mucoadhesive membrane could reside on the surface of mucosa for a long period, it ensures a controlled release of drugs for a long duration (Smart, 2004). Figure 21D-G discusses the fitting of cumulative drug permeation with different mathematical models. The best-fit model was Korsmeyer Peppas with an R^2 value of 0.99. As a matter of fact, the cell junctions remain closed after

material treatment, the inference regarding the mechanism of drug permeation fits with the transcellular mechanism.

4.1.20 *Ex-vivo* drug permeation evaluation

Transcellular transport of PL across epithelial monolayer has been confirmed by TEER measurement and *in-vitro* drug permeation studies. If transcellular transport happens across the epithelial cell monolayer, the same has to be verified in *ex-vivo* conditions also. Therefore, PL permeation from UV crosslinked Zein/PEO was verified through porcine buccal mucosa using Franz diffusion cell apparatus. Figure 22A demonstrates the cumulative release profile *ex-vivo*. It was noted that 33.4 ± 6.7 % of PL permeated across mucosa to the basolateral receptor compartment within 8 h of the experiment. The permeation release was investigated for finding the best fit mathematical models based on the correlation coefficient. Table 9 is showing R^2 values of various mathematical models of drug release. Korsmeyer Peppas model of drug release showed maximum fit with R^2 value 0.996. The PL permeation across porcine buccal mucosa was compared with a control system where 20 μg/mL of PL was added directly to the donor chamber. It was observed that 72.3 ± 4.3 % of PL happened within 6 h of the experiment. Permeation coefficients of control and test systems were calculated from the cumulative drug permeation curve. The permeation coefficient of the control system and PL-loaded UV crosslinked Zein/PEO are 1.584 ± 0.258 cm/h and 0.808 ± 0.114 % respectively (figure 22B). A significant change in permeation coefficient hasn't been observed (p-value = 0.058) after keeping the material of interest over the mucosa as no junction opening happens in the epithelial layer. A comparable permeation coefficient to that of the control system was obtained. Still, slow permeation of PL from the electrospun membrane compared to PL is observed because additional time is being taken by drug molecules to

diffuse out of the electrospun membrane which is not required in direct drug administration.

Table 9 Correlation coefficients of various drug release models in *ex-vivo* PL permeation through porcine buccal mucosa from UV crosslinked Zein/PEO

Mathematical model	R^2 value
Zero order	0.991
First order	0.980
Higuchi model	0.976
Korsmeyer Peppas model	0.996

4.2 THIOL-MODIFIED ZEIN/PEO ELECTROSPUN MEMBRANE AND ITS CHARACTERIZATION

4.2.1 Thiol modification of zein

Thiol modification of zein with cysteine amino acid was carried out via EDC crosslinker. EDC is known as a zero-length crosslinker because it does not involve the amide bond formed between the carboxyl and amino functional groups (Deng et al., 2020). An O-acylisourea active intermediate is formed during the mechanism of crosslinking which is further getting substituted with amino groups. At the last step of modification, EDC will be removed in the form of isourea which is water soluble (Pham et al., 2018). Figure 23A demonstrates the mechanism of thiol modification happening between zein and cysteine (CY) in the presence of EDC. The research work involved preparation of five formulations of thiol-modified zein. The details of quantities of zein, cysteine and EDC taken for the preparation of the formulations are given in table 10. After the preparation of thiol-modified zein solution at room temperature, the solution was solvent cast to get

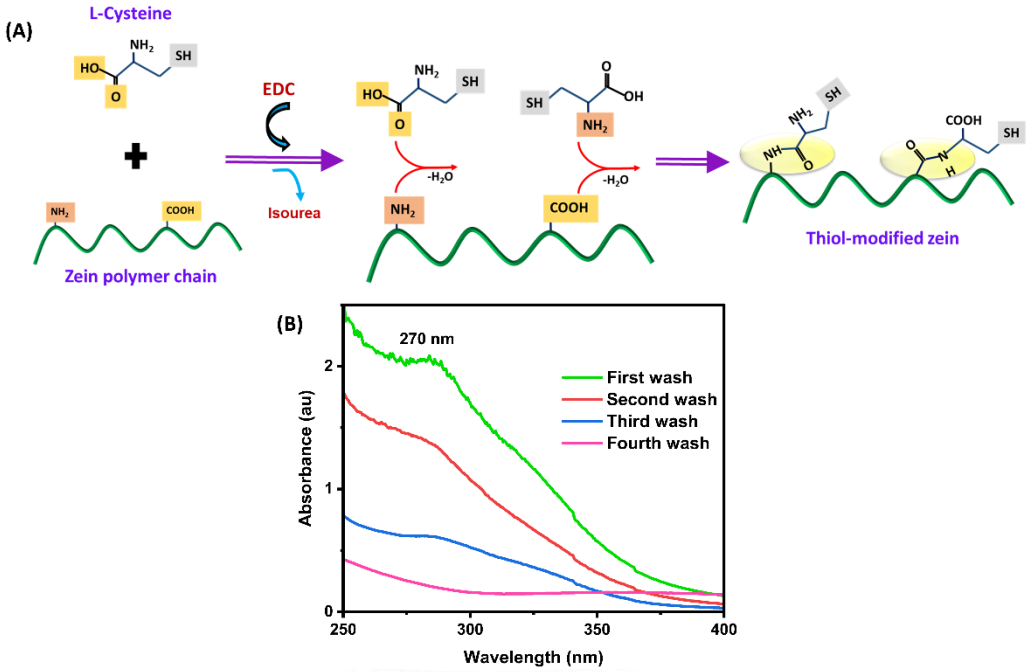

Figure 23 A) Scheme showing EDC mediated conjugation of cysteine on polymer chain of zein B) UV spectra of washed-off water showing absorption maxima at 270 nm

a film. Isourea by-product of EDC reaction will be entrapped in the film after casting, which has to be washed off. Hence, solvent cast film of thiol-modified zein was washed in distilled water several times. UV spectra of the washed off water was analysed and observed a peak maximum at 270 nm as shown in figure 23B, which corresponds to the $n \rightarrow \pi^*$ transition of carbonyl groups in isourea (Potthast et al., 2005). The washing was continued till the peak maximum disappeared from the washing solution in the UV spectra. The film was then again dried and crushed into small pieces before storage.

Table 10 Composition details of various thiol-modified zein films

Sample Name	Zein (g)	Cysteine (g)	EDC (mM)
Z30CY5	3	0.15	2
Z30CY10	3	0.3	2
Z30CY15	3	0.45	2
Z30CY30	3	0.9	2
Z30CY50	3	1.5	2

4.2.2 Electrospinning of thiol-modified Zein/PEO solution

Thiol-modified zein was taken in 3.3 g for all formulations. PEO was taken as 3 % (w/w) of total zein present in thiol-modified zein films. Table 11 describes a detailed calculation of the weight ratio of each component. For example, for Z30CY50PEO3 composition, the total weight of Z30CY0 film will be 4.5 g (3 g zein and 1.5 g cysteine). Out of 4.5 g of film obtained, 3.3 g was taken which would contain 2.2 g zein and 1.1 g cysteine in it. PEO was taken as the 3 % (w/w) of zein, which would be approximately 0.67 g. Thiol-modified zein film and PEO were dissolved in an 8:2 EtOH/H_2O solvent mixture at room temperature (27 ± 2 °C).

Table 11 Detailed composition of thiol-modified Zein/PEO solutions

Composition	Total weight of film (g)	Weight of zein (g)	Weight of cysteine (g)	Weight of PEO (g)
Z30CY05PEO3	3.3	3.14	0.16	0.094
Z30CY10PEO3	3.3	3	0.3	0.09
Z30CY15PEO3	3.3	2.86	0.44	0.086
Z30CY30PEO3	3.3	2.54	0.76	0.076
Z30CY50PEO3	3.3	2.20	1.1	0.066

Electrospinning was carried out using an 18 G needle at a flow rate of 5 mL/h and 15-18 kV voltage. The distance between mandrel and needle was fixed to 10 cm and mandrel rotation was set to 1500 rpm. To prepare electrospun membranes loaded with PL, thiol-modified zein and PEO were dissolved in PL solutions in 8:2 EtOH/H_2O having various concentrations of 0.01 mM, 0.02 mM, 0.03 mM, 0.04 mM and 0.05 mM. Electrospinning of drug-loaded membranes also followed the same experimental parameters (Surendranath, M Ramesan, et al., 2023).

4.2.3 Surface morphology evaluation by SEM

Figure 24A demonstrates the bar diagram representation of the fibre diameter of five thiol-modified Zein/PEO electrospun membranes. ImageJ software was employed for determining the fibre diameter from scanning electron microscope images. From the bar diagram, it is evident that fibre diameter decreased with an increase in the percentage of thiolation. The average fibre diameter is 5 ± 0.3 µm, 5 ± 0.4 µm, 3 ± 0.3 µm, 2 ± 0.2 µm and 1.5 ± 0.3 µm for Z30CY5PEO3, Z30CY10PEO3, Z30CY15PEO3, Z30CY30PEO3 and Z30CY50PEO3 respectively. A significant difference in fibre diameter is observed after 15 % thiolation. The 5 % and 10 % thiol-modified zein does not exhibit a considerable difference in fibre diameter among themselves. The observation of

decreased fibre diameter for Z30CY15PEO3 is attributed to the low concentration of PEO added to it. But for 5 % and 10 % thiol-modified Zein/PEO samples, the concentration of PEO added is almost equal. That is why, fibre diameter is observed to be the same. Z30CY50PEO3 is prepared by adding 0.066 g PEO which is very less compared to other compositions. Hence, the fibre diameter is the least compared to all other compositions. The SEM images of electrospun membranes are depicted in figure 24B-F.

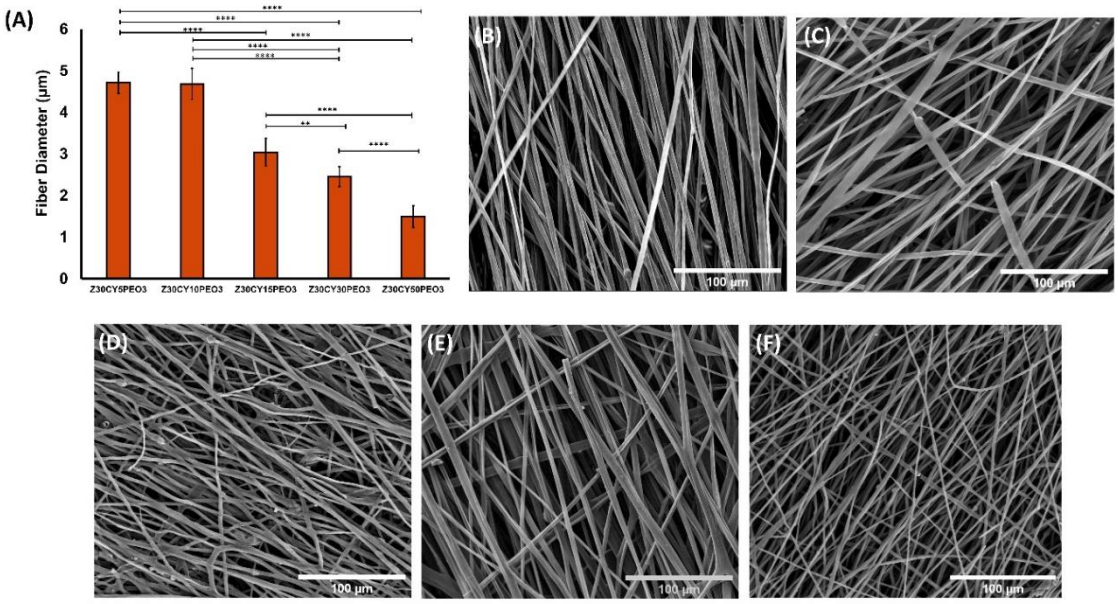

Figure 24 A) Graph showing fibre diameter of different thiol-modified Zein/PEO membranes B-F) SEM images of Z30CY5PEO3, Z30CY10PEO3, Z30CY15PEO3, Z30CY30PEO3 and Z30CY50PEO3 respectively (1000X magnification)

4.2.4 Porosity evaluation by density method

A decrease in fibre diameter has been observed with an increase in the extent of thiol modification. SEM images and further ImageJ analysis asserted this fact. Fibre diameter has a direct influence on the porosity of the electrospun membrane. The porosity of the fibrous matrix increases with the decrease in fibre diameter. Figure 25 denotes the bar diagram representation of porosity (%) of various thiol-modified Zein/PEO matrices.

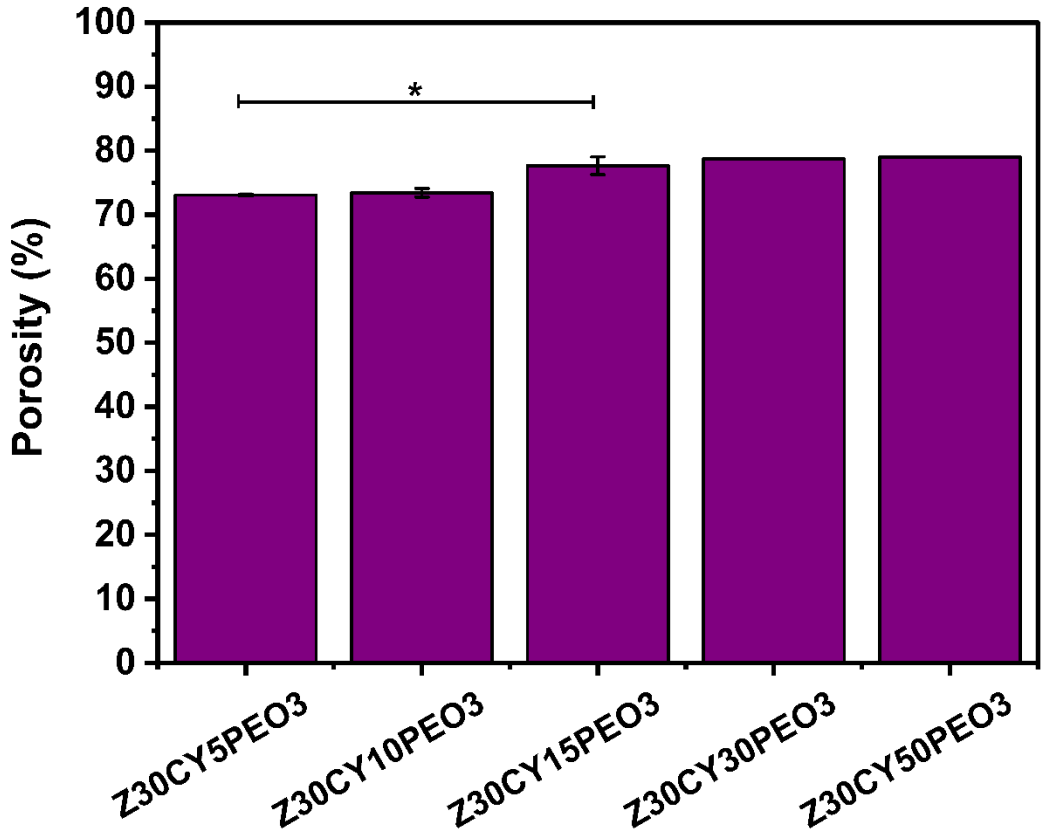

Figure 25 Porosity (%) of different thiol-modified Zein/PEO electrospun matrices

Z30CY15PEO3 exhibited a higher value for porosity (78 ± 1 %) which was statistically significant (p-value=0.01) compared to lower thiol concentration samples like Z30CY5PEO3 and Z30CY10PEO3. Porosity values of lower thiol-modified samples were 73 ± 0.1 % and 73 ± 0.6 % respectively. Further increase in porosity was not observed for Z30CY30PEO3 and Z30CY50PEO3. Drug delivery devices are extensively benefitted with a higher percentage of porosity (Ahuja and Pathak, 2009).

4.2.5 Ellman's assay to quantify thiol modification

Ellman's assay quantifies the free thiol groups present in samples so that the extent of thiolation of zein can be evaluated. With the increase in the concentration of cysteine used for modifying zein, the concentration of thiol groups increased in thiolated zein samples. Figure 26A represents the graphical representation of thiol concentrations. 5,10,15,30 and 50 % thiol-modified zein pose thiol concentrations like 421 ± 5

µmole/gram, 658 ± 31 µmole/gram, 806 ± 49 µmole/gram, 935 ± 22 µmole/gram and 1492 ± 14 µmole/gram respectively. Thiol concentration is considerably more for 50 % thiol-modified zein compared to all other compositions (p-value < 0.05).

4.2.6 Raman spectra

Raman spectra give identifiable peaks for thiol functional groups (Bazylewski et al., 2017). Raman spectra were taken for unmodified Zein/PEO and thiol-modified Zein/PEO electrospun samples (figure 26B). Literature suggests that S-H stretching vibration appears at 2550 cm^{-1} in Raman spectra (Pawlukojć et al., 2005). Thiol-modified Zein/PEO has shown its peak for S-H stretching at 2684 cm^{-1}. Though zein also contains thiol groups in its native structure, it was not observed in the Raman spectra of the unmodified sample. It might be because the quantity of thiol for the observable expression of the peak is less in native zein compared to thiol-modified zein. The other peaks observed in Raman spectra are 1655 cm^{-1}, 2930 cm^{-1} and 3400 cm^{-1} which correspond to -C=O vibration mixed with N-H deformation, N-H vibration and O-H vibration (Wang et al., 2013) respectively.

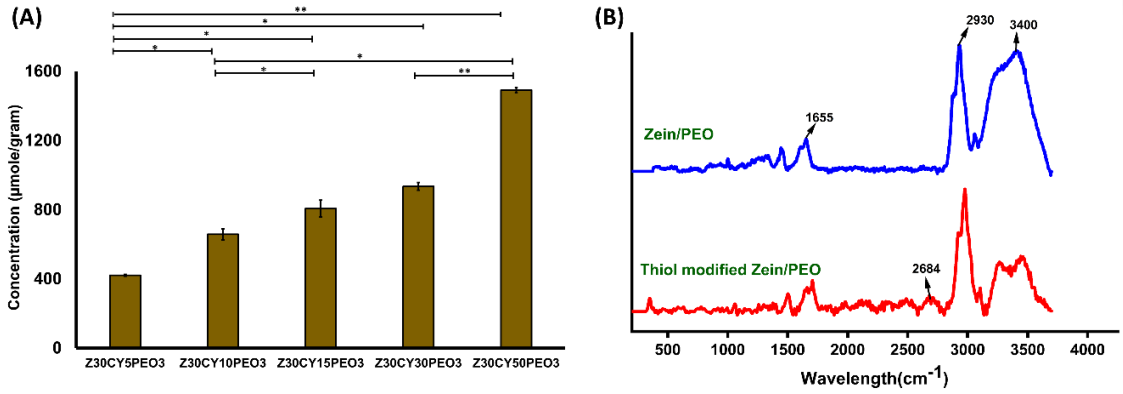

Figure 26 A) Result of estimation of thiol groups by Ellman's assay B) Raman spectra of thiol-modified and unmodified Zein/PEO

4.2.7 Mechanical property evaluation by UTM

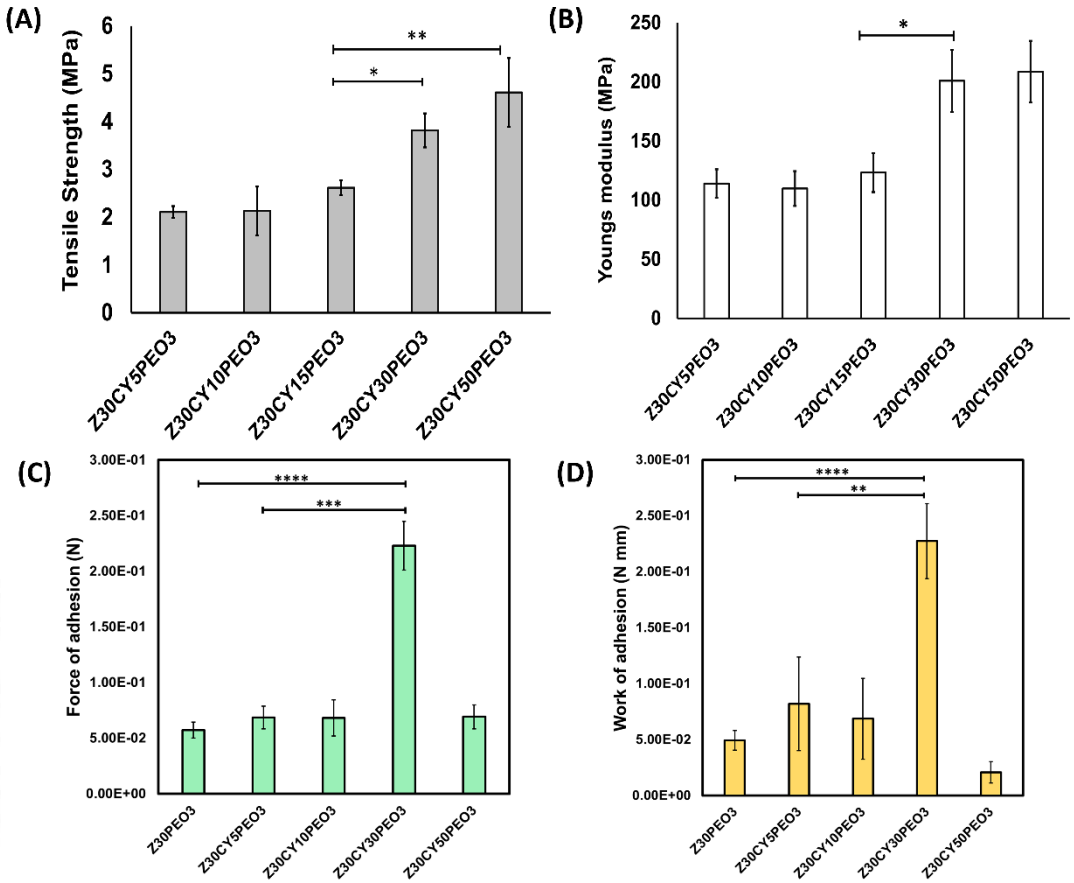

Figure 27 A) Bar diagram representing tensile strength values of thiol-modified samples B) Bar diagram representing Youngs modulus of thiol-modified samples C) Graphical representation of force of adhesion of thiol-modified samples with porcine buccal mucosa D) Graphical representation of work of adhesion of samples with porcine buccal mucosa

Mechanical properties in terms of tensile strength and Youngs modulus were evaluated for five compositions of thiol-modified Zein/PEO electrospun membranes. A higher percentage of thiol-modified zein samples showed augmentation in tensile strength. From figure 27A, it is evident that the tensile strength didn't show considerable change for the initial 5 %, 10 % and 15 % thiol-modified Zein/PEO compositions. A significant increase in tensile property was observed for Z30CY30PEO3 (p-value = 0.01). Similarly, Z30CY50PEO3 also exhibited a considerable increase in the tensile property (p-value = 0.002). Tensile strength values of 5 %, 10 %, 15 %, 30 % and 50 % thiol-modified samples are 2.10 ± 0.12 MPa, 2.13 ± 0.50 MPa, 2.61 ± 0.15 MPa, 3.81 ± 0.36 MPa and

4.61 ± 0.72 MPa respectively. An interesting point to be noted is that amount of PEO blended with a higher percentage of thiol-modified zein is less. Despite decreased PEO concentration also, mechanical property is improved which is solely due to the contribution of thiolation of zein polymer chains. It has already been reported that the thiolation technique is capable of improving the mechanical properties of polymer along with mucoadhesive properties (Puri et al., 2020). The possible disulfide-sulfhydryl exchange reactions in thiolated polymer would cause inter and intra-disulfide interactions and further lead to increased mechanical stability (Dicharry et al., 2006). Since a commendable increase is observed after the 30 % modification, it is expected that a higher extent of chemical crosslinking is happening after this point. A similar trend of improvement has been observed for Youngs modulus also. Youngs modulus increased significantly at Z30CY30PEO3. For the initial three compositions, values of Youngs modulus are 114 ± 12 MPa, 110 ± 15 MPa and 123 ± 16.5 MPa. For Z30CY30PEO3, this tremendously increased to 200 ± 26 MPa. Z30CY50PEO3 also exhibited approximately the same value for Youngs modulus ie., 208.6 ± 26 MPa which is represented in figure 27B.

4.2.8 Mucoadhesion by Texture analysis

Cysteine moieties are capable of establishing disulfide interactions with the cysteine residues of mucin glycoprotein (Mfoafo et al., 2023). Trends in mucoadhesive properties for the five compositions were analysed in this regard. Carcass tissue collected from rabbit intestine was used for the adhesion study. A linear pattern of increase in the force of adhesion is expected with an increase in cysteine concentration in thiol-modified zein samples. Linear increase was observed till Z30CY30PEO3, further adhesive force got decreased for Z30CY50PEO3 (figure 27C). The values of work of adhesion also exhibited a similar pattern of linear increase till Z30CY30PEO3 and then a drastic

decrease (figure 27D). The force of adhesion of thiol-modified samples with porcine buccal mucosal tissue is $6.85 \times 10^{-2} \pm 1.01 \times 10^{-2}$ N, $6.81 \times 10^{-2} \pm 1.61 \times 10^{-2}$ N, $2.23 \times 10^{-1} \pm 2.18 \times 10^{-2}$ N, and $6.92 \times 10^{-2} \pm 1.08 \times 10^{-2}$ N in the respective order of 5 %, 10 %, 30 % and 50 % modification. Similarly, the work of adhesion values of thiol-modified samples is $8.20 \times 10^{-2} \pm 4.18 \times 10^{-2}$ N mm, $6.87 \times 10^{-2} \pm 3.62 \times 10^{-2}$ N mm, $2.27 \times 10^{-1} \pm 3.36 \times 10^{-2}$ N mm, and $2.08 \times 10^{-2} \pm 9.57 \times 10^{-3}$ N mm respectively. Compared to the unmodified Zein/PEO blend, thiol modification has been observed to bring about enhanced mucoadhesion. A considerable increase in the force of adhesion from $5.70 \times 10^{-2} \pm 7.15 \times 10^{-3}$ N to $2.23 \times 10^{-1} \pm 2.18 \times 10^{-2}$ N mm after 30 % thiol modification is an intriguing observation to be noted (p-value= 2.19×10^{-8}). It can also be noted that 5 % thiol modification is not showing much mucoadhesive properties. These observations are the same for both force of adhesion and work of adhesion. The 30 % modified samples showed maximum work of adhesion and it further decreased for the 50 % thiol-modified sample. The maximum work of adhesion observed for the 30 % thiol-modified sample was $2.27 \times 10^{-1} \pm 3.36 \times 10^{-2}$ N mm which is significantly much higher than unmodified Zein/PEO ($4.94 \times 10^{-2} \pm 8.88 \times 10^{-3}$ N mm) with p value 4.48×10^{-6}. Though the concentration of thiol group is higher in 50 % modified sample, a proportional increase in mucoadhesion was not observed. Mucoadhesion is complex phenomenon involving chemical interaction, polymer chain interpenetration and adhesive interaction. That being the case, the phenomenon of mucoadhesion can be explained in terms of a bell-shaped distribution rather a sigmoidal distribution. Therefore, 30 % modification would be the point of optimum maximum, later which adhesion decreases. Since Z30CY30PEO3 exhibited better adhesive properties, it was selected for further studies.

4.2.9 Drug dissolution studies

Five formulations of PL-incorporated thiol-modified Zein/PEO electrospun membranes were prepared. The formulations were prepared by dissolving 260 μg, 520 μg, 780 μg, 1040 μg and 1300 μg PL in an 8:2 EtOH/H_2O solvent mixture. Thiol-modified zein films and PEO were weighed and added to the above PL containing the solvent mixture and electrospinning was done. The entire process of PL loading into the polymer solution and electrospinning is known as blend electrospinning (Nangare et al., 2020). Electrospinning operation involves the loss of a certain amount of polymer solution and spun fibres. It is difficult to get 100 % yield after electrospinning. Relative loss is expected in the quantity

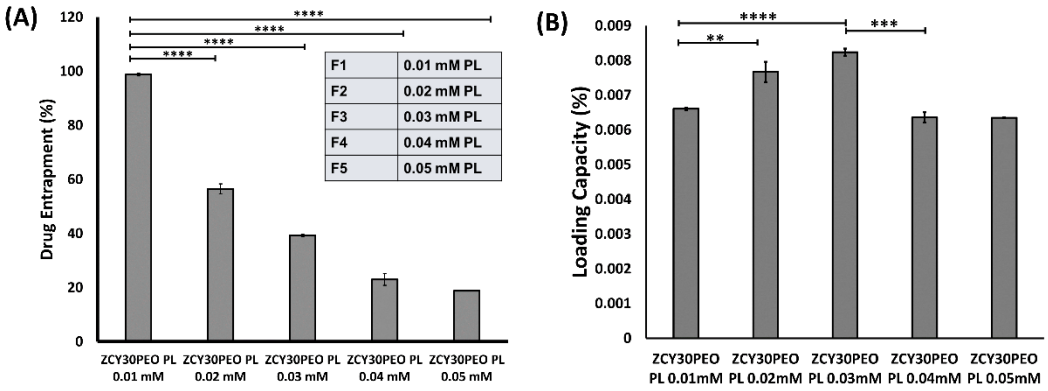

Figure 28 A) Bar graph representation of drug entrapment (%) B) Bar graph representation of loading capacity (%)

of drug entrapped also. Table 12 denotes the tabulation of the quantity of drug-loaded in the membrane after electrospinning. The quantity of drug dissolved before electrospinning is given under title of 'drug loaded' in the table. Weight of the electrospun mat after electrospinning denotes the weight of the electrospun membrane obtained after all kinds of wastage. Expected drug loaded after electrospinning is the theoretical calculation of the drug-loaded based on the weight of the membrane obtained. That much quantity of PL would be entrapped only if the entrapment percentage is 100 %. The experimental concentration of PL loaded was analysed by subjecting the membranes to

UV spectroscopy. A drug dissolution study was employed for this calculation at a wavelength of 290 nm. Drug-loaded samples dissolved in 8:2 EtOH/H_2O were subjected to UV analysis with no drug-loaded samples dissolved in the same solvent mixture as blank.

One example for the calculation is, F1 formulation was prepared by dissolving 3.3 g thiol-modified zein and 0.076 g PEO in the solvent mixture containing PL. Out of a total of 3.376 g polymer taken for electrospinning, the weight of the final electrospun membrane obtained was just 2.3056 g and the corresponding amount of drug expected to be entrapped is 177.56 µg. But UV analysis has shown that the actual amount of drug entrapped within the membrane is 175.35 µg. A similar logical calculation was applied for all formulations.

Table 12 Detailed tabulation of the amount of drug-loaded, expected to be entrapped, actually loaded and percentage drug entrapment of F1-F5 formulations

Formulation	Drug-loaded (µg)	Weight of electrospun mat after electrospinning (g)	Expected drug-loaded after electrospinning (µg)	Actual drug-loaded (µg)	Drug entrapment (%)
Z30CY30PEO3 PL 0.01 mM –F1	260	2.3056	177.56	175.35	98.8
Z30CY30PEO3 PL 0.02 mM-F2	520	2.208	340.09	192.11	56.5
Z30CY30PEO3 PL 0.03 mM-F3	780	2.6304	607.73	238.62	39.3
Z30CY30PEO3 PL 0.04 mM-F4	1040	1.9776	609.21	140.07	23.0
Z30CY30PEO3 PL 0.05 mM-F5	1300	2.5536	983.31	184.94	18.8

The percentage of drug entrapment was calculated from the theoretical amount of drug-loaded and the actual drug-loaded. In the case of the F1 formulation, the expected amount

of drug entrapped was 177.56 μg and in actual case it had 175.35 μg of PL loading. Hence, the drug entrapment percentage was 98.7 ± 0.5 %. Other formulations showed a considerable decrease in the value of drug entrapment percentage. It can be noted from figure 28A that the amount of drug entrapped is increasing with increasing the concentration of PL loading but far less than the drug-loaded. That is the reason for less drug entrapment percentage. Figure 28A denotes the bar diagram representation of drug entrapment percentage. F2-F5 formulations exhibited 56.5 ± 1.9 %, 39.3 ± 0.4 %, 23.0 ± 2.1 % and 18.8 ± 0.02 % percentage entrapment respectively. The maximum was observed for F1. Nevertheless, it can also be concluded that the maximum concentration of PL that could be loaded onto the matrix is 238.62 μg irrespective of the concentration loaded. Entrapment concentration does not increase beyond a level even if the loading concentration is increased. This might be because of the aggregation of drug molecules in the membrane and the subsequent non-uniform distribution of drug molecules (Lian and Meng, 2017).

The percentage of loading capacity was calculated from the weight of the actual amount of drug entrapped and the total weight of the membrane. The percentage of loading capacity increased till F3 formulation then decreased. Figure 28B is the bar diagram representation of percentage loading capacity. It could be concluded that loading capacity significantly increases until an optimum value and then decrease. And also, the amount of drug-loaded is in the microgram range and the total weight of the membrane falls in the gram range, therefore the loading capacity value is very small.

4.2.10 Cumulative drug release kinetics in PBS

The third formulation which showed the highest loading capacity was selected for cumulative drug release studies in PBS of pH 7.4. The trend of drug release followed an initial burst release in the first 1 h, continuous release till 6 h and then a sustained release.

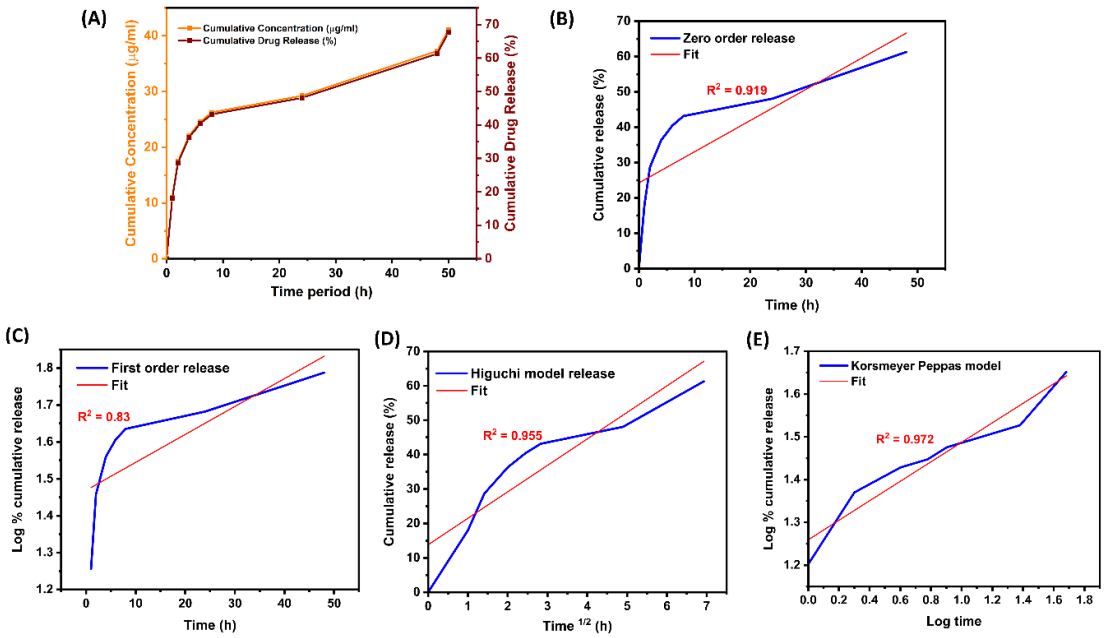

Figure 29 A) *In-vitro* drug release of PL from thiol-modified Zein/PEO in PBS (pH=7.4), B-E) Mathematical models of drug release fitted with the cumulative release (%)- Zero order release, First order release, Higuchi model of release and Korsmeyer Peppas model respectively

Figure 29A describes the cumulative drug release profile of PL from thiol-modified Zein/PEO. Within 48 h of the study, 37.3 ± 2.9 µg/mL PL was released into PBS which was 61.3 ± 4.8 %. The release profile had to fit with different mathematical models to find the best fit. Mathematical models considered for porous membranes are Zero order, First order, Higuchi model and Korsmeyer Peppas model (Bruschi, 2015). Figure 29B represents the Zero-order release graph which had a 0.919 correlation with the actual data. First order release profile in Figure 29C showed the poorest fit with a correlation coefficient of 0.823. The Higuchi model of drug release shown in figure 29D showed a much better fit and the best fit was observed with the Korsmeyer Peppas model (R^2 value = 0.972). Figure 29E describes Korsmeyer Peppas release with a k value of 23.63 and an n value of 0.255. Korsmeyer Peppas model having n value less than 0.5 describes a diffusion-controlled release mechanism (Costa and Sousa Lobo, 2001; Permanadewi et al., 2019).

4.2.11 MTT assay

MTT assay is a metabolic assay to determine the cytotoxicity of materials quantitatively. Quantification of percentage cell viability was done by MTT assay in RPMI 2650 cells. Materials loaded with and without PL were subjected to MTT assay. Extracts of materials in DMEM media and PBS were taken for the analysis and the results showed that around 100 % cell viability has been exhibited by thiol-modified Zein/PEO electrospun membranes with and without PL loading. Figure 30A is the graphical representation of cell viability with phenol as a positive control.

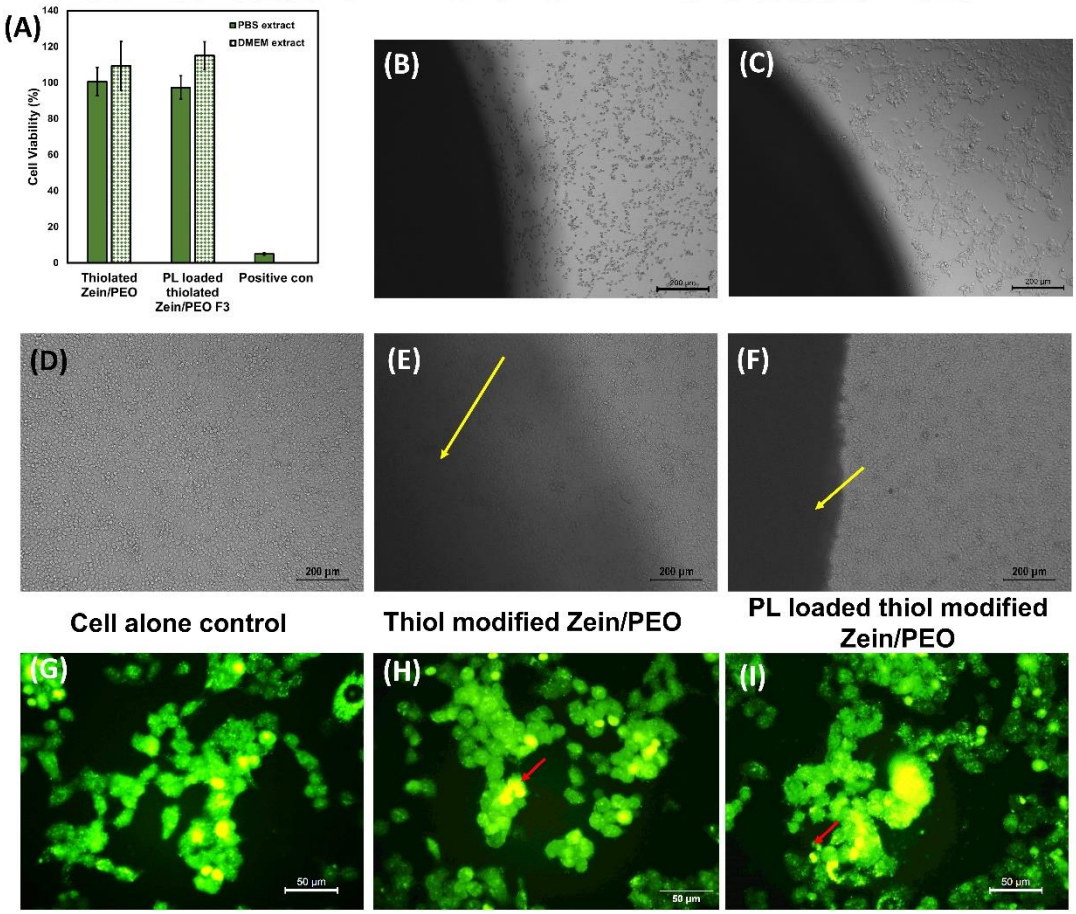

Figure 30 A) Bar graph representation of percentage cell viability obtained from MTT assay B-F) Phase contrast images after direct contact assay (10X magnification) of positive control cells, negative control cells, cell alone control, thiol-modified Zein/PEO treated cells and PL loaded thiol-modified Zein/PEO treated cells respectively G-I) Fluorescent images of control cells, thiol-modified Zein/PEO treated cells and PL loaded thiol-modified Zein/PEO treated cells respectively after live/dead assay (40X magnification)

4.2.12 Direct contact assay

Direct contact assay evaluates cytotoxicity by investigating the structure and morphology of cells after coming in direct contact with the materials of interest for 24 h. Phase contrast images are the means of analysis. Figure 30B-F is the phase contrast images taken. Figure 30B and 30C are the positive and negative control images of cells treated with tin coated PVC and UHMWPE respectively. Figure 30D is the reference image of untreated cells. The morphology of cells and the number of dead cells were compared with the reference for the material-treated cells shown in figure 30E and 30F. It is seen that the cells were maintaining their monolayer and morphology even after coming in contact with thiol-modified Zein/PEO electrospun membranes for 24 h. The incorporation of PL into the membrane does not make any change. Therefore, the non-cytotoxicity of the materials is confirmed.

4.2.13 Live/dead assay

Live/dead assay evaluates cytotoxicity by dual staining live and dead cells after exposing the cells to materials for 24 h. Fluorescent images are the means of analysis. Live/dead assay stains live cells as green and dead cells as red (K Liu et al., 2015). Akin to direct contact assay, untreated cells were stained and their fluorescent images were taken as a reference control system (figure 30G). Figures 30H-I are the live/dead images of cells treated with thiol-modified Zein/PEO with and without PL loaded. Dead cells are marked in the figure using arrows. These fluorescent images conclude that, since the number of green-coloured live cells is more compared to a few red-coloured red dead cells, the materials are non-cytotoxic.

4.2.14 F-actin staining

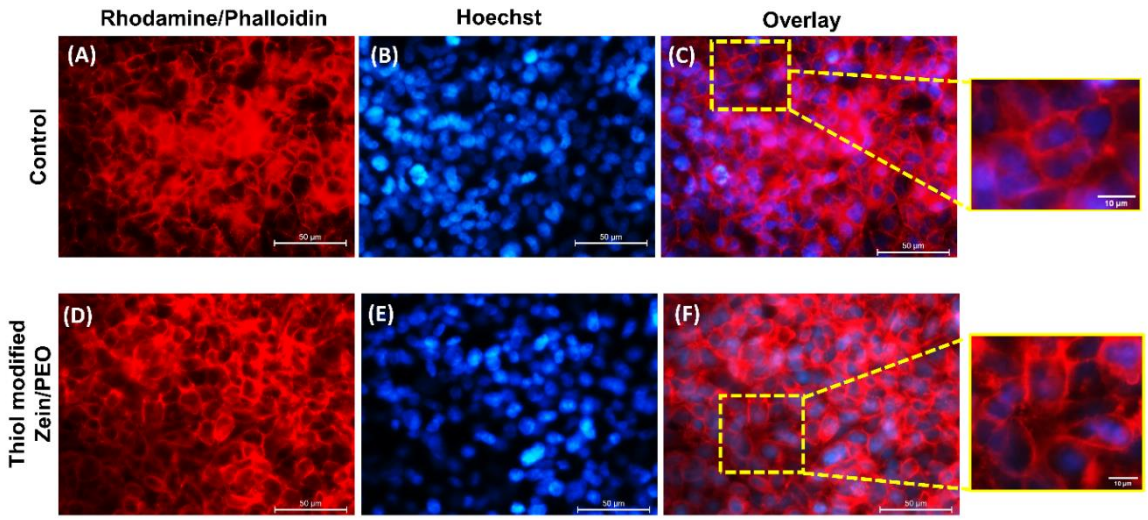

Figure 31 Fluorescent images of A-C) Control cells- F-actin stained with Rhodamine/phalloidin, nucleus stained with Hoechst, and overlay respectively D-F) Cells treated with thiol-modified Zein/PEO- F-actin stained with Rhodamine/phalloidin, nucleus stained with Hoechst, and overlay respectively (40X magnification). Enalrged images of overlay are showed on the right side of each panel.

F-actin cytoskeletal filaments of epithelial cells have been reported to support the architecture and integrity of tight junctions (Van Itallie and Anderson, 2014). Rhodamine-labelled phalloidin has been used to stain F-actin filaments and visualized under the fluorescent microscope. The nucleus was counter-stained using Hoechst. RPMI 2650 cells which are kept untreated with materials were considered as the reference control. A comparative evaluation of the F-actin morphology of control cells in figure 31A-C and test material treated cells in figure 31D-F was carried out. It is observed that treatment of RPMI 2650 cells with thiol-modified Zein/PEO does not cause changes to the structure, integrity and continuity of the F-actin filaments. Similar to the control cells, extensive epithelial filamentous structure was maintained after material treatment for 24 h. The magnified image on the right side of each panel helped to evidently confirm the observation.

4.2.15 Beta-catenin immunostaining

Cell junctions like tight junctions, adherens junctions and gap junctions seal the intercellular space of epithelial cells and regulate movement across cells (Anderson and Van Itallie, 2009). Tight junctions are present on the apical side and adherens junctions lie beneath them (Shukla et al., 2016). Beta-catenin is the protein seen in the adherens junction of epithelial cells (Kürti et al., 2012). Perturbations to the architecture and morphology of beta-catenin would reflect on the integrity of adherens junction which would further impact on the structure and coalition of tight junctions. Therefore, evaluation of the intactness of beta-catenin proteins would enlighten the tight junctional

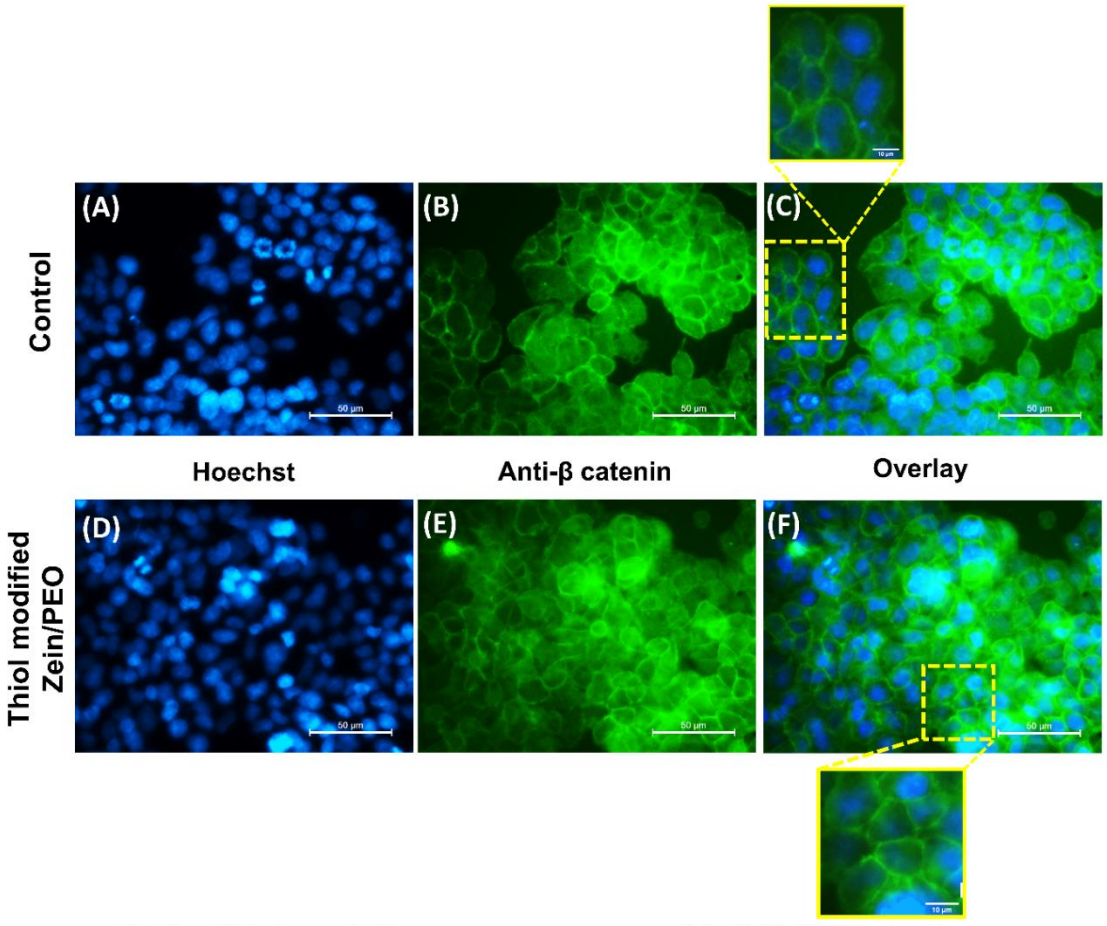

Figure 32 A-C) Immunostaining images of beta-catenin proteins of adherens junction of control cells – nucleus staining, beta-catenin staining and overlay respectively D-F) Immunostaining images of RPMI 2650 cells after treatment with thiol-modified Zein/PEO- nucleus staining, beta-catenin staining and overlay respectively (40X magnification). Enlarged images of beta-catenin staining are also shown above and below each panel.

opening. Anti-beta-catenin antibody was used to immunostaining beta-catenin proteins and visualized using fluorescent images. Hoechst was used to counterstain nuclei in cells. Figure 32A-C was taken as the control for the experiment where the cells are untreated with material and their structure was considered as the comparative reference for material-treated cells. Figure 32D-F represents fluorescent images of RPMI 2650 cells which are treated with thiol-modified Zein/PEO electrospun samples for 24 h. Magnified images on the top and bottom of each panel would help to identify the continuity of filamentous protein structure. It can be concluded from the comparative evaluation of these images that thiol-modified Zein/PEO is not causing changes in the structure of beta-catenin proteins and cell junctions are maintained close during the material treatment.

Thiolated polymers (thiomers) have been immensely probed for their ability to open tight junctions (Zhang et al., 2018). It is highly recommended for the transport of large-sized molecules like proteins (up to 16 Å diameter) and peptide drug across the mucosa. The associated disadvantage of tight junction opening is the chance of permeation of toxins, bacteria or other noxious substances across mucosa (Hasegawa et al., 2021). The traditional thiol functionalized polymers like those that have been discussed in this article pose an inherent oxidation tendency to form disulfide moieties at pH ≥5 (Zhang et al., 2018). The oxidation of cysteine to cystine under normoxic condition suppress junctional barrier dysfunction (Yin et al., 2016). The proposed drug molecule to transport across the mucosal epithelium is PL, which is comparatively very small in size and lipophilic enough to cross the epithelium via a transcellular pathway.

4.2.16 TEER measurement and drug permeation studies

Transepithelial electrical resistance (TEER) is the quantitative measure of epithelial barrier integrity. Apart from the qualitative evaluations like F-actin and beta-catenin

staining images, TEER evaluation will help in asserting junctional opening in terms of change in transepithelial electrical resistance. Figure 33A is the graphical representation of absolute TEER value and TEER (%). TEER readings were taken before and after treatment with thiol-modified Zein/PEO. The measurements reveal that TEER values stay the same even after material treatment. The impairment in the junctional opening is attributed to the oxidation of thiol groups which exist without S-protected, to disulfide groups (Federer et al., 2021; Wang et al., 2012).

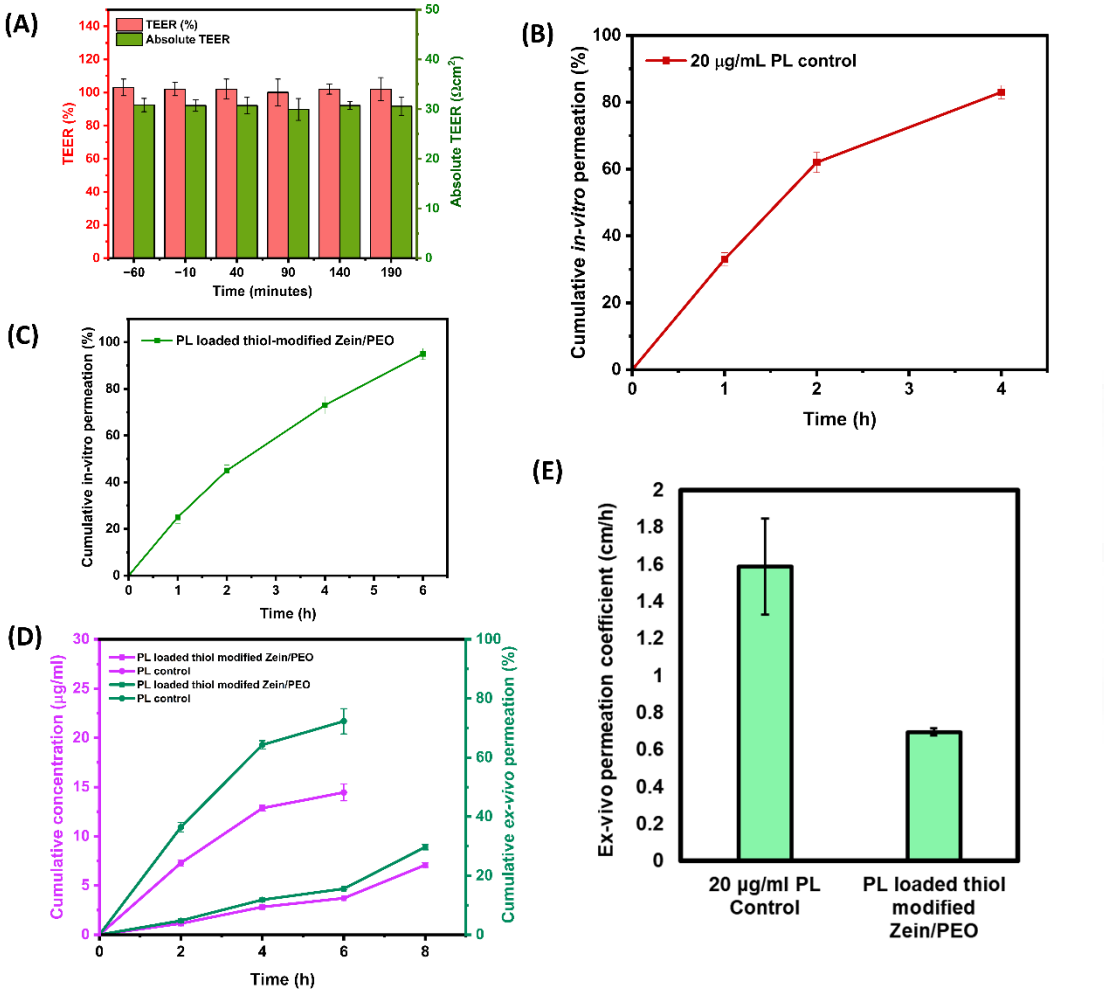

Figure 33 A) Graphical representation of absolute TEER values and TEER (%) of confluent RPMI 2650 cells before and after material treatment B) Cumulative release (%) curve of 20 µg/mL PL control obtained from *in-vitro* drug permeation study C) Cumulative release (%) curve of PL loaded thiol-modified Zein/PEO obtained from *in-vitro* drug permeation study D) Representation of *ex-vivo* permeation of PL through porcine buccal mucosa- test material and control system E) Bar diagram demonstrating *ex-vivo* permeation coefficient of test and control system

Absence of junctional opening questions the mechanism of drug transport across epithelial cells. Since paracellular transport is impossible due to junction closing. The possibility of transcellular transport has to be confirmed via *in-vitro* drug permeation through RPMI 2650 cells. PL solution of concentration 20 μg/mL prepared in HBSS was added over the cell monolayer as the control experiment. 20 μg/mL PL loaded thiol-modified Zein/PEO was placed over the cell monolayer as the test system. Within 4 h of direct administration of PL over the cell monolayer, 83 ± 2 % PL permeated across the barrier as shown in figure 33B. It took 6 h for 96 ± 2.4 % (20.8 ± 0.53 μg/mL) of PL to permeate across the barrier when it is administered as entrapped in thiol-modified Zein/PEO (figure 33C). The observed type of slow-release mechanism from thiol-modified Zein/PEO is preferable. Apart from that, direct administration of drug over mucosa is not recommended due to local irritation and patient incompliance. In account of the fact that cell junctions are not opening after material treatment, the permeation coefficient of PL-incorporated thiol-modified Zein/PEO needs to be lower than the control. The permeation coefficient of PL control and PL-incorporated thiol-modified Zein/PEO are 0.565 ± 0.025 cm/h and 0.408 ± 0.02 cm/h respectively (table 13). The permeation coefficient of PL control is high not because of junctional opening but because direct administration of PL led to immediate transport of the drug across epithelia. In the case of PL-incorporated thiol-modified Zein/PEO, an initial diffusion of PL from the electrospun matrix is required which has to be followed by epithelial transport. And also, since no junction is open, fast transport wouldn't happen. Therefore, the delay due to the diffusion of PL from the matrix caused a reduced permeation coefficient.

Table 13 *In-vitro* permeation coefficients of PL control and PL loaded thiol-modified Zein/PEO

Material	Permeation Coefficient (cm/h)
PL control	0.565 ± 0.025
PL loaded thiol-modified Zein/PEO	0.408 ± 0.02

4.2.17 *Ex-vivo* permeation through porcine buccal mucosa

In-vitro permeation of PL through RPMI 2650 cells has to be supported with evidence for *ex-vivo* permeation through porcine buccal mucosa. The porcine buccal mucosa is chosen because of its close similarity with human buccal mucosa in terms of permeation characteristics, enzyme activity and ultra-structure (Amores et al., 2014). Thiol-modified Zein/PEO placed on mucosa which is mounted in a Franz diffusion cell was the experimental system. Mucosa without adding material in diffusion cell apparatus was considered as the control. The PL permeation reached 29.7 ± 0.95 % within 8 h of the study as shown in figure 33D. It showed the best fit with the First order of drug release with an R^2 value of 0.980. A PL solution of concentration 20 µg/mL directly added over the mucosa in the donor chamber was considered as the control system. The control system exhibited 72.3 ± 4.3 % PL permeation within 6 h of the study. Though a fast permeation was observed for the control system, the permeation coefficient of the control and test material doesn't differ substantially (p-value = 0.08). The permeation coefficient of PL-loaded thiol-modified Zein/PEO is 0.694 ± 0.02 cm/h whereas that of the PL control system is 1.584 ± 0.69 cm/h (figure 33E). Both the control and test system are not causing junctional openings to augment the permeation. Still, PL permeation is fast in the control system because it bypasses the step of diffusion from the electrospun membrane. As already been discussed, direct administration of the drug is not recommended and PL-loaded electrospun membrane is facilitating adequate permeation of the drug across the mucosa.

4.3 THERMALLY CROSSLINKED ZEIN/PVP ELECTROSPUN MEMBRANE AND ITS CHARACTERIZATION

4.3.1 Preparation, drug loading and optimization of thermal crosslinking

Zein/PVP blend solutions of three different ratios of 20:2, 15:5 and 10:10 were prepared. The feasibility of electrospinning of these solutions were analysed and found that only 20:2 and 15:5 Zein/PVP blend solutions could electrospun. Higher PVP concentration caused a considerable increase in solution viscosity and therefore, electrospinning was not possible. Among 20:2 and 15:5 polymer blends, 15:5 was finalized for the study because of the assumption that higher PVP concentration would have higher adhesion over mucosa. PL was added to the 15:5 ratio of Zein/PVP blend solution at various concentrations of 0.01 mM, 0.02 mM, 0.03 mM, 0.04 mM and 0.05 mM.

The electrospun membranes of the Zein/PVP blend were subjected to thermal crosslinking at 120 °C. The time of thermal crosslinking was optimized based on the stability of electrospun matrices in contact with water. PVP is a water-soluble polymer

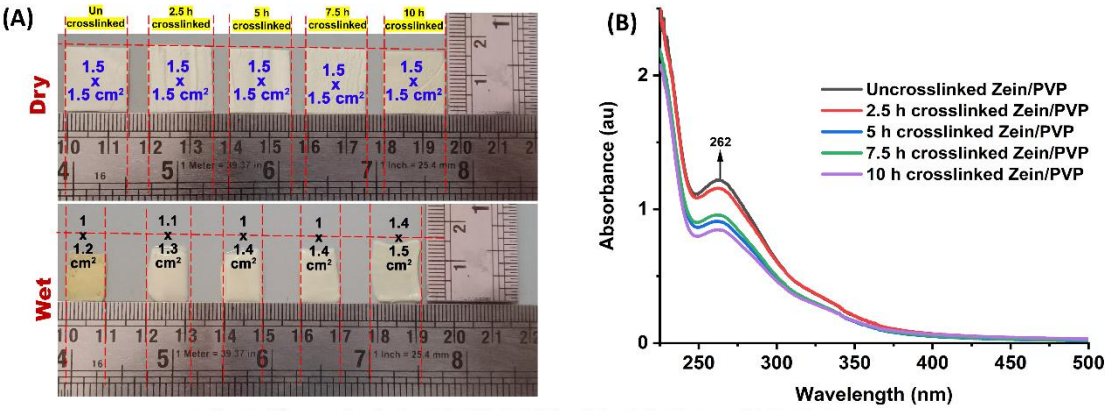

Figure 34 A) Image showing the response of different crosslinked materials after contacting water B) UV absorbance spectra of PVP leach out of thermally crosslinked Zein/PVP matrices for varying time periods

and will leach out from the matrices during immersion in water. Thermal crosslinking aims at crosslinking of PVP chains to reduce its leaching. Electrospun samples of size 1 cm x 1 cm and approximately 0.13 mm thickness were immersed in water and noted for their change in shape and strength. The samples were subjected to crosslinking for different time periods of 2.5 h, 5 h, 7.5 h and 10 h and were further evaluated. Figure 34A describes the change in the dimension of samples after coming in contact with water. With an increase in the time of crosslinking, the membranes exhibited increased stability in aqueous conditions. However, 10 h crosslinking at 120 °C exhibited sufficient stability to the matrices. UV spectra of PVP exhibited an absorbance maximum of 262 nm (Shen et al., 2005). Figure 34B describes the reduced PVP leach out with an increased time of crosslinking. The intensity of absorption maximum at 262 nm has been considerably reduced after 10 h crosslinking. Since the leaching out of PVP hasn't completely disappeared after 10 h crosslinking at 120 °C, PVP is expected to exist in uncrosslinked stage also to an extent. Literature has reported high temperature crosslinking of PVP, especially at 200 °C for 2 h (Tan et al., 2014). If so, reducing the temperature of crosslinking and increasing the time of crosslinking is expected to cause the same result. In that case, following the thumb rule of doubling the rate of reaction with every 10 °C rise in temperature, 120 °C crosslinking has to be continued to 384 h or 16 days. In this work, the only concern to employ thermal crosslinking was to impart water stability to the matrices and it had been achieved after 10 h crosslinking. The extent of crosslinking would be less after 10 h of crosslinking.

4.3.2 Surface morphology analysis by SEM

Scanning electron microscopy images of uncrosslinked and thermally crosslinked Zein/PVP were taken for the evaluation of the surface morphology of fibres (figure 35A-B). It is evident from the images that thermal crosslinking has increased the compactness

of fibres though there are no visible changes in their morphology and fibre diameter. ImageJ software was used to analyse the fibre diameter and found that thermal crosslinking hasn't resulted in any significant changes in the fibre diameter. The fibre diameter of uncrosslinked and thermally crosslinked Zein/PVP is same and is 3 ± 1 µm. Figure 35C-D represents the fibre diameter distribution curves of uncrosslinked and thermally crosslinked Zein/PVP.

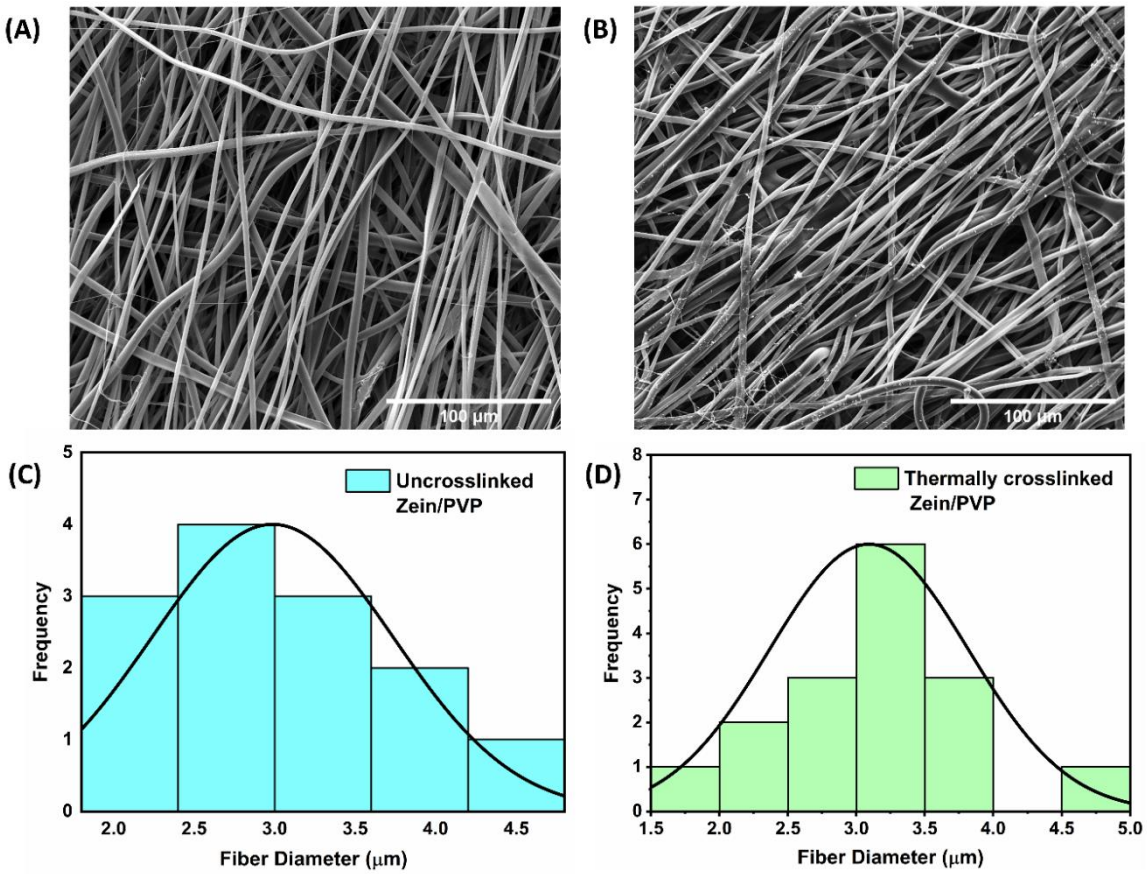

Figure 35 A-B) SEM images of uncrosslinked and thermally crosslinked Zein/PVP electrospun membranes respectively (1000X magnification) C-D) Fibre diameter distribution curve of uncrosslinked Zein/PVP and thermally crosslinked Zein/PVP respectively

4.3.3 FTIR Spectroscopy for characterization of functional groups

FTIR spectra of zein, PVP, and thermally crosslinked PVP are stacked in figure 36A. Six characteristic peaks of zein were observed in its spectra. N-H stretching vibration, also

known as amide A vibration was observed at 3280 cm^{-1}. The amide I peak, which corresponds to C=O stretching was observed at 1648 cm^{-1}. N-H bending vibration, also known as amide II vibration was noted at 1533 cm^{-1}. C-N stretching vibration was observed at 1242 cm^{-1} and C-H stretching vibration was observed at 2947 cm^{-1}. C-H bending vibration appeared at 1447 cm^{-1} (Corradini et al., 2014).

Characteristic peaks of PVP are also marked in figure 36A. N-H stretching vibration was observed at 3400 cm^{-1}, C=O stretching vibration was observed at 1645 cm^{-1}, C-N stretching vibration was noted at 1290 cm^{-1} and C-H asymmetric stretching vibration was noted at 2960 cm^{-1} (El-Batal et al., 2019). After thermal crosslinking of PVP, few changes were observed for the -CH asymmetric stretching vibration. The peak which shifted to 2970 cm^{-1} and had a decreased intensity compared to uncrosslinked PVP. It is because

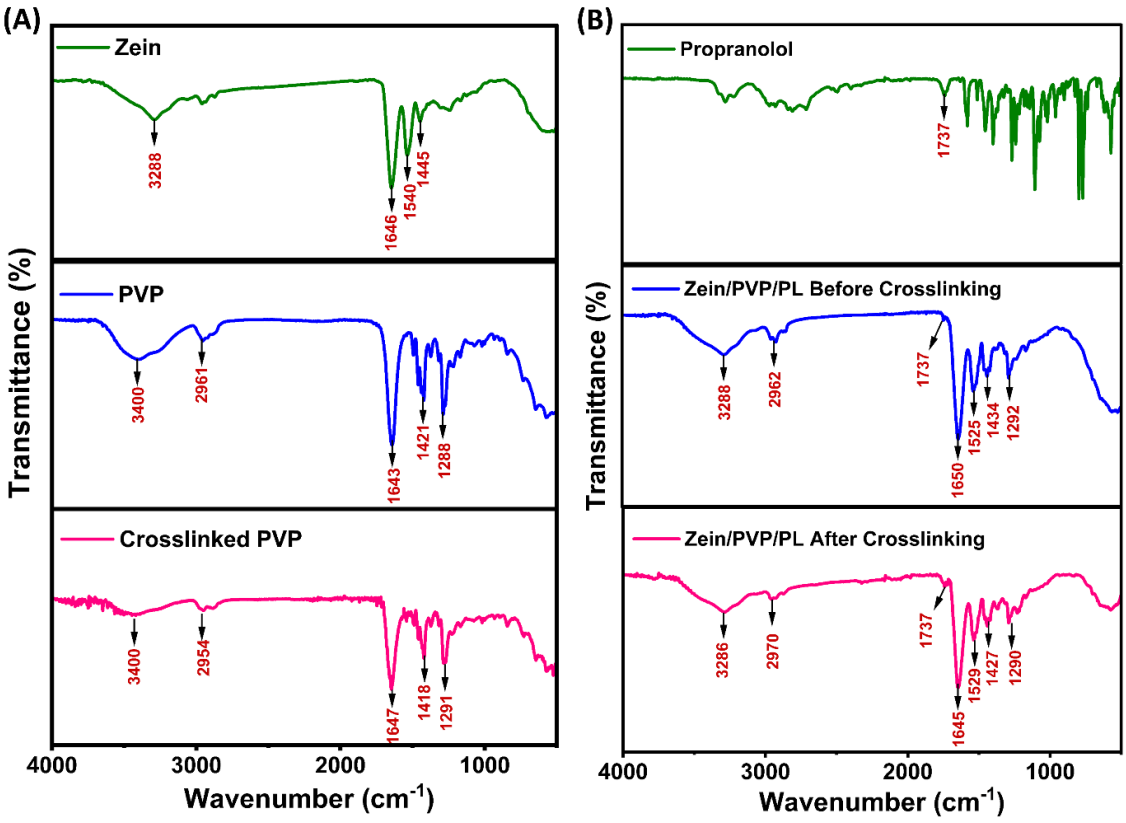

Figure 36 A) FTIR spectra of zein, PVP and thermally crosslinked PVP B) PL, uncrosslinked Zein/PVP/PL, and thermally crosslinked Zein/PVP/PL

C-H groups are involved in the crosslinking of PVP. During thermal crosslinking, -CH groups get converted to tertiary radicals and these radicals join to form crosslinked PVP structure (Tan et al., 2014). Therefore, after thermal crosslinking, the number of -CH groups will be reduced and that is the reason for the reduced intensity of C-H asymmetric stretching vibration.

FTIR spectra of PL, uncrosslinked Zein/PVP/PL and thermally crosslinked Zein/PVP/PL are stacked in figure 36B. The aromatic C=C stretching vibration found at 1737 cm^{-1} is the characteristic vibration of PL. The incorporation of PL into the electrospun membrane also resulted in the appearance of aromatic C=C stretching vibration at 1737 cm^{-1}. The appearance of aromatic C=C stretching vibration is undisturbed by thermal crosslinking. Similar to PVP and thermally crosslinked PVP spectra, a reduction of the intensity of C-H stretching vibration was observed in the case of uncrosslinked Zein/PVP and thermally crosslinked Zein/PVP.

4.3.4 Raman spectroscopy

Raman spectroscopy is another tool used to further confirm the thermal crosslinking of PVP. The main characteristic Raman vibrations of PVP were observed at 753 cm^{-1}, 934 cm^{-1}, 1372 cm^{-1} and 1670 cm^{-1} which all correspond to C-C vibration, C-C breathing vibration, C-H deformation and C=O stretching vibration respectively. A significant vibration at 934 cm^{-1} was observed in the Raman spectra of PVP which corresponds to C-C ring breathing mode (RBM) vibration (Alibe et al., 2019; Grant et al., 2021) (figure 37A). Due to thermal crosslinking, the RBM of PVP shifted to 930 cm^{-1}. From figure 37B, it can be seen that the RBM of uncrosslinked Zein/PVP appeared at 934 cm^{-1} which downshifted to 930 cm^{-1} after thermal crosslinking. The shift happened within 2.5 h of crosslinking itself. The shift was observed for both 2.5 h and 10 h crosslinked Zein/PVP samples. The literature proposes that the shift in RBM is attributed to either conversion

of the pyrrolidone ring structure of PVP or the stiffening of fibre structure due to crosslinking (Maciejewska et al., 2019).

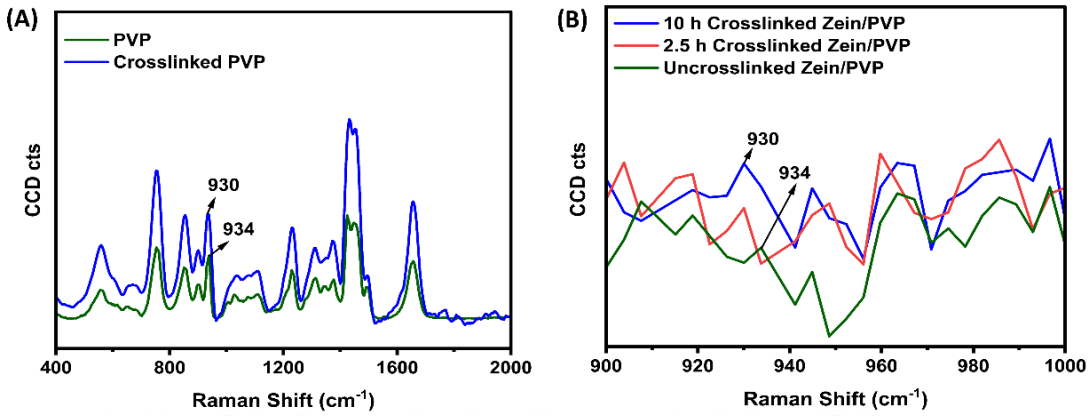

Figure 37 A) Raman spectra of PVP and crosslinked PVP B) Raman spectra of uncrosslinked and thermally crosslinked electrospun samples of Zein/PVP for varying time periods

4.3.5 Thiol estimation using Ellman's assay

Ellman's assay quantifies the concentration of free sulfhydryl groups in the polymer system. Thermal treatment of zein would cause heat-induced disulfide bond breakage. Federici *et al* have reported conformational changes happening to the alpha-helical structure of zein to beta-sheet structure (Federici et al., 2021). During higher temperature thermal treatment, disulfide bonds in the terminals of protein structure would break and set more thiol groups free. The thermal stability of the majority of globular proteins is aided by the disulfide bonds present in their native conformation. Ogawa *et al* have reported the susceptibility of bonds to thermal treatment (Akazawa-Ogawa et al., 2016). Disulfide-thiol exchange reactions mediate the destabilization of disulfide bonds during thermal treatment (Futami et al., 2017). Sulfhydryl groups would be acting as reducing agents to cleave the intramolecular disulfide bonds in the structure of the protein under non-aqueous conditions (Cabra et al., 2008). Ellman's assay and associated quantification of thiol concentration in Zein/PVP electrospun samples crosslinked for varying time

periods are represented as a bar diagram in figure 38A. It is observed that, up to 7.5 h crosslinking at 120 °C, a considerable change in thiol concentration was not observed. But thiol concentration considerably increased after 10 h crosslinking (p-value = 0.02). This indicates that appreciable amount of disulfide breakage is happening during long time exposure of temperature rather than short-term exposure. The thiol group concentration of uncrosslinked Zein/PVP is 100 ± 1 µM. After 2.5 h, 5 h and 7.5 h crosslinking, thiol concentrations were 113 ± 4 µM, 120 ± 3 µM and 117 ± 4 µM respectively. However, 10 h treatment at 120 °C caused an increase in thiol concentration to 127 ± 1 µM.

Table 14 Tabular representation of percentage content of different protein conformations in uncrosslinked and thermally crosslinked samples of Zein/PVP

	α helix (%)	**β sheet parallel (%)**	**β sheet antiparallel (%)**	**Random coil (%)**
Uncrosslinked Zein/PVP	73.9	26.1	0	0
Thermally crosslinked Zein/PVP	0.5	23.2	44.9	31.4

4.3.6 CD spectroscopy

Thermal treatment has been reported to cause conformational changes to the protein structure of zein. Since zein is a natural protein extracted from corn and is having a native alpha-helical conformation (Wei et al., 2021). It is expected according to literature reports that thermal crosslinking of zein would change the conformation to beta sheet (Drummy et al., 2005; Federici et al., 2021). In accordance with the anticipation, the alpha-helical content of zein significantly reduced from 73.9 % to 0.5 %. And on the other hand, anti-parallel beta-sheet content increased to 44.9 %. Table 14 has included the percentage content details of individual conformations of Zein/PVP electrospun membrane before

and after thermal treatment. It is evident from the table that thermal crosslinking has caused an increase in random coil content to 31.4 %. Sun *et al* have reported an increase in the random coil content of zein due to thermal crosslinking (Sun et al., 2016). A higher percentage of random coil conformation is an indication of more uncoiling happening to the protein structure during thermal crosslinking. In summary, both breakage of disulfide bonds and uncoiling of protein conformation takes place during thermal crosslinking of zein for 10 h.

4.3.7 Percentage of water uptake and Porosity evaluation

Evaluation of the percentage of water uptake is an approach to confirm crosslinking of polymer chains. The percentage of water uptake will decrease with an increased degree of crosslinking (Chen et al., 2019). Therefore, thermally crosslinked samples for different periods were subjected to percentage water uptake, analysed and depicted in figure 38B. At 1 h of study, the percentage water uptake of 2.5 h crosslinked samples was high compared to other time crosslinked samples. The water uptake percentage of 2.5 h crosslinked samples was 1056 ± 31 %, which was significantly higher than 593 ± 56 % of the 10 h crosslinked sample (p-value = 0.001). At 4 h, 9 h and 25 h of evaluation also, the water uptake percentage followed a similar trend where the water uptake percentage of 10 h crosslinked samples was much lesser than 2.5 h crosslinked samples.

The percentage of water uptake is expected to increase with time of immersion. But in this case, for a particular sample, the water uptake percentage decreased with time and later became constant. This is expected to be because of the leaching out of uncrosslinked PVP at initial periods. Because not all PVP chains are crosslinked during thermal treatment. Uncrosslinked PVP will leach out initially within 4 h of the experiment. After 4 h of the experiment, the water uptake percentage remained constant for all crosslinked samples.

It is expected that both PVP and zein are undergoing crosslinking during thermal crosslinking. The mechanism of crosslinking of PVP is chemical in nature whereas that of zein is physical in nature. PVP undergoes a radical-mediated crosslinking and zein undergoes a conformational change-mediated crosslinking. Both happen independently of each other. Schematic representations of crosslinking of PVP and zein are depicted in figure 38C.

The density method calculation of the porosity of thermally crosslinked Zein/PVP resulted in 73 ± 1 % of porosity.

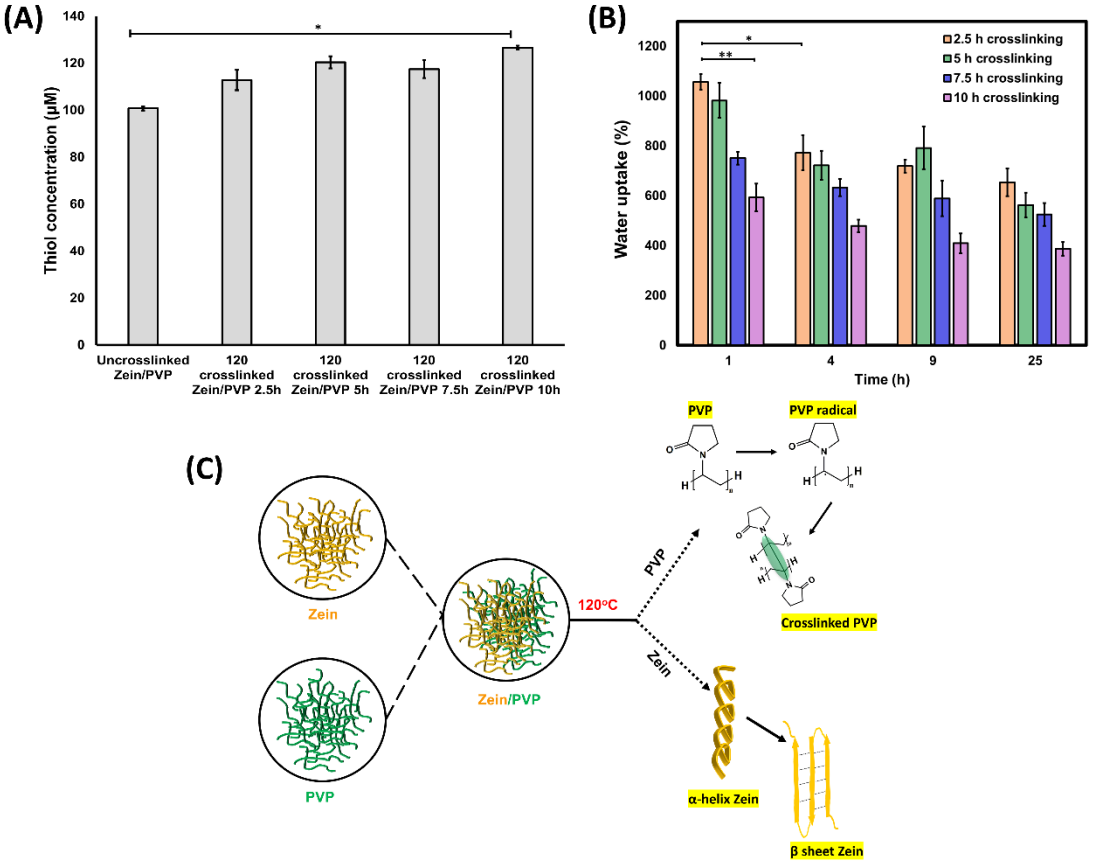

Figure 38 A) Graphical representation of thiol concentration of thermally crosslinked samples for varying time periods B) Graphical representation of % water uptake of thermally crosslinked Zein/PVP for varying time periods (n =3) C) Schematic representation of crosslinking of PVP and zein during thermal treatment

Table 15 Table representing the temperature of completion of decomposition of uncrosslinked and thermally crosslinked Zein/PVP

Material	Temperature onset of decomposition (°C)	The temperature of completion of degradation(°C)
Uncrosslinked Zein/PVP	261.92	922.62
2.5 crosslinked Zein/PVP	251.41	852.22
10 h crosslinked Zein/PVP	222.57	849.59

4.3.8 Thermogravimetric analysis

Thermogravimetric analysis of uncrosslinked and thermally crosslinked Zein/PVP was performed and thermal stability was evaluated. It has been reported that the thermal decomposition of zein starts at 250 °C and 80 % weight loss happens between 250 °C and 490 °C (Altan et al., 2018). Similarly, thermal degradation of PVP has been reported to start at 190 °C and 80 % weight loss happens between 200 °C to 460 °C (Azeez, 2016). Thermal degradation of the electrospun polymer blend of zein and PVP will be collectively influenced by the individual degradation profiles of zein and PVP. The decomposition of uncrosslinked Zein/PVP started at 261.9 °C. The temperature onset of degradation of 2.5 h and 20 h crosslinked samples are 251.4 °C and 225.6 °C respectively. Thermal crosslinking has resulted in early start of thermal degradation for Zein/PVP samples. In the case of uncrosslinked Zein/PVP electrospun matrix, 100 % decomposition was noted at 922.6 °C. But, thermal crosslinking after electrospinning has downshifted the temperature of completion of decomposition. Though the pattern of degradation is same for uncrosslinked and thermally crosslinked samples (figure 39A), pre-mature decomposition was noted after thermal crosslinking. 2.5 h crosslinked Zein/PVP exhibited its complete decomposition at 852.2 °C and 10 h crosslinked Zein/PVP

exhibited its complete decomposition at 845.6 °C. Details of temperature of decomposition are given in table 15.

4.3.9 Mechanical characterization

The tensile strength of different time-crosslinked samples was evaluated. A significant increase in tensile strength was observed after 5 h of thermal crosslinking. Uncrosslinked Zein/PVP was having a tensile strength of 2.66 ± 0.21 MPa. Tensile strength of 2.5 h and 5 h crosslinked Zein/PVP are 2.68 ± 0.24 MPa and 2.97 ± 0.27 MPa respectively. A significant increase in tensile strength to 3.5 ± 0.17 MPa was observed for 7.5 h crosslinked Zein/PVP compared to uncrosslinked Zein/PVP (p-value = 0.01) and 2.5 h crosslinked Zein/PVP (p-value = 0.002). A much higher value of tensile strength was demonstrated by 10 h crosslinked Zein/PVP which is 3.92 ± 0.13 MPa (p-value = 1.76 x 10^{-5}). This observation is attributed to the efficient crosslinking happening with an increase in the time of crosslinking. Due to increased efficiency in crosslinking, the free motion of polymer chains would be restricted and thus strength would be increased. Graphical representations of the tensile strength of Zein/PVP electrospun matrices crosslinked for varying time periods are shown in figure 39B. In addition to crosslinking, prolonged thermal treatment would be causing ordered arrangement of polymer chains and thus increasing crystallinity. This would also be contributing to the improvement in tensile properties. Conformational changes of zein from alpha-helix to beta-sheet would also be contributing to this observation.

Figure 39C discusses the changes in mechanical properties of PVP alone before and after thermal crosslinking. The tensile strength of uncrosslinked PVP was 7.6 ± 0.25 MPa which considerably increased to 10.8 ± 1.05 MPa after thermal crosslinking for 10 h. In

this case also, the improvement in mechanical properties would be collectively contributed by crosslinking of PVP chains and increased crystallinity.

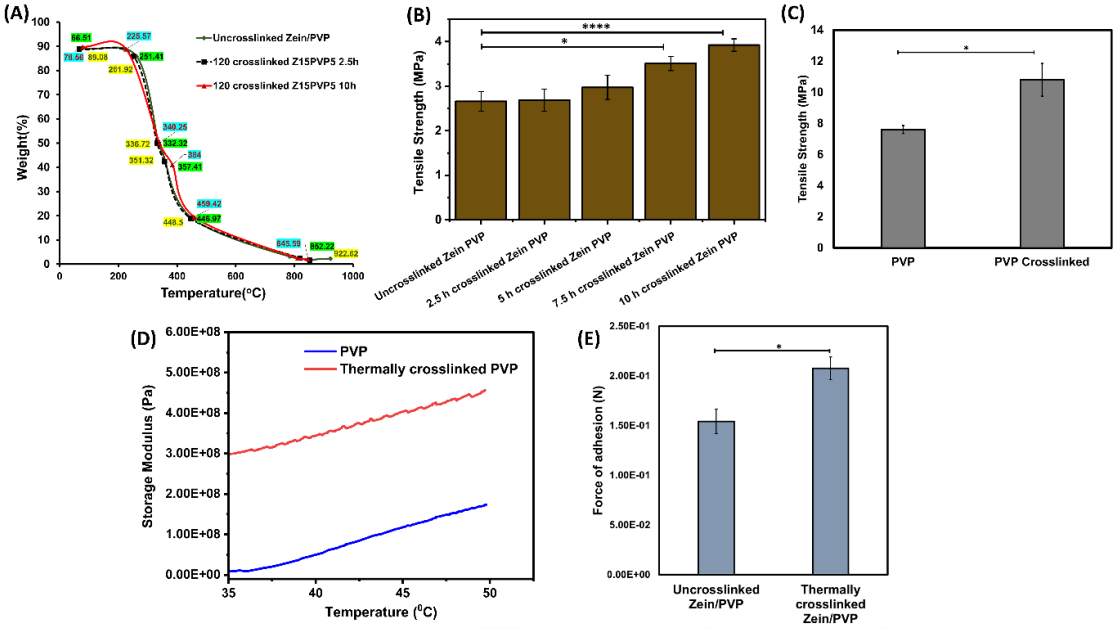

Figure 39 A) TGA thermogram of uncrosslinked and thermally crosslinked Zein/PVP B) Tensile strength representation of Zein/PVP samples with and without thermal crosslinking C) Tensile strength representation of PVP before and after thermal crosslinking D) DMA thermogram of PVP before and after thermal crosslinking E) Force of adhesion of uncrosslinked Zein/PVP and thermally crosslinked Zein/PVP on porcine buccal mucosa represented as bar graph

4.3.10 Dynamic Mechanical Analysis

Solvent cast PVP films were subjected to DMA analysis. Temperature sweep under tension mode of analysis was continued till 50 °C. The initial storage modulus of uncrosslinked PVP was 3.8 x 10^6 Pa whereas that of crosslinked PVP was 3.0 x 10^8 Pa at 35 °C. This observation itself is an indication of crosslinking happening (Zhang et al., 2019). The DMA thermogram in figure 39D shows that the storage modulus is increasing with the increase of the temperature of analysis. Similar to tensile strength analysis, an increase in storage modulus with increase in testing temperature is attributed to two phenomena. One is the crosslinking of PVP chains happening during temperature treatment and the second one is an increase in crystallinity. Already crosslinked PVP also

showed an increase in storage modulus because uncrosslinked sites in the polymer structure are getting crosslinked during the temperature exposure.

4.3.11 Texture analysis for mucoadhesion

Mucoadhesion of uncrosslinked Zein/PVP and thermally crosslinked Zein/PVP were analysed using porcine buccal mucosa and compared. From figure 39E it can be seen that thermal crosslinking has resulted in an increase in the force of adhesion over porcine buccal mucosa. Thermally crosslinked Zein/PVP exhibited $2.08 \times 10^{-1} \pm 1.12 \times 10^{-2}$ N of adhesion which was significantly higher than the $1.54 \times 10^{-1} \pm 1.22 \times 10^{-2}$ N of uncrosslinked Zein/PVP (p-value = 0.015).

The contribution of PVP towards mucoadhesion is regarding its hydrophilicity which very well fits with the wetting theory of mucoadhesion (Alsarra et al., 2011; Tort et al., 2019). And also, polymer chains of PVP can easily penetrate through the mucin glycoprotein chains and establish mucoadhesion via the diffusion model of mucoadhesion. Mucoadhesive properties of PVP can also be explained based on the adsorption model because of its ability to form hydrogen bonds and van der Walls interactions with mucin (Vecchi et al., 2021).

Mucoadhesion is highly favoured with the presence of thiol functional groups because of the establishment of disulfide interaction with the cysteine moieties of mucin (Bernkop-Schnürch, 2005; Leichner et al., 2019). Zein is known for carrying many disulfide bonds in its structure. During thermal treatment, disulfide bonds get broken and thiol groups are set free for binding. As a result of increased thiol content, the mucoadhesive property increased after thermal treatment. Along with that, uncoiling of protein conformations of zein would be enabling free interpenetration of zein polymer chains with mucin chains to establish a diffusion model of mucoadhesion. A cumulative effect of all these factors might be the reason for improved mucoadhesion after thermal crosslinking of Zein/PVP.

4.3.12 Drug dissolution studies

Table 16 Table describing the entrapped concentration of PL in different formulations

Formulation	Blended amount of drug (µg)	The expected amount of drug in the membrane (µg)	The actual amount of drug entrapped (µg)	Drug entrapment (%)
F1	130	94	90	96.2
F2	260	246	115	47.2
F3	390	360	102	28.4
F4	520	211	54	25.8
F5	600	556	157	28.2

A drug dissolution study was done by dissolving pre-weighed pieces of drug-loaded membranes in ethanol and noting the UV absorbance at 290 nm. A drug dissolution study is important to analyse and quantify the amount of drug entrapped in the membrane based on the final weight of the electrospun membrane. Zein/PVP membranes loaded with five different concentrations of PL were prepared by taking 0.75 g zein and 0.25 g PVP in ethanol solvent. The preparation of F1 formulation was done by dissolving 130 µg PL into the polymer solution carrying 1 g polymers in total. After electrospinning, 1 g of membrane was expected to be collected from the mandrel, but in reality, 0.72 g membrane was obtained. The remaining polymer was lost during the process of electrospinning. If so, the whole 130 µg of PL can't be expected to be entrapped in the membrane. The membrane having 0.72 g weight is theoretically expected to entrap 94 µg PL in it. UV absorbance measurement at 290 nm experimentally quantifies the actual entrapped concentration of PL in the membrane, which was 90 µg. Therefore, the entrapment percentage of the F1 formulation is 96.2 ± 0.1 %. Details of the theoretical amount of

drug loading and experimental amount of drug loading of F1 to F5 formulations are given in table 16.

Out of five formulations, F1 formulation showed a maximum entrapment percentage of 96.2 ± 0.1 %. Other formulations exhibited less than 50 % of entrapment. It can be seen from table 16 that an increase in the concentration of drug loading is causing the increase in the amount of drug entrapped but not proportionate to the amount of drug blended.

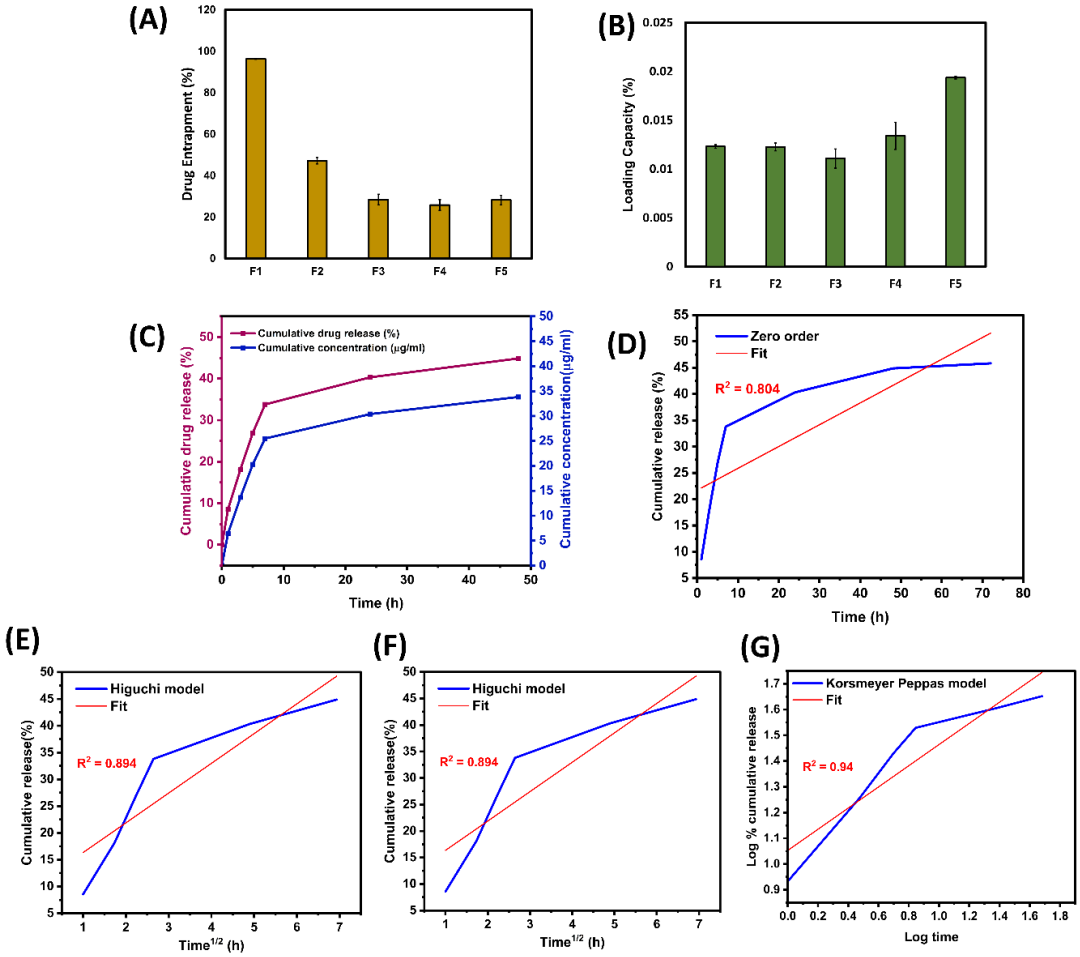

Figure 40 A) Drug entrapment (%) of F1-F5 formulations B) Loading capacity (%) of F1-F5 formulations C) Drug release kinetics of thermally crosslinked Zein/PVP and D-G) Mathematical model fitting with cumulative release – Zero order, First order, Higuchi model and Korsmeyer Peppas model respectively

Therefore, a sequential increase in drug entrapment can't be observed which might be due to aggregation of drug molecules at higher concentrations and consequent non-uniform distribution in the electrospun membrane (Lian and Meng, 2017). A simple

blending electrospinning technique for drug entrapment has been reported for low efficiency in entrapment percentage and uneven distribution of drug in the electrospun membrane (Sun et al., 2019). The drug entrapment percentage of F2 formulation decreased to 47.2 ± 1.6 %. It further decreased to 28.4 ± 2.5 % in the F3 formulation and later maintained the entrapment percentage constant. Figure 40A is the graphical representation of the drug entrapment percentage of all five formulations.

Loading capacity is the percentage ratio of the amount of drug-loaded and the total weight of the drug-loaded membrane. Figure 40B demonstrated the graphical diagram of loading capacity. The highest loading capacity was exhibited by the F5 formulation which is 0.019 ± 0.0001 %. The magnitude of loading capacity is very low because PL was loaded in microgram quantity and the weight of the polymer membrane falls in the gram range. The loading capacity of the F5 formulation is high, even though the entrapment percentage is more for the F1 formulation because the amount of drug entrapped is more in F5 than in F1. F1 contains only 90 μg PL entrapped whereas the amount of PL entrapped in F5 is 157 μg.

4.3.13 Drug release studies

F5 formulation of thermally crosslinked Zein/PVP having the highest loading capacity was selected for drug release kinetics evaluation. Figure 40C indicates the drug release trend from thermally crosslinked Zein/PVP which initially had an initial release profile and later a sustained release profile. The cumulative release of PL was 8.6 ± 0.3 % at 1 h of study which further increased to 18 ± 0.1 % after 5 h. Within 48 h of the study, 44.9 ± 0.5 % of PL was released into the PBS media. Figure 40C also describes the trend of cumulative concentration of PL release in μg/mL. From the figure, it is clear that 33.8 ± 0.4 μg/mL of PL release happened within 48 h from thermally crosslinked Zein/PVP. Out of four mathematical models tried for fitting with the release profile, the Korsmeyer

Peppas model showed the best fit with an R^2 value of 0.94. Zero order, First order and Higuchi model of release showed poor fit as the correlation coefficients were 0.804, 0.687 and 0.894 respectively. Cumulative release graphs showing the extent of fit with different mathematical models are given in figure 40D-G. The 'n' value of the Korsmeyer Peppas fitting equation was 0.14 which corresponds to quasi-fickian diffusion (Olejnik et al., 2017), where drug release is facilitated by diffusion rather erosion or swelling.

4.3.14 Direct contact assay for cytotoxicity evaluation

Cytotoxicity responses of RPMI 2650 cells due to contact with thermally crosslinked Zein/PVP were evaluated by direct contact assay. The impact of PL loading on the viability of cells was also analysed. Thermally crosslinked Zein/PVP electrospun membranes with and without PL loading were placed over the RPMI 2650 cell monolayer for 24 h and incubated. F5 formulation having a higher loading capacity was selected for the cytotoxicity analysis. The phase contrast images of the cell-material system were taken after 24 h and analysed. The harmful influence of materials will be reflected as dead cells, morphology-lost cells or disturbance to cell monolayer. Figure 41A-E represents the phase contrast direct contact images of RPMI 2650 cells. Figure 41A and 41B are the positive and negative control images. Figure 41C is the reference or cell alone control where the real morphology of live cells and intactness of cell monolayer can be seen. Reference cells are just media-treated cells. Figure 41D and 41E are cells treated with thermally crosslinked Zein/PVP without and with PL loading. In reference to the control cells, material treatment hasn't resulted in toxicity to the cells. Direct contact assay concludes the materials as non-cytotoxic.

4.3.15 Live/dead assay

Fluorescent imaging of RPMI 2650 cells, distinguishing live and dead cells using different stains enriches information obtained from direct contact assay. Acridine orange/ethidium bromide stains were used for the staining where the former stains live

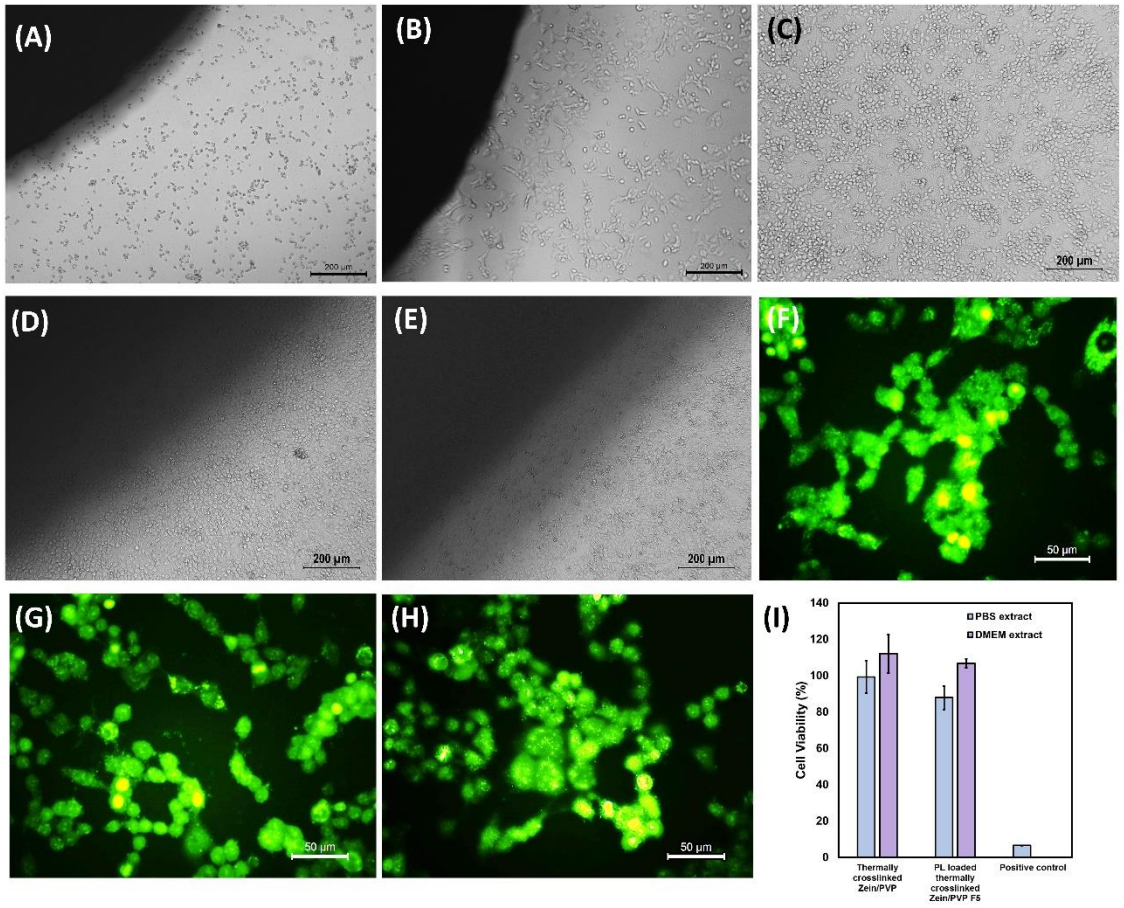

Figure 41 Direct contact images of A) Positive control cells B) Negative control cells C) Cell alone control D) Thermally crosslinked Zein/PVP treated cells E) PL loaded thermally crosslinked Zein/PVP treated cells (Images were taken in 10X magnification), live/dead assay images of F) Control cells G) Thermally crosslinked Zein/PVP treated cells H) PL loaded thermally crosslinked Zein/PVP treated cells and (images were taken in 40X magnification) I) % cell viability as bar diagram representation

cells and the latter stains dead cells. Live cells are visualized as green and dead cells as red. Figure 41F is the control image. The appearance of the majority of live cells in green colour is the reference for the test material analysis. Figures 41G and 41H are the live/dead fluorescent images of cells treated with thermally crosslinked Zein/PVP without and with PL loading respectively. The images are self-explanatory regarding the

non-cytotoxic properties of the materials under study. The majority of the cells appeared live in the images and few cells are red. The red cells are marked using arrows. Since a majority of cells stayed live after material treatment live/dead assay also concluded non-cytotoxicity of materials of interest.

4.3.16 MTT assay

Unlike direct contact assay and live/dead assay, MTT assay is a quantitative estimation technique. MTT assay measures the metabolic activity of viable cells via their ability to convert MTT to formazan complexes. If the material is not toxic to cells, the conversion of MTT to formazan is possible. Higher the number of live cells present, the higher the conversion happens. Quantification of formazan is the direct indication of cell viability (Präbst et al., 2017). MTT assay was carried out using material extracts in PBS and DMEM media. PBS extracts of thermally crosslinked Zein/PVP showed 99.3 ± 9 % cell viability after 24 h incubation with RPMI 2650 cells. Incorporation of PL into thermally crosslinked Zein/PVP also hasn't harmed the viability of cells. F5 formulation showed 87.8 ± 6.4 % viability after 24 h incubation (figure 41I). A similar trend was observed when material extracts in DMEM media were used for the MTT assay. Thermally crosslinked Zein/PVP and PL loaded thermally crosslinked Zein/PVP demonstrated cell viability of 112 ± 11 % and 107 ± 2 % in respective order. However, cell viability of thermally crosslinked Zein/PVP hasn't exhibited a significant difference with PL loaded system (p-value = 0.05). Therefore, PL loading is not causing cytotoxicity to RPMI 2650 cells in particular. Phenol-added cells were taken as the positive control in the experiment.

4.3.17 F-actin staining for the evaluation of cytoskeleton morphology

Fluorescent staining of F-actin filaments using Rhodamine/phalloidin staining helps to visualize and analyse the filament structure and integrity. Along with F-actin staining, nucleus staining was done using Hoechst. Figure 42A-B represents untreated control cells after nucleus and F-actin staining respectively. Figure 42C is the overlay of both. The morphology and cytoskeleton intactness could be considered as the reference for the analysis of material-treated cells. After treating RPMI 2650 cells with thermally crosslinked Zein/PVP, fluorescent images were taken. It can be visualized from figure 42D-F that the integrity of F-actin filaments is left undisturbed after material treatment. F-actin filaments play a crucial role in maintaining junctional protein integrity. Therefore, the absence of alteration in the continuity of F-actin filaments points towards the absence of junctional openings in epithelial cells.

4.3.18 Immunostaining of beta-catenin proteins in adherens junction

Since F-actin filaments stay unchanged in terms of morphology as well as intactness, disturbance causing epithelial cell junction is unlikely. Fluorescent antibody staining of beta-catenin proteins of adherens junctions (Kürti et al., 2012) in RPMI 2650 cells will help to confirm the hypothesis. Figure 42G-I demonstrates the images of control cells where the unperturbed beta-catenin proteins are visible with perfect morphology and barrier integrity. Changes happening to this structure after treating with thermally crosslinked Zein/PVP are analysed in figure 42J-L. It was found that treating RPMI 2650 cells with thermally crosslinked Zein/PVP doesn’t permute the coherence of beta-catenin proteins.

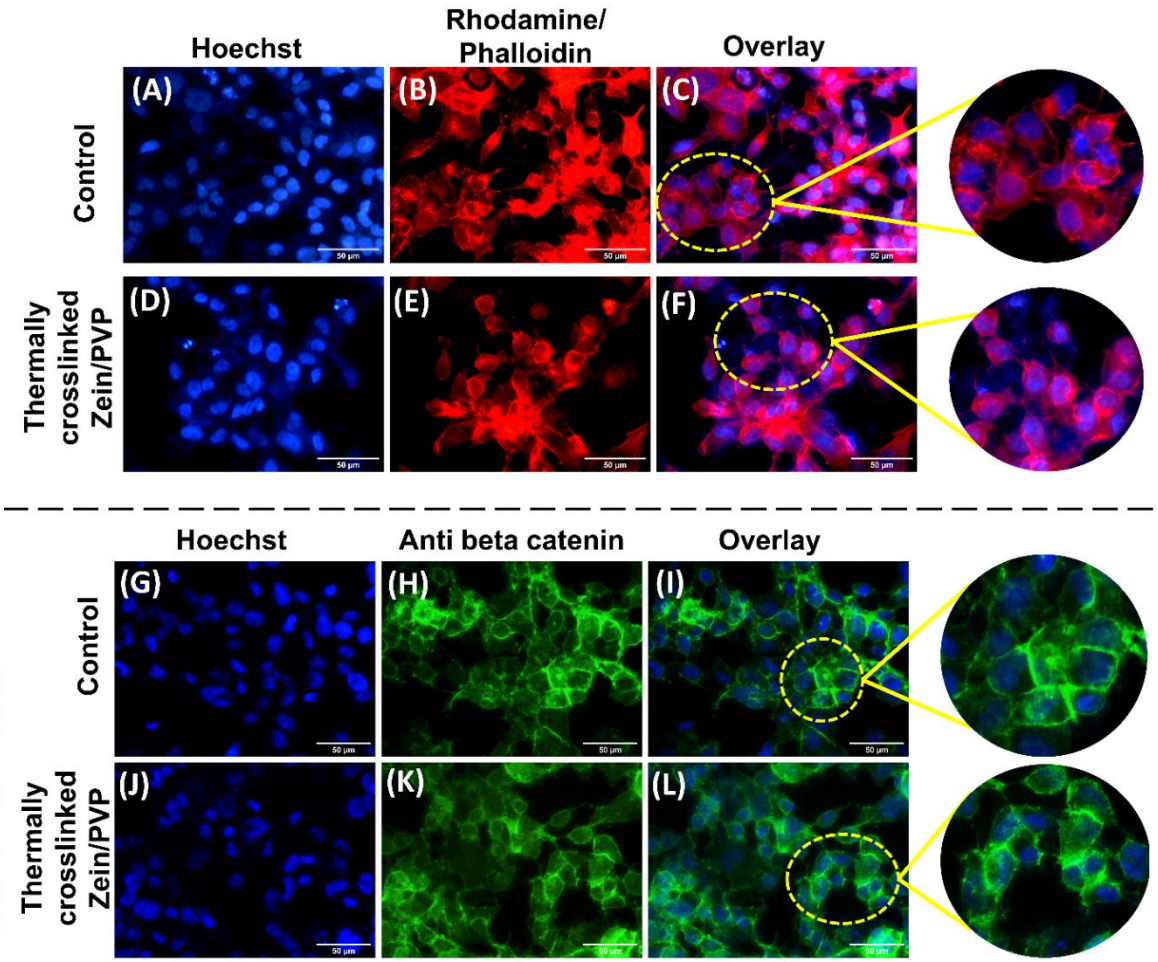

Figure 42 F-actin staining of A-C) Control cells D-F) Cells after treatment with thermally crosslinked Zein/PVP and Immunostaining of beta-catenin junctional protein of G-I) Control cells J-L) Cells after treatment with thermally crosslinked Zein/PVP (all images taken in 63X magnification) [The magnified overlay images are kept on the right side of each panel]

Biomaterials known for causing disturbance to junctional integrity are calcium chelators, ionic liquids surfactants and cationic polymers (Brunner et al., 2021). Zein and PVP don't fall under any of these categories and not causing disturbance to adherens junctions. Even though the adherens junction is not directly controlling paracellular transport, it helps to maintain tight junction assembly and thus indirectly regulates paracellular activity. Disruption of the tight junction will reflect in the structural coherence of the adherens junction also (Han et al., 2019). Notwithstanding the junctional opening, the mode of transport of drug molecules across the epithelial monolayer is anticipated to be

transcellular. Paracellular transport could be anticipated only if there is a loss of barrier integrity.

4.3.19 TEER measurement

Transepithelial Electrical Resistance (TEER) evaluates the integrity of the cell monolayer. The absolute TEER values and TEER (%) calculated are plotted in figure 43A. The absolute TEER value of confluent RPMI 2650 cells lies in the range of 25-30 Ωcm^2 (Kim et al., 2018). In this experiment also, the observed values of absolute TEER of cultured RPMI 2650 cells in a liquid-liquid interface were around 30-33 Ωcm^2. The value didn't change with time before and after material treatment. Similarly, TEER (%) also hasn't changed significantly before and after treatment with thermally crosslinked Zein/PVP. And also, thermal crosslinking of the Zein/PVP blend hasn't influenced the ability of the material to cause changes in the barrier integrity in any way. The TEER (%) values as well as absolute TEER values of RPMI 2650 cells do not considerably differ with the treatment of uncrosslinked and thermally crosslinked Zein/PVP. These observations abide by the above-discussed facts regarding the opening of junctional proteins. Immunostaining of beta-catenin proteins revealed that there is no opening of

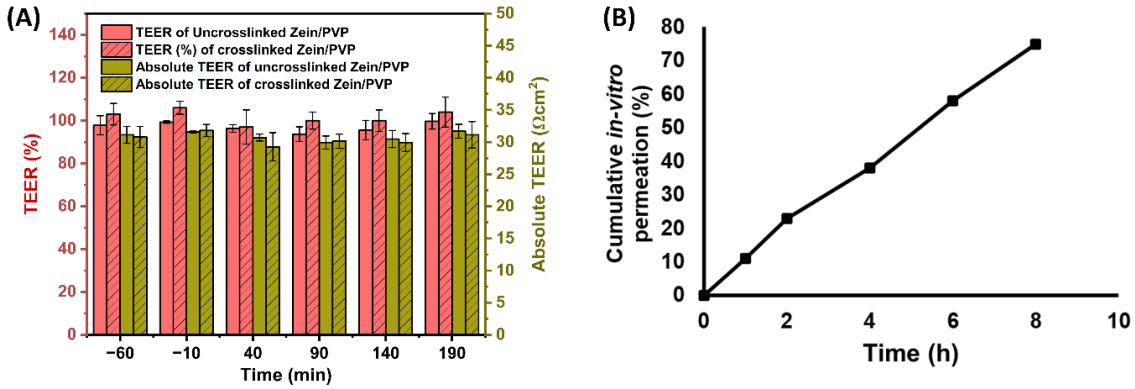

Figure 43 A) Graphical representation of TEER (%) and absolute TEER of uncrosslinked and thermally crosslinked Zein/PVP B) Zero order *in-vitro* drug permeation profile of PL loaded thermally crosslinked Zein/PVP

cell junctions happening due to the influence of material added. Hence TEER is not expected to vary with time. Hence, drug transport through the cell monolayer is expected to happen through the transcellular pathway.

4.3.20 *In-vitro* PL permeation study

In-vitro drug permeation studies through culture inserts were done to confirm the permeation of the drug through the cell monolayer even in the absence of cell junction opening. The release kinetics of PL control was also studied. 75 ± 2 % cumulative release of PL is observed within 8 h from PL loaded thermally crosslinked Zein/PVP. The *in-vitro* drug permeation profile is best fitted with Zero-order kinetics of drug release (figure 43B). The correlation coefficient of fitting of drug release profile with different drug release models is shown in table 17. Zero-order permeation of the drug through the cell monolayer facilitated the release of the drug at a constant rate and overcomes the issue of immediate release (Laracuente et al., 2020). As a control system of study, PL of the same concentration as in the above system but without incorporating in electrospun matrix was also added over the cell monolayer. In control, 88 ± 3 % of cumulative release of PL happened within 4 h of study in control. The easiness of permeation of PL through the cell monolayer would vary for drug samples directly delivered over the cell and delivered through a matrix system. It is advised to deliver the drug through polymeric carriers to reduce the local irritation expected due to the direct administration of the drug (Rabiee et al., 2021). Moreover, direct drug administration without a carrier is practically impossible and it is not patient- friendly also. Drug samples delivered through a matrix system like an electrospun membrane would take time for the drug to release out of the matrix and then to permeate through the cell monolayer. Hence, the permeation coefficient of PL control was found to be 0.402 ± 0.012 cm/h which is higher than that

of PL loaded thermally crosslinked Zein/PVP system which is only 0.173 ± 0.002 cm/h (table 18). This slow-release profile helped to avoid the burst release of the drug.

The permeation coefficient of thermally crosslinked Zein/PVP was less because tight junctions were not opened in contact with the membrane. It is to be noted that PL is lipophilic enough to cause transcellular permeation (Gumina and Yan, 2019; Vogelpoel et al., 2004). Therefore, the role of the membrane system as a carrier for PL and the ability of PL to permeate through the cell layer enabled the constant release of PL for a prolonged time.

Table 17 Correlation coefficients of various mathematical models of drug release in *in-vitro* drug permeation of PL from thermally crosslinked Zein/PVP

Mathematical Model	R^2 value
Zero order	0.998
First order	0.958
Higuchi model	0.991
Korsmeyer-Peppas model	0.998

Table 18 *In-vitro* permeation coefficients of PL control and PL loaded thermally crosslinked Zein/PVP

Material	Permeation Coefficient (cm/h)
PL control	0.402 ± 0.012
PL loaded thermally crosslinked Zein/PVP	0.173 ± 0.002

4.3.21 *Ex-vivo* PL permeation study through porcine buccal mucosa

Ex-vivo drug permeation study was usually carried out using porcine buccal mucosa because of its resemblance in structure, morphology and permeability characteristics with human buccal mucosa (Pinto et al., 2020). Cumulative drug permeation was evaluated

for thermally crosslinked Zein/PVP. Similar to the observations of *in-vitro* drug release studies in PBS media, the *ex-vivo* drug permeation profile also followed an initial burst release trend followed by sustained release. It was observed that 6.3 ± 1.04 % of PL permeation happened through porcine buccal mucosa within 8 h. In terms of cumulative released concentration, 1.9 ± 0.3 µg/mL PL permeation happened in 8 h as shown in figure 44A. Mathematical model fitting was done with the cumulative permeation profile and found that the Higuchi model exhibited the best fit. Zero order, First order, Higuchi model and Korsmeyer Peppas model were evaluated for fitting with the drug permeation

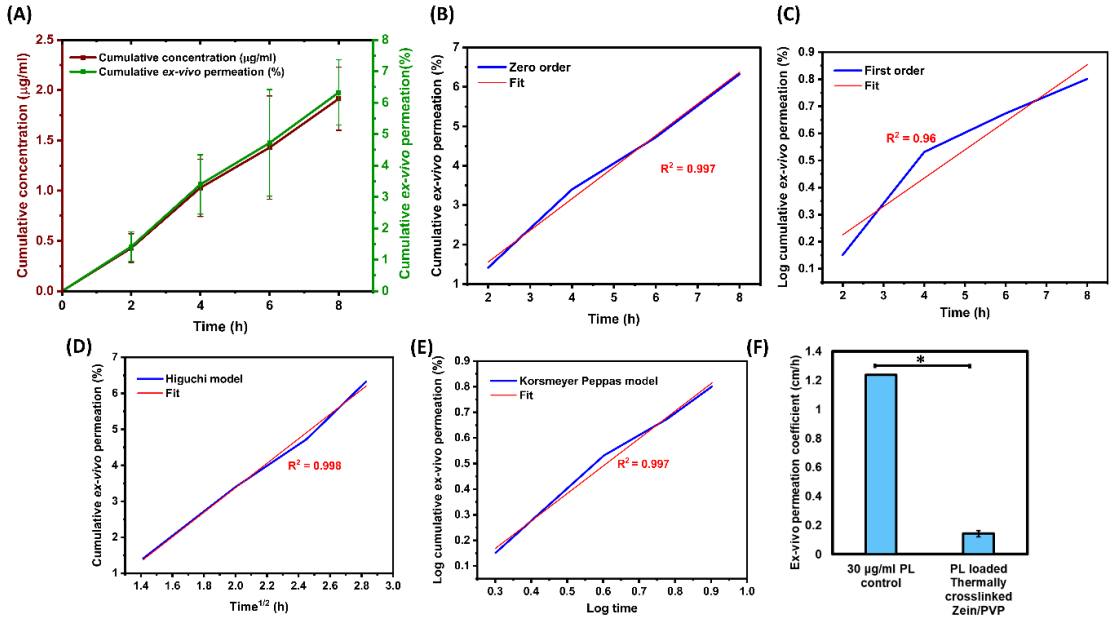

Figure 44 A) Cumulative drug permeation *ex-vivo* B-E) Mathematical model fitting with Zero order, First order, Higuchi model and Korsmeyer Peppas model respectively F) *Ex-vivo* permeation coefficient of control and test system represented as bar graph

profile. Correlation coefficients are 0.997, 0.797, 0.960, and 0.997 respectively for Zero order, First order, Higuchi model and Korsmeyer Peppas model (figure 44B-E). The *ex-vivo* drug permeation experiment was conducted keeping 30 µg/mL PL directly added over the mucosa as the control system. Permeation coefficients of control and test systems were calculated from the cumulative drug permeation curves. The permeation coefficient of the control system is considerably more than test system (p-value = 0.006). In the

control system, 67.7 ± 1.4 % of PL permeation happened in 8 h of the experiment and subsequently permeation coefficient appeared to be 1.238 ± 0.0008 cm/h. On the other hand, in the test system, only 6.3 ± 1.04 % PL permeation was noticed within 8 h of the experiment. This slow permeation resulted in a 0.142 ± 0.021 cm/h permeation coefficient for PL-loaded thermally crosslinked Zein/PVP (figure 44F). Previous experiments have confirmed the absence of junctional openings in epithelial cell junctions of mucosal tissue after material treatment. Therefore, it is not expected to have a higher permeation coefficient than the control. The huge difference in permeation coefficient is not because of the reason that junctional opening is happening in the control system. It is because, an abrupt PL permeation occurs when the drug solution is applied directly over the mucosa whereas, in the control system, an additional time for diffusing out of the electrospun membrane is required. Diffusion of PL from thermally crosslinked Zein/PVP could be concluded to be very slow and weak so that only a few drugs are getting permeated across the mucosa.

4.4 MUCIN CROSSLINKED ZEIN/PVP ELECTROSPUN MEMBRANE AND ITS CHARACTERIZATION

4.4.1 Preparation of mucin crosslinked zein (MUZ)

Crosslinking between mucin and zein was carried out expecting the formation of peptide bonds between amino groups of zein and carboxylic acid groups of oligosaccharide side chains of mucin via EDC activation. The structure of mucin is composed of a central protein core with O-linked oligosaccharide side chains (Pinzón Martín et al., 2019). N-acetylgalactosamine, N-acetylglucosamine, fucose, galactose, N-acetylneuraminic acid (sialic acid) and mannose were found in the oligosaccharide side chains of mucin (Chatterjee et al., 2020). Sialic acids are usually seen on the terminals of O-glycans in the

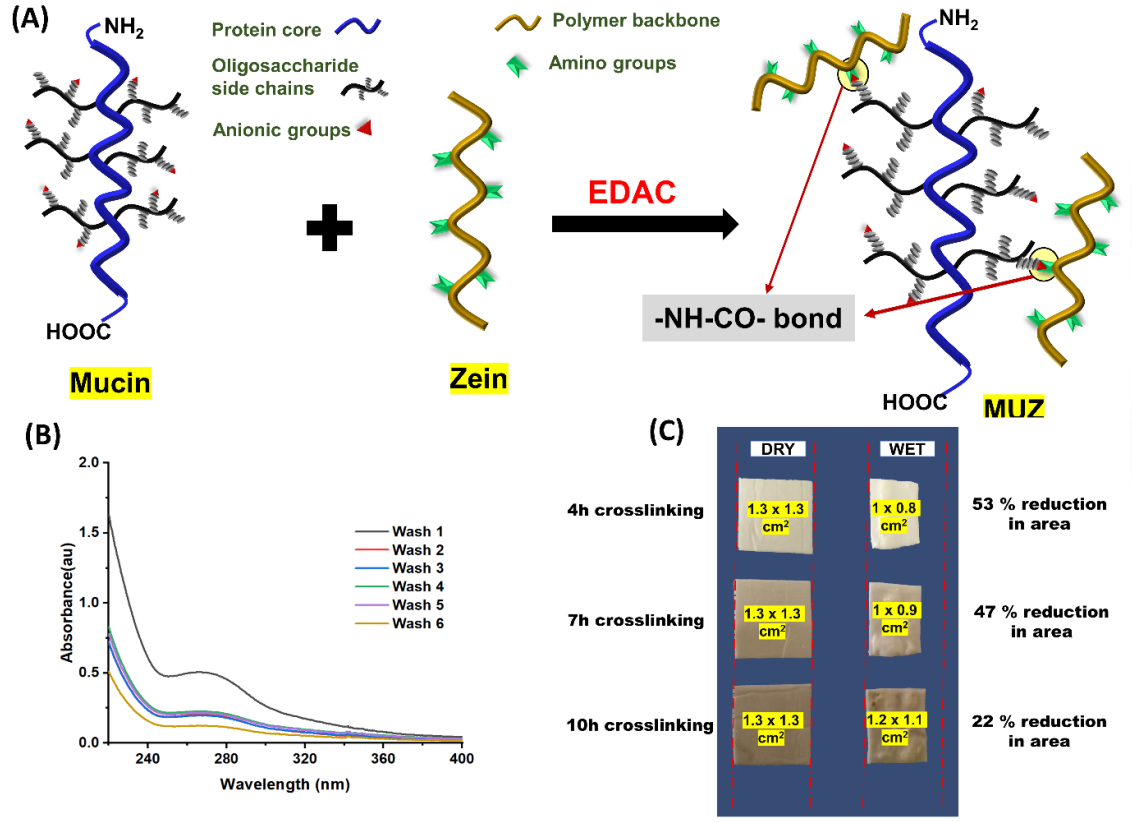

Figure 45 A) Schematic diagram depicting the mechanism of crosslinking between mucin and zein by EDC crosslinking B) UV spectra of MUZ after washing which shows absorption maxima of isourea which disappear after a number of washing C) Captured images of size reduction of MUZPVP matrices after water contact which are crosslinked for 4 h, 7 h and 10 h

mucin (Varki and Schauer, 2009). Sialic acid is a monosaccharide carrying carboxylic acid groups in the 2nd position (Ghosh, 2020). These carboxylic acid residues bind with the amino groups present in the structure of zein via EDC activation. Figure 45A depicts the schematic representation of EDC-mediated crosslinking of zein and mucin (MUZ). EDC crosslinking generates iso-urea by-product which is water-soluble. Since zein is water-insoluble, mucin crosslinked zein will also be not soluble in water. Hence, unreacted mucin and iso-urea by-products could be washed off using distilled water from the casted films of MUZ (Bhattacharjee and Ahearne, 2021). UV spectra of distilled water after washing off iso-urea exhibited an absorption maximum of 265 nm. Therefore, the complete removal of iso-urea was confirmed by the disappearance of this peak in UV spectra (figure 45B). Out of two compositions of MUZ prepared with 0.5 % and 1 % (w/v) mucin, MUZ with large mucin content was selected for further evaluations.

4.4.2 TNBS assay to estimate the degree of crosslinking

TNBS assay to estimate the concentration of primary amino groups will benefit to quantify the degree of crosslinking between mucin and zein. Both zein and mucin carry amino groups in their structure. Hence reduction in the concentration of amino groups after MUZ preparation has to be compared with zein/mucin polymer blend film rather with zein or mucin alone. Zein/mucin blend film was prepared in 7:3 EtOH/PBS without EDC activation in view of the above perspective. It was observed that EDC activation and subsequent crosslinking between mucin and zein caused a reduction in the concentration of amino groups. Zein/mucin polymer blend film carrying 2.75 ± 0.07 µg/mL primary amino groups, which considerably decreased to 1.67 ± 0.02 µg/mL after EDC crosslinking (p-value = 0.001). If that is the case, the degree of crosslinking was calculated as 39 ± 0.008 %.

4.4.3 Electrospinning of MUZPVP and post-electrospinning thermal crosslinking

The electrospun membrane of zein had insufficient mechanical properties and it could not meet the demands of a membrane which is easy to handle (Qu et al., 2019). Crosslinking of mucin with zein also hadn't improved the mechanical properties. Blending with a synthetic adhesive polymer like PVP will improve the mechanical property of MUZ. Hence polymer solution of MUZ blended with 5 % (w/v) PVP was electrospun. Further, PVP is a water-soluble polymer which immediately leaches out of the electrospun membrane after water contact. Post-electrospinning crosslinking of PVP has to be carried out to resolve this issue. Thermal crosslinking of PVP has already been recommended by various research groups (Tan et al., 2014). They have proposed thermal crosslinking of PVP at 200 °C for 1 h. In this particular case, the temperature can't be raised to 200 °C because mucin has a melting point in the range of 115-120 °C (Eraga et al., 2016). The thermal crosslinking temperature selected in the present study is 100 °C and extended for 10 h. The time of crosslinking was optimized based on the stable response of the matrix to water. The crosslinking time was varied and compared in terms of shrinkage response after water contact (figure 45C). After 4 h of crosslinking, around 53 % of shrinkage was observed which considerably decreased to 22 % after 10 h of crosslinking. Therefore, a 10 h time has been finalised for thermal crosslinking of PVP in MUZPVP.

4.4.4 Surface morphology analysis by SEM

Scanning electron microscopy images of MUZPVP and Zein/Mucin/PVP blend electrospun membranes were taken and compared. ImageJ software was used for the calculation of fibre diameter. Figures 46A and 46B represent SEM images of the Zein/Mucin/PVP blend and MUZPVP electrospun membranes. Figure 46C is the bar diagram representation of fibre diameter. EDC crosslinking between mucin and zein has

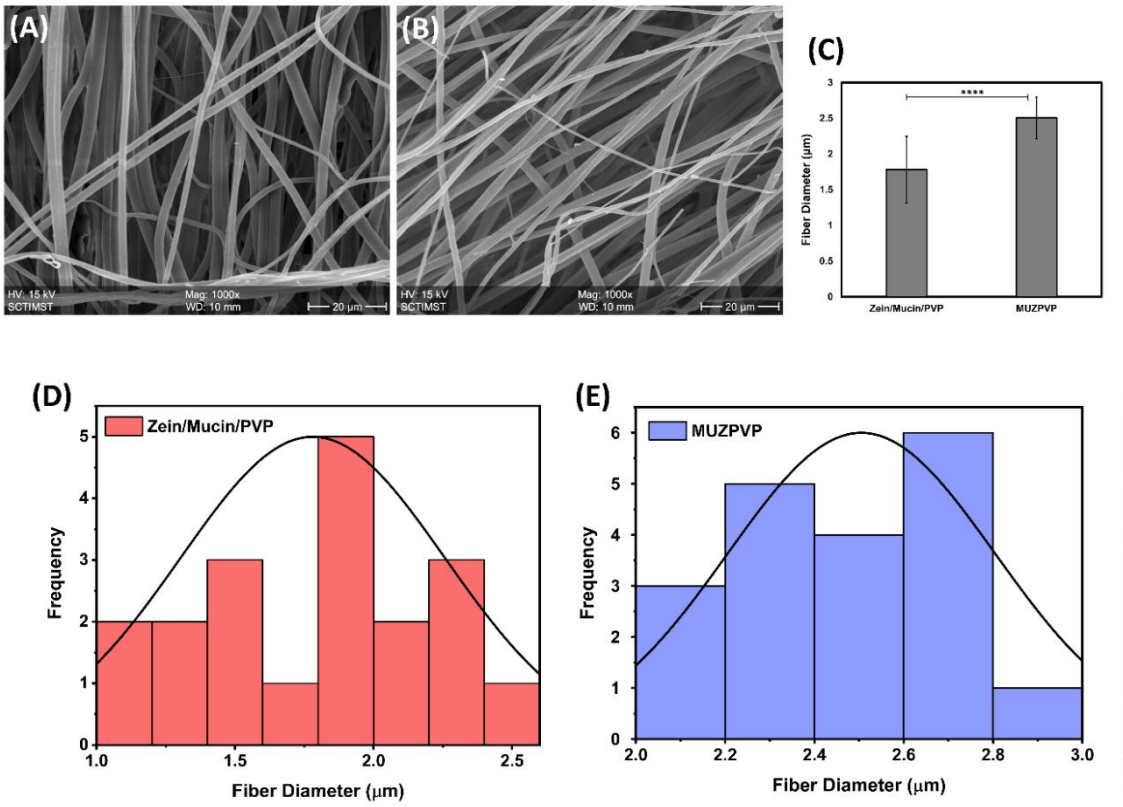

Figure 46 A-B) SEM images of Zein/Mucin/PVP blend electropsun matrix and MUZPVP matrix respectively C) Bar diagramatic representation of fibre diameter of Zein/Mucin/PVP blend and MUZPVP matrix D-E) Histrogram distribution of fibre diameter of Zein/Mucin/PVP and MUZPVP respectively

been observed to cause an increase in the fibre diameter of the electrospun membrane. The fibre diameter of the Zein/Mucin/PVP electrospun membrane was 1.8 ± 0.5 μm and that of MUZPVP was 2.5 ± 0.3 μm. Statistical analysis of fibre diameter has shown that fibre has increased significantly (p-value = 1.36 x 10^{-6}) after EDC crosslinking. This might be because of the increased viscosity of the polymer solution after crosslinking

(Jiang et al., 2010; Tian et al., 2019). Figure 46D and 46E represents the fibre diameter distribution of the Zein/Mucin/PVP blend and MUZPVP electrospun membranes respectively. Electrospun fibres of Zein/Mucin/PVP are found to be distributed within 1 to 2.5 μm whereas that of MUZPVP was distributed within 2 to 3 μm.

4.4.5 FTIR spectroscopy for chemical characterization

FTIR spectra of mucin and MUZPVP were taken and identified unique functional groups. FTIR spectra of mucin shown in figure 47A have several characteristic vibrational peaks. A broad peak observed at 3272 cm^{-1} corresponds to overlapping vibrations of the -OH group of alcohol and carboxylic acid functionalities and the -NH group of amide functionality. Aliphatic C-H stretching was observed at 2919 cm^{-1}. Amide linkages in mucin were evident in the FTIR spectra as amide I and amide II vibrations. They were observed respectively at 1638 cm^{-1} and 1538 cm^{-1}. FTIR peaks observed at 1375 cm^{-1} and

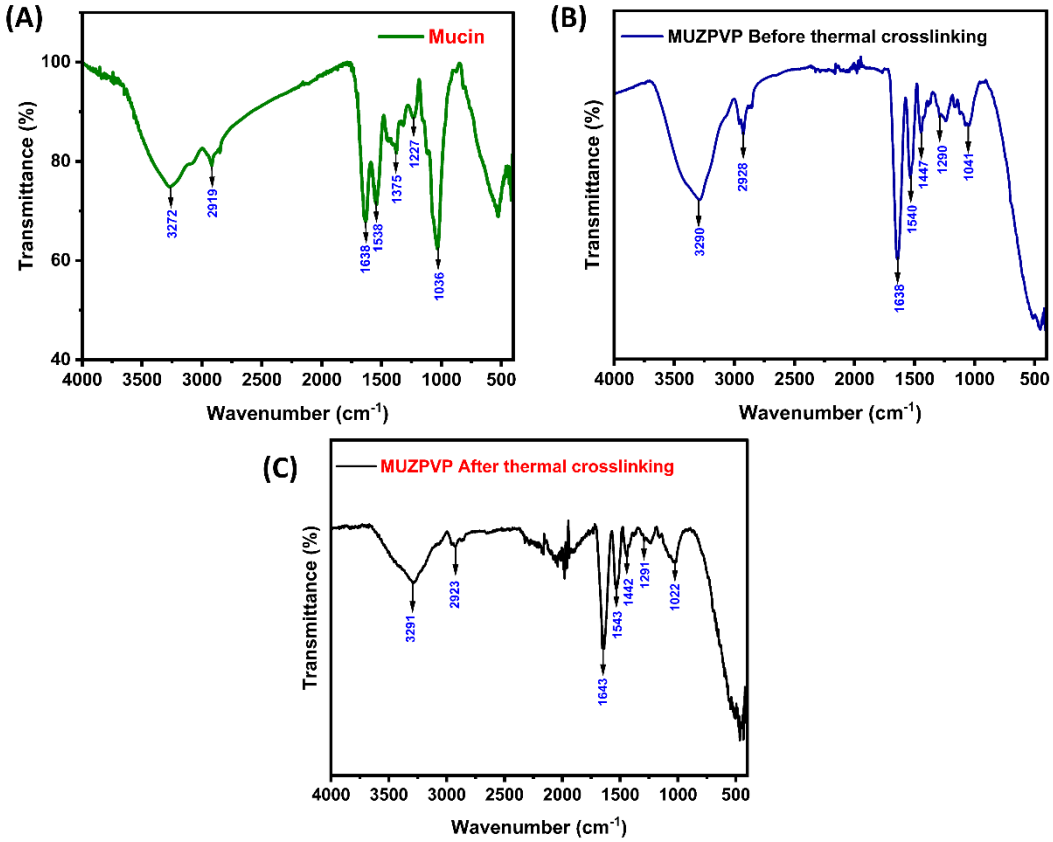

Figure 47 FTIR Spectra of A) Mucin alone B) MUZPVP before thermal crosslinking C) MUZPVP after thermal crosslinking

1227 cm^{-1} corresponded to C-N and C-O stretching vibrations. A sharp peak observed at 1036 cm^{-1} is due to the C-O stretching vibration of primary alcohol groups in oligosaccharide side chains of mucin (Johnson et al., 2009).

Figure 47B represent the FTIR spectra of MUZPVP-before crosslinking. Characteristic peaks of mucin and zein were expected to be present in MUZPVP. But in most cases, vibrations of chemical bonds overlap for zein and mucin. That being the case, vibrations corresponding to amide linkage, C-H and O-H bonds in mucin and zein overlap. The broad peak observed at 3290 cm^{-1} corresponds to the overlap of N-H and O-H stretching vibration. A slight shift has been observed for the C-H stretching vibration of MUZPVP to 2928 cm^{-1} compared to similar vibration of mucin. This might be due to the combined influence of zein and PVP. No notable shift was observed for amide I and amide II linkages. C-N vibration of the pyrrolidone ring structure of PVP appeared at 1290 cm^{-1} (Huang et al., 2019). C-N vibration of mucin was expected to be present at 1375 cm^{-1}, however it was absent. C-N vibration of PVP ring structure dominated in appearance. It is because the MUZPVP is composed of 20 % (w/w) mucin with respect to the total weight of PVP. The concentration of PVP is more compared to the concentration of mucin and naturally, its vibrations will dominate. The stretching vibrations of O-H bonds in primary alcohol groups of mucin appeared at 1041 cm^{-1} but with a low intensity. This is also as a result of less percentage composition of mucin in MUZPVP. Figure 47C presents the FTIR spectra of MUZPVP-after thermal crosslinking. Nevertheless, the characteristic peaks of MUZPVP before and after thermal crosslinking remain the same, but C-H asymmetric stretching vibration differ for MUZPVP before and after thermal crosslinking. Thermal crosslinking of PVP is occurring at the -CH group of the PVP polymer chain via a radical-initiated mechanism at high temperature conditions (Tan et al., 2014). That being the case, asymmetrical stretching vibration of the -CH group

decreases in intensity after crosslinking. As previously discussed, thermal crosslinking of MUZPVP was carried out under 100 °C for 10 h, which is not enough for the entire polymer chains to crosslink. Despite that fact, thermal crosslinking at 100 °C for 10 h was performed to enable adequate water stability to the matrix by preventing immediate and complete dissolution of PVP.

4.4.6 Mechanical property evaluation by UTM

Tensile strength, Youngs modulus and elongation at break (%) of MUZPVP were analysed. The impact of crosslinking between mucin and zein will be reflected in the mechanical property of MUZPVP. To analyse the reverberations, the mechanical properties of MUZPVP were compared with Zein/Mucin/PVP blend electrospun matrix without any crosslinking. MUZPVP was evaluated before and after thermal crosslinking.

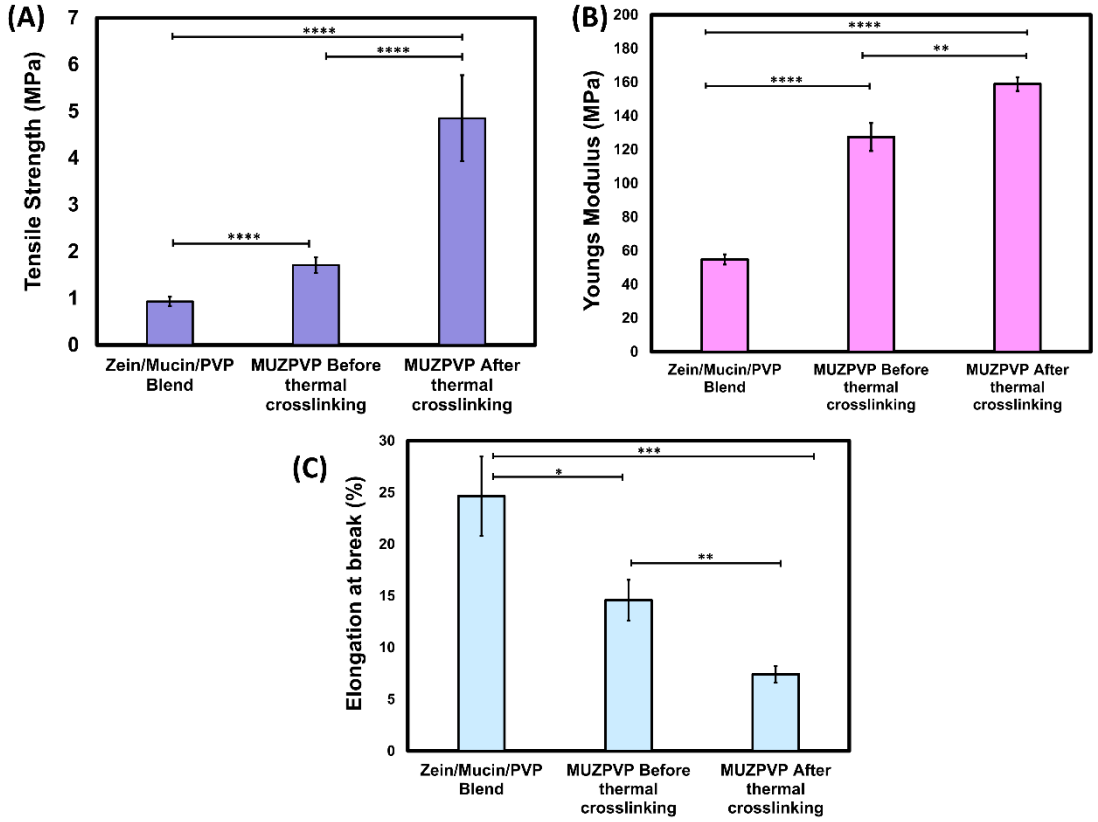

Figure 48 Representations of mechanical property and comparison between Zein/Mucin/PVP blend and MUZPVP electrospun matrices – a) Tensile strength b) Youngs modulus c) Elongation at break (%)

It was observed that the effect of crosslinking has been reflected in the tensile and modulus properties of MUZPVP. The tensile strength of the Zein/Mucin/PVP blend was 0.93 ± 0.09 MPa and that of MUZPVP-before thermal crosslinking was 1.71 ± 0.17 MPa. After thermal crosslinking, the tensile strength of MUZPVP increased to 4.85 ± 0.92 MPa. Similarly, Youngs modulus of Zein/Mucin/PVP blend was 54.8 ± 3 MPa and that of MUZPVP-before thermal crosslinking was 127 ± 8 MPa. Youngs modulus of MUZPVP also considerably increased after thermal crosslinking to 159 ± 4 MPa (p-value = 1.6×10^{-8}). Figures 48A-C are bar diagram representations of tensile strength, Youngs modulus and elongation at break (%) respectively. Observations regarding elongation at break (%) led to the fact that crosslinking of the polymer chains of mucin and zein significantly reduced elongation at break (%) (p-value = 0.0003). After crosslinking, free slipping of polymer chains over each other would be reduced and consequently, elongation at break (%) also will reduce. That is the reason behind the reduction in elongation at break (%) from 24.6 ± 3.8 % of Zein/Mucin/PVP blend to 14.6 ± 1.9 % of MUZPVP-before thermal crosslinking. This reasonable decrease is confirmative evidence for crosslinking between mucin and zein. Thermal crosslinking of PVP caused decrease in elongation at break (%) again to 7.43 ± 0.8 %.

4.4.7 Mucoadhesion by Texture analysis

The degree of adhesiveness of materials on porcine buccal mucosa was evaluated using texture analysis. Zein and PVP have already been investigated extensively for their ability to adhere to the mucosa either individually or in combination (Alsarra et al., 2011; Surendranath, Ramesan, et al., 2023; Vecchi et al., 2021). The interesting aspect of texture analysis of MUZPVP is to investigate the effect of mucin on mucoadhesion. Mucoadhesion is being defined as the adhesive interaction between the polymer system of interest and with mucin glycoprotein of the mucosal surface (Szilágyi et al., 2020).

The force of adhesion between the polymer system and mucosa can be attributed to establishing electrostatic interaction, covalent interaction, hydrogen bond interactions or physical interpenetrations (Surendranath, R, et al., 2022). That being the case, analysis of the cohesive interaction of mucin in the mucosa with mucin incorporated polymer system is a novel approach. This can be confirmed by comparing the mucoadhesive properties of MUZPVP with Zein/PVP electrospun membrane, in which no mucin is incorporated. This comparison allows us to know the additional benefit of mucin incorporation. The Zein/PVP electrospun membrane exhibited a maximum force of adhesion of $1.20 \times 10^{-1} \pm 1.28 \times 10^{-2}$ N. After mucin incorporation via crosslinking with zein significantly increased (p-value = 5.9×10^{-5}) the force of adhesion to $3.25 \times 10^{-1} \pm 2.85 \times 10^{-2}$ N. The bar diagram representation of the force of adhesion is shown in figure 49A. A similar

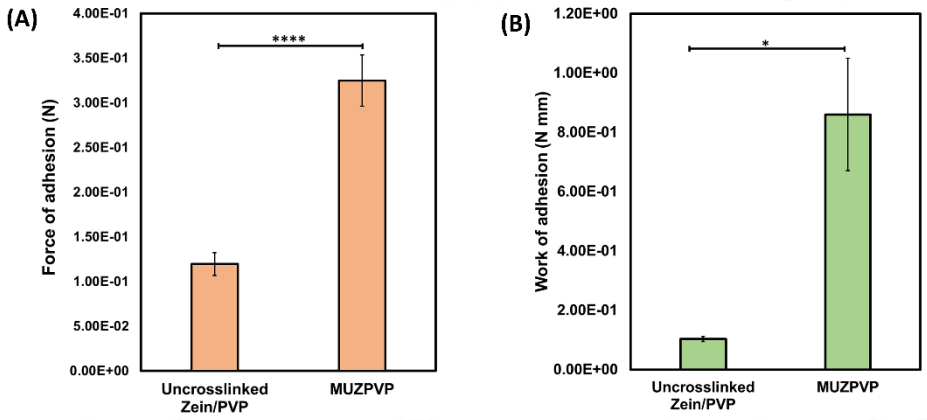

Figure 49 Comparative graphical representation of A) Force of adhesion B) Work of adhesion of Zein/PVP and MUZPVP

trend was observed for work of adhesion also. MUZPVP exhibited reasonably higher value of work of adhesion compared to Zein/PVP blend (p-value = 0.006). Incorporation of mucin caused increase in work of adhesion from $1.03 \times 10^{-1} \pm 8.80 \times 10^{-3}$ N mm to $8.60 \times 10^{-1} \pm 1.89 \times 10^{-1}$ N mm as expressed in figure 49B. Hydrogen bond interaction of oligosaccharide side chains of mucin glycoproteins (Bansil and Turner, 2006) and flexible interpenetration of mucin chains might be contributing to this enhancement in adhesive properties.

4.4.8 Drug dissolution study

Table 19 Detailed calculation of the weight of expected and actual drug entrapped in F1-F5 formulations

Formulation	Total weight of polymers (g)	Amount of drug loaded (µg)	Weight of membrane after electrospinning (g)	Expected amount of entrapped drug (µg)	Actual amount of entrapped drug (µg)	Drug entrapment (%)
F1	2.1	260	1.173	145.2	38.25	26.4
F2	2.1	520	1.30	322	75.23	23.3
F3	2.1	780	0.9503	353	57.32	16.2
F4	2.1	1040	0.8432	417.58	54.04	12.9
F5	2.1	1200	1.479	845.1	112.04	13.3

PL incorporations to MUZPVP were done by preparing five formulations of concentrations 0.01 mM, 0.02 mM, 0.03 mM, 0.04 mM and 0.05 mM. F1 to F5 formulations were then subjected to a drug dissolution study for calculating drug entrapment (%) and loading capacity (%). Pre-weighed samples of drug-loaded electrospun membranes were dissolved in 7:3 EtOH/PBS. UV measurements were taken at 290 nm and further calculations gave percentage entrapment and loading capacity. The final membrane collected after electrospinning will not be having the same weight as that of the total weight of polymers because of the loss of fibre during the process. That being the case, additional calculation has to be done to find out the exact amount of drug entrapped in the membrane. Table 19 included the calculations of the amount of drug-loaded, expected drug entrapment and actual drug entrapment. The total weight of zein, mucin and PVP will be 2.1 g in the polymer solution containing 7:3 EtOH/PBS. F1 formulation was prepared by dissolving 260 µg PL in a 2.1 g polymer solution. The final weight of the electrospun membrane was 1.173 g which was expected to carry 145.2 µg

of PL if 100 % of drug entrapment happened. This concentration is absolutely a theoretical value which demands an additional calculation for the experimental amount of drug entrapment. UV measurements of F1 formulation after dissolving in 7:3 EtOH/PBS have calculated the exact entrapped PL concentration as 38.25 µg. This means the experimental concentration of PL entrapment is only 26.4 ± 0.5 % of the theoretical concentration of drug entrapment. Though F2 to F5 formulations were prepared by dissolving higher PL concentrations, a proportionate increase in entrapment has not been observed. Figure 50A represents the graphical representation of drug entrapment for five formulations. Maximum drug entrapment was observed for F1 formulation and other formulations showed much less entrapment percentage. Usually, electrospinning enables the preparation of electrospun membranes with more than 95 % drug entrapment. The

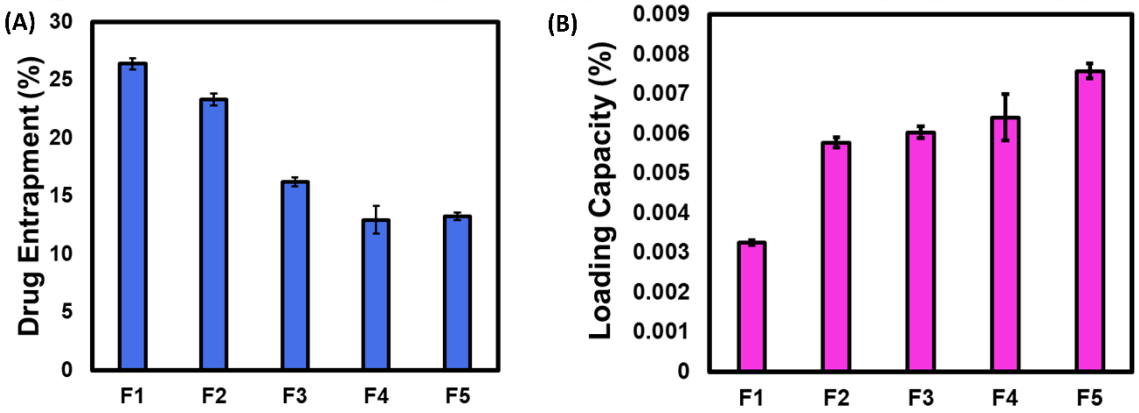

Figure 50 A) Drug entrapment (%) of F1-F5 formulations B) Loading capacity (%) of F1-F5 formulations of MUZPVP

efficiency of drug entrapment into the fibres of the electrospun matrix is determined by the compatibility of the drug and polymer in the solvent mixture as well as the volatility of the drug (Arthanari et al., 2016). Mucin is a polymer showing highly pH-dependent behaviour. Changes in pH conditions will cause conformational changes to mucin and further lead to sol-gel transitions (Curnutt et al., 2020). The solubility of mucin is enhanced at higher pH conditions (Cao et al., 1999). Conversely, the solubility of PL is enhanced at acidic conditions. This compatibility issue will be the reason for poor PL

entrapment in MUZPVP (Perez-Marcos et al., 1996). From figure 50A, drug entrapment percentage of F1 to F5 formulations can be observed as 26.4 ± 0.5 %, 23.3 ± 0.5 %, 16.2 ± 0.4 %, 12.9 ± 1.2 % and 13.3 ± 0.3 % respectively. The consecutive decrease in drug entrapment percentage from F1 to F5 formulation might be credited to the aggregation of drug molecules and non-uniform distribution in the electrospun membrane (Lian and Meng, 2017).

Loading capacity (%) was calculated from the amount of drug entrapped and the total weight of the membrane. Figure 50B is the loading capacity (%) graph. Loading capacity percentage of F1-F4 formulations are $0.0033 \pm 6.15 \times 10^{-5}$ %, 0.0058 ± 0.0001 %, 0.0060 ± 0.0001 % and 0.0064 ± 0.0006 % respectively. F5 formulation showed a maximum loading capacity of 0.0076 ± 0.0002 %. Loading capacity is low because PL is loaded in microgram quantity to polymer membrane having weight in 'gram'.

4.4.9 Drug release kinetics in PBS

A drug release study was done for the F5 formulation having the highest loading capacity (%). Figure 51A demonstrates the drug release profile in PBS which had initial burst release characteristics followed by a sustained release trend. Electrospun membrane carrying 70 μg/mL PL was analysed for release kinetics in PBS. At 1 h of the release study, 5.2 ± 1.2 μg/mL PL got released into the PBS media. After 8 h of the experiment, 31.6 ± 1.8 % of PL release happened. Later, the release profile had a slow releasing mechanism as the release reached 41.3 ± 2.8 % in 48 h of the experiment. The release profile was fitted with different mathematical models and found that the Korsmeyer Peppas model exhibited the best fit with an R^2 value of 0.937. Figure 51B-E is the

mathematical model fitting curves with Zero order, First order, Higuchi model and Korsmeyer Peppas model kinetics.

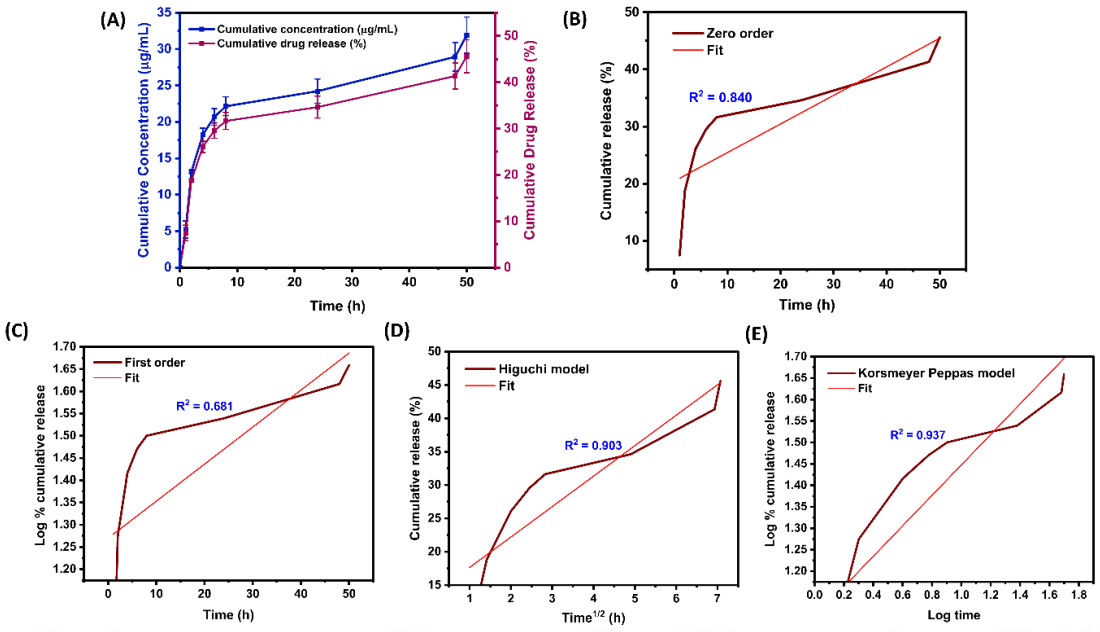

Figure 51 A) Cumulative drug release of MUZPVP loaded with PL in PBS B-E) Fitting curves with mathematical models of drug release- respectively in the order of Zero order, First order, Higuchi model and Korsmeyer Peppas model

4.4.10 Direct contact assay for evaluation of cytotoxicity

In-vitro cytotoxicity of MUZPVP was evaluated on human nasal epithelial cells, RPMI 2650. The reverberations of PL loading on cytotoxicity were also evaluated. Samples with and without PL were kept over an epithelial cell monolayer of RPMI 2650 cells for 24 h and visualized under the microscope. Phase contrast images of figure 52A and 52B represent positive and negative control. Figure 52C is the control image of untreated RPMI 2650 cells. Figures 52D and 52E are the phase contrast images after keeping MUZPVP without PL and with PL over the cell monolayer. The dark regions marked using arrows are the materials placed over cells. In comparison with the actual live morphology of cells, figures 52D and 52E were also maintaining the same morphology. Zein and PVP are already acknowledged for their non-cytotoxic properties to cells

(Surendranath, Ramesan, et al., 2023). The incorporation of mucin hasn't been observed to cause cytotoxicity to the cells.

4.4.11 MTT assay for quantitative evaluation of cytotoxicity

MTT assay was performed to confirm and quantify the non-cytotoxicity of MUZPVP. It is a metabolic assay where the number of viable cells was estimated based on their capability to reduce tetrazolium salt to formazan crystals. More the number of viable cells after material treatment, more is the production of formazan crystals. MTT assay was

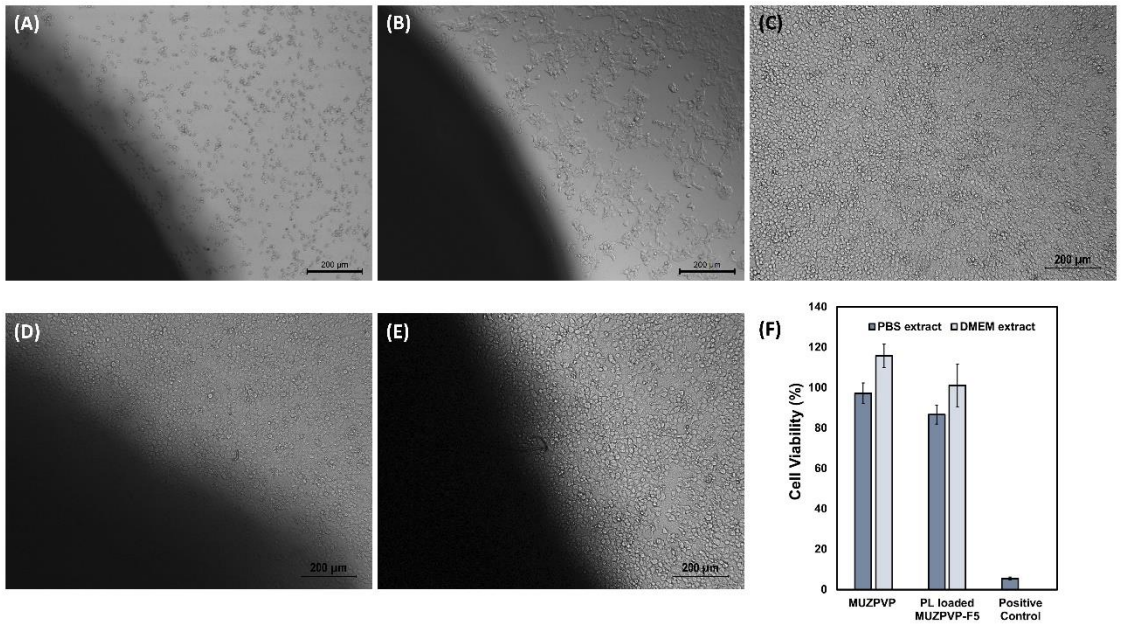

Figure 52 Phase contrast imaging of direct contact assay in RPMI 2650 cells A) Positive control cells B) Negative control cells C) Cell alone control D) Cells treated with MUZPVP matrix E) Cells treated with PL loaded MUZPVP matrix (NB: The yellow arrow points towards the material placed over the cell monolayer, which is seen as dark) F) Cell viability (%) of MUZPVP and PL loaded MUZPVP in MTT assay with phenol as positive control

done using material extract in PBS and DMEM media. It was observed that the addition of material extracts and incubation for 24 h hasn't resulted in toxicity to the cells. Even, PL incorporation hasn't caused toxic responses to RPMI 2650 cells. The percentage cell viability for PBS extracts of MUZPVP and PL-loaded MUZPVP are 97.2 ± 5.1 % and 86.6 ± 4.7 % respectively. These results differ significantly as the p-value is 0.03. Even

then, percentage cell viability is more than 85 % for both membranes and can be considered non-cytotoxic. The % cell viability for DMEM extracts of MUZPVP and PL-loaded MUZPVP are 115.7 ± 5.8 % and 101 ± 10.7 % respectively. Figure 52F represents the graphical representation of cell viability.

4.4.12 Fluorescent visualization of cytotoxicity via live/dead assay

Live/dead assay is a technique to qualitatively evaluate cytotoxicity via fluorescent imaging. Acridine orange/ethidium bromide stain was used for imaging. Acridine orange will stain live cells in green and ethidium bromide-stained dead cells in red. Untreated control cells are shown in figure 53A-C where live and dead cell staining and their

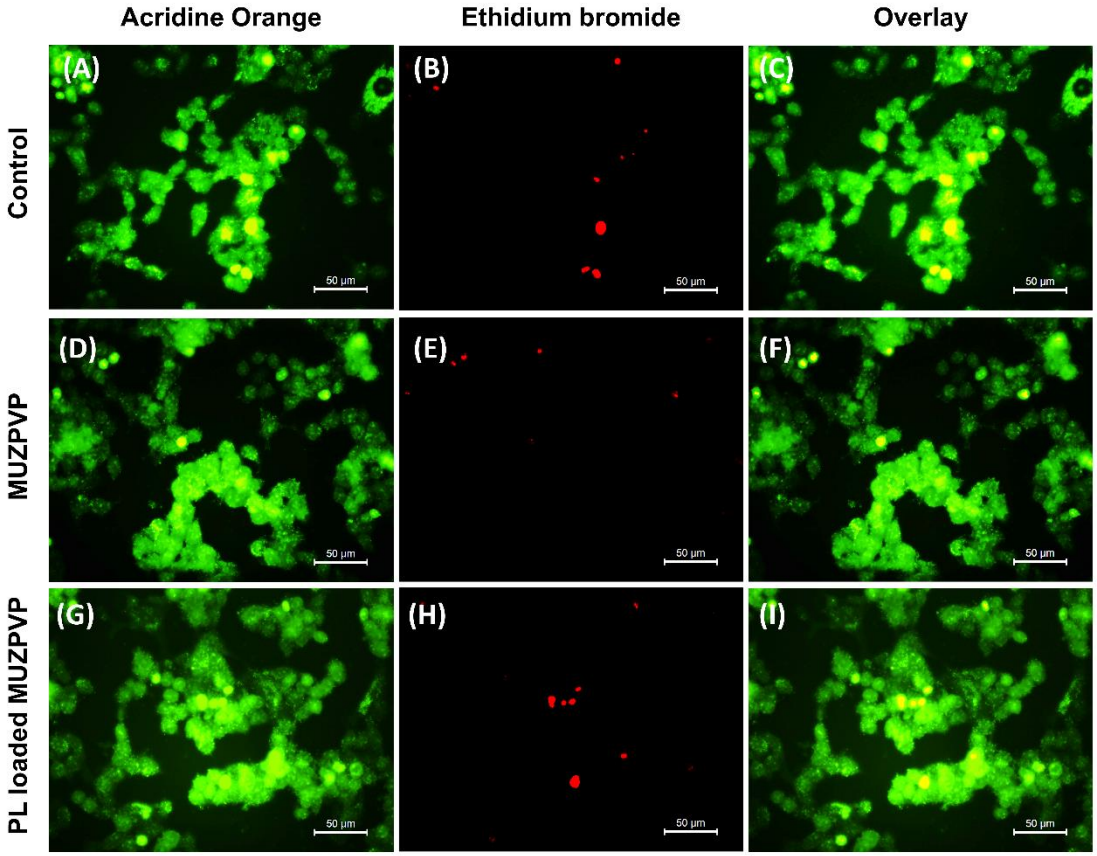

Figure 53 Live dead assay fluorescent images – acridine orange staining, ethidium bromide staining and overlay respectively of A-C) Control RPMI 2650 cells D-F) Cells treated with MUZPVP matrix and G-I) Cells treated with PL loaded MUZPVP (40X magnification)

overlay are arranged respectively. RPMI 2650 cells after treating MUZPVP for 24 h were alive since the majority of cells appeared green in figure 53D. Only very few dead cells are observed in figure 53E in red colour. Figure 53F is the overlay of live and dead cell images after MUZPVP treatment. Direct contact assay and MTT assay proved that the PL-loaded MUZPVP won't cause toxicity to RPMI 2650 cells. Likewise, live/dead assay also confirmed the non-cytotoxicity of PL-loaded MUZPVP. Figures 53G-I are the fluorescent images after acridine orange staining, ethidium bromide staining and their overlay respectively. In this case, also, the majority of cells appeared as live and certified the non-cytotoxicity of PL-loaded MUZPVP.

4.4.13 Evaluation of F-actin morphology

The logical relevance of evaluating F-actin morphology lies in understanding the integrity of epithelial tight junctions. F-actin filaments play a critical role in maintaining the architecture of tight junctions and the coherence of junctional proteins (Van Itallie and Anderson, 2014). Disturbance to the structure and continuity of F-actin filaments would lead to loss of barrier integrity of tight junctional proteins. The evaluation has been carried out by comparing the morphology of untreated control cells with that of MUZPVP-treated cells. Figures 54A-C are fluorescent images of nucleus staining, F-actin staining and their overlay respectively of control cells. The overlay has been enlarged and placed on the right side of the panel. The actual structure and distribution of F-actin filaments are evident in figure 54A-C. The main focus of the experiment is to make observations regarding changes happening to F-actin filaments after MUZPVP treatment. Figure 54D-F are fluorescent images after MUZPVP treatment. It is clear from the images that the F-actin cytoskeleton of RPMI 2650 cells stay intact even after maintaining 24 h direct contact with MUZPVP. Neither zein, PVP nor mucin cause

disturbances to F-actin filaments and consequently tight junctions remain closed after material treatment.

4.4.14 Immunostaining of adherens junctions

Inter-cellular junctions like tight junctions, gap junctions and adherens junctions provide cell-cell adhesion (Samiei et al., 2019). Zonal occludens proteins act as physical linkages between tight junctions and adherens junctions. Hence, they perpetuate a high level of

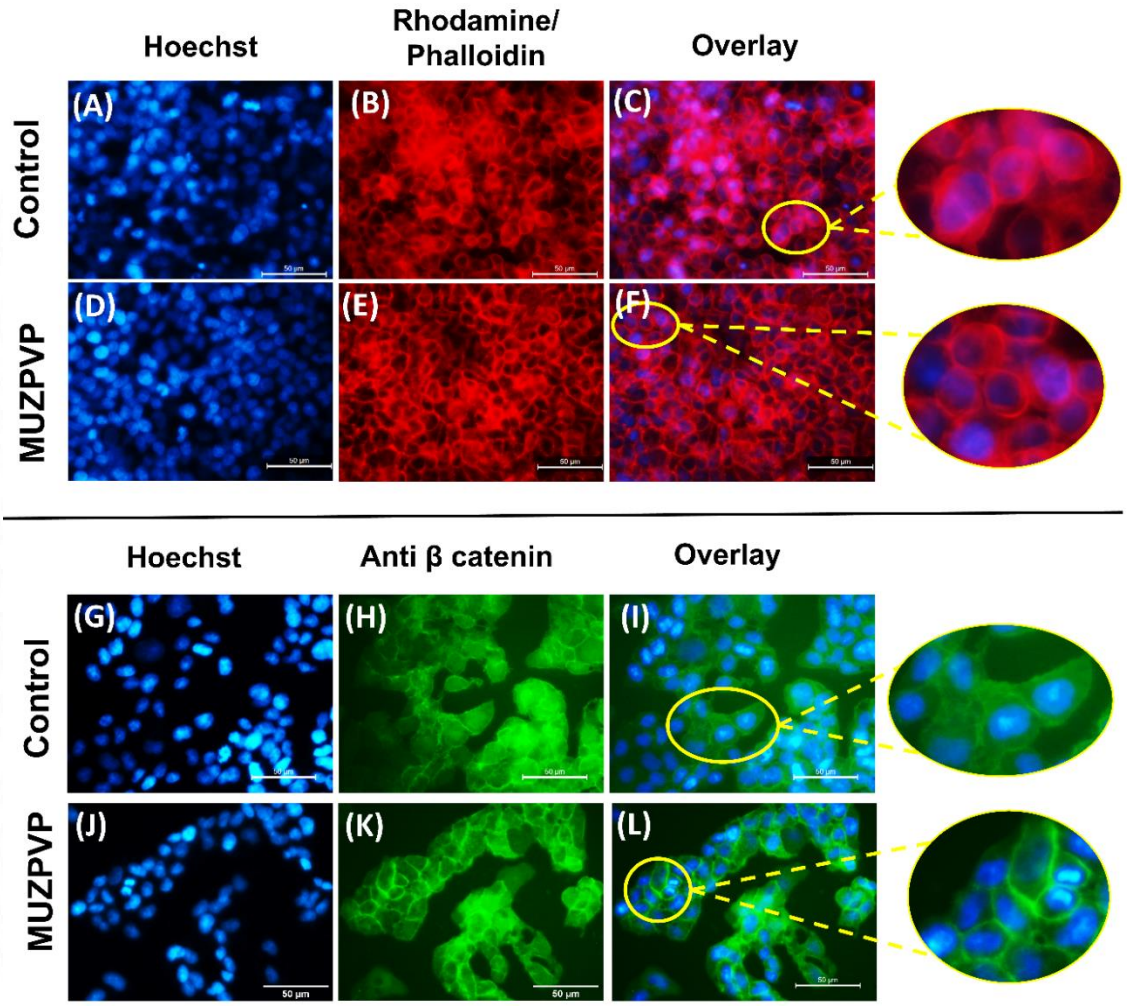

Figure 54 Top panel- Fluorescent images of nucleus staining(Hoechst), F-actin staining (rhodamine/phalloidin) and overlay respectively of A-C) Control cells D-F) Cells after treatment with MUZPVP.

Bottom panel- Fluorescent images of nucleus staining (Hoechst), β catenin adherens protein immunostaining (anti β-catenin) and overlay respectively of G-I) Control cells J-L) Cells after treatment with MUZPVP

interdependency (Campbell et al., 2017). Cadherin proteins of the adherens junction comprise α catenin, β catenin and p-120 catenin. Actin filaments are attached to α catenin, which is linked with epithelial cadherin and β catenin (Drees et al., 2005). Previous experiments have proven that MUZPVP is causing disturbances to F-actin filaments. Even though, material impact over adherens junction proteins also has to be investigated. Therefore, immunostaining of β catenin proteins has been done and visualized. Just like in the previous case, untreated cells were considered as the control for the reference. Figure 54G-I are the nucleus staining, β catenin staining images and their overlay image in the sequence of control cells. The β catenin proteins appeared green and the nucleus was blue. The real structure and integrity of β catenin proteins could be noted from those images. Treatment of cells with MUZPVP hasn't been noticed causing any changes to β catenin proteins. Alike observations and inferences of F-actin staining, perturbations to the epithelial junctions after MUZPVP can be ruled out. Figure 54J-L represents the MUZPVP-treated cells after nucleus, β catenin staining and their overlay in sequence. Maintaining junctional integrity and keeping junctions closed after material treatment is desirable in the aspect of preventing pathogen entry and other damages (Lu et al., 2014).

4.4.15 Transepithelial electrical resistance (TEER) evaluation

F-actin staining and immunostaining of β catenin proteins have qualitatively confirmed the lack of junctional opening occurring during MUZPVP treatment. TEER measurement and its calculation is a quantitative step to validate the same. It is relevant in the aspect of determining the mechanism of PL transport across epithelial cell monolayers. The absolute TEER value calculated before and after placing MUZPVP over RPMI 2650 cell monolayer is depicted in figure 55A. No considerable difference in absolute TEER value, as well as TEER (%) value, was observed. Literature has reported the absolute TEER value of RPMI 2650 cells under liquid-liquid interface culturing as 30 Ωcm^2 (Kreft et al.,

2015; Sibinovska et al., 2019). The experimental results of absolute TEER value after MUZPVP also fall in the same range.

4.4.16 *In-vitro* drug permeation study

The possibility of PL permeation in the absence of a junctional opening has to be verified. *In-vitro* drug permeability through complete cell monolayer is a wise technique for the same. PL-loaded MUZPVP was kept over RPMI 2650 cell monolayer and the amount of PL permeated across cell monolayer was quantified. Within 8 h of the experiment, 44.9 ± 2.5 % of PL permeated across the cell monolayer to the basolateral compartment of the cell culture insert. The control system of the experiment was PL (10 µg/mL) added directly over the cell monolayer. In that case, 93 ± 4 % of PL permeated across the cell monolayer within an initial 2 h. The cumulative drug permeation curve of test system is depicted in figure 55B. The beneficial aspect of mucoadhesive drug delivery is bypassing of hepatic metabolism to increase drug bioavailability. Even if that is the case, direct drug administration over the mucosal surface is not recommended in any circumstances. It may cause local irritations and lead to the loss of a greater amount of drug through saliva secretion and mucus turnover. Employing a drug-carrying matrix for adhesive drug delivery through mucosa will facilitate a diffusion-controlled release of PL from the matrix and subsequent permeation through the mucosa. It prevents uncontrolled drug release at the mucosal surface. Especially, mucoadhesive formulations assured targeted delivery of PL at the mucosa and retains the formulation as such at the site of interest. A specific and controlled release of the drug would be facilitated by the adhesive

electrospun matrix (Smart, 2004). The permeation of PL through the cell monolayer was fitted with various mathematical models- Zero order, First order, Higuchi model and Korsmeyer Peppas model. The best fit model found was Korsmeyer Peppas with a R^2 value of 0.960. The correlation coefficient for model fitting with Zero order, First order and Higuchi release models were 0.853, 0.741 and 0.939 respectively (figure 55C-F).

Nevertheless, cell junctions remained intact after material treatment, PL permeated through the cell monolayer. The mechanism of PL transport followed a transcellular

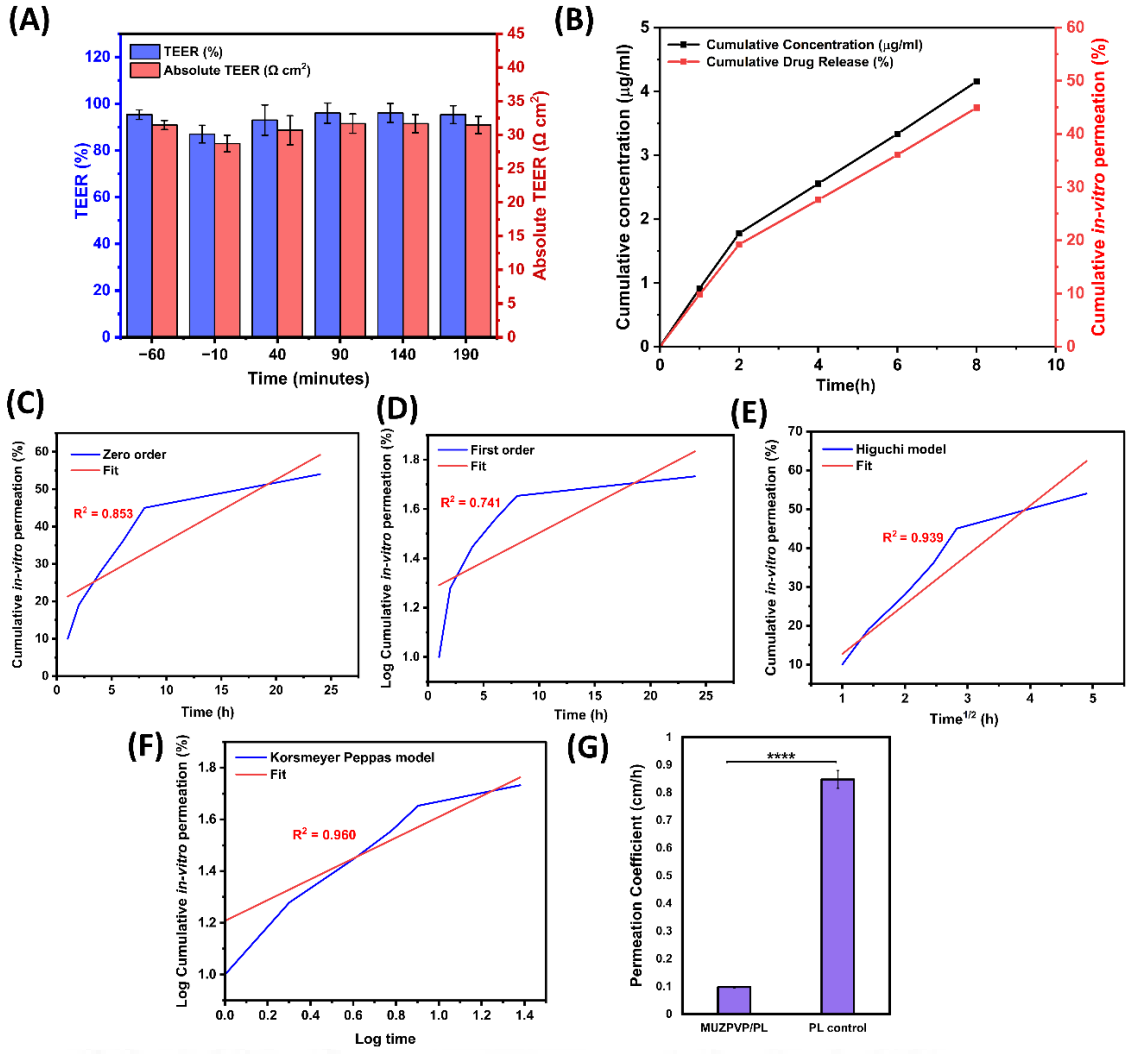

Figure 55 A) TEER (%) and absolute TEER (Ω cm^2) before and after MUZPVP treatment B) Cumulative Permeation (%) through RPMI 2650 cells of PL from PL loaded MUZPVP, Cumulative Permeation (%) fitting with C) Zero order D) First order E) Higuchi model F) Korsmeyer Peppas models G) Bar diagram representation of permeation coefficient of PL loaded MUZPVP and PL control

pathway. The extent of permeation was compared for PL control and PL-loaded MUZPVP. As already discussed, PL control had burst release followed by a fast permeation profile. Therefore, the permeation coefficient of PL control was too high, ie., 0.847 ± 0.032 cm/h. On the other hand, PL-loaded MUZPVP showed a slow permeation profile (figure 55G) with a substantially low permeation coefficient ie., 0.097± 0.002 cm/h (p-value = 3.7×10^{-5}).

4.4.17 *Ex-vivo* drug permeation through porcine buccal mucosa

Transmucosal permeation of PL through porcine buccal mucosa will be a piece of additional information to verify the transcellular permeation happening. The amount of PL permeated across mucosa was quantified using UV spectroscopy. Within 8 h of the study, 84 ± 35 % PL permeation was observed. Figure 56A represents the cumulative drug permeation graph. A liner profile of drug permeation was observed till 8 h. Mathematical model fitting of drug permeation was carried out. Zero-order kinetics had the best fit with the PL permeation profile from MUZPVP with an R^2 value of 0.997 (figure 56B). First order, the Higuchi model and Korsmeyer Peppas model fitting curves are shown in figure 56C-E in sequence. Permeation coefficients of PL-loaded MUZPVP and 10 µg/mL PL control were calculated from the cumulative drug permeation graph. Figure 56F demonstrates the cumulative drug permeation graph of 10 µg/mL PL control. It has been observed that 97.4 ± 6 % of PL permeation happens *ex-vivo* through porcine buccal mucosa within 6 h of the experiment. As a consequence, the permeation coefficient of PL control is high compared to PL loaded MUZPVP system. Figure 56G is the bar diagram representation of the permeation coefficient of the control and test system. Permeation coefficients of control and test systems are 3.99 ± 1.06 cm/h and 2.06 ± 0.77 cm/h respectively. A significantly lower permeation coefficient for the test system (p-value = 0.04) is an indication of a lack of cell junction opening after MUZPVP

treatment. Fast permeation in the control system is not attributed to junction opening but rather due to immediate release at the site of action. Drug release from electrospun material happens in a while as drug diffusion should happen initially from the electrospun material and it has to be followed by permeation.

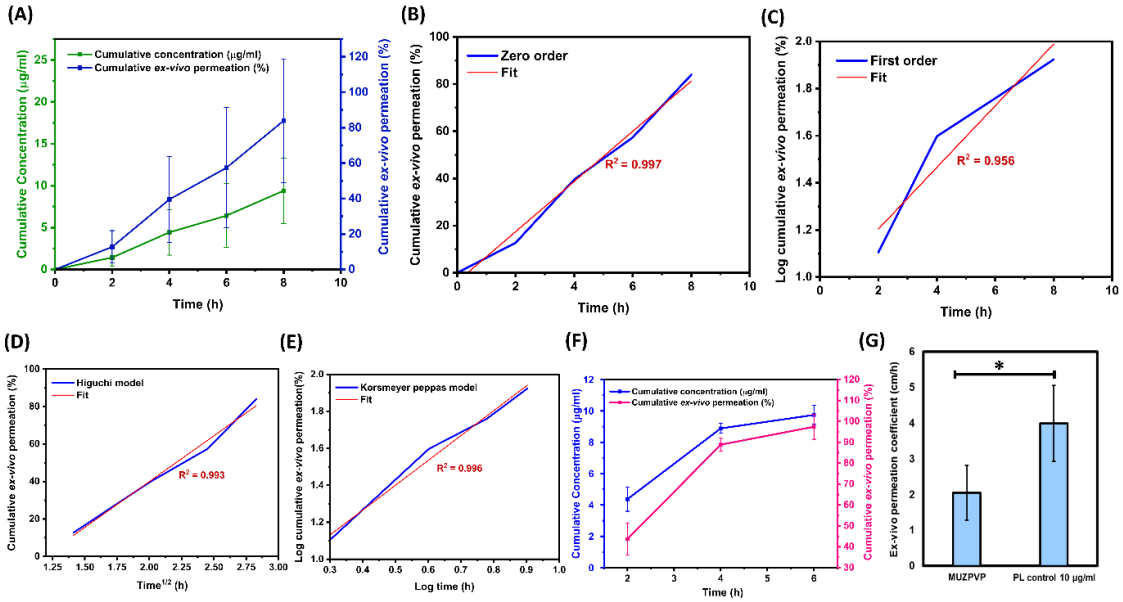

Figure 56 A) Cumulative drug permeation graph *ex-vivo* B) Zero order drug permeation C) First order drug permeation D) Higuchi model drug of permeation E) Korsmeyer Peppas model of drug permeation F) *Ex-vivo* cumulative drug permeation of 10 µg/mL PL control G) Bar graph representation of permeation coefficients

4.5 ZEIN/APBA CONJUGATED PVP ELECTROSPUN MEMBRANE AND ITS CHARACTERIZATION

4.5.1 APBA conjugation with PVP

Initially, 3-aminophenyl boronic acid (APBA) solutions were prepared in 10 mL EtOH. Three concentrations of 10 mM, 20 mM, and 50 mM were prepared by dissolving 0.01 g, 0.02 g and 0.05 g APBA respectively. The meta position of the benzene ring in APBA

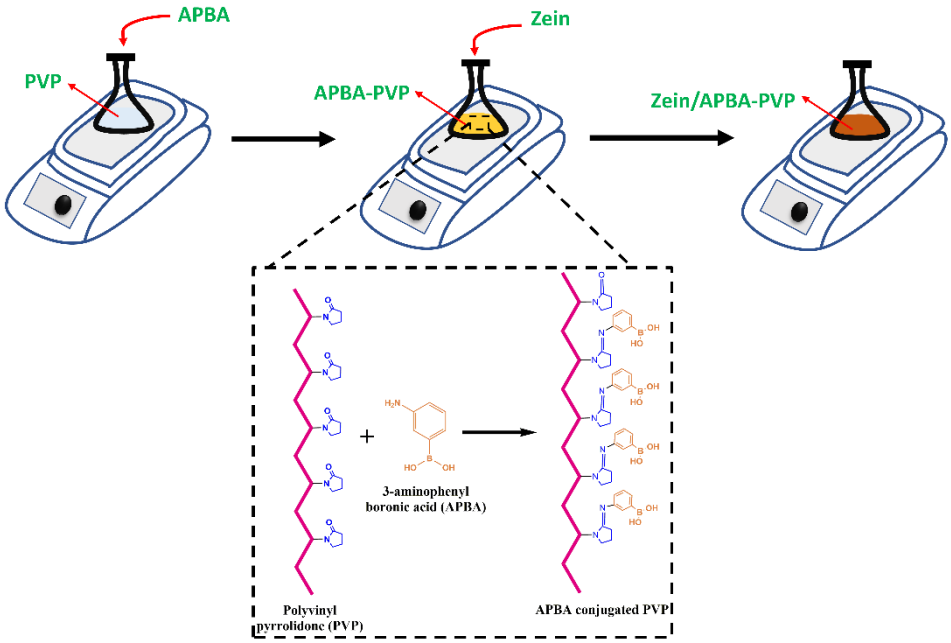

Figure 57 Pictorial representation of scheme of APBA conjugation with PVP and further blending with zein. Mechanism of APBA-PVP conjugation is shown in dotted rectangle.

contains an amino group. It is susceptible to bind with the C=O group of the pyrrolidone ring of PVP and establishing a Schiff base (Manju et al., 2011). Thereafter, APBA would be present as a pendant group on the principal polymer chain of PVP. Figure 57 is the pictorial representation of the scheme and mechanism of APBA conjugation with PVP.

4.5.2 Electrospinning of Zein/APBA-PVP

Zein is a natural protein known for mucoadhesive properties due to the presence of thiol functional groups in the cysteine amino acid. Zein is extracted from corn and it is rich in

proline content (Abe et al., 1985). On the other hand, PVP has also been broadly explored for developing electrospun fibres (Maciejewska et al., 2019; Tort et al., 2019). PVP is hydrophilic, and hygroscopic (Kurakula and Rao, 2020) and its superior adhesive property can be explained in terms of the wettability theory of mucoadhesion. Despite all these, the practical difficulty of electrospinning of PVP is to separate the electrospun membrane from the collector. Moreover, electrospinning of PVP alone in EtOH developed a membrane with a fused fibrous structure. In that scenario, it is preferred to prepare a blend of PVP with another polymer having better spinnability. Therefore, 5 % (w/v) PVP conjugated with APBA solution (APBA-PVP) was added with 15 % (w/v) zein. Zein was chosen purposively because of its adhesive property and hydrophobicity (Gonçalves et al., 2020). The addition of zein results in reducing the hygroscopic property of PVP and ends up in obtaining an electrospun membrane with unfused fibrous structure and adhesive properties.

4.5.3 Scanning electron microscopy (SEM) for morphological analysis

SEM images of 10 mM, 20 mM and 50 mM Zein/APBA-PVP electrospun membranes are represented in figure 58A-C in sequence. Primary visual analysis of change in fibre diameter with an increase in APBA concentration concludes that fibre diameter increases with an increase in APBA concentration. ImageJ analysis of fibre diameter was done to assess the changes quantitatively. The Zein/10 mM APBA-PVP electrospun fibres were having 1.6 ± 1.4 μm. A wide distribution of fibre diameter was observed for Zein/10 mM APBA-PVP, which spanned from 0.2 μm to 4.5 μm (figure 58D). Fibre diameter of Zein/20 mM APBA-PVP was 1.9 ± 1.3 μm. Just like in the previous case, the fibre diameter distribution of Zein/20 mM APBA-PVP spanned between 0.3 μm and 5.5 μm

(figure 58E). A commendable increase in fibre diameter hasn't been observed for Zein/20 mM APBA-PVP compared to Zein/10 mM APBA-PVP (p-value = 0.1). Increasing the concentration of APBA from 20 mM to 50 mM resulted in an increase in fibre diameter as well as a narrow distribution of fibre diameter (figure 58F). The fibre diameter of Zein/50 mM APBA-PVP was 3.2 ± 1.5 μm, which was a considerable increase compared to 10 mM and 20 mM APBA conjugated membranes (p-value = 0.0002 and 0.002 respectively).

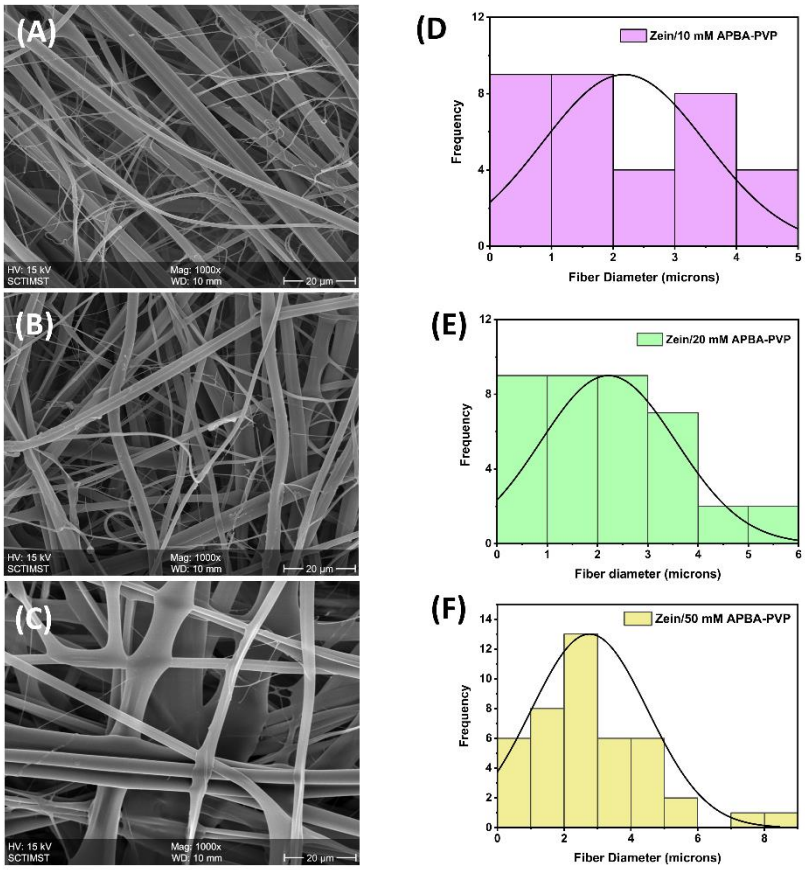

Figure 58 A-C) SEM images of Zein/APBA-PVP with 10 mM, 20 mM and 50 mM APBA concentration respectively (each of 1000X magnification) D-F) Fibre diameter distribution curves for 10 mM, 20 mM and 50 mM APBA conjugated electrospun membranes of Zein/PVP.

4.5.4 Quantification of the percentage of conjugation

UV spectra of APBA have been taken and observed an absorption maximum at 305 nm (J Yang et al., 2016) which corresponded to $\pi \rightarrow \pi^*$ transition in the benzene ring (Jayeoye, Olatunde, et al., 2020). The amino group of APBA and the carbonyl group of PVP interact

and establish the Schiff base during the conjugation mechanism. In that case, also, the benzene ring in APBA will be maintained intact and similar absorbance was noticed

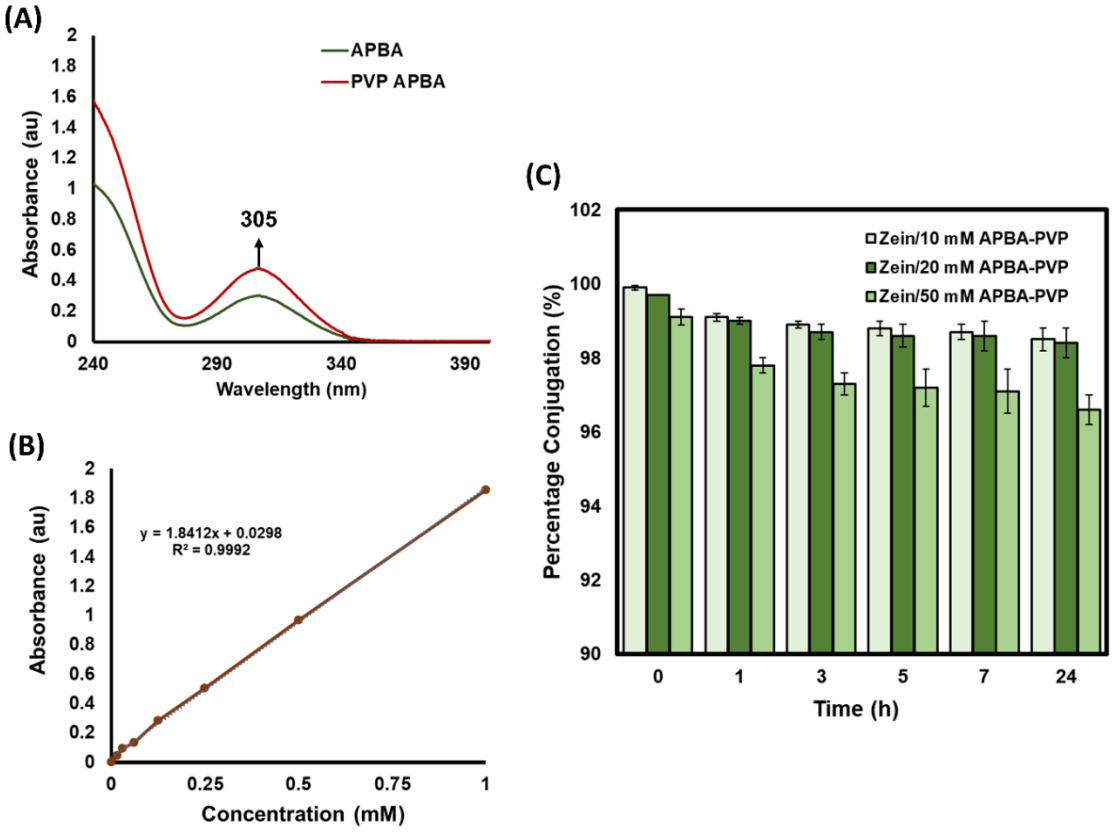

Figure 59 A) UV-visible spectra of APBA showing absorbance maximum (water taken as blank) B) Standard calibration curve of APBA in water C) Bar diagram representation of degree of conjugation of 10 mM, 20 mM and 50 mM APBA conjugated samples of Zein/PVP.

(figure 59A). Taking this observation into account, a standard calibration curve of APBA was plotted by measuring absorbance at 305 nm. Figure 59B represents the standard calibration curve of APBA in distilled water. Pre-weighed samples of 10 mM, 20 mM and 50 mM APBA conjugated samples of Zein/PVP were immersed in distilled water and the concentration of APBA leached out from the matrices were quantified taking the standard calibration curve as reference. Percentage of APBA conjugation was determined from the initial APBA concentration conjugated and the leached-out concentration. Figure 59C represents the graphical representation of percentage of APBA conjugation for different Zein/APBA-PVP samples at various time periods. In the case of 10 mM and

20 mM conjugated samples, almost 99 % conjugation was calculated. With increase in the concentration of APBA conjugated, percentage conjugation was observed to decrease to 98 % after 1 h of leach out study. Further after 3 h of experiment, percentage conjugation of Zein/50 mM APBA-PVP significantly decreased to 97 % (p-value = 0.01). It was observed that, for all three compositions of Zein/APBA-PVP, percentage of conjugation remained constant after 3 h of release study.

4.5.5 FTIR spectroscopy

Figure 60A represents the stacked FTIR spectra of PVP, APBA, APBA-PVP and Zein/APBA-PVP. The major distinguishable peak for APBA is the peak observed at 1440 cm^{-1} which corresponded to vibrations of the benzene ring (Jayeoye, Nwabor, et al., 2020) which is absent in PVP. A similar peak was observed for APBA-PVP and Zein/APBA-

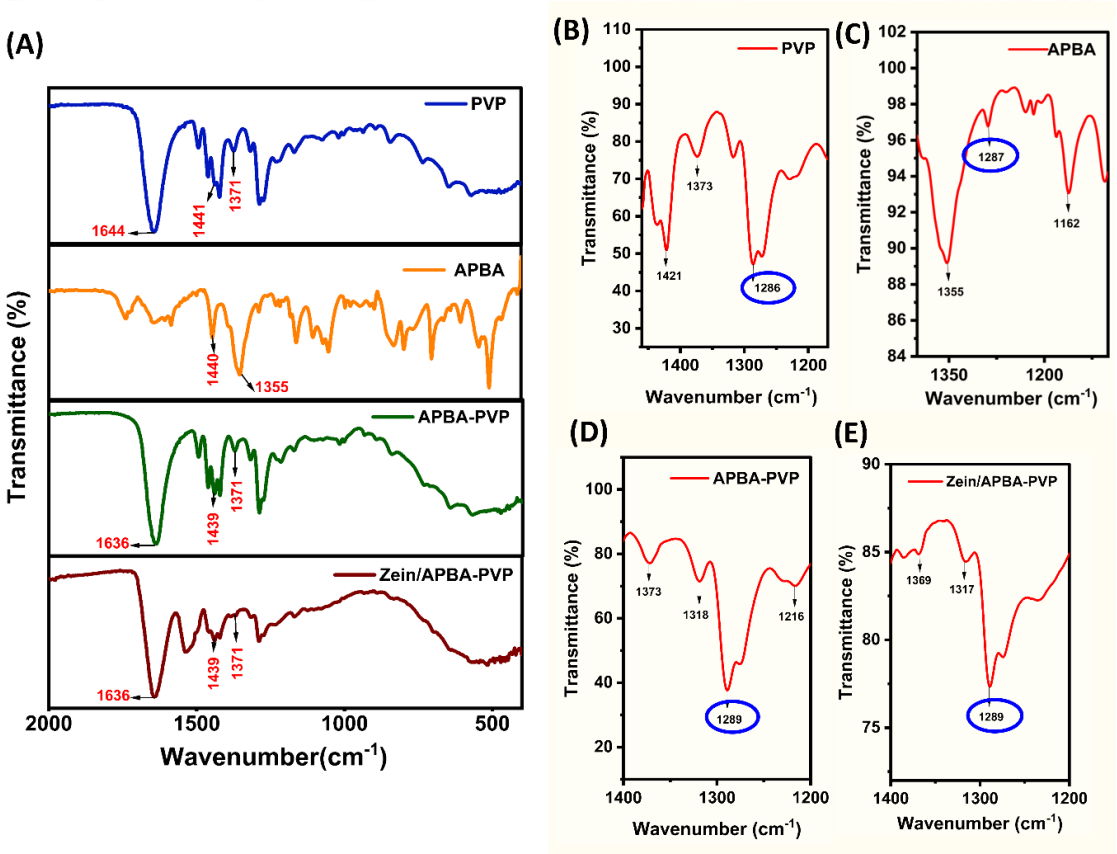

Figure 60 A) FTIR overlay spectra of PVP, APBA, APBA-PVP and Zein/APBA-PVP, Fraction of FTIR spectra of B) PVP C) APBA D) APBA-PVP E) Zein/APBA-PVP

PVP at 1439 cm^{-1}. In addition to that, C=O stretching vibrations observed in PVP at 1644 cm^{-1} has been observed to shift to 1636 cm^{-1} due to the formation of new C=N bonds. This confirmed the Schiff base formation between the amino group of APBA and the carbonyl group of PVP. Bending vibration of CH_2 groups of PVP was observed at 1371 cm^{-1}. The peak at 1355 cm^{-1} in the FTIR spectra of APBA corresponded to B-O stretching vibrations. APBA-PVP exhibited an overlap between CH_2 bending vibration and B-O stretching vibrations and only bending vibrations of CH_2 were dominant in the FTIR spectra of APBA-PVP and Zein/APBA-PVP. The asymmetrical O-B-O stretching vibration of APBA was noted at 1287 cm^{-1} as a strong peak. This was observed to be prominent in APBA-PVP and Zein/APBA-PVP as shown in figure 60B-E.

4.5.6 X-ray Photoelectron Spectroscopy (XPS)

X-ray Photoelectron Spectroscopy was done to confirm the presence of elements. Figure 61A represents the XPS survey spectra showing elemental peaks of C1s, N1s, O1s and B1s. B1s elemental peak in survey spectra confirmed the presence of APBA moieties in

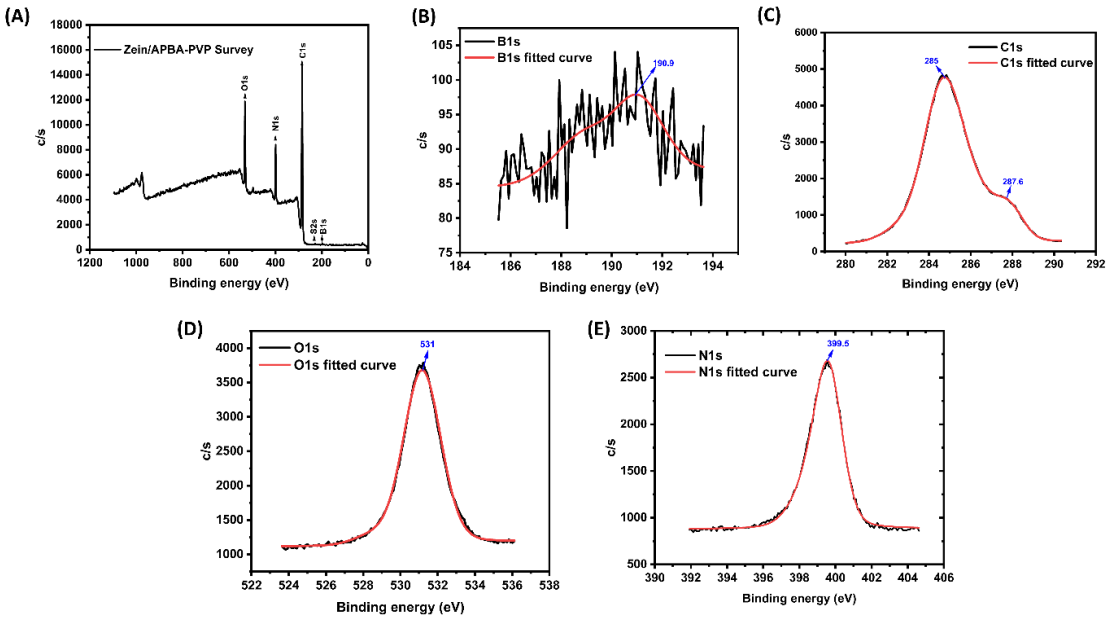

Figure 61 A) XPS survey spectra of Zein/APBA-PVP electrospun membrane, High resolution spectra of B) B1s C) C1s D) O1s and E) N1s

the polymer matrix. High-resolution spectra of B1s in figure 61B had a characteristic peak maximum at 190.9 eV (Sarıarslan et al., 2020). High-resolution spectra of C1s showed two peaks at 285.0 eV and 287.6 eV (figure 61C). The strong peak at 285 eV is attributed to unresolved contributions from aromatic and alkyl carbons. The weak peak noticed at 287.6 eV is attributed to carbon atoms bound to heteroatoms. This peak again is a validation of the presence of boronic acid moieties. Figure 61D-E are the high-resolution XPS spectra of O1s and N1s in sequence.

4.5.7 The water contact angle for the wettability study

APBA conjugation with polymers is reported to cause changes in the wettability characteristics. Boronic acid groups exhibit hydrophobic properties below pKa values and hydrophilic properties above pKa values (Brooks and Sumerlin, 2016; Yoshinaga et al., 2023). This fact has been verified by comparing the water contact angle of Zein/PVP polymer before and after APBA conjugation. Zein/PVP polymer film is hydrophilic and exhibited a contact angle of 75 ± 2 °. APBA conjugation with PVP has resulted in an increase in contact angle to 92 ± 4 °. The commendable increase in contact angle (p-value = 0.015) is depicted in figure 62A-B. According to reports in the literature, the pKa of 3-aminophenyl boronic acid is 8.8 (Surendranath, R, et al., 2022). In that case, at neutral pH conditions, APBA is supposed to demonstrate hydrophobic properties. Thus, and so, Zein/APBA-PVP showed higher contact angle values which is a valid confirmation of conjugation happening. Mucoadhesion and hydrophilicity of polymers possess a direct proportionate relation. In that case, an increase in hydrophobicity could retard adhesive interaction between the polymer matrix and mucosa. Hydrophilic property-mediated mucoadhesion is completely non-specific and it belongs to first-generation materials. On the contrary, APBA moieties establish adhesive interaction via the formation of a boronate ester complex with cis-diols groups of mucins. It is highly specific and targeted.

Though APBA conjugation increases hydrophobicity, the targeted binding would be enough for adhesion over mucosa.

4.5.8 Mechanical property evaluation

The consequences of APBA conjugation on static mechanical properties were evaluated using UTM. Mechanical properties were observed to change with an increase in the concentrations of APBA. Figure 62C represents the bar diagram representation of tensile strength of 10 mM, 20 mM and 50 mM APBA conjugated Zein/PVP electrospun membranes. It is reported that the electrospun membrane of a simple polymer blend of Zein and PVP has a tensile strength of 2.67 ± 0.21 MPa. After 10 mM APBA conjugation,

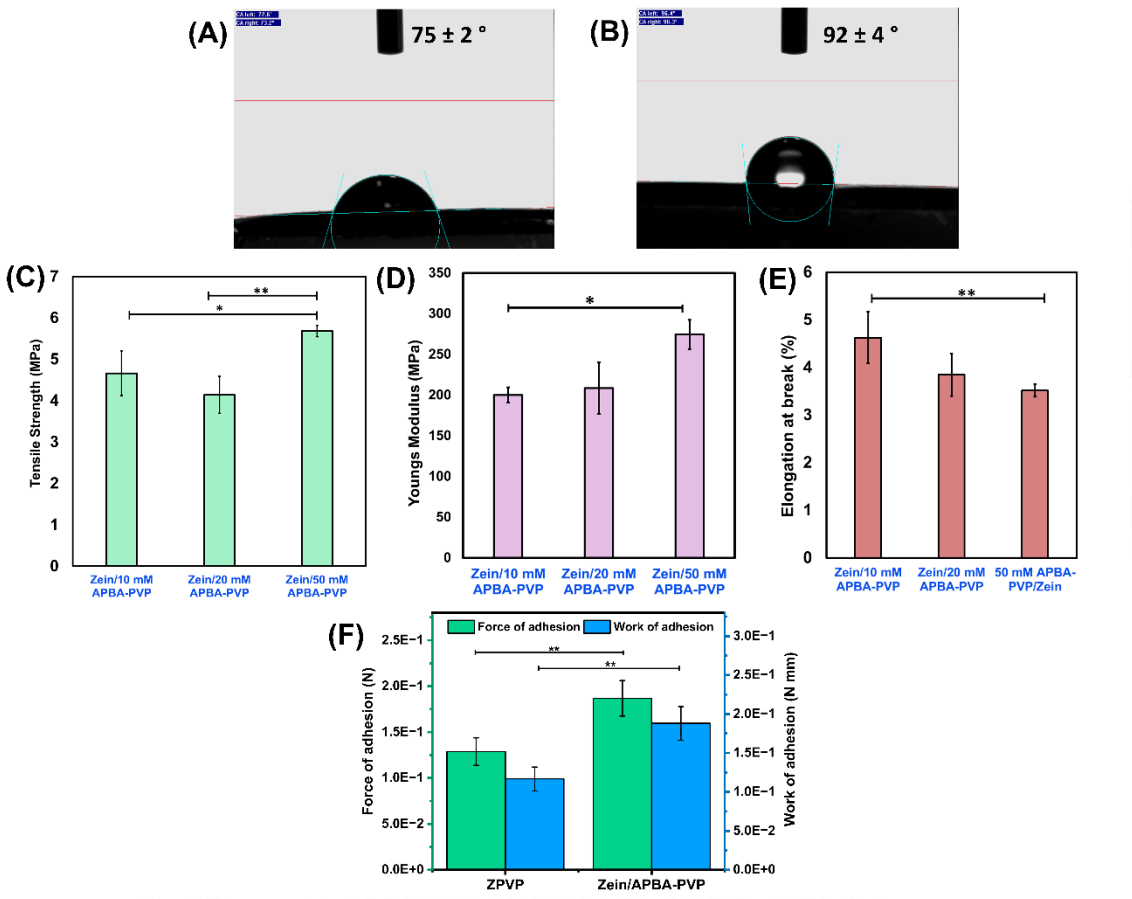

Figure 62 Water contact angle images of A) Zein/PVP film B) Zein/APBA-PVP film, mechanical property evaluation of Zein/APBA-PVP electrospun membranes with 10 mM, 20 mM and 50 mM APBA conjugation represented in terms of C) Tensile strength D) Youngs modulus E) Elongation at break (%) and F) Mucoadhesion results represented in terms of force of adhesion and work of adhesion

tensile strength predominantly increased to 4.66 ± 0.22 MPa. A significant increase can't be observed further for Zein/20 mM APBA-PVP whereas, Zein/50 mM APBA-PVP showed a perfect improvement in tensile strength compared to 10 mM (p-value = 0.03) and 20 mM APBA conjugated membranes (p-value = 0.002). Tensile strength of Zein/50 mM APBA-PVP is 5.68 ± 0.47 MPa. As shown in figure 62D, APBA conjugation has improved the Youngs modulus also. The 50 mM APBA conjugation augmented Youngs modulus to 274 ± 18 MPa from 200 ± 9 MPa of Zein/10 mM APBA-PVP (p-value = 0.03). As a consequence of the increase in brittleness after APBA conjugation as noted in terms of tensile strength and Youngs modulus, elongation at break (%) exhibited an appreciable decrease. Figure 62E represents the bar diagram representation of elongation at break (%). An appreciable decrease was recorded after increasing APBA concentration to 50 mM from 10 mM. The elongation at break (%) of 10 mM, 20 mM and 50 mM APBA conjugated membranes was 4.62 ± 0.54 %, 3.84 ± 0.45 %, and 3.52 ± 0.14 % respectively. The highest percentage APBA conjugated system ie., Zein/50 mM APBA-PVP which exhibited best results for mechanical properties was selected for further evaluations.

4.5.9 Evaluation of mucoadhesion by Texture analysis

Boronate-containing polymers (BCP) are capable of establishing irreversible covalent complexes with cis-diol groups in mucin (d'Amone et al., 2023). Zein/PVP blend electrospun matrix itself is capable of adhering to the surface of mucosa due to its wettability and swelling properties (Surendranath, Ramesan, et al., 2023). The additional benefit of pendant APBA groups on the polymer chain was evaluated by comparing the mucoadhesive properties of Zein/PVP and Zein/APBA-PVP electrospun matrices. Texture analysis for mucoadhesion was carried out in porcine buccal mucosa. The peak maximum of the force-distance curve was considered as the maximum force of adhesion

and the area under the curve represents the work of adhesion. After APBA conjugation to the polymer chain, the force of adhesion considerably increased to 1.87 x 10^{-1} ± 1.94 x 10^{-2} N from 1.29 x 10^{-1} ± 1.50 x 10^{-2} N of that of Zein/PVP blend (p-value= 0.003). Following the same trend, work of adhesion also increased after APBA conjugation from 1.17 x 10^{-1} ± 1.53 x 10^{-2} N mm to 1.88 x 10^{-1} ± 2.16 x 10^{-2} N mm (p-value = 0.004). Graphical representation of force of adhesion and work of adhesion is given in figure 62F. Collective contribution of zein, PVP and APBA in terms of establishing disulfide bonds, swelling and boronate ester complex formation respectively resulted in increased force of adhesion and work of adhesion. The improvement observed in mucoadhesion after APBA conjugation would be enabling prolonged stay of material on the mucosal surface and thus facilitating prolonged drug release.

4.5.10 Drug dissolution and drug release studies

Zein/APBA-PVP electrospun matrix has been loaded with propranolol hydrochloride (PL), an anti-hypertensive drug for transmucosal delivery. The drug was loaded in five formulations and electrospun. Blending electrospinning was employed for the preparation of drug-loaded membranes, where PL of concentrations 0.01 mM, 0.02 mM, 0.03 mM, 0.04 mM and 0.05 mM were mixed into the polymer solution before

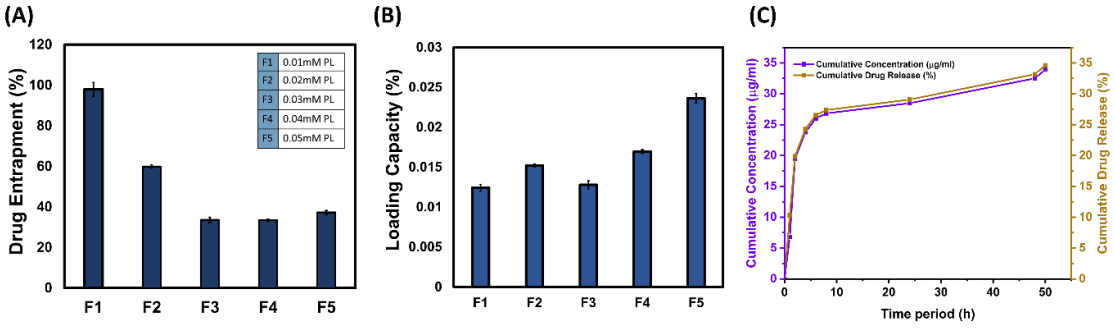

Figure 63 A) Drug entrapment (%) of F1-F5 formulations B) Graphical representation of loading capacity (%) of F1-F5 formulations C) Drug release profile of PL loaded Zein/APBA-PVP in terms of cumulative concentration (µg/mL) and cumulative release (%) done in PBS

electrospinning. A drug dissolution study was carried out by dissolving triplicate pieces of pre-weighed samples in EtOH. Since PL and polymers are miscible in the solvent taken, 100 % of drug entrapment was expected for all electrospun formulations (Ajmal et al., 2019). But the same was true only for the F1 formulation. Drug entrapment was not calculated based on the amount of drug dissolved in the polymer solution. This is because, electrospinning involves loss of polymer fibres during the process. Therefore, the expected amount of drug loading can be calculated based on the final weight of the polymer membrane obtained. For example, the F1 formulation was prepared by mixing 130 μg of PL in the polymer solution. The weight of polymers to which PL was mixed was 1.025, but after electrospinning, the membrane was having only 0.6045 g weight. If so, 76.67 μg of PL would have been entrapped in the membrane. In that case, the membrane was dissolved back in EtOH and absorbance was noted at 290 nm. It was found that 75.05 μg of PL is actually entrapped in it, which is 97.9 ± 3.4 % entrapment. Further, in other formulations, a higher concentration of PL was loaded but a proportionate increase in entrapment percentage was not observed. Figure 63A describes the drug entrapment of five formulations of PL-loaded Zein/APBA-PVP electrospun membranes. Detailed tabulation of the calculation of drug entrapment is given in table 20. F2 formulation was having only 59.9 ± 0.8 % of drug entrapment. F3 to F5 formulations had drug entrapment in the range of 35 %. PL aggregation happening at higher concentration drug loading can be expected as the cause of the decrease of drug entrapment form F1 to F5 formulations (Surendranath, Ramesan, et al., 2023).

Even if the drug entrapment percentage is getting decreased from F1 to F5 formulations, the quantity of drug entrapped is increasing as evident from table 20. Increasing the quantity of PL loading from 130 μg to 650 μg, the quantity of drug entrapped also

increased from 75.02 µg to 198.22 µg. But the problem is that the increase in the quantity of entrapped drug is not in proportion with increase in the quantity of drug loading.

Loading capacity was calculated from the quantity of drug entrapped and the final weight of the electrospun membrane. Unlike drug entrapment percentage, loading capacity percentage increased from F1 to F5 formulation because the quantity of drug entrapped is increasing from 75.02 µg to 198.22 µg. Figure 63B is the graphical representation of the loading capacity of F1-F5 formulations. F5 formulation exhibited a maximum loading capacity of 0.0236 ± 0.006 %. The low magnitude for loading capacity is because the amount of drug loaded is in the microgram range and the weight of the membrane ranges in grams.

Table 20 Tabulation of drug entrapment (%) and loading capacity (%) based on the experimental concentration of entrapped drug in F1-F5 formulations

Formulation	Weight of polymer (g)	Loaded drug (µg)	Expected weight of drug after electrospinning (µg)	The actual concentration of the drug (µg)	Drug entrapment (%)	Loading capacity (%)
F1	1.025	130	76.67	75.05	97.9	0.0124
F2	1.025	260	173.12	103.75	59.9	0.0152
F3	1.025	390	171.22	57.54	33.6	0.0127
F4	1.025	520	362.22	121.00	33.4	0.0169
F5	1.025	650	531.73	198.22	37.3	0.023

The highest-loading F5 formulation was chosen for drug release studies in PBS at pH 7.4. Figure 63C is the cumulative drug release curve of PL from the Zein/APBA-PVP electrospun matrix. The release trend followed an initial burst release followed by a sustained release. Within 1 h of release, 10.3 ± 4.9 % of PL release happened. The PL release approached 33.2 ± 2 % within 48 h of the study. The release profile was fitted

with Zero order, First order, Higuchi model and Korsmeyer Peppas model and found to be fitting best with the Korsmeyer Peppas model with an R^2 value of 0.915. Table 21 gives the calculated R^2 values for the different mathematical models after fitting with the PL release curve. Korsmeyer Peppas model is best fitted with an n value less than 0.5, suggesting a diffusion-controlled release mechanism of PL from the electrospun matrix.

Table 21 R^2 values of mathematical models of drug release

Mathematical models	R^2 values
Zero order	0.959
First order	0.936
Higuchi model	0.983
Korsmeyer-Peppas model	0.985

4.5.11 *In-vitro* cytotoxicity studies

In-vitro cytotoxicity evaluation of Zein/APBA-PVP electrospun matrix was done in RPMI 2650 epithelial cells. PL-loaded Zein/APBA-PVP membranes were also analysed. Qualitative estimation of cytotoxicity was done by direct contact and live/dead assays. Direct contact assay gives the phase contrast images of RPMI 2650 cells after incubating with materials of interest for 24 h. On the other hand, cells were visualized under a fluorescent microscope after live/dead fluorescent staining in live/dead assay. Phase contrast images of direct contact assay are shown in figure 64A-E. Cells treated with tin coated PVC and UHMWPE were considered as positive and negative control. The epithelial RPMI 2650 cells without any treatment were considered as the cell alone control (figure 64C). Zein/APBA-PVP and PL-loaded Zein/APBA-PVP treated cells are depicted in figure 64D and 64E respectively. The cells after material treatment were retaining their morphology and monolayer after 24 h. Therefore, the materials were

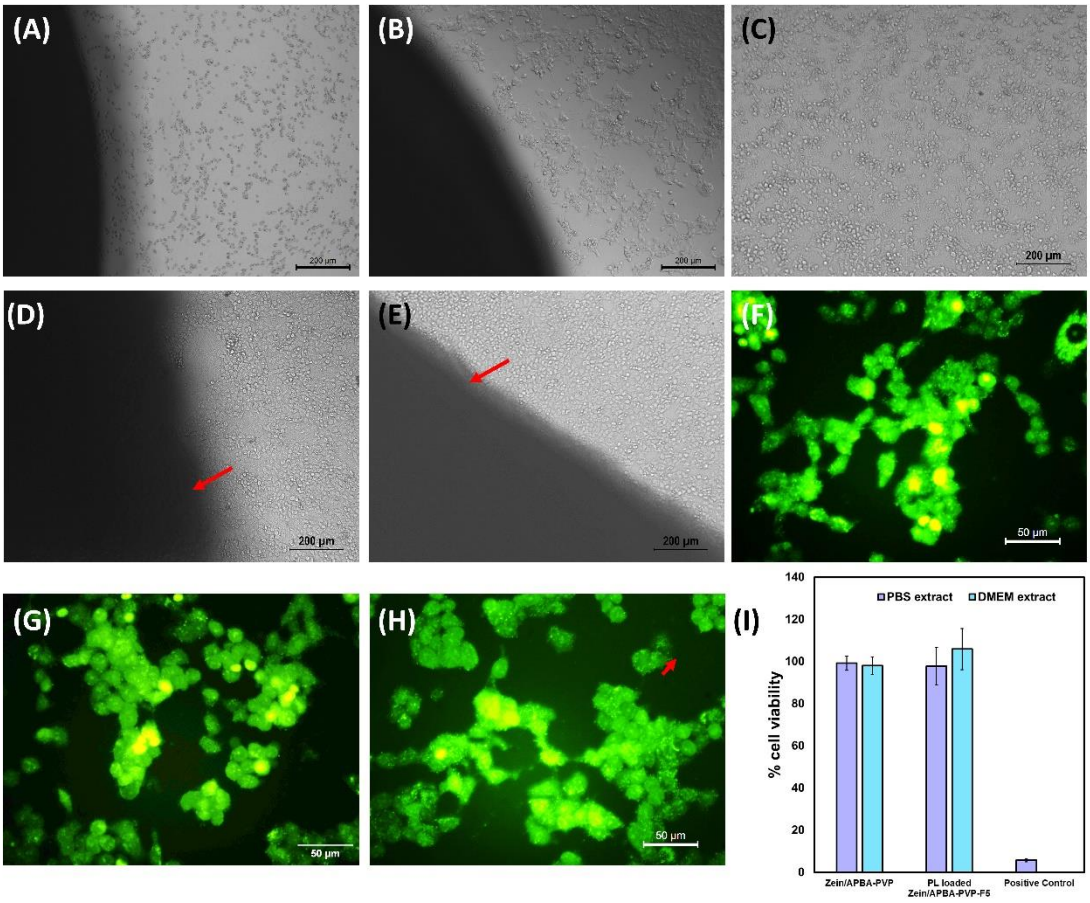

Figure 64 Direct contact phase contrast images (10X magnification) of A) Positive control cells B) Negative control cells C) Cell alone control D) Zein/APBA-PVP treated cells E) Zein/APBA-PVP/PL treated cells, Live/dead assay fluorescent images (40X magnification) of F) Control cells G) Zein/APBA-PVP treated cells and H) Zein/APBA-PVP/PL treated cells I) Representation of % cell viability after MTT assay

confirmed to be non-cytotoxic to RPMI 2650 cells. Live/dead assay images also go on par with the results of direct contact assay. Figure 64F is the control cell images where the live cells are stained using acridine orange in green colour and dead cells are visible as red colour after ethidium bromide staining. Figures 64G and 64H are live/dead fluorescent images after Zein/APBA-PVP and PL-loaded Zein/APBA-PVP treatment. In both cases, the number of live cells is observed in the majority in green colour. A few of the cells, which were observed as dead were marked using arrow points. Quantitative estimation of cell viability using MTT assay is a next step confirmation to the above observations. Material extracts in PBS and DMEM media were collected for MTT assay.

The metabolic viability of cells after Zein/APBA-PVP and PL-loaded Zein/APBA-PVP was almost 100 %. The positive control cells which were treated with phenol showed 5.7 ± 0.8 % viability. The graphical representation of cell viability obtained from the MTT assay is depicted in figure 64I. Zein and PVP are already known for their cytocompatibility (Demir et al., 2017) and hence are widely used in biomedical applications. The additional presence of APBA with these non-cytotoxic polymers has not caused toxicity to the cells.

4.5.12 F-actin staining for the evaluation of cell-junction integrity

Evaluation of F-actin cytoskeletal filaments of epithelial cells is important in the perspective of analysing the mechanism of drug transport. In paracellular drug transport, where the drug passes through the inter cellular space, cell junctions get opened. In that

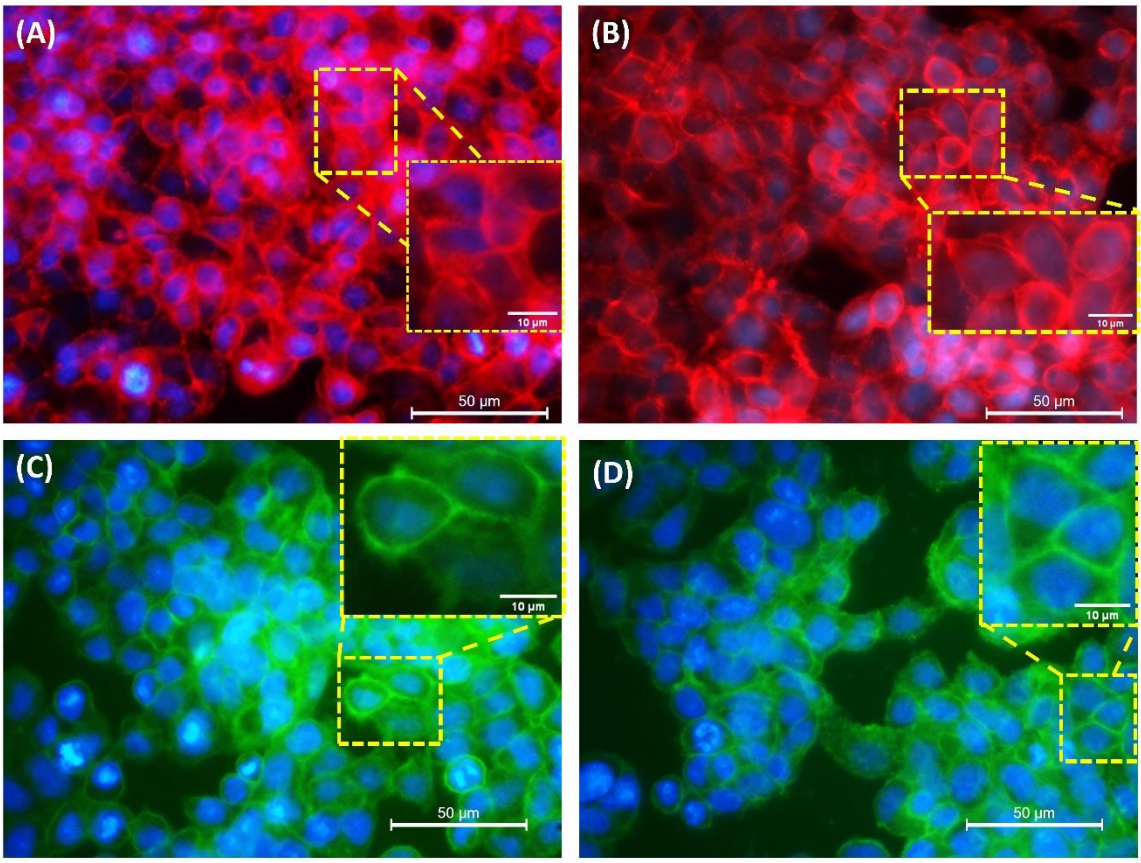

Figure 65 Overlay F-actin staining images of A) Control cells B) Zein/APBA-PVP treated cells and Overlay beta-catenin immunostaining images of C) Control cells D) Zein/APBA-PVP treated cells

case, the coherence of tight junction, adherens junction and desmosomes are important. Changes happening in the structure of tight junction proteins will be reflected in the integrity of adherens junction proteins and further in F-actin filaments which are inter-connected through catenin proteins (Campbell et al., 2017; Hartsock and Nelson, 2008). Therefore, the evaluation of F-actin structural integrity is a key point to describe the mechanism of drug transport.

Rhodamine-labelled phalloidin was used to stain F-actin filaments in red colour. The nucleus of the cells was stained using Hoechst in blue colour. Figure 65A represents the control cells after F-actin/nucleus staining. Magnified images of F-actin filaments are shown in the inset of the image. The continuity and integrity of the filamentous structure of F-actin is visible from the image. The cells after treatment with Zein/APBA-PVP for 24 h also retained the structural integrity of F-actin filaments. Figure 65B is the fluorescent image after material treatment. A magnified image is given in the inset where the structural coalition of F-actin filaments was seen undisturbed.

4.5.13 Immunostaining of beta-catenin proteins of adherens junction

In continuation with the above discussion, the changes happening to the tight junction of epithelial cell junction will be reflected in the structure of adherens junction proteins also. In that scenario, the β-catenin proteins of adherens junctions (Giepmans and van IJzendoorn, 2009) were stained using anti-β catenin antibody. Immunostaining images of untreated cells in figure 65C with the magnified image shown in the inset can be considered as the reference for the natural appearance of β-catenin proteins. Figure 65D is the cell image after Zein/APBA-PVP treatment for 24 h. Just like the control cells, material-treated cells also retained the continuity, integrity and structure of β-catenin

proteins of the adherens junction. This observation confirms the junctional coherence and rules out the possibility of paracellular transport of PL across epithelial cell monolayer.

4.5.14 TEER measurement and *in-vitro* drug permeation study

F-actin staining and β-catenin immunostaining have qualitatively confirmed the lack of junctional opening during material treatment. Transepithelial electrical resistance (TEER) measurement is a quantitative method adopted to confirm the integrity of the cell monolayer. Changes in TEER values after material treatment indicate junctional opening and therefore a comparative study of TEER values before and after material treatment has to be carried out. Figure 66A represents the schematic setup for TEER experimentation. RPMI 2650 cells were cultured in a 24-well insert till achieving a constant TEER value, ie., complete formation of a monolayer. Once the TEER has become constant, the material was placed over the monolayer and TEER values were noted before and after placing the material at different periods. The extent of retaining the TEER integrity was calculated and stated in terms of TEER (%). Figure 66B is the graphical presentation of absolute TEER and TEER (%) values at different periods. Liquid-liquid interface culturing of RPMI 2650 cells has been reported to have an absolute TEER value in the range of 30 Ωcm^2 (Sibinovska et al., 2019). RPMI 2650 cells after treatment with Zein/APBA-PVP also demonstrated an absolute TEER value of 30 Ωcm^2. Similarly, TEER (%) values also ranged at 100 % at all periods of the experiment. Hence, the epithelial cell junction integrity was proved quantitatively.

In the absence of a cell junction opening, the drug transport across the epithelial cell monolayer has to follow the transcellular pathway. It has to be verified whether PL is capable of permeating through the cell membrane or not. A drug permeation study was done in the same experiment setup as that of TEER measurement. Drug-loaded

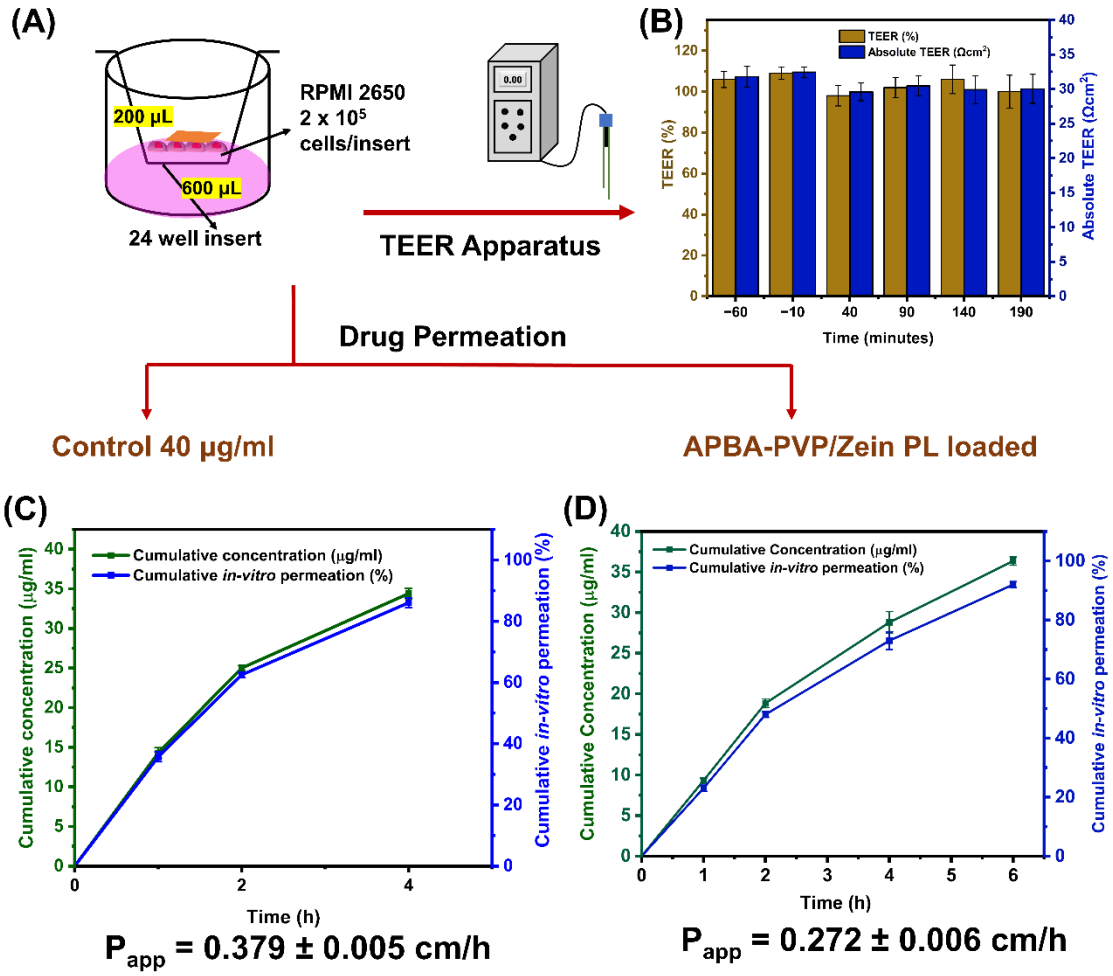

Figure 66 A) Schematic representation of experimental setup for TEER measurement and drug permeation using cell culture inserts B) TEER (%) values of RPMI 2650 cells before and after Zein/APBA-PVP treatment C) Cumulative drug release profile of PL directly added (40 µg/mL) over the cell monolayer D) Cumulative release profile of PL delivered via electrospun Zein/APBA-PVP [Permeation coefficient of control and test material are denoted on the bottom of the graphs]

Zein/APBA-PVP electrospun membrane was placed in the apical chamber of 24 well inserts and permeated amount of drug was collected from the basolateral compartment. Quantification of drug permeation was done using UV spectroscopy at 290 nm. The control system of the experiment was 40 µg/mL of PL directly added to the top of the cell monolayer. The cumulative drug permeation curve was plotted for both control and test systems. Figures 66C and 66D represent both in respective order. The permeation coefficient (P_{app}) was calculated from the slope of the curve. In case, the mechanism of

drug transport is paracellular for the material-treated system, P_{app} would be a higher value compared to the control. But, here P_{app} of PL from the Zein/APBA-PVP system was 0.272 ± 0.006 cm/h, and that of control was 0.379 ± 0.006 cm/h. Since the P_{app} of the material-treated system is lesser than the control (p-value = 0.0003), the mechanism of drug permeation can only be transcellular. A higher P_{app} value for the control system doesn't mean that direct drug administration is causing a junctional opening, rather it means that the direct addition of the drug is causing abrupt drug permeation. When PL is applied through an adhesive membrane carrier, the drug permeation is controlled as it has to first diffuse out of the membrane and then permeate across the cell monolayer. Such a controlled delivery is highly favoured for many of the drug delivery applications.

4.5.15 Transmucosal drug permeation through porcine buccal mucosa

In-vitro drug permeation through RPMI 2650 cell monolayer has confirmed transcellular transport which has to be further verified in *ex-vivo* conditions. The *ex-vivo* drug permeation was done by Franz diffusion cell apparatus with porcine buccal mucosa. The permeation study was conducted till 8 h and the cumulative drug release curve was plotted. Figure 67A demonstrates the cumulative PL permeation curve through porcine buccal mucosa from the PL-loaded Zein/APBA-PVP electrospun membrane. Within 8 h of the experiment, 31.3 ± 5.7 % of PL permeation was observed. Figure 67B-E are the mathematical model fitting curves of cumulative drug permeation. The best-fit model was Zero order since the R^2 value is high. The effective permeation through buccal mucosa has to be compared with a control system, which is 40 µg/mL PL directly administered over mucosa. Figure 67F is the cumulative drug permeation through porcine buccal mucosa after direct administration of the control drug system. The observation for

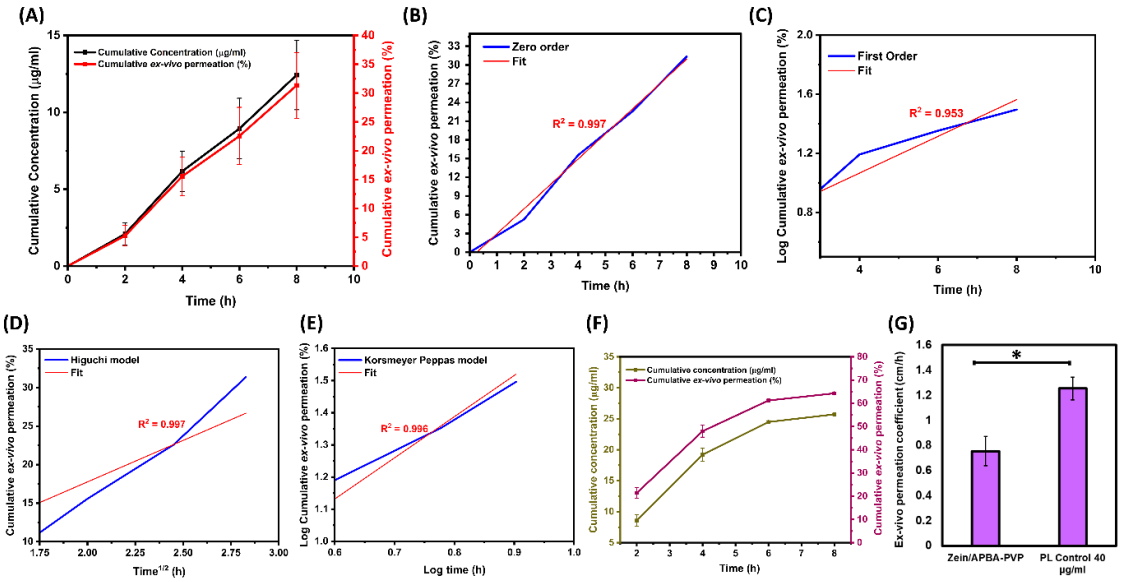

Figure 67 A) *Ex-vivo* permeation profile of PL through porcine buccal mucosa B) Fitting curve with Zero order kinetics C) Fitting curve with First order kinetics D) Fitting curve with Higuchi model E) Fitting curve with Korsmeyer Peppas model F) Drug permeation from 40 µg/mL PL control through porcine buccal mucosa G) Permeation coefficients of test and control system represented as bar diagram

the control system was that 64.3 ± 0.4 % of the drug permeated within 8 h of the experiment which was almost double the amount of drug permeation of that from test material. Fast and immediate drug permeation was absent in the test system because of the additional time requirement for the drug diffusion from the electrospun material of interest. In test material drug permeation through the mucosa happens only after drug diffusion whereas in the control system direct drug permeation will be facilitated. Due to this difference, the permeation coefficient of PL control was observed to be higher than that of PL loaded Zein/APBA-PVP system (p-value = 0.01). Permeation coefficients are 1.25 ± 0.09 cm/h and 0.75 ± 0.12 cm/h respectively for 40 µg/mL PL control and PL loaded Zein/APBA-PVP which are given as a bar diagram in figure 67G. The smaller permeation coefficient for the test material indicates the lack of cell junction opening. At the same time, higher permeation for the control system doesn't mean junction opening. It is just an indication of fast permeation due to direct drug administration.

5 SUMMARY, CONLCUSION AND FUTURE PERSPECTIVES

5.1 SUMMARY AND CONCLUSION

The aim of the present study was to evaluate the potential of zein based electrospun membranes for mucoadhesive drug delivery applications. Taking into consideration of the fact that electrospun zein is mechanically weak due to its brittleness, different crosslinking techniques, blending with synthetic polymers like polyethylene oxide and polyvinyl pyrrolidone and different functional modifications were evaluated and compared in this research.

5.1.1 UV crosslinked Zein/PEO

UV crosslinking of Zein/PEO electrospun membrane resulted in conformational changes. The inherent alpha helical conformation of zein gets transformed to beta-sheet after UV irradiation for 24 h. Also, the disulfide linkages at the end of each helix break during UV crosslinking and thiol-containing cysteine amino acids become free following an electron transfer mechanism. Blending of PEO with zein caused increase in mechanical property of the electrospun membrane. UV crosslinking further improved the tensile strength from 1.78 ± 0.29 MPa to 3.52 ± 0.38 MPa. UV crosslinking hasn't caused changes in the thermal decomposition pattern of zein. DSC analysis of UV crosslinked Zein/PEO membrane exhibited protein unfolding peak at 255.1 °C indicating the absence of complete unfolding of native protein structure of zein after 24 h UV irradiation. PEO blending resulted in decrease in the water contact angle which further got decreased after long UV exposure. The evaluation of mucoadhesion in porcine buccal mucosa showed increase in force of adhesion and work of adhesion after UV crosslinking of Zein/PEO electrospun membrane. This is a result of the presence of more thiol groups on the

polymer chain of zein after UV crosslinking. UV crosslinked Zein/PEO electrospun membrane with and without PL loading has showed non-cytotoxic properties with RPMI 2650 cells. The result has been confirmed with direct contact assay, MTT assay and live/dead assay. The cumulative percentage release of PL in PBS, *in-vitro* conditions and *ex-vivo* conditions were 31.8 ± 2.3 % in 48 h, 46.4 ± 1.4 % in 8 h and 33.4 ± 6.7 % in 8 h respectively. The release kinetics of PL from UV crosslinked Zein/PEO best fitted with Korsmeyer Peppas model in PBS, *in-vitro* conditions and *ex-vivo* conditions. Treatment of RPMI 2650 cells with UV crosslinked Zein/PEO hasn't resulted in perturbations to the epithelial cell junctions which pointed towards transcellular mechanism of drug transport. Fluorescent imaging of F-actin filaments and immunostaining of β-catenin protein of adherens junction confirmed this fact. Since the TEER (%) values remained unchanged after material treatment, possibility of transcellular mechanism of transport was again confirmed. Occurrence of drug permeation through porcine buccal mucosa in the absence of the opening of cell junction further confirmed the mechanism of transport.

5.1.2 Thiol-modified Zein/PEO

Thiol modification of zein with cysteine amino acid has been carried out in the presence of EDC crosslinker. The functionalised thiol groups were assessed for the presence of thiol via Ellman's assay and Raman spectra. Electrospun membrane of thiol-modified zein was prepared by blending with PEO. Thiol-modified samples of zein were prepared with 5 %, 10 %, 15 %, 30 % and 50 % cysteine concentrations to which 3 % (w/w) of PEO was added to prepare the blend. The quantity of PEO blended with the thiol-modified zein decreases with increase in the percentage of thiol concentration. As a result, the fibre diameter of electrospun samples were observed to be significantly decreasing from 5 % to 50 % thiol-modified Zein/PEO. An improvement in the mechanical property of zein was observed after thiol modification and PEO blending. The tensile strength

values significantly increased from 2.10 ± 0.12 MPa to 4.61 ± 0.72 MPa for the 5 % and 50 % thiol-modified zein/PEO electrospun membranes. Even if the amount of PEO blended with thiol-modified zein is less for higher percentage modified samples, the improvement in mechanical property is solely due to the contribution of thiolation of zein polymer chains. Even though the concentration of thiol groups sequentially improved from 5 % to 50 % thiol-modification, the maximum force of adhesion in porcine buccal mucosa was noted for the 30 % modified sample. The PL loaded and non-loaded samples of 30 % thiol-modified Zein/PEO electrospun membrane were subjected to cytocompatibility evaluation using RPMI 2650 cells and their non-cytotoxicity was confirmed. The result has been confirmed with direct contact assay, MTT assay and live/dead assay. The cumulative percentage release of PL in PBS, *in-vitro* conditions and *ex-vivo* conditions are 67.6 ± 6.3 % in 48 h, 96 ± 2.4 % in 6 h and 34.0 ± 1.43 % in 8 h respectively. Drug permeation kinetics in PBS media, *in-vitro* conditions and *ex-vivo* conditions best fitted with Korsmeyer-Peppas model, Higuchi model and First order kinetics respectively. Drug transport mechanism from thiol-modified Zein/PEO also followed a transcellular mechanism as no changes in the barrier integrity was noted for epithelial cell junctions as visualized from F-actin staining and β-catenin immunostaining. The evaluation of TEER (%) after material treatment quantitatively confirmed transcellular mechanism of transport.

5.1.3 Thermally crosslinked Zein/PVP

Polymer blend of Zein/PVP was prepared in 15:5 ratio. Thermal crosslinking of electrospun membrane of Zein/PVP blend was done at 120 °C. High temperature treatment for 10 h caused radical mediated crosslinking of PVP chains in the systems. The diminished intensity of -CH asymmetric stretching vibration of PVP polymer after thermal crosslinking is confirmative evidence for the radical mediated crosslinking

mechanism. The shift observed for the RBM vibration of PVP in Raman spectra after thermal crosslinking also confirmed the crosslinking. According to the results of CD spectroscopy, the crosslinking technique also resulted in conformational change of zein from alpha-helix to beta-sheet. Uncrosslinked PVP chains in the system get arranged in an ordered fashion in such a way that the crystallinity is increased. The cumulative effect of PVP crosslinking, conformational change of zein and increased crystallinity contributed to the enhanced mechanical property of thermally crosslinked Zein/PVP electrospun membrane. A significant increase in tensile strength was observed after 5 h of crosslinking. The 10 h crosslinked Zein/PVP exhibited the maximum tensile strength value of 3.92 ± 0.13 MPa. Increasing the time of thermal crosslinking resulted in premature decomposition of polymer system as evidenced from TGA results. The breakage of disulfide bonds in zein after 10 h temperature treatment set more thiol groups free on the polymer chain which resulted in better mucoadhesion. *In-vitro* cytotoxicity analysis in RPMI 2650 cells concluded that the thermally crosslinked Zein/PVP electrospun membrane as non-cytotoxic even after incorporating PL. The result has been confirmed with direct contact assay, MTT assay and live/dead assay. The cumulative percentage release of PL in PBS, *in-vitro* conditions and *ex-vivo* conditions are 44.9 ± 0.5 % in 48 h, 75 ± 2 % in 8 h and 6.3 ± 1.03 % in 8 h respectively. The best fit mathematical models were Korsmeyer Peppas, Zero order and Higuchi model for drug release studies in PBS, *in-vitro* conditions and *ex-vivo* conditions respectively. Immunostaining showed that the beta catenin proteins in the epithelial cell junction do not open up during material treatment. TEER (%) evaluation also confirmed the observations of F-actin staining and immunostaining. Hence the transport of PL through epithelial cells and porcine buccal mucosa has been assumed to follow a transcellular mechanism of transport.

5.1.4 Mucin crosslinked Zein/PVP

Mucin incorporated electrospun membrane for mucoadhesive drug delivery is a novel concept to investigate. Mucin of concentration 1 % (w/v) was crosslinked with 15 % (w/v) zein in the presence of EDC crosslinker so that the amino group of zein binds with carboxyl group of mucins. TNBS assay quantified the degree of mucin/zein crosslinking to 39 %. Mucin crosslinked zein film was then blended with 5 % (w/v) PVP for the preparation of electrospun membrane. Post-electrospinning crosslinking of electrospun MUZPVP enabled PVP chain crosslinking. Mucin/zein crosslinking has resulted in increase of fibre diameter for MUZPVP compared to uncrosslinked blend of mucin, zein and PVP. Both crosslinking mechanisms contributed towards increased tensile strength. Tensile strength of Zein/Mucin/PVP blend electrospun membrane was observed to be 0.93 ± 0.09 MPa whereas that of MUZPVP after thermal crosslinking was 4.85 ± 0.92 MPa. Evaluation of FTIR spectra of MUZPVP also confirmed the presence of mucin by the vibrational peaks of O-H bonds of primary alcohols. It also gave evidence for the thermal crosslinking of PVP by showing decreased intensity for C-H asymmetric stretching vibration compared to that of MUZPVP without thermal crosslinking. The cohesive interaction and mutual interpenetration mucin chains in the polymer system and mucin in the mucosal surface enhanced the mucoadhesive property of MUZPVP in terms of force of adhesion and work of adhesion. MUZPVP with and without PL loading were observed to be non-cytotoxic to RPMI 2650 cells. The result has been confirmed with direct contact assay, MTT assay and live/dead assay. A decreased drug entrapment was observed due to lack of compatibility between mucin and PL. However, PL release in PBS, *in-vitro* drug permeation and *ex-vivo* drug permeation was evident. The cumulative percentage release of PL in PBS, *in-vitro* and *ex-vivo* conditions are 33.2 ± 7 % in 48 h, 44.9 ± 2.5 % in 8 h and 83.9 ± 34.9 % in 8 h respectively. The release kinetics is best

fitted with Korsmeyer Peppas model for PBS media and *in-vitro* conditions whereas for the *ex-vivo* conditions the best fit model was Zero order kinetics. Fluorescent staining of F-actin filaments and beta-catenin proteins confirmed the barrier integrity of epithelial cells after material treatment. That being the case, PL permeation through the cell monolayer happened through a transcellular pathway. TEER (%) evaluation results also confirmed the transcellular mechanism of transport.

5.1.5 Zein/APBA conjugated PVP

3-aminophenyl boronic acid (APBA) was conjugated to the polymer chain of PVP by forming a Schiff base. The conjugation was done with 10 mM, 20 mM and 50 mM APBA to 5 % (w/v) of PVP. A polymer blend of 15 % (w/v) zein with APBA conjugated PVP was prepared to fabricate electrospun membrane. FTIR and XPS analysis confirmed the presence of APBA in the system after conjugation. UV spectroscopy quantification technique was adopted to find out the degree of conjugation which appeared to be 97 %. APBA conjugation to PVP resulted in increase in contact angle compared to unconjugated Zein/PVP. This is a result of hydrophobic behaviour of APBA at a pH lower than its pKa values. Augmentation in tensile strength also confirmed conjugation of APBA with PVP. Comparatively higher force and work of adhesion with respect to unconjugated Zein/PVP blend grounded boronate ester mediated mucoadhesion. The cumulative percentage release of PL in PBS, *in-vitro* conditions and *ex-vivo* conditions are 39.05 ± 1.18 % in 48 h, 92 ± 1 % in 6 h and 31.35 ± 5.65 % in 8 h respectively. PL release in PBS, *in-vitro* condition and *ex-vivo* conditions demonstrated Korsmeyer Peppas model, Higuchi model and Zero order fitting respectively. Zein/APBA-PVP electrospun membrane was observed to be non-cytotoxic to RPMI 2650 cells with and without PL loading. The result has been confirmed with direct contact assay, MTT assay and live/dead assay. After material treatment, F-actin and immunostaining unveiled the

intactness of cytoskeleton and adherens junction proteins. Despite that, *in-vitro* drug permeation of PL was observed through RPMI 2650 cells which pointed towards the transcellular mechanism of transport. The TEER (%) evaluation and *Ex-vivo* drug permeation studies also confirmed the possible mechanism of transport to be transcellular.

5.1.6 System comparison- conclusion

All the five systems under investigations were noted to be non-cytotoxic to RPMI 2650 cells. The drug loaded samples showed an initial burst release profile and a sustained release afterwards. The integrity and continuity of F-actin filaments and beta-catenin proteins in the adherens junctions were observed to be maintaining intact. Quantitative evaluation of epithelial junction integrity by TEER value evaluation also showed no significant change after treating the cells with all electrospun membranes. *In-vitro* drug permeation observed in the absence of epithelial junction openings confirmed the transcellular mechanism of transport. Transmucosal drug permeation of PL observed in *ex-vivo* conditions also validated the conclusion of transcellular transport of PL.

Among all the five systems, thiol modification, mucin incorporation and APBA conjugation improved the performance of electrospun polymer membranes as mucoadhesive PL delivery system compared to simple polymer blends like UV crosslinked Zein/PEO and thermally crosslinked Zein/PVP.

- Thiol-modified Zein/PEO performed excellent in cumulative drug release in PBS, *in-vitro* drug permeation and *ex-vivo* drug permeation.
- Mucin crosslinked Zein/PVP was the best mucoadhesive polymeric system and it performed well in *ex-vivo* drug permeation studies.

- Zein/APBA conjugated PVP system exhibited maximum mechanical property and its permeation results were excellent in *in-vitro* as well as *ex-vivo* conditions.

5.2 FUTURE PERSPECTIVES

The present study confirmed the potential of five types of zein based electrospun membranes for mucoadhesive drug delivery applications. Propranolol hydrochloride has been incorporated and evaluated for drug release as a model analysis. The results of this particular research shed light towards incorporating other drug molecules which are much compatible with the electrospun membranes and use of the same for either local or systemic drug delivery.

The present study has evaluated the electrospun membranes only up to *ex-vivo* conditions. It is necessary to comprehensively understand the drug release profile in *in-vivo* conditions. *In-vivo* evaluation has to be carried out in suitable animal model with appropriate disease conditions. It needs to verified that whether the plasma level concentration of the drug falls within the therapeutic window of the drug molecule.

REFERENCES:

Abe M, Miyasaka S and Arai S (1985) Analysis of Sulfhydryl Groups in Zein. *Agricultural and Biological Chemistry* 49(5). Taylor & Francis: 1417–1422.

Adams GDJ, Cook I and Ward KR (2015) The Principles of Freeze-Drying. In: Wolkers WF and Oldenhof H (eds) *Cryopreservation and Freeze-Drying Protocols*. Methods in Molecular Biology. New York, NY: Springer New York, pp. 121–143. Available at: http://link.springer.com/10.1007/978-1-4939-2193-5_4 (accessed 28 April 2022).

Ahmed HT and Abdullah OG (2019) Preparation and Composition Optimization of PEO:MC Polymer Blend Films to Enhance Electrical Conductivity. *Polymers* 11(5). 5. Multidisciplinary Digital Publishing Institute: 853.

Ahuja G and Pathak K (2009) Porous Carriers for Controlled/Modulated Drug Delivery. *Indian Journal of Pharmaceutical Sciences* 71(6): 599–607.

Ajmal G, Bonde GV, Thokala S, et al. (2019) Ciprofloxacin HCl and quercetin functionalized electrospun nanofibre membrane: fabrication and its evaluation in full thickness wound healing. *Artificial Cells, Nanomedicine, and Biotechnology* 47(1). Taylor & Francis: 228–240.

Akazawa-Ogawa Y, Uegaki K and Hagihara Y (2016) The role of intra-domain disulfide bonds in heat-induced irreversible denaturation of camelid single domain VHH antibodies. *The Journal of Biochemistry* 159(1): 111–121.

AlHusban F, Perrie Y and Mohammed AR (2010) Formulation and characterisation of lyophilised rapid disintegrating tablets using amino acids as matrix forming agents. *European Journal of Pharmaceutics and Biopharmaceutics* 75(2): 254–262.

Alibe IM, Matori KA, Sidek HAA, et al. (2019) Effects of polyvinylpyrrolidone on structural and optical properties of willemite semiconductor nanoparticles by polymer thermal treatment method. *Journal of Thermal Analysis and Calorimetry* 136(6): 2249–2268.

Alsarra IA, Hamed AY, Alanazi FK, et al. (2011) Rheological and mucoadhesive characterization of poly(vinylpyrrolidone) hydrogels designed for nasal mucosal drug delivery. *Archives of Pharmacal Research* 34(4): 573.

Altan A, Aytac Z and Uyar T (2018) Carvacrol loaded electrospun fibrous films from zein and poly(lactic acid) for active food packaging. *Food Hydrocolloids* 81: 48–59.

Amores S, Domenech J, Colom H, et al. (2014) An improved cryopreservation method for porcine buccal mucosa in ex vivo drug permeation studies using Franz diffusion cells. *European Journal of Pharmaceutical Sciences* 60: 49–54.

Anand U, Feridooni T and Agu RU (2012) Novel Mucoadhesive Polymers for Nasal Drug Delivery. *Recent Advances in Novel Drug Carrier Systems*. IntechOpen. Epub ahead of print 31 October 2012. DOI: 10.5772/52560.

Anderson JM and Van Itallie CM (2009) Physiology and Function of the Tight Junction. *Cold Spring Harbor Perspectives in Biology* 1(2): a002584.

Arthanari S, Mani G, Jang JH, et al. (2016) Preparation and characterization of gatifloxacin-loaded alginate/poly (vinyl alcohol) electrospun nanofibres. *Artificial Cells, Nanomedicine, and Biotechnology* 44(3). Taylor & Francis: 847–852.

Azeez N (2016) Thermogravimetric Analysis on PVA / PVP Blend Under Air Atmosphere. Epub ahead of print 1 January 2016.

Baltzley S, Malkawi AA, Alsmadi M, et al. (2018) Sublingual spray drug delivery of ketorolac-loaded chitosan nanoparticles. *Drug Development and Industrial Pharmacy* 44(9). Taylor & Francis: 1467–1472.

Bansil R and Turner BS (2006) Mucin structure, aggregation, physiological functions and biomedical applications. *Current Opinion in Colloid & Interface Science* 2–3(11): 164–170.

Bansil R, Stanley E and LaMont JT (1995) Mucin biophysics. *Annual Review of Physiology* 57: 635–657.

Barratt G, Couarraze G, Couvreur P, et al. (2001) Polymeric Micro- and Nanoparticles as Drug Carriers. In: *Polymeric Biomaterials, Revised and Expanded*. 2nd ed. CRC Press.

Bazylewski P, Divigalpitiya R and Fanchini G (2017) In situ Raman spectroscopy distinguishes between reversible and irreversible thiol modifications in l -cysteine. *RSC Advances* 7(5). Royal Society of Chemistry: 2964–2970.

Becucci L, Innocenti M, Salvietti E, et al. (2008) Potassium ion transport by gramicidin and valinomycin across a Ag(111)-supported tethered bilayer lipid membrane. *Electrochimica Acta* 53(22): 6372–6379.

Bell SL, Xu G, Khatri IA, et al. (2003) N-linked oligosaccharides play a role in disulphide-dependent dimerization of intestinal mucin Muc2. *The Biochemical Journal* 373(Pt 3): 893–900.

Bernkop-Schnürch A (2005) Thiomers: A new generation of mucoadhesive polymers. *Advanced Drug Delivery Reviews* 57(11). Mucoadhesive Polymers: Strategies, Achievements and Future Challenges: 1569–1582.

Bernkop-Schnürch A and Steininger S (2000) Synthesis and characterisation of mucoadhesive thiolated polymers. *International Journal of Pharmaceutics* 194(2): 239–247.

Bernkop-Schnürch A, Guggi D and Pinter Y (2004) Thiolated chitosans: development and in vitro evaluation of a mucoadhesive, permeation enhancing oral drug delivery system. *Journal of Controlled Release* 94(1): 177–186.

Bhardwaj N and Kundu SC (2010) Electrospinning: A fascinating fibre fabrication technique. *Biotechnology Advances* 28(3): 325–347.

Bhattacharjee P and Ahearne M (2021) Significance of Crosslinking Approaches in the Development of Next Generation Hydrogels for Corneal Tissue Engineering. *Pharmaceutics* 13(3). 3. Multidisciplinary Digital Publishing Institute: 319.

Bhurke AS, Askeland PA and Drzal LT (2007) Surface Modification of Polycarbonate by Ultraviolet Radiation and Ozone. *The Journal of Adhesion* 83(1). Taylor & Francis: 43–66.

Bognitzki M, Frese T, Steinhart M, et al. (2001) Preparation of fibres with nanoscaled morphologies: Electrospinning of polymer blends. *Polymer Engineering & Science* 41(6): 982–989.

Brannigan RP and Khutoryanskiy VV (2019) Progress and Current Trends in the Synthesis of Novel Polymers with Enhanced Mucoadhesive Properties. *Macromolecular Bioscience* 19(10): 1900194.

Bravo-Osuna I, Vauthier C, Farabollini A, et al. (2007) Mucoadhesion mechanism of chitosan and thiolated chitosan-poly(isobutyl cyanoacrylate) core-shell nanoparticles. *Biomaterials* 28(13): 2233–2243.

Brizuela M and Winters R (2022) Histology, Oral Mucosa. In: *StatPearls*. Treasure Island (FL): StatPearls Publishing. Available at: http://www.ncbi.nlm.nih.gov/books/NBK572115/ (accessed 3 April 2022).

Brooks WLA and Sumerlin BS (2016) Synthesis and Applications of Boronic Acid-Containing Polymers: From Materials to Medicine. *Chemical Reviews* 116(3). American Chemical Society: 1375–1397.

Brunner J, Ragupathy S and Borchard G (2021) Target specific tight junction modulators. *Advanced Drug Delivery Reviews* 171: 266–288.

Bruschi ML (ed.) (2015) 5 - Mathematical models of drug release. In: *Strategies to Modify the Drug Release from Pharmaceutical Systems*. Woodhead Publishing, pp. 63–86. Available at: https://www.sciencedirect.com/science/article/pii/B9780081000922000059 (accessed 4 June 2022).

Cabra V, Vázquez-Contreras E, Moreno A, et al. (2008) The effect of sulfhydryl groups and disulphide linkage in the thermal aggregation of Z19 alpha-zein. *Biochimica Et Biophysica Acta* 1784(7–8): 1028–1036.

Campbell HK, Maiers JL and DeMali KA (2017) Interplay between tight junctions & adherens junctions. *Experimental Cell Research* 358(1): 39–44.

Cao X, Bansil R, Bhaskar KR, et al. (1999) pH-Dependent Conformational Change of Gastric Mucin Leads to Sol-Gel Transition. *Biophysical Journal* 76(3): 1250–1258.

Carvalho FC, Bruschi ML, Evangelista RC, et al. (2010) Mucoadhesive drug delivery systems. *Brazilian Journal of Pharmaceutical Sciences* 46(1): 1–17.

Casettari L, Vllasaliu D, Castagnino E, et al. (2012) PEGylated chitosan derivatives: Synthesis, characterizations and pharmaceutical applications. *Progress in Polymer Science* 37(5). Topical Issue on Biorelated polymers: 659–685.

Cesari A, Fabiano A, Piras AM, et al. (2020) Binding and mucoadhesion of sulfurated derivatives of quaternary ammonium-chitosans and their nanoaggregates: An NMR investigation. *Journal of Pharmaceutical and Biomedical Analysis* 177: 112852.

Chatterjee M, van Putten JPM and Strijbis K (2020) Defensive Properties of Mucin Glycoproteins during Respiratory Infections—Relevance for SARS-CoV-2. *mBio* 11(6). American Society for Microbiology: e02374-20.

Chaturvedi M, Kumar M and Pathak K (2011) A review on mucoadhesive polymer used in nasal drug delivery system. *Journal of Advanced Pharmaceutical Technology & Research* 2(4): 215.

Chen C-H, Lin Y-S, Wu S-J, et al. (2018) Mutlifunctional nanoparticles prepared from arginine-modified chitosan and thiolated fucoidan for oral delivery of hydrophobic and hydrophilic drugs. *Carbohydrate Polymers* 193: 163–172.

Chen X, Zhou L, Xu H, et al. (2019) The structure and properties of natural sheep casing and artificial films prepared from natural collagen with various crosslinking treatments. *International Journal of Biological Macromolecules* 135: 959–968.

Cheng J, Amin D, Latona J, et al. (2019) Supramolecular Polymer Hydrogels for Drug-Induced Tissue Regeneration. *ACS Nano* 13(5). American Chemical Society: 5493–5501.

Chettri D, Boro M, Sarkar L, et al. (2021) Lectins: Biological significance to biotechnological application. *Carbohydrate Research* 506: 108367.

Cheung RCF, Ng TB, Wong JH, et al. (2015) Chitosan: An Update on Potential Biomedical and Pharmaceutical Applications. *Marine Drugs* 13(8): 5156–5186.

Chou S-F, Carson D and Woodrow KA (2015) Current strategies for sustaining drug release from electrospun nanofibres. *Journal of Controlled Release: Official Journal of the Controlled Release Society* 220(Pt B): 584–591.

Chowdary KPR and Rao YS (2004) Mucoadhesive Microspheres for Controlled Drug Delivery. *Biological and Pharmaceutical Bulletin* 27(11): 1717–1724.

Cicinelli E, de Ziegler D, Bulletti C, et al. (2000) Direct transport of progesterone from vagina to uterus. *Obstetrics and Gynecology* 95(3): 403–406.

Clitherow KH, Murdoch C, Spain SG, et al. (2019) Mucoadhesive Electrospun Patch Delivery of Lidocaine to the Oral Mucosa and Investigation of Spatial Distribution in a Tissue Using MALDI-Mass Spectrometry Imaging. *Molecular Pharmaceutics* 16(9): 3948–3956.

Colley HE, Said Z, Santocildes-Romero ME, et al. (2018) Pre-clinical evaluation of novel mucoadhesive bilayer patches for local delivery of clobetasol-17-propionate to the oral mucosa. *Biomaterials* 178: 134–146.

Cook SL, Woods S, Methven L, et al. (2018) Mucoadhesive polysaccharides modulate sodium retention, release and taste perception. *Food Chemistry* 240: 482–489.

Corradini E, Curti PS, Meniqueti AB, et al. (2014) Recent advances in food-packing, pharmaceutical and biomedical applications of zein and zein-based materials. *International Journal of Molecular Sciences* 15(12): 22438–22470.

Costa P and Sousa Lobo JM (2001) Modeling and comparison of dissolution profiles. *European Journal of Pharmaceutical Sciences* 13(2): 123–133.

Couvreur P and Vauthier C (1991) Polyalkylcyanoacrylate nanoparticles as drug carrier: present state and perspectives. *Journal of Controlled Release* 17(2): 187–198.

Couvreur P, Kante B, Roland M, et al. (1979) Polycyanoacrylate nanocapsules as potential lysosomotropic carriers: preparation, morphological and sorptive properties. *The Journal of Pharmacy and Pharmacology* 31(5): 331–332.

Curnutt A, Smith K, Darrow E, et al. (2020) Chemical and Microstructural Characterization of pH and [Ca2+] Dependent Sol-Gel Transitions in Mucin Biopolymer. *Scientific Reports* 10(1). 1. Nature Publishing Group: 8760.

Czerkinsky C and Holmgren J (2012) Mucosal Delivery Routes for Optimal Immunization: Targeting Immunity to the Right Tissues. In: Kozlowski PA (ed.) *Mucosal Vaccines: Modern Concepts, Strategies, and Challenges*. Current Topics in Microbiology and Immunology. Berlin, Heidelberg: Springer, pp. 1–18. Available at: https://doi.org/10.1007/82_2010_112 (accessed 23 April 2022).

d'Amone L, Sahoo JK, Ostrovsky-Snider N, et al. (2023) Boronic Acid-Tethered Silk Fibroin for pH-Dependent Mucoadhesion. *Biomacromolecules*. American Chemical Society. Epub ahead of print 10 February 2023. DOI: 10.1021/acs.biomac.2c01349.

da Silva JB, dos Santos RS, da Silva MB, et al. (2021) Interaction between mucoadhesive cellulose derivatives and Pluronic F127: Investigation on the micelle structure and mucoadhesive performance. *Materials Science and Engineering: C* 119: 111643.

Das S, Bhattacharya K, Blaker JJ, et al. (2023) Beyond traditional therapy: Mucoadhesive polymers as a new frontier in oral cancer management. *Biopolymers* 114(9). John Wiley & Sons, Ltd: e23556.

Davidovich-Pinhas M and Bianco-Peled H (2010) Novel mucoadhesive system based on sulfhydryl-acrylate interactions. *Journal of Materials Science. Materials in Medicine* 21(7): 2027–2034.

De Ziegler D, Bulletti C, De Monstier B, et al. (1997) The first uterine pass effect. *Annals of the New York Academy of Sciences* 828: 291–299.

Deitzel JM, Kleinmeyer JD, Hirvonen JK, et al. (2001) Controlled deposition of electrospun poly(ethylene oxide) fibres. *Polymer* 42(19): 8163–8170.

Demir M, Ramos-Rivera L, Silva R, et al. (2017) Zein-based composites in biomedical applications. *Journal of Biomedical Materials Research Part A* 105(6): 1656–1665.

Deng L, Zhang X, Li Y, et al. (2018) Characterization of gelatin/zein nanofibres by hybrid electrospinning. *Food Hydrocolloids* 75: 72–80.

Deng L, Li X, Miao K, et al. (2020) Development of Disulfide Bond Crosslinked Gelatin/ε-Polylysine Active Edible Film with Antibacterial and Antioxidant Activities. *Food and Bioprocess Technology* 13(4): 577–588.

Dias Antunes M, da Silva Dannenberg G, Fiorentini ÂM, et al. (2017) Antimicrobial electrospun ultrafine fibres from zein containing eucalyptus essential oil/cyclodextrin inclusion complex. *International Journal of Biological Macromolecules* 104: 874–882.

Diaz-Salmeron R, Toussaint B, Huang N, et al. (2021) Mucoadhesive Poloxamer-Based Hydrogels for the Release of HP-β-CD-Complexed Dexamethasone in the Treatment of Buccal Diseases. *Pharmaceutics* 13(1). 1. Multidisciplinary Digital Publishing Institute: 117.

Dicharry RM, Ye P, Saha G, et al. (2006) Wheat Gluten−Thiolated Poly(vinyl alcohol) Blends with Improved Mechanical Properties. *Biomacromolecules* 7(10). American Chemical Society: 2837–2844.

Drees F, Pokutta S, Yamada S, et al. (2005) α-Catenin Is a Molecular Switch that Binds E-Cadherin-β-Catenin and Regulates Actin-Filament Assembly. *Cell* 123(5): 903–915.

Drummy LF, Phillips DM, Stone MO, et al. (2005) Thermally induced alpha-helix to beta-sheet transition in regenerated silk fibres and films. *Biomacromolecules* 6(6): 3328–3333.

Duggan S, Cummins W, O' Donovan O, et al. (2017) Thiolated polymers as mucoadhesive drug delivery systems. *European Journal of Pharmaceutical Sciences* 100: 64–78.

Edmans JG, Murdoch C, Santocildes-Romero ME, et al. (2020) Incorporation of lysozyme into a mucoadhesive electrospun patch for rapid protein delivery to the oral mucosa. *Materials Science and Engineering: C* 112: 110917.

El Sharawy AM, Shukr MH and Elshafeey AH (2017) Formulation and optimization of duloxetine hydrochloride buccal films: in vitro and in vivo evaluation. *Drug Delivery* 24(1): 1762–1769.

El-Batal AI, El-Sayyad GS, Al-Hazmi NE, et al. (2019) Antibiofilm and Antimicrobial Activities of Silver Boron Nanoparticles Synthesized by PVP Polymer and Gamma Rays Against Urinary Tract Pathogens. *Journal of Cluster Science* 30(4): 947–964.

El-Leithy Eman S., Shaker DS, Ghorab MK, et al. (2010) Evaluation of Mucoadhesive Hydrogels Loaded with Diclofenac Sodium–Chitosan Microspheres for Rectal Administration. *AAPS PharmSciTech* 11(4): 1695–1702.

El-Leithy E. S., Shaker DS, Ghorab MK, et al. (2010) Optimization and characterization of diclofenac sodium microspheres prepared by a modified coacervation method. *Drug Discoveries & Therapeutics* 4(3): 208–216.

Eraga SO, Ofeogbu PU, Ovu EO, et al. (2016) An investigation of the properties of mucin obtained from three sources. *The Pharma Innovation Journal* 5(12). AkiNik Publications: 08–12.

Erickson DP, Ozturk OK, Selling G, et al. (2020) Corn zein undergoes conformational changes to higher β-sheet content during its self-assembly in an increasingly hydrophilic solvent. *International Journal of Biological Macromolecules* 157: 232–239.

Eshel-Green T and Bianco-Peled H (2016) Mucoadhesive acrylated block copolymers micelles for the delivery of hydrophobic drugs. *Colloids and Surfaces B: Biointerfaces* 139: 42–51.

Federer C, Kurpiers M and Bernkop-Schnürch A (2021) Thiolated Chitosans: A Multi-talented Class of Polymers for Various Applications. *Biomacromolecules* 22(1). American Chemical Society: 24–56.

Federici E, Selling GW, Campanella OH, et al. (2021) Thermal treatment of dry zein to improve rheological properties in gluten-free dough. *Food Hydrocolloids* 115: 106629.

Fonseca-Santos B and Chorilli M (2017) An overview of carboxymethyl derivatives of chitosan: Their use as biomaterials and drug delivery systems. *Materials Science and Engineering: C* 77: 1349–1362.

Futami J, Miyamoto A, Hagimoto A, et al. (2017) Evaluation of irreversible protein thermal inactivation caused by breakage of disulphide bonds using methanethiosulphonate. *Scientific Reports* 7(1): 12471.

Gao Y, Almalki WH, Afzal O, et al. (2021) Systematic development of lectin conjugated microspheres for nose-to-brain delivery of rivastigmine for the treatment of Alzheimer's disease. *Biomedicine & Pharmacotherapy* 141: 111829.

Garcia-Amezquita LE, Welti-Chanes J, Vergara-Balderas FT, et al. (2016) Freeze-drying: The Basic Process. In: Caballero B, Finglas PM, and Toldrá F (eds) *Encyclopedia of Food and Health*. Oxford: Academic Press, pp. 104–109. Available at: https://www.sciencedirect.com/science/article/pii/B9780123849472003287 (accessed 28 April 2022).

Gaudana R, Ananthula HK, Parenky A, et al. (2010) Ocular Drug Delivery. *The AAPS Journal* 12(3): 348–360.

Geraghty D, Peifer MA, Rubenstein I, et al. (1981) The primary structure of a plant storage protein: zein. *Nucleic Acids Research* 9(19): 5163–5174.

Ghosh S (2020) Sialic acid and biology of life: An introduction. *Sialic Acids and Sialoglycoconjugates in the Biology of Life, Health and Disease*: 1–61.

Giepmans BNG and van IJzendoorn SCD (2009) Epithelial cell–cell junctions and plasma membrane domains. *Biochimica et Biophysica Acta (BBA) - Biomembranes* 1788(4). Apical Junctional Complexes Part II: 820–831.

Gonçalves J, Torres N, Silva S, et al. (2020) Zein impart hydrophobic and antimicrobial properties to cotton textiles. *Reactive and Functional Polymers* 154: 104664.

Gorantla S, Krishna Rapalli V, Waghule T, et al. (2020) Nanocarriers for ocular drug delivery: current status and translational opportunity. *RSC Advances* 10(46). Royal Society of Chemistry: 27835–27855.

Grant JJ, Pillai SC, Perova TS, et al. (2021) Electrospun Fibres of Chitosan/PVP for the Effective Chemotherapeutic Drug Delivery of 5-Fluorouracil. *Chemosensors* 9(4). 4. Multidisciplinary Digital Publishing Institute: 70.

Groeger S and Meyle J (2019) Oral Mucosal Epithelial Cells. *Frontiers in Immunology* 10.

Grządka E (2012) The Adsorption Layer in the System: Carboxymethylcellulose/Surfactants/NaCl/MnO2. *Journal of Surfactants and Detergents* 15(4): 513–521.

Gu JM, Robinson JR and Leung SH (1988) Binding of acrylic polymers to mucin/epithelial surfaces: structure-property relationships. *Critical Reviews in Therapeutic Drug Carrier Systems* 5(1): 21–67.

Gumina ME and Yan AC (2019) Atenolol as an alternative to propranolol for the management of sleep disturbances in the treatment of infantile hemangiomas. *Pediatric Dermatology* 36(4): 556–557.

Gupta B, Anjum S and Ikram S (2013) Preparation of thiolated polyvinyl alcohol hydrogels. *Journal of Applied Polymer Science* 129(2): 815–821.

Hägerström H (2003) Polymer Gels as Pharmaceutical Dosage Forms : Rheological Performance and Physicochemical Interactions at the Gel-Mucus Interface for Formulations Intended for Mucosal Drug Delivery. Acta Universitatis Upsaliensis. Epub ahead of print 2003.

Hajighasemi F and Mirshafiey A (2009) In Vitro Sensitivity of Leukemia Cells to Propranolol. *Journal of Clinical Medicine Research* 1(3): 144–149.

Han X, Zhang E, Shi Y, et al. (2019) Biomaterial–tight junction interaction and potential impacts. *Journal of Materials Chemistry B* 7(41). Royal Society of Chemistry: 6310–6320.

Hanafy NAN, Leporatti S and El-Kemary MA (2019) Mucoadhesive Hydrogel Nanoparticles as Smart Biomedical Drug Delivery System. *Applied Sciences* 9(5). 5. Multidisciplinary Digital Publishing Institute: 825.

Hanisch FG and Müller S (2000) MUC1: the polymorphic appearance of a human mucin. *Glycobiology* 10(5): 439–449.

Hartsock A and Nelson WJ (2008) Adherens and tight junctions: Structure, function and connections to the actin cytoskeleton. *Biochimica et Biophysica Acta (BBA) - Biomembranes* 1778(3): 660–669.

Hasegawa T, Mizugaki A, Inoue Y, et al. (2021) Cystine reduces tight junction permeability and intestinal inflammation induced by oxidative stress in Caco-2 cells. *Amino Acids* 53(7): 1021–1032.

Hearnden V, Sankar V, Hull K, et al. (2012) New developments and opportunities in oral mucosal drug delivery for local and systemic disease. *Advanced Drug Delivery Reviews* 64(1): 16–28.

Horvát G, Gyarmati B, Berkó S, et al. (2015) Thiolated poly(aspartic acid) as potential in situ gelling, ocular mucoadhesive drug delivery system. *European Journal of Pharmaceutical Sciences* 67: 1–11.

Hu X, Liu S, Zhou G, et al. (2014) Electrospinning of polymeric nanofibres for drug delivery applications. *Journal of Controlled Release* 185: 12–21.

Hua S (2019) Advances in Nanoparticulate Drug Delivery Approaches for Sublingual and Buccal Administration. *Frontiers in Pharmacology* 10.

Huang S-W, Lin Y-F, Li Y-X, et al. (2019) Synthesis of Fluorescent Carbon Dots as Selective and Sensitive Probes for Cupric Ions and Cell Imaging. *Molecules* 24(9): 1785.

Illum L (2002) Nasal drug delivery: new developments and strategies. *Drug Discovery Today* 7(23): 1184–1189.

Illum L (2003) Nasal drug delivery—possibilities, problems and solutions. *Journal of Controlled Release* 87(1). Proceeding of the Seventh European Symposium on Controlled Drug Delivery: 187–198.

Ingole SA and Kumbharkhane A (2021) Temperature dependent Broadband dielectric relaxation study of Aqueous Polyvinylpyrrolidone (PVP K-15, K-30 & K-90) using a TDR. *Physics and Chemistry of Liquids* 59(5). Taylor & Francis: 806–816.

Jabbal-Gill I, Watts P and Smith A (2012) Chitosan-based delivery systems for mucosal vaccines. *Expert Opinion on Drug Delivery* 9(9): 1051–1067.

Javadzadeh Y, Musaalrezaei L and Nokhodchi A (2008) Liquisolid technique as a new approach to sustain propranolol hydrochloride release from tablet matrices. *International Journal of Pharmaceutics* 362(1–2): 102–108.

Jayeoye TJ, Olatunde OO, Benjakul S, et al. (2020) Synthesis and characterization of novel poly(3-aminophenyl boronic acid-co-vinyl alcohol) nanocomposite polymer stabilized silver nanoparticles with antibacterial and antioxidant applications. *Colloids and Surfaces B: Biointerfaces* 193: 111112.

Jayeoye TJ, Nwabor OF and Rujiralai T (2020) Synthesis of highly stable and dispersed silver nanoparticles/poly(vinyl alcohol-co-ethylene glycol)/poly(3-aminophenyl boronic acid) nanocomposite: Characterization and antibacterial, hemolytic and cytotoxicity studies. *Journal of Industrial and Engineering Chemistry* 89: 288–300.

Jelkmann M, Leichner C, Zaichik S, et al. (2020) A gellan gum derivative as in-situ gelling cationic polymer for nasal drug delivery. *International Journal of Biological Macromolecules* 158: 1037–1046.

Ji Y, Song W, Xu L, et al. (2022) A Review on Electrospun Poly(amino acid) Nanofibres and Their Applications of Hemostasis and Wound Healing. *Biomolecules* 12(6). 6. Multidisciplinary Digital Publishing Institute: 794.

Jiang H, Zhang M and Adhikari B (2013) 21 - Fruit and vegetable powders. In: Bhandari B, Bansal N, Zhang Min, et al. (eds) *Handbook of Food Powders*. Woodhead Publishing Series in Food Science, Technology and Nutrition. Woodhead Publishing, pp. 532–552. Available at: https://www.sciencedirect.com/science/article/pii/B9780857095138500212 (accessed 28 April 2022).

Jiang Q, Reddy N and Yang Y (2010) Cytocompatible cross-linking of electrospun zein fibres for the development of water-stable tissue engineering scaffolds. *Acta Biomaterialia* 6(10): 4042–4051.

Jiménez-castellanos MR, Zia H and Rhodes CT (1993) Mucoadhesive Drug Delivery Systems. *Drug Development and Industrial Pharmacy* 19(1–2). Taylor & Francis: 143–194.

Jin P, Jan LY and Jan Y-N (2020) Mechanosensitive Ion Channels: Structural Features Relevant to Mechanotransduction Mechanisms. *Annual review of neuroscience* 43(1): 207–229.

Johnson KT, Fath KR, Henricus MM, et al. (2009) Self-Assembly and Growth of Smart Cell-Adhesive Mucin-Bound Microtubes. *Soft Materials* 7(1). Taylor & Francis: 21–36.

Kafedjiiski K, Jetti RKR, Föger F, et al. (2007) Synthesis and in vitro evaluation of thiolated hyaluronic acid for mucoadhesive drug delivery. *International Journal of Pharmaceutics* 343(1): 48–58.

Karavas E, Georgarakis E and Bikiaris D (2006) Application of PVP/HPMC miscible blends with enhanced mucoadhesive properties for adjusting drug release in predictable pulsatile chronotherapeutics. *European Journal of Pharmaceutics and Biopharmaceutics* 64(1): 115–126.

Kariduraganavar MY, Heggannavar GB, Amado S, et al. (2019) Chapter 6 - Protein Nanocarriers for Targeted Drug Delivery for Cancer Therapy. In: Mohapatra SS, Ranjan S, Dasgupta N, et al. (eds) *Nanocarriers for Drug Delivery*. Micro and Nano Technologies. Elsevier, pp. 173–204. Available at: http://www.sciencedirect.com/science/article/pii/B9780128140338000060 (accessed 18 May 2020).

Kast CE and Bernkop-Schnürch A (2001) Thiolated polymers — thiomers: development and in vitro evaluation of chitosan–thioglycolic acid conjugates. *Biomaterials* 22(17): 2345–2352.

Kelly SM, Jess TJ and Price NC (2005) How to study proteins by circular dichroism. *Biochimica et Biophysica Acta (BBA) - Proteins and Proteomics* 1751(2): 119–139.

Khan S, Patil K, Bobade N, et al. (2010) Formulation of intranasal mucoadhesive temperature-mediated in situ gel containing ropinirole and evaluation of brain targeting efficiency in rats. *Journal of Drug Targeting* 18(3): 223–234.

Khutoryanskiy VV (2011) Advances in Mucoadhesion and Mucoadhesive Polymers. *Macromolecular Bioscience* 11(6): 748–764.

Kianfar P, Vitale A, Dalle Vacche S, et al. (2019) Photo-crosslinking of chitosan/poly(ethylene oxide) electrospun nanofibres. *Carbohydrate Polymers* 217: 144–151.

Kim D, Kim YH and Kwon S (2018) Enhanced nasal drug delivery efficiency by increasing mechanical loading using hypergravity. *Scientific Reports* 8: 168.

Kim J and De Jesus O (2022) Medication Routes of Administration. In: *StatPearls*. Treasure Island (FL): StatPearls Publishing. Available at: http://www.ncbi.nlm.nih.gov/books/NBK568677/ (accessed 21 April 2022).

Koczkur KM, Mourdikoudis S, Polavarapu L, et al. (2015) Polyvinylpyrrolidone (PVP) in nanoparticle synthesis. *Dalton Transactions* 44(41). The Royal Society of Chemistry: 17883–17905.

Kofuji K, Qian C-J, Nishimura M, et al. (2005) Relationship between physicochemical characteristics and functional properties of chitosan. *European Polymer Journal* 41(11): 2784–2791.

Kolawole OM, Lau WM and Khutoryanskiy VV (2019) Synthesis and Evaluation of Boronated Chitosan as a Mucoadhesive Polymer for Intravesical Drug Delivery. *Journal of Pharmaceutical Sciences* 108(9): 3046–3053.

Kolawole OM, Ifeanafor AR, Ifade WA, et al. (2023) Formulation and evaluation of paclitaxel-loaded boronated chitosan/alginate nanoparticles as a mucoadhesive system for localized cervical cancer drug delivery. *Journal of Drug Delivery Science and Technology* 87: 104810.

Koombhongse S, Liu W and Reneker DH (2001) Flat polymer ribbons and other shapes by electrospinning. *Journal of Polymer Science Part B: Polymer Physics* 39(21): 2598–2606.

Kreft ME, Jerman UD, Lasič E, et al. (2015) The characterization of the human nasal epithelial cell line RPMI 2650 under different culture conditions and their optimization for an appropriate in vitro nasal model. *Pharmaceutical Research* 32(2): 665–679.

Krogstad EA, Ramanathan R, Nhan C, et al. (2017) Nanoparticle-releasing nanofibre composites for enhanced in vivo vaginal retention. *Biomaterials* 144: 1–16.

Kulkarni AD, Patel HM, Surana SJ, et al. (2017) N,N,N-Trimethyl chitosan: An advanced polymer with myriad of opportunities in nanomedicine. *Carbohydrate Polymers* 157: 875–902.

Kulkarni R, Fanse S and Burgess DJ (2023a) Mucoadhesive drug delivery systems: a promising non-invasive approach to bioavailability enhancement. Part I: biophysical considerations. *Expert Opinion on Drug Delivery* 20(3). Taylor & Francis: 395–412.

Kulkarni R, Fanse S and Burgess DJ (2023b) Mucoadhesive drug delivery systems: a promising noninvasive approach to bioavailability enhancement. Part II: formulation considerations. *Expert Opinion on Drug Delivery* 20(3). Taylor & Francis: 413–434.

Kulkarni U, Mahalingam R, Pather SI, et al. (2009) Porcine Buccal Mucosa as an In Vitro Model: Relative Contribution of Epithelium and Connective Tissue as Permeability Barriers. *Journal of Pharmaceutical Sciences* 98(2): 471–483.

Kumar P, Nagarajan A and Uchil PD (2018) Analysis of Cell Viability by the MTT Assay. *Cold Spring Harbor Protocols* 2018(6).

Kurakula M and Rao GSNK (2020) Pharmaceutical assessment of polyvinylpyrrolidone (PVP): As excipient from conventional to controlled delivery systems with a spotlight on COVID-19 inhibition. *Journal of Drug Delivery Science and Technology* 60: 102046.

Kurniawan A, Gunawan F, Nugraha AT, et al. (2017) Biocompatibility and drug release behavior of curcumin conjugated gold nanoparticles from aminosilane-functionalized electrospun poly(N-vinyl-2-pyrrolidone) fibres. *International Journal of Pharmaceutics* 516(1–2): 158–169.

Kürti L, Veszelka S, Bocsik A, et al. (2012) Retinoic acid and hydrocortisone strengthen the barrier function of human RPMI 2650 cells, a model for nasal epithelial permeability. *Cytotechnology* 65.

Kydd WL and Daly CH (1982) The biologic and mechanical effects of stress on oral mucosa. *The Journal of Prosthetic Dentistry* 47(3): 317–329.

Laffleur F (2018) Nasal adhesive patches - Approach for topical application for dry nasal syndrome. *International Journal of Biological Macromolecules* 111: 493–497.

Laksitorini M, Prasasty VD, Kiptoo PK, et al. (2014) Pathways and Progress in Improving Drug Delivery through the Intestinal Mucosa and Blood-Brain Barriers. *Therapeutic delivery* 5(10): 1143–1163.

Lal M (2020) Freeze-dried tablets for oral vaccine delivery: Ease of administration and potential for production in existing facilities. *Vaccine* 38(26): 4142–4145.

Lam HT, Zupančič O, Laffleur F, et al. (2021) Mucoadhesive properties of polyacrylates: Structure – Function relationship. *International Journal of Adhesion and Adhesives* 107: 102857.

Lan D, Liu Z, Zhou J, et al. (2022) Preparation and characterization of silk fibroin/polyethylene oxide nanofibre membranes with antibacterial activity. *Journal of Biomedical Materials Research Part A* 110(2): 287–297.

Laracuente M-L, Yu MH and McHugh KJ (2020) Zero-order drug delivery: State of the art and future prospects. *Journal of Controlled Release* 327: 834–856.

Lee J, Lee H and Andrade J (1995) Blood compatibility of polyethylene oxide surfaces. *Progress in Polymer Science* 20(6): 1043–1079.

Lee M, Park CG, Huh BK, et al. (2017) Sinonasal Delivery of Resveratrol via Mucoadhesive Nanostructured Microparticles in a Nasal Polyp Mouse Model. *Scientific Reports* 7(1). 1. Nature Publishing Group: 40249.

Lehr CM (2000) Lectin-mediated drug delivery: the second generation of bioadhesives. *Journal of Controlled Release: Official Journal of the Controlled Release Society* 65(1–2): 19–29.

Leichner C, Wulz P, Baus RA, et al. (2019) N-Hydroxysulfosuccinimide Esters versus Thiomers: A Comparative Study Regarding Mucoadhesiveness. *Molecular Pharmaceutics* 16(3). American Chemical Society: 1211–1219.

Leonard TE, Liko AF, Gustiananda M, et al. (2023) Thiolated pectin-chitosan composites: Potential mucoadhesive drug delivery system with selective cytotoxicity towards colorectal cancer. *International Journal of Biological Macromolecules* 225: 1–12.

Li A, Xu Z, Sun N, et al. (2019) Cellulose-reinforced catechol-modified polyacrylic acid-Zn2+ coacervate as strong composite adhesive. *Journal of Applied Polymer Science* 136(9): 47126.

Li J, Feng H, He J, et al. (2013) Coaxial electrospun zein nanofibrous membrane for sustained release. *Journal of Biomaterials Science, Polymer Edition* 24(17). Taylor & Francis: 1923–1934.

Li J, Pan H, Ye Q, et al. (2020) Carvedilol-loaded polyvinylpyrrolidone electrospun nanofibre film for sublingual delivery. *Journal of Drug Delivery Science and Technology* 58: 101726.

Lian H and Meng Z (2017) Melt electrospinning of daunorubicin hydrochloride-loaded poly (ε-caprolactone) fibrous membrane for tumor therapy. *Bioactive Materials* 2(2): 96–100.

Liang D, Hsiao BS and Chu B (2007) Functional electrospun nanofibrous scaffolds for biomedical applications. *Advanced Drug Delivery Reviews* 59(14): 1392–1412.

Liu K, Liu P, Liu R, et al. (2015) Dual AO/EB Staining to Detect Apoptosis in Osteosarcoma Cells Compared with Flow Cytometry. *Medical Science Monitor Basic Research* 21: 15–20.

Liu P, Xu H, Mi X, et al. (2015) Oxidized Sucrose: A Potent and Biocompatible Crosslinker for Three-Dimensional Fibrous Protein Scaffolds. *Macromolecular Materials and Engineering* 300(4): 414–422.

Liu S, Chang CN, Verma MS, et al. (2015) Phenylboronic acid modified mucoadhesive nanoparticle drug carriers facilitate weekly treatment of experimentallyinduced dry eye syndrome. *Nano Research* 8(2): 621–635.

Liu Y, Huang R, Han L, et al. (2009) Brain-targeting gene delivery and cellular internalization mechanisms for modified rabies virus glycoprotein RVG29 nanoparticles. *Biomaterials* 30(25): 4195–4202.

Liu Yangdan, Wang X, Liu Youping, et al. (2018) Thermosensitive In Situ Gel Based on Solid Dispersion for Rectal Delivery of Ibuprofen. *AAPS PharmSciTech* 19(1): 338–347.

Lu R-Y, Yang W-X and Hu Y-J (2014) The role of epithelial tight junctions involved in pathogen infections. *Molecular Biology Reports* 41(10): 6591–6610.

Ludwig A (2005) The use of mucoadhesive polymers in ocular drug delivery. *Advanced Drug Delivery Reviews* 57(11). Mucoadhesive Polymers: Strategies, Achievements and Future Challenges: 1595–1639.

Luís Â, Domingues F and Ramos A (2019) Production of Hydrophobic Zein-Based Films Bioinspired by The Lotus Leaf Surface: Characterization and Bioactive Properties. *Microorganisms* 7(8): 267.

Maciejewska BM, Wychowaniec JK, Woźniak-Budych M, et al. (2019) UV cross-linked polyvinylpyrrolidone electrospun fibres as antibacterial surfaces. *Science and Technology of Advanced Materials* 20(1). Taylor & Francis: 979–991.

Maher S, Brayden DJ, Casettari L, et al. (2019) Application of Permeation Enhancers in Oral Delivery of Macromolecules: An Update. *Pharmaceutics* 11(1).

Majzoob S, Atyabi F, Dorkoosh F, et al. (2006) Pectin-cysteine conjugate: synthesis and in-vitro evaluation of its potential for drug delivery. *The Journal of Pharmacy and Pharmacology* 58(12): 1601–1610.

Makhlof A, Fujimoto S, Tozuka Y, et al. (2011) In vitro and in vivo evaluation of WGA–carbopol modified liposomes as carriers for oral peptide delivery. *European Journal of Pharmaceutics and Biopharmaceutics* 77(2): 216–224.

Manju S, Muraleedharan CV, Rajeev A, et al. (2011) Evaluation of alginate dialdehyde cross-linked gelatin hydrogel as a biodegradable sealant for polyester vascular graft. *Journal of Biomedical Materials Research Part B: Applied Biomaterials* 98B(1): 139–149.

Mann G, Gurave PM, Kaul A, et al. (2022) Polymeric and electrospun patches for drug delivery through buccal route: Formulation and biointerface evaluation. *Journal of Drug Delivery Science and Technology* 68: 103030.

María Pineda-Reyes A, Delgado MH, Luz Zambrano-Zaragoza M de la, et al. (2021) Implementation of the emulsification-diffusion method by solvent displacement for polystyrene nanoparticles prepared from recycled material. *RSC Advances* 11(4). Royal Society of Chemistry: 2226–2234.

Marsh N and Marsh A (2000) A short history of nitroglycerine and nitric oxide in pharmacology and physiology. *Clinical and Experimental Pharmacology & Physiology* 27(4): 313–319.

Masserini M (2013) Nanoparticles for Brain Drug Delivery. *ISRN Biochemistry* 2013. Hindawi: e238428.

Mathiowitz E, III DEC and Lehr C-M (eds) (1999) *Bioadhesive Drug Delivery Systems: Fundamentals, Novel Approaches, and Development*. Boca Raton: CRC Press.

Matsumoto M, Udomsinprasert W, Laengee P, et al. (2016) A Water-Based Chitosan-Maleimide Precursor for Bioconjugation: An Example of a Rapid Pathway for an In Situ Injectable Adhesive Gel. *Macromolecular Rapid Communications* 37(19): 1618–1622.

McBain JW and Hopkins DG (1925) On Adhesives and Adhesive Action. *The Journal of Physical Chemistry* 29(2). American Chemical Society: 188–204.

Medha S, Resmi R, Rekha MR, et al. (2023) An Investigation into the Efficacy of Low Temperature and UV Irradiated Citric Acid Crosslinked Zein/PEO Electrospun Membranes for Wound Healing Using Human Dermal Fibroblast Cells. *ChemistrySelect* 8(34): e202204493.

Mfoafo K, Mittal R, Eshraghi A, et al. (2023) Thiolated polymers: An overview of mucoadhesive properties and their potential in drug delivery via mucosal tissues. *Journal of Drug Delivery Science and Technology* 85: 104596.

Milligan JJ and Saha S (2022) A Nanoparticle's Journey to the Tumor: Strategies to Overcome First-Pass Metabolism and Their Limitations. *Cancers* 14(7). 7. Multidisciplinary Digital Publishing Institute: 1741.

Miri MA, Movaffagh J, Najafi MBH, et al. (2016) Optimization of elecrospinning process of zein using central composite design. *Fibres and Polymers* 17(5): 769–777.

Mittal D, Ali A, Md S, et al. (2014) Insights into direct nose to brain delivery: current status and future perspective. *Drug Delivery* 21(2). Taylor & Francis: 75–86.

Miyoshi T, Toyohara K and Minematsu H (2005) Preparation of ultrafine fibrous zein membranes via electrospinning. *Polymer International* 54(8): 1187–1190.

Mortazavi SA and Moghimi HR (2010) Effect of Surfactant Type and Concentration on the Duration of Mucoadhesion of Carbopol 934 and HPMC Solid Compacts. *Iranian Journal of Pharmaceutical Research* 0(Number 4). School of Pharmacy, Shahid Beheshti University of Medical Sciences: 191–199.

Muller V, Piai J, Fajardo A, et al. (2011) Preparation and Characterization of Zein and Zein-Chitosan Microspheres with Great Prospective of Application in Controlled Drug Release. *Journal of Nanomaterials* 2011: 10.

Mythri G, Kavitha K, Kumar MR, et al. (2011) Novel mucoadhesive polymers- A review. *Journal of Applied Pharmaceutical Science* 1: 37–42.

Nair AB, Shah J, Jacob S, et al. (2021) Development of Mucoadhesive Buccal Film for Rizatriptan: In Vitro and In Vivo Evaluation. *Pharmaceutics* 13(5). 5. Multidisciplinary Digital Publishing Institute: 728.

Nair B (1998) Final Report On the Safety Assessment of Polyvinylpyrrolidone (PVP). *International Journal of Toxicology* 17(4_suppl). SAGE Publications Inc: 95–130.

Nangare S, Jadhav N, Ghagare P, et al. (2020) Pharmaceutical applications of electrospinning. *Annales Pharmaceutiques Françaises* 78(1): 1–11.

Nazar H, Fatouros DG, van der Merwe SM, et al. (2011) Thermosensitive hydrogels for nasal drug delivery: the formulation and characterisation of systems based on N-

trimethyl chitosan chloride. *European Journal of Pharmaceutics and Biopharmaceutics: Official Journal of Arbeitsgemeinschaft Fur Pharmazeutische Verfahrenstechnik e.V* 77(2): 225–232.

Novilla MN (2018) Ionophores. In: *Veterinary Toxicology*. Elsevier, pp. 1073–1092. Available at: https://linkinghub.elsevier.com/retrieve/pii/B9780128114100000787 (accessed 20 June 2022).

Ochoa Machiste E, Segale L, Conti S, et al. (2005) Effect of UV light exposure on hydrophilic polymers used as drug release modulators in solid dosage forms. *Journal of Drug Delivery Science and Technology* 15(2): 151–157.

Olejnik A, Kapuscinska A, Schroeder G, et al. (2017) Physico-chemical characterization of formulations containing endomorphin-2 derivatives. *Amino Acids* 49(10): 1719–1731.

Oliveira MF, Suarez D, Rocha JCB, et al. (2015) Electrospun nanofibres of polyCD/PMAA polymers and their potential application as drug delivery system. *Materials Science and Engineering: C* 54: 252–261.

Orkwis JA, Wolf AK, Shahid SM, et al. (2020) Development of a Piezoelectric PVDF-TrFE Fibrous Scaffold to Guide Cell Adhesion, Proliferation, and Alignment. *Macromolecular Bioscience* 20(9): 2000197.

Ottenbrite RM and Javan R (2005) Biological Structures. In: Bassani F, Liedl GL, and Wyder P (eds) *Encyclopedia of Condensed Matter Physics*. Oxford: Elsevier, pp. 99–108. Available at: https://www.sciencedirect.com/science/article/pii/B0123694019006987 (accessed 9 May 2022).

Pai C-L, Boyce MC and Rutledge GC (2011) On the importance of fibre curvature to the elastic moduli of electrospun nonwoven fibre meshes. *Polymer* 52(26): 6126–6133.

Painuly D, Nisha U, Arya S, et al. (2019) Effect on in-vitro release of individual and dual contraceptive drug loading from gelatin electrospun fibres. *Journal of Drug Delivery Science and Technology* 51: 454–463.

Paliwal R and Palakurthi S (2014) Zein in controlled drug delivery and tissue engineering. *Journal of Controlled Release: Official Journal of the Controlled Release Society* 189: 108–122.

Pamlényi K, Kristó K, Jójárt-Laczkovich O, et al. (2021) Formulation and Optimization of Sodium Alginate Polymer Film as a Buccal Mucoadhesive Drug Delivery System Containing Cetirizine Dihydrochloride. *Pharmaceutics* 13(5). 5. Multidisciplinary Digital Publishing Institute: 619.

Paraman I and Lamsal BP (2011) Recovery and Characterization of α-Zein from Corn Fermentation Coproducts. *Journal of Agricultural and Food Chemistry* 59(7). American Chemical Society: 3071–3077.

Paris A-L, Caridade S, Colomb E, et al. (2021) Sublingual protein delivery by a mucoadhesive patch made of natural polymers. *Acta Biomaterialia* 128: 222–235.

Patel VM, Prajapati BG and Patel MM (2007) Formulation, evaluation, and comparison of bilayered and multilayered mucoadhesive buccal devices of propranolol hydrochloride. *AAPS PharmSciTech* 8(1): E147–E154.

Pawlukojć A, Leciejewicz J, Ramirez-Cuesta AJ, et al. (2005) l-Cysteine: Neutron spectroscopy, Raman, IR and ab initio study. *Spectrochimica Acta Part A: Molecular and Biomolecular Spectroscopy* 61(11): 2474–2481.

Peppas NA and Buri PA (1985) Surface, interfacial and molecular aspects of polymer bioadhesion on soft tissues. *Journal of Controlled Release* 2: 257–275.

Pérez-González GL, Villarreal-Gómez LJ, Serrano-Medina A, et al. (2019) Mucoadhesive electrospun nanofibres for drug delivery systems: applications of polymers and the parameters' roles. *International Journal of Nanomedicine* 14. Dove Medical Press: 5271–5285.

Pérez-González GL, Cornejo-Bravo JM, Vera-Graciano R, et al. (2022) Development, characterization, and in vitro evaluation of adhesive fibrous mat for mucosal propranolol delivery. *e-Polymers* 22(1). De Gruyter: 58–68.

Perez-Marcos B, Ford JL, Armstrong DJ, et al. (1996) Influence of pH on the release of propranolol hydrochloride from matrices containing hydroxypropylmethylcellulose K4M and carbopol 974. *Journal of Pharmaceutical Sciences* 85(3): 330–334.

Permanadewi I, Kumoro AC, Wardhani DH, et al. (2019) Modelling of controlled drug release in gastrointestinal tract simulation. *Journal of Physics: Conference Series* 1295(1). IOP Publishing: 012063.

Pham DT, Saelim N and Tiyaboonchai W (2018) Crosslinked fibroin nanoparticles using EDC or PEI for drug delivery: physicochemical properties, crystallinity and structure. *Journal of Materials Science* 53(20): 14087–14103.

Pinto S, Pintado ME and Sarmento B (2020) In vivo, ex vivo and in vitro assessment of buccal permeation of drugs from delivery systems. *Expert Opinion on Drug Delivery* 17(1): 33–48.

Pinzón Martín S, Seeberger PH and Varón Silva D (2019) Mucins and Pathogenic Mucin-Like Molecules Are Immunomodulators During Infection and Targets for Diagnostics and Vaccines. *Frontiers in Chemistry* 7.

Porfiryeva NN, Nasibullin SF, Abdullina SG, et al. (2019) Acrylated Eudragit® E PO as a novel polymeric excipient with enhanced mucoadhesive properties for application in nasal drug delivery. *International Journal of Pharmaceutics* 562: 241–248.

Potthast A, Rosenau T, Kosma P, et al. (2005) On the Nature of Carbonyl Groups in Cellulosic Pulps. *Cellulose* 12(1): 43–50.

Präbst K, Engelhardt H, Ringgeler S, et al. (2017) Basic Colorimetric Proliferation Assays: MTT, WST, and Resazurin. In: Gilbert DF and Friedrich O (eds) *Cell Viability Assays: Methods and Protocols*. Methods in Molecular Biology. New York, NY: Springer, pp. 1–17. Available at: https://doi.org/10.1007/978-1-4939-6960-9_1 (accessed 18 January 2023).

Prezotti FG, Siedle I, Boni FI, et al. (2020) Mucoadhesive films based on gellan gum/pectin blends as potential platform for buccal drug delivery. *Pharmaceutical Development and Technology* 25(2): 159–167.

Prosperi-Porta G, Kedzior S, Muirhead B, et al. (2016) Phenylboronic-Acid-Based Polymeric Micelles for Mucoadhesive Anterior Segment Ocular Drug Delivery. *Biomacromolecules* 17(4). American Chemical Society: 1449–1457.

Puri V, Sharma A, Kumar P, et al. (2020) Thiolation of Biopolymers for Developing Drug Delivery Systems with Enhanced Mechanical and Mucoadhesive Properties: A Review. *Polymers* 12(8). 8. Multidisciplinary Digital Publishing Institute: 1803.

Puri V, Sharma A, Kumar P, et al. (2021) Synthesis and Characterization of Thiolated Gum Ghatti as a Novel Excipient: Development of Compression-Coated Mucoadhesive Tablets of Domperidone. *ACS Omega* 6(24). American Chemical Society: 15844–15854.

Purohit TJ, Hanning SM and Wu Z (2018) Advances in rectal drug delivery systems. *Pharmaceutical Development and Technology* 23(10). Taylor & Francis: 942–952.

Putri AP, Picchioni F, Harjanto S, et al. (2021) Alginate Modification and Lectin-Conjugation Approach to Synthesize the Mucoadhesive Matrix. *Applied Sciences* 11(24). 24. Multidisciplinary Digital Publishing Institute: 11818.

Qin Z and Buehler MJ (2010) Molecular dynamics simulation of the α-helix to β-sheet transition in coiled protein filaments: evidence for a critical filament length scale. *Physical Review Letters* 104(19): 198304.

Qu L, Chen G, Dong S, et al. (2019) Improved mechanical and antimicrobial properties of zein/chitosan films by adding highly dispersed nano-TiO2. *Industrial Crops and Products* 130: 450–458.

Rabiee N, Ahmadi S, Afshari R, et al. (2021) Polymeric Nanoparticles for Nasal Drug Delivery to the Brain: Relevance to Alzheimer's Disease. *Advanced Therapeutics* 4(3): 2000076.

Rajalekshmi R, Kaladevi Shaji A, Joseph R, et al. (2021) Scaffold for liver tissue engineering: Exploring the potential of fibrin incorporated alginate dialdehyde–gelatin hydrogel. *International Journal of Biological Macromolecules* 166: 999–1008.

Ramesh Babu V, Krishna Rao KSV, Sairam M, et al. (2006) pH sensitive interpenetrating network microgels of sodium alginate-acrylic acid for the controlled release of ibuprofen. *Journal of Applied Polymer Science* 99(5): 2671–2678.

Reddy N, Li Y and Yang Y (2009) Alkali-catalyzed low temperature wet crosslinking of plant proteins using carboxylic acids. *Biotechnology Progress* 25(1): 139–146.

Remya KR, Chandran S, Mani S, et al. (2018) Hybrid polycaprolactone/polyethylene oxide scaffolds with tunable fibre surface morphology, improved hydrophilicity and biodegradability for bone tissue engineering applications. *Journal of Biomaterials Science, Polymer Edition* 29(12): 1444–1462.

Reuss L (2012) Water Transport Across Cell Membranes. In: *eLS*. John Wiley & Sons, Ltd. Available at: https://onlinelibrary.wiley.com/doi/abs/10.1002/9780470015902.a0020621.pub2 (accessed 20 June 2022).

Rhim JW, Gennadios A, Fu D, et al. (1999) Properties of Ultraviolet Irradiated Protein Films. *LWT - Food Science and Technology* 32(3): 129–133.

Ritthidej GC (2011) Chapter 3 - Nasal Delivery of Peptides and Proteins with Chitosan and Related Mucoadhesive Polymers. In: Van Der Walle C (ed.) *Peptide and Protein Delivery*. Boston: Academic Press, pp. 47–68. Available at: https://www.sciencedirect.com/science/article/pii/B9780123849359100033 (accessed 26 April 2022).

Robinson JR and Bologna WJ (1994) Vaginal and reproductive system treatments using a bioadhesive polymer. In: Anderson JM, Kim SW, Kopeček J, et al. (eds) *Advances in Drug Delivery Systems, 6*. Elsevier, pp. 87–94. Available at: http://www.sciencedirect.com/science/article/pii/B9780444820273500134 (accessed 25 August 2020).

Rohani Shirvan A, Bashari A and Hemmatinejad N (2019) New insight into the fabrication of smart mucoadhesive buccal patches as a novel controlled-drug delivery system. *European Polymer Journal* 119: 541–550.

Rohani Shirvan A, Hemmatinejad N, Bahrami SH, et al. (2021) Fabrication of multifunctional mucoadhesive buccal patch for drug delivery applications. *Journal of Biomedical Materials Research Part A* 109(12): 2640–2656.

Sadeghi-avalshahr AR, Nokhasteh S, Molavi AM, et al. (2020) Tailored PCL Scaffolds as Skin Substitutes Using Sacrificial PVP Fibres and Collagen/Chitosan Blends. *International Journal of Molecular Sciences* 21(7). 7. Multidisciplinary Digital Publishing Institute: 2311.

Sahatsapan N, Ngawhirunpat T, Rojanarata T, et al. (2020) Catechol-Functionalized Alginate Nanoparticles as Mucoadhesive Carriers for Intravesical Chemotherapy. *AAPS PharmSciTech* 21(6): 212.

Sahoo J, Murthy PN, Biswal S, et al. (2008) Comparative Study of Propranolol hydrochloride Release from Matrix Tablets with Kollidon®SR or Hydroxy Propyl Methyl Cellulose. *AAPS PharmSciTech* 9(2): 577–582.

Sajomsang W, Rungsardthong Ruktanonchai U, Gonil P, et al. (2009) Mucoadhesive property and biocompatibility of methylated N-aryl chitosan derivatives. *Carbohydrate Polymers* 78(4): 945–952.

Samiei M, Ahmadian E, Eftekhari A, et al. (2019) Cell junctions and oral health. *EXCLI Journal* 18: 317–330.

Sarıarslan H, Karaca E, Şahin M, et al. (2020) Electrochemical synthesis and corrosion protection of poly(3-aminophenylboronic acid- co -pyrrole) on mild steel. *RSC Advances* 10(63). Royal Society of Chemistry: 38548–38560.

Sarti F and Bernkop-Schnürch A (2011) Chitosan and Thiolated Chitosan. In: Jayakumar R, Prabaharan M, and Muzzarelli RAA (eds) *Chitosan for Biomaterials I*. Advances in Polymer Science. Berlin, Heidelberg: Springer, pp. 93–110. Available at: https://doi.org/10.1007/12_2011_109 (accessed 27 April 2022).

Sattar M, Sayed OM and Lane ME (2014) Oral transmucosal drug delivery--current status and future prospects. *International Journal of Pharmaceutics* 471(1–2): 498–506.

Sau-Hung Spence Leung and Robinson JR (1987) The contribution of anionic polymer structural features to mucoadhesion. *Journal of Controlled Release* 5(3): 223–231.

Selling GW, Hamaker SAH and Sessa DJ (2007) Effect of Solvent and Temperature on Secondary and Tertiary Structure of Zein by Circular Dichroism. *Cereal Chemistry Journal* 84(3): 265–270.

Selling GW, Biswas A, Patel A, et al. (2007) Impact of Solvent on Electrospinning of Zein and Analysis of Resulting Fibres. *Macromolecular Chemistry and Physics* 208(9): 1002–1010.

Selling GW, Woods KK and Biswas A (2012) Electrospun zein fibres using glyoxal as the crosslinking reagent. *Journal of Applied Polymer Science* 123(5): 2651–2661.

Shaikh R, Raj Singh TR, Garland MJ, Woolfson A David, et al. (2011) Mucoadhesive drug delivery systems. *Journal of Pharmacy and Bioallied Sciences* 3(1): 89–100.

Shaikh R, Raj Singh TR, Garland MJ, Woolfson A. David, et al. (2011) Mucoadhesive drug delivery systems. *Journal of Pharmacy & Bioallied Sciences* 3(1): 89–100.

Shen H, Cheng BL, Lu GW, et al. (2005) Picosecond nonlinear optical responses of Au/PVP composite films. 39(1). IOP Publishing: 233–236.

Shi H, Wang Y, Bao Z, et al. (2019) Thermosensitive glycol chitosan-based hydrogel as a topical ocular drug delivery system for enhanced ocular bioavailability. *International Journal of Pharmaceutics* 570: 118688.

Shi K, Huang Y, Yu H, et al. (2011) Reducing the Brittleness of Zein Films through Chemical Modification. *Journal of Agricultural and Food Chemistry* 59(1). American Chemical Society: 56–61.

Shukla PK, Gangwar R, Manda B, et al. (2016) Rapid disruption of intestinal epithelial tight junction and barrier dysfunction by ionizing radiation in mouse colon in vivo: protection by N-acetyl-l-cysteine. *American Journal of Physiology - Gastrointestinal and Liver Physiology* 310(9): G705–G715.

Sibinovska N, Žakelj S and Kristan K (2019) Suitability of RPMI 2650 cell models for nasal drug permeability prediction. *European Journal of Pharmaceutics and Biopharmaceutics* 145: 85–95.

Siemann U (2005) Solvent cast technology – a versatile tool for thin film production. In: *Scattering Methods and the Properties of Polymer Materials*. Berlin, Heidelberg: Springer Berlin Heidelberg, pp. 1–14. Available at: http://link.springer.com/10.1007/b107336 (accessed 29 April 2022).

Silva MM, Calado R, Marto J, et al. (2017) Chitosan Nanoparticles as a Mucoadhesive Drug Delivery System for Ocular Administration. *Marine Drugs* 15(12). 12. Multidisciplinary Digital Publishing Institute: 370.

Singh I, Pawar P, Sanusi EA, et al. (2017) Mucoadhesive Polymers for Drug Delivery Systems. In: *Adhesion in Pharmaceutical, Biomedical and Dental Fields*. John Wiley & Sons, Ltd, pp. 89–113. Available at: https://onlinelibrary.wiley.com/doi/abs/10.1002/9781119323716.ch5 (accessed 27 April 2022).

Siow CRS, Wan Sia Heng P and Chan LW (2016) Application of freeze-drying in the development of oral drug delivery systems. *Expert Opinion on Drug Delivery* 13(11): 1595–1608.

Smart JD (2004) Lectin-mediated drug delivery in the oral cavity. *Advanced Drug Delivery Reviews* 56(4). Lectins and Glycoconjugates in Drug Delivery and Targeting: 481–489.

Smart JD (2005) The basics and underlying mechanisms of mucoadhesion. *Advanced Drug Delivery Reviews* 57(11): 1556–1568.

Sobiesk JL and Munakomi S (2022) Anatomy, Head and Neck, Nasal Cavity. In: *StatPearls*. Treasure Island (FL): StatPearls Publishing. Available at: http://www.ncbi.nlm.nih.gov/books/NBK544232/ (accessed 24 April 2022).

Son WK, Youk JH, Lee TS, et al. (2004) The effects of solution properties and polyelectrolyte on electrospinning of ultrafine poly(ethylene oxide) fibres. *Polymer* 45(9): 2959–2966.

Soni V, Pandey V, Tiwari R, et al. (2019) Chapter 13 - Design and Evaluation of Ophthalmic Delivery Formulations. In: Tekade RK (ed.) *Basic Fundamentals of Drug Delivery*. Advances in Pharmaceutical Product Development and Research. Academic Press, pp. 473–538. Available at: https://www.sciencedirect.com/science/article/pii/B9780128179093000133 (accessed 26 April 2022).

Srinivasan B, Kolli AR, Esch MB, et al. (2015) TEER measurement techniques for in vitro barrier model systems. *Journal of laboratory automation* 20(2): 107–126.

Stankus JJ, Guan J, Fujimoto K, et al. (2006) Microintegrating smooth muscle cells into a biodegradable, elastomeric fibre matrix. *Biomaterials* 27(5): 735–744.

Stephan AM and Thomas S (2009) ELECTROLYTES | Gel. In: *Encyclopedia of Electrochemical Power Sources*. Elsevier, pp. 140–152. Available at: https://linkinghub.elsevier.com/retrieve/pii/B9780444527455000137 (accessed 9 May 2022).

Suchaoin W, Pereira de Sousa I, Netsomboon K, et al. (2016) Mucoadhesive polymers: Synthesis and in vitro characterization of thiolated poly(vinyl alcohol). *International Journal of Pharmaceutics* 503(1): 141–149.

Sun C, Dai L, He X, et al. (2016) Effect of heat treatment on physical, structural, thermal and morphological characteristics of zein in ethanol-water solution. *Food Hydrocolloids* 58: 11–19.

Sun Y, Cheng S, Lu W, et al. (2019) Electrospun fibres and their application in drug controlled release, biological dressings, tissue repair, and enzyme immobilization. *RSC Advances* 9(44). The Royal Society of Chemistry: 25712–25729.

Surendranath M, R RM and Parameswaran R (2022) Recent advances in functionally modified polymers for mucoadhesive drug delivery. *Journal of Materials Chemistry B*. The Royal Society of Chemistry. Epub ahead of print 7 July 2022. DOI: 10.1039/D2TB00856D.

Surendranath M, Rajalekshmi R, Ramesan RM, et al. (2022) UV-Crosslinked Electrospun Zein/PEO Fibroporous Membranes for Wound Dressing. *ACS Applied Bio Materials* 5(4). American Chemical Society: 1538–1551.

Surendranath M, M Ramesan R, Nair P, et al. (2023) Design and evaluation of propranolol hydrochloride loaded thiolated Zein/PEO electrospun fibrous matrix for transmucosal drug delivery. *Journal of Materials Chemistry B* 11(32). Royal Society of Chemistry: 7778–7791.

Surendranath M, Ramesan RM, Nair P, et al. (2023) Electrospun Mucoadhesive Zein/PVP Fibroporous Membrane for Transepithelial Delivery of Propranolol Hydrochloride. *Molecular Pharmaceutics* 20(1). American Chemical Society: 508–523.

Szekalska M, Wróblewska M, Czajkowska-Kośnik A, et al. (2023) The Spray-Dried Alginate/Gelatin Microparticles with Luliconazole as Mucoadhesive Drug Delivery System. *Materials* 16(1). 1. Multidisciplinary Digital Publishing Institute: 403.

Szilágyi BÁ, Mammadova A, Gyarmati B, et al. (2020) Mucoadhesive interactions between synthetic polyaspartamides and porcine gastric mucin on the colloid size scale. *Colloids and Surfaces B: Biointerfaces* 194: 111219.

Takeuchi H, Yamamoto H and Kawashima Y (2001) Mucoadhesive nanoparticulate systems for peptide drug delivery. *Advanced Drug Delivery Reviews* 47(1): 39–54.

Tan G, Li J, Song Y, et al. (2019) Phenylboronic acid-tethered chondroitin sulfate-based mucoadhesive nanostructured lipid carriers for the treatment of dry eye syndrome. *Acta Biomaterialia* 99: 350–362.

Tan L, Zheng X, Chen L, et al. (2014) Quality testing of human albumin by capillary electrophoresis using thermally crosslinked poly(vinyl pyrrolidone)-coated fused-silica capillary. *Journal of Separation Science* 37.

Tang Z, Miao Y, Zhao J, et al. (2021) Mussel-inspired biocompatible polydopamine/carboxymethyl cellulose/polyacrylic acid adhesive hydrogels with UV-shielding capacity. *Cellulose* 28(3): 1527–1540.

Taylor G (1969) Electrically driven jets. *Proceedings of the Royal Society of London. A. Mathematical and Physical Sciences*. Epub ahead of print 1969. DOI: 10.1098/rspa.1969.0205.

Tian H, Yuan L, Wang J, et al. (2019) Electrospinning of polyvinyl alcohol into crosslinked nanofibres: An approach to fabricate functional adsorbent for heavy metals. *Journal of Hazardous Materials* 378: 120751.

Timur SS, Yüksel S, Akca G, et al. (2019) Localized drug delivery with mono and bilayered mucoadhesive films and wafers for oral mucosal infections. *International Journal of Pharmaceutics* 559: 102–112.

Tort S, Yıldız A, Tuğcu-Demiröz F, et al. (2019) Development and characterization of rapid dissolving ornidazole loaded PVP electrospun fibres. *Pharmaceutical Development and Technology* 24(7). Taylor & Francis: 864–873.

Tuğcu-Demiröz F, Saar S, Tort S, et al. (2020) Electrospun metronidazole-loaded nanofibres for vaginal drug delivery. *Drug Development and Industrial Pharmacy* 46(6). Taylor & Francis: 1015–1025.

Turasan H and Kokini JL (2017) Advances in Understanding the Molecular Structures and Functionalities of Biodegradable Zein-Based Materials Using Spectroscopic Techniques: A Review. *Biomacromolecules* 18(2): 331–354.

Ugwoke MI, Agu RU, Verbeke N, et al. (2005) Nasal mucoadhesive drug delivery: Background, applications, trends and future perspectives. *Advanced Drug*

Delivery Reviews 57(11). Mucoadhesive Polymers: Strategies, Achievements and Future Challenges: 1640–1665.

Ullah S, Hashmi M, Khan MQ, et al. (2019) Silver sulfadiazine loaded zein nanofibre mats as a novel wound dressing. *RSC Advances* 9(1): 268–277.

Upadhyaya L, Singh J, Agarwal V, et al. (2014) The implications of recent advances in carboxymethyl chitosan based targeted drug delivery and tissue engineering applications. *Journal of Controlled Release: Official Journal of the Controlled Release Society* 186: 54–87.

Vakili MR, Mohammed-Saeid W, Aljasser A, et al. (2021) Development of mucoadhesive hydrogels based on polyacrylic acid grafted cellulose nanocrystals for local cisplatin delivery. *Carbohydrate Polymers* 255: 117332.

Valenta C (2005) The use of mucoadhesive polymers in vaginal delivery. *Advanced Drug Delivery Reviews* 57(11). Mucoadhesive Polymers: Strategies, Achievements and Future Challenges: 1692–1712.

Van Itallie CM and Anderson JM (2014) Architecture of tight junctions and principles of molecular composition. *Seminars in Cell & Developmental Biology* 36: 157–165.

Varki A and Schauer R (2009) Sialic Acids. In: Varki A, Cummings RD, Esko JD, et al. (eds) *Essentials of Glycobiology*. 2nd ed. Cold Spring Harbor (NY): Cold Spring Harbor Laboratory Press. Available at: http://www.ncbi.nlm.nih.gov/books/NBK1920/ (accessed 23 January 2023).

Vashisth P, Raghuwanshi N, Srivastava AK, et al. (2017) Ofloxacin loaded gellan/PVA nanofibres - Synthesis, characterization and evaluation of their gastroretentive/mucoadhesive drug delivery potential. *Materials Science and Engineering: C* 71: 611–619.

Vauthier C and Bouchemal K (2009) Methods for the Preparation and Manufacture of Polymeric Nanoparticles. *Pharmaceutical Research* 26(5): 1025–1058.

Vecchi CF, Cesar GB, Souza PR de, et al. (2021) Mucoadhesive polymeric films comprising polyvinyl alcohol, polyvinylpyrrolidone, and poloxamer 407 for pharmaceutical applications. *Pharmaceutical Development and Technology* 26(2). Taylor & Francis: 138–149.

Vogelpoel H, Welink J, Amidon GL, et al. (2004) Biowaiver monographs for immediate release solid oral dosage forms based on biopharmaceutics classification system (BCS) literature data: Verapamil hydrochloride, propranolol hydrochloride, and atenolol. *Journal of Pharmaceutical Sciences* 93(8): 1945–1956.

Voronova A, Prieto C, Pardo-Figuerez M, et al. (2022) Photothermal Activatable Mucoadhesive Fibre Mats for On-Demand Delivery of Insulin via Buccal and Corneal Mucosa. *ACS Applied Bio Materials* 5(2). American Chemical Society: 771–778.

Waite JH and Tanzer ML (1981) Polyphenolic Substance of Mytilus edulis: Novel Adhesive Containing L-Dopa and Hydroxyproline. *Science* 212(4498). American Association for the Advancement of Science: 1038–1040.

Wang X, Iqbal J, Rahmat D, et al. (2012) Preactivated thiomers: Permeation enhancing properties. *International Journal of Pharmaceutics* 438(1–2): 217–224.

Wang Y, Su C-P, Schulmerich M, et al. (2013) Characterization of core–shell structures formed by zein. *Food Hydrocolloids* 30(2): 487–494.

Weber CR (2012) Dynamic properties of the tight junction barrier. *Annals of the New York Academy of Sciences* 1257: 77–84.

Wei Y, Wang C, Liu X, et al. (2021) Effects of microfluidization and thermal treatment on the characterization and digestion of curcumin loaded protein–polysaccharide–tea saponin complex nanoparticles. *Food & Function* 12(3). The Royal Society of Chemistry: 1192–1206.

Winning TA and Townsend GC (2000) Oral mucosal embryology and histology. *Clinics in Dermatology* 18(5). Elsevier: 499–511.

Woodley J (2001) Bioadhesion: new possibilities for drug administration? *Clinical Pharmacokinetics* 40(2): 77–84.

Woody RW (1994) Contributions of tryptophan side chains to the far-ultraviolet circular dichroism of proteins. *European biophysics journal: EBJ* 23(4): 253–262.

Woolfson AD, McCafferty DF and Moss GP (1998) Development and characterisation of a moisture-activated bioadhesive drug delivery system for percutaneous local anaesthesia. *International Journal of Pharmaceutics* 169(1): 83–94.

Wu H, Li J, Zhang Q, et al. (2012) A novel small Odorranalectin-bearing cubosomes: preparation, brain delivery and pharmacodynamic study on amyloid-β_{25-35}-treated rats following intranasal administration. *European Journal of Pharmaceutics and Biopharmaceutics: Official Journal of Arbeitsgemeinschaft Fur Pharmazeutische Verfahrenstechnik e.V* 80(2): 368–378.

Xu H, Canisag H, Mu B, et al. (2015) Robust and Flexible Films from 100% Starch Cross-Linked by Biobased Disaccharide Derivative. *ACS Sustainable Chemistry & Engineering* 3(11). American Chemical Society: 2631–2639.

Xu X, Wang H, Jiang L, et al. (2014) Comparison between Cellulose Nanocrystal and Cellulose Nanofibril Reinforced Poly(ethylene oxide) Nanofibres and Their Novel Shish-Kebab-Like Crystalline Structures. *Macromolecules* 47(10). American Chemical Society: 3409–3416.

Xu X, Sun L, Zhou L, et al. (2020) Functional chitosan oligosaccharide nanomicelles for topical ocular drug delivery of dexamethasone. *Carbohydrate Polymers* 227: 115356.

Xue J, Wu T, Dai Y, et al. (2019) Electrospinning and Electrospun Nanofibres: Methods, Materials, and Applications. *Chemical reviews* 119(8): 5298–5415.

Yang J, He X, Chen L, et al. (2016) The selective detection of galactose based on boronic acid functionalized fluorescent carbon dots. *Analytical Methods* 8(47). The Royal Society of Chemistry: 8345–8351.

Yang NJ and Hinner MJ (2015) Getting Across the Cell Membrane: An Overview for Small Molecules, Peptides, and Proteins. In: Gautier A and Hinner MJ (eds) *Site-Specific Protein Labeling*. Methods in Molecular Biology. New York, NY: Springer New York, pp. 29–53. Available at: http://link.springer.com/10.1007/978-1-4939-2272-7_3 (accessed 29 May 2020).

Yang Q, Li Z, Hong Y, et al. (2004) Influence of solvents on the formation of ultrathin uniform poly(vinyl pyrrolidone) nanofibres with electrospinning. *Journal of Polymer Science Part B: Polymer Physics* 42(20): 3721–3726.

Yang SB, Rabbani MM, Ji BC, et al. (2016) Optimum Conditions for the Fabrication of Zein/Ag Composite Nanoparticles from Ethanol/H2O Co-Solvents Using Electrospinning. *Nanomaterials* 6(12).

Yang Y, Wang L and Li S (1996) Formaldehyde-free zein fibre—preparation and investigation. *Journal of Applied Polymer Science* 59(3): 433–441.

Yang Y, Jia Z, Li Q, et al. (2006) Experimental investigation of the governing parameters in the electrospinning of polyethylene oxide solution. *IEEE Transactions on Dielectrics and Electrical Insulation* 13(3): 580–585.

Yao C, Li X and Song T (2007) Electrospinning and crosslinking of zein nanofibre mats. *Journal of Applied Polymer Science* 103(1): 380–385.

Yarin A l. (2011) Coaxial electrospinning and emulsion electrospinning of core–shell fibres. *Polymers for Advanced Technologies* 22(3): 310–317.

Yeh T-H, Hsu L-W, Tseng MT, et al. (2011) Mechanism and consequence of chitosan-mediated reversible epithelial tight junction opening. *Biomaterials* 32(26): 6164–6173.

Yin J, Ren W, Yang G, et al. (2016) l-Cysteine metabolism and its nutritional implications. *Molecular Nutrition & Food Research* 60(1): 134–146.

Ying W (2008) The nose may help the brain: intranasal drug delivery for treating neurological diseases. *Future Neurology* 3(1). Future Medicine: 1–4.

Yoshinaga N, Zhou JK, Xu C, et al. (2023) Phenylboronic Acid-Functionalized Polyplexes Tailored to Oral CRISPR Delivery. *Nano Letters* 23(3). American Chemical Society: 757–764.

Yu D-G, Zhang X-F, Shen X-X, et al. (2009) Ultrafine ibuprofen-loaded polyvinylpyrrolidone fibre mats using electrospinning. *Polymer International* 58(9): 1010–1013.

Yu S, Zhang X, Tan G, et al. (2017) A novel pH-induced thermosensitive hydrogel composed of carboxymethyl chitosan and poloxamer cross-linked by glutaraldehyde for ophthalmic drug delivery. *Carbohydrate Polymers* 155: 208–217.

Yu T, Andrews GP and Jones DS (2014) Mucoadhesion and Characterization of Mucoadhesive Properties. In: das Neves J and Sarmento B (eds) *Mucosal Delivery of Biopharmaceuticals: Biology, Challenges and Strategies*. Boston, MA: Springer US, pp. 35–58. Available at: https://doi.org/10.1007/978-1-4614-9524-6_2 (accessed 4 May 2020).

Zaman M, Saeed S, Imtiaz Bajwa R, et al. (2021) Synthesis and Evaluation of Thiol-Conjugated Poloxamer and Its Pharmaceutical Applications. *Pharmaceutics* 13(5). 5. Multidisciplinary Digital Publishing Institute: 693.

Zaman M, Bajwa RI, Qureshi OS, et al. (2021) Synthesis of Thiol-Modified Hemicellulose, Its Biocompatibility, Studies, and Appraisal as a Sustained Release Carrier of Ticagrelor. *Frontiers in Pharmacology* 12: 550020.

Zhang B, M. Jayalath I, Ke J, et al. (2019) Chemically fueled covalent crosslinking of polymer materials. *Chemical Communications* 55(14). Royal Society of Chemistry: 2086–2089.

Zhang M, Liu Y, Yi H, et al. (2014) Electrospun zein/PVA fibrous mats as three-dimensional surface for embryonic stem cell culture. *The Journal of The Textile Institute* 105(3). Taylor & Francis: 246–255.

Zhang Q, Li X and Jasti BR (2021) Role of physicochemical properties of some grades of hydroxypropyl methylcellulose on in vitro mucoadhesion. *International Journal of Pharmaceutics* 609: 121218.

Zhang Y, Zhou S, Deng F, et al. (2018) The function and mechanism of preactivated thiomers in triggering epithelial tight junctions opening. *European Journal of Pharmaceutics and Biopharmaceutics* 133: 188–199.

ANNEXURES

LIST OF PUBLICATIONS

PUBLICATIONS FROM THE THESIS

[1]. Surendranath, Medha, Resmi Rajalekshmi, Rekha M. Ramesan, Prakash Nair, and Ramesh Parameswaran. "UV-Crosslinked electrospun Zein/PEO fibroporous membranes for wound dressing." *ACS Applied Bio Materials* 5, no. 4 (2022): 1538-1551. **(IF: 4.7)**

[2]. Surendranath, Medha, M. R. Rekha, and Ramesh Parameswaran. "Recent advances in functionally modified polymers for mucoadhesive drug delivery." *Journal of Materials Chemistry B* 10, no. 31 (2022): 5913-5924. **(IF: 7)**

[3]. Surendranath, Medha, Rekha M. Ramesan, Prakash Nair, and Ramesh Parameswaran. "Electrospun Mucoadhesive Zein/PVP Fibroporous Membrane for Transepithelial Delivery of Propranolol Hydrochloride." *Molecular Pharmaceutics* 20, no. 1 (2022): 508-523. **(IF: 4.9)**

[4]. Surendranath, Medha, Rekha M. Ramesan, Prakash Nair, and Ramesh Parameswaran. "Design and evaluation of propranolol hydrochloride loaded thiolated Zein/PEO electrospun fibrous matrix for transmucosal drug delivery." *Journal of Materials Chemistry B* 11, no. 32 (2023): 7778-7791. **(IF: 7)**

[5]. Surendranath, Medha, Rekha M. Ramesan, Prakash Nair, and Ramesh Parameswaran. “Novel design of mucin incorporated fibrous matrix for mucoadhesion and its evaluation for transmucosal propranolol hydrochloride delivery” (Under communication)

[6]. Surendranath, Medha, Rekha M. Ramesan, Prakash Nair, and Ramesh Parameswaran. “3-aminophenyl boronic acid (APBA) conjugated PVP/Zein fibrous membrane for propranolol delivery” (Under communication)

OTHER PUBLICATIONS

[1]. Medha, Surendranath, Rajalekshmi Resmi, M. R. Rekha, Prakash Nair, and P. Ramesh. "An Investigation into the Efficacy of Low Temperature and UV Irradiated Citric Acid Crosslinked Zein/PEO Electrospun Membranes for Wound Healing Using Human Dermal Fibroblast Cells." *ChemistrySelect* 8, no. 34 (2023): e202204493. **(IF: 2.1)**

BIODATA

Name **:** Medha Surendranath

Permanent address **:** Medha Nivas, Kisan Road, Pannenpara, Chalad P.O, Kannur-14, Kerala

Date of birth **:** 14.02.1993

Educational qualifications :

2019-2023: - PhD Scholar at Sree Chitra Tirunal Institute for Medical Sciences and Technology, Division of Polymeric Medical Devices, Biomedical Technology Wing, Trivandrum, Kerala, India.

2015-2017: - Master of Science in Chemical Sciences, Department of Chemistry, Pondicherry University, Pondicherry, India

2012-2015: - Bachelor of Science in Chemistry, Department of Chemistry, CMS College, Mahathma Gandhi University, Kottayam, Kerala, India